

Proteomics of mouse cortex following conditional deletion of *Psmc1* proteasomal subunit in neurones

Jamal Ibrahim Elkharaz, B.Pharm, M.Sc.

Thesis submitted to The University of Nottingham

For the degree of Doctor of Philosophy

October 2013

Abstract

Neurodegenerative diseases are characterized by progressive degeneration of selective neurones in the nervous system and the formation of protein inclusions in surviving neurones. The mechanisms underlying neurodegeneration and neuroprotection in the nervous system remain elusive. Ubiquitin is one of the hallmarks of neuropathological inclusions in the majority of neurodegenerative diseases, including Alzheimer's disease and Parkinson's disease. Therefore, dysfunction of the ubiquitin proteasome system has been implicated in disease cause and/or progression. This thesis investigates a unique conditional genetic mouse model of neurodegeneration caused by conditional genetic 26S proteasomal depletion in mouse forebrain neurones. We have identified potential proteins targeted for ubiquitination in brain using bio-affinity chromatography of zinc finger protein ZNF216 coupled with mass spectrometry. This led to the identification of several potential ubiquitinated proteins involved in gene expression and regulation. We have also investigated the global brain proteome in response to 26S proteasomal depletion in neurones using two-dimensional fluorescence difference in-gel electrophoresis coupled to mass spectrometry for protein identification. Several differentially expressed proteins were identified in the 26S proteasome-depleted cortex. Astrocytic intermediate filament proteins glial acid fibrillary protein and vimentin, as well as the antioxidant peroxiredoxin-6, were upregulated. Mitochondrial fumarate hydratase and stathmin-1, involved in the tricarboxylic acid cycle and cytoskeletal microtubule dynamics respectively, were downregulated. These proteins have been validated by biochemical and immunohistochemical approaches. Further analysis of oxidative stress revealed increased lipid and protein oxidation that may be involved in the neurodegeneration associated with 26S proteasomal depletion. However, we also show increased phospholipase A₂ activity associated with peroxiredoxin-6 expression that may have additional roles in neurodegenerative and/or neuroprotective functions. Interestingly, the levels of reactive oxygen species were inversely correlated with the upregulation of peroxiredoxin-6. We suggest that peroxiredoxin-6 may play an important role in the brain in the protection against oxidative stress and our studies may improve our physiological and pathological understanding of neurodegenerative disease.

Acknowledgments

First and foremost, I would like to acknowledge my gratitude to my supervisor Dr. Lynn Bedford, for her efforts, encouragement and shrewd advice throughout my time as her student. I was very lucky to have a supervisor who was so interested in my research work and who worked so keenly to provide me with the mouse model of dementia to work with for my *PhD* study.

I must also express my appreciation to my second supervisor Dr. Layfield Robert for his helpful suggestions, encouragement and kindness by providing me with some materials I needed for my research.

I must also acknowledge Prof. John Mayer for welcoming me to his lab before he retired, and he even continued to visit us in the lab from time to time and encouraged me during my work, giving me suggestions and advice; for which I thank him.

Finishing this work would have not been possible without the help of Dr. Aslihan Ugun-Klusek, who gave me valuable advice and performed the mass spectrometry analysis, so my thanks also go out to her.

Thanks to my colleagues in the past and in the present Dr. Simon Paine, Dr. Zahra Nooshin, Dr. Joanna Strachan, Dr. James Cavy, Zakok Ahmed, for all their help and support.

Many thanks to Maureen Mee and Karen Lawler.

Also many thanks to Dr. Constantin Teodosiu for his advice and who allowed me to use the spectrophotometer in his lab and to Dr. David Tooth for mass spectrometry analysis.

Finally I would also like to thank my wife Intissar for her support, encouragement and patience throughout my study, and to thank my parents who prayed for me.

Publications

Elkharaz J, Ugun-Klusek A, Constantin-Teodosiu D, Lawler K, Mayer RJ, Billett E, Lowe J, Bedford L (2013). Implications for oxidative stress and astrocytes following 26S proteasomal depletion in mouse forebrain neurones. *Biochim Biophys Acta*. 1832 (12): 1959-1968.

Rezvani N, Elkharaz J, Lawler K, Mee M, Mayer RJ, Bedford L (2012). Heterozygosity for the proteasomal Psmc1 ATPase is insufficient to cause neuropathology in mouse brain, but causes cell cycle defects in mouse embryonic fibroblasts. *Neurosci Lett*. 521(2):130-135.

Abbreviations

1DG	one dimensional gel
2D-DIGE	two dimensional fluorescence difference in-gel electrophoresis
ACTN	β -actin
AD	Alzheimer's disease
AMPS	ammonium per-sulphate
ANOVA	analysis of variance
ApoE	apolipoprotein E
Bcl-2	B-cell lymphoma 2
BSA	bovine serum albumin
CaMKII α	calcium calmodulin-dependent protein kinase II α
CNBr	cyanogen bromide activated-Sepharose-4B
CP	20S proteolytic core particle
COX5A	cytochrome c oxidase subunit 5A, mitochondrial
Cre	causes <u>re</u> combination
DCFDA	2, 7- dichlororfluorescein diacetate
DLB	dementia with Lewy bodies
DNPH	2,4- dinitrophenylhydrazine
DUB	deubiquitination
ECL	chemiluminescent substrate
GAB	gel application buffer
GAPDH	glyceraldehyde-3-phosphate dehydrogenase
GFAP	glial acidic fibrillary protein
GST	gluthathion-S-transferase
HSP7C	heat shock cognate 71 kDa protein
IEF	isoelectric focusing
IF	intermediate filaments
IL-1 β	interleukins-1 β
IPG	immobilized pH gradient

IPTG	isopropyl- β -D-thiogalactopyranosid
Iso-T	isopeptidase T
LB	Lewy bodies
LC/MS-MS	liquid chromatography/mass spectrometry
MAP2	microtubule-associated protein-2
MDA	malondialdehyde
mFUMH	mitochondrial fumarate hydratase
MJ33	1-hexadecyl-3-trifluoroethylglycero-sn-2-phosphomethanol
MPTP	1-methyl-4-phenyl-1, 2, 3, 6-tetrahydropyridine
MALDI-TOF	matrix-associated laser desorption ionization-time of flight
MT	microtubule
NEM	N-ethylmaleimide
NEUG	neurogranin
NF- κ B	nuclear factor kappa-B
NO	nitric oxide
ONOO	peroxynitrite
P53	protein 53 or tumor protein 53
PB	pale body
PBST	phosphate buffered saline-Triton
PD	Parkinson's disease
PDD	Parkinson's disease with dementia
PLA ₂	phospholipase A ₂
PRDX-6	peroxiredoxin-6
PSMA	proteasome subunit mouse-A
PSMB	proteasome subunit mouse-B
PSMC	proteasome subunit mouse-C
PSMD	proteasome subunit mouse-D
RIPA	radioimmunoprecipitation assay buffer
ROS	reactive oxygen species

RNS	reactive nitrogen species
RP	19S regulatory particle
Rpn	regulatory particle <u>n</u> on-ATPase subunits
Rpt	regulatory particle <u>A</u> TPase subunits
RpS27A	ribosomal protein S27a
SEM	standard error of the mean
SEPT-7	septin-7
SNAB	beta-soluble NSF attachment protein
STMN-1	stathmin-1
TBHP	tert-butyl hydrogen peroxide
TBS	Tris-buffered saline
TBS-T	Tris-buffered saline-Triton
TCA	trichloroacetic acid
TCB	thrombin cleavage buffer
TEMED	N, N, N, N- tetramethylene diamine
TMOP	1, 1, 3, 3-tetramethoxypropane
VIME	vimentin
Uba52	ubiquitin A-52 residue ribosomal gene
Ubb	polyubiquitin-B gene
UBD	ubiquitin binding domains
Ubc	ubiquitin conjugating enzyme
UBP	ubiquitin binding proteins
UCHL1	ubiquitin carboxyl-terminal esterase L1
UCH	ubiquitin carboxy-terminal hydrolases
UPS	ubiquitin proteasome system
USP	ubiquitin-specific proteases
ZNF216	zinc finger protein-216

Table of contents

Chapter 1: The Introduction	1
1.1 Introduction.....	2
1.2 The ubiquitin 26S proteasome system	4
1.2.1 The 26S proteasome.....	4
1.2.2 The 20S core particle	4
1.2.3 The 19S regulatory particle.....	5
1.2.4 Proteasome assembly	5
1.2.5 Ubiquitin	9
1.2.6 Ubiquitination	9
1.2.6.1 The ubiquitin activation enzyme (E1):	10
1.2.6.2 The ubiquitin conjugating enzyme (E2):	10
1.2.6.3 The ubiquitin ligase enzyme (E3):.....	10
1.2.7 Unanchored polyubiquitin chains	12
1.2.8 Ubiquitin specific peptidases (deubiquitinating enzymes)	12
1.2.9 Ubiquitin binding proteins	12
1.3 Protein homeostasis and neurodegenerative diseases	13
1.3.1 Lewy body diseases	13
1.3.2 The Lewy body	14
1.3.3 Parkinson’s disease	14
1.3.4 Dementia with Lewy bodies	15
1.3.5 Dysfunction of the UPS and neurodegenerative disease	16
1.4 Oxidative stress and neurodegeneration	18
1.4.1 Lipid peroxidation.....	19
1.4.2 Protein oxidation.....	21
1.5 Reactivation of astrocytes in neurodegenerative diseases	22

1.5.1 The role of astrocytes.....	22
1.5.2 Reactive astrogliosis	23
1.6 26S proteasomal depletion mouse model; <i>Psmc1^{fl/fl}</i> ; <i>CaMKIIα-Cre</i>	23
Aim	27
Chapter 2: Materials and Methods.....	28
2.1 Experimental animals.....	29
2.1.1 Generation of <i>Psmc1^{fl/fl}</i> ; <i>CaMKIIα-Cre</i> Mice	29
2.1.2 Extraction of genomic DNA from mouse tissues	29
2.1.2.1 Reagents	29
2.1.2.2 Protocol	29
2.1.3 Polymerase Chain Reaction (PCR).....	30
2.1.3.1 Reagents	30
2.1.3.2 Protocol.....	30
2.1.4 Agarose gel electrophoresis	30
2.1.4.1 Reagents	30
2.1.4.2 Protocol.....	30
2.2 Preparation of affinity chromatography matrices and capture of ubiquitinated proteins.....	32
2.2.1 Preparation of <i>E. coli</i> glycerol stock.....	32
2.2.1.1 Reagents	32
2.2.1.2 Protocol	32
2.2.2 Plasmid purification for sequencing	32
2.2.2.1 Reagents	32
2.2.2.2 Protocol	32
2.2.3 Preparation of 20 ml overnight <i>E. coli</i> culture.....	33
2.2.3.1 Reagents	33

2.2.3.2 Protocol	33
2.2.4 Bacterial expression of recombinant proteins	33
2.2.4.1 Reagents	33
2.2.4.2 Protocol	33
2.2.5 Purification of GST-ZNF216 recombinant proteins	34
2.2.5.1 Reagents	34
2.2.5.2 Protocol	34
2.2.6 Thrombin cleavage of GST-recombinant proteins	35
2.2.6.1 Reagents	35
2.2.6.2 Protocol	35
2.2.7 Coupling ZNF 216 purified proteins to Sepharose beads - preparation of ZNF216 affinity matrices	35
2.2.7.1 Reagents	35
2.2.7.2 Protocol	36
2.2.8 Capture of ubiquitinated proteins from brain tissue homogenate	36
2.2.8.1 Reagents	36
2.2.8.2 Protocol	37
2.2.9 Capture of Lysine- 48 synthetic polyubiquitin chain	37
2.2.9.1 Reagents	37
2.2.9.2 Protocol	37
2.2.10 Deubiquitination using ubiquitin-specific protease (USP2) enzyme	38
2.2.10.1 Reagents	38
2.2.10.2 Protocol	38
2.3 Protein analysis	39
2.3.1 Bradford assay for protein quantitation	39
2.3.1.1 Reagents	39
2.3.1.2 Protocol	39

2.3.2 One dimensional (1DG) sodium dodecyl sulphate polyacrylamide gel electrophoresis (SDS-PAGE) - large gradient gel (5-20 %)	39
2.3.2.1 Reagents	39
2.3.2.2 Protocol	40
2.3.3 1DG SDS-PAGE - mini gradient (10-18%) and 12% gel	40
2.3.3.1 Protocol	40
2.3.4 Two dimensional (2DG) gel electrophoresis	41
2.3.4.1 Reagents	41
2.3.4.2 Protocol	42
1) Sample preparation:	42
2) First dimension isoelectric focusing (IEF)	42
3) Equilibration of IPG strips.....	42
4) Second dimension electrophoresis.....	42
2.3.5 Coomassie Blue staining.....	43
2.3.5.1 Reagents	43
2.3.5.2 Protocol	43
2.3.6 Colloidal Coomassie staining	43
2.3.6.1 Reagents	43
2.3.6.2 Protocol	43
2.3.7 Silver staining	44
2.3.7.1 Reagents	44
2.3.7.2 Protocol	44
2.3.8 Western blotting analysis.....	44
2.3.8.1 Reagents	44
2.3.8.2 Protocol	45
2.3.9 Striping of antibody from the nitrocellulose membrane.....	45
2.3.9.1 Reagents	45

2.3.9.2 Protocol	45
2.4 Two-dimensional fluorescence difference in-gel electrophoresis (2D-DIGE)	46
2.4.1 Reagents	46
2.4.2 Protocol	46
2.4.2.1 Sample preparation	46
2.4.2.2 Experimental design and CyDye labeling.....	46
2.4.2.3 First dimension isoelectric focusing (IEF).....	47
2.4.2.4 Equilibration of IPG strips	47
2.4.2.5 Second dimension electrophoresis	47
2.4.2.6 Gel imaging.....	47
2.4.2.7 Analysis of 2D-DIGE images to identify differential abundant spots	48
2.4.3 Preparative 2DG and spot picking	48
2.4.4 Protein extraction for MALDI-TOF-MS	48
2.4.4.1 Reagents	48
2.4.4.2 Protocol	48
2.4.5 Protein validation following MALDI-TOF-MS	49
2.5 Histological studies of brain sections - protein localization	50
2.5.1 Double immunofluorescent.....	50
2.5.1.1 Material and reagents	50
2.5.1.2 Protocol	50
2.6 Measures of oxidative stress markers	52
2.6.1 Determination of Malondialdehyde (MDA)	52
2.6.1.1 Reagents and solutions.....	52
2.6.1.2 Preparation of stock solutions.....	52
2.6.1.3 Preparation of MDA Standard Curve.	52
2.6.1.4 Sample Preparation for MDA Measurement.	53
2.6.1.5 Assay procedure for MDA measurement	53

2.6.2 Estimation of protein carbonyl group	55
2.6.2.1 Reagents and solutions.....	55
2.6.2.2 Protocol	55
2.6.3 Determination of nitrated proteins	56
2.6.3.1 Reagents and solutions.....	56
2.6.3.2 Preparation of peroxy nitrite solution	56
2.6.3.3 Preparation of positive control of nitrated proteins	57
2.6.4 Measurement of reactive oxygen species (ROS) in cortical tissue.....	57
2.6.4.1 Reagents and solutions.....	57
2.6.4.2 Protocol	57
2.7 Assay of total phospholipase activity (PLA ₂).....	58
2.7.1 Reagents and solutions.....	58
2.7.1.1 Preparation of solutions	58
2.7.1.2 Preparation of sample	58
2.7.2 Protocol.....	59
Chapter 3: Investigation into ubiquitinated proteins in the <i>Psmc1^{fl/fl};CaMKIIα-Cre</i> mouse cortex.....	61
3.1 Introduction.....	62
3.2. Results.....	63
3.2.1. Accumulation of polyubiquitinated proteins in <i>Psmc1^{fl/fl};CaMKIIα-Cre</i> mouse cortex	63
3.2.2 Purification of ZNF216 recombinant proteins	66
3.2.3 Preparation of ZNF216 affinity matrices for the capture of ubiquitinated proteins	69
3.2.4 Binding of ubiquitinated proteins to ZNF216 affinity matrices	71
3.2.5 Evaluation of the binding capacity of ZNF216-Wt affinity matrices	74

3.2.6 Deubiquitination of captured ubiquitinated proteins using ubiquitin specific protease 2	76
3.2.7 Two dimensional profile of proteins bound to ZNF216 affinity matrices.....	79
3.2.8 One dimensional profile of proteins bound to ZNF216 affinity matrices	81
3.3 Discussion	84
3.3.1 Age-related accumulation of polyubiquitinated proteins and unanchored polyubiquitin chains.....	84
3.3.2 Capture of ubiquitinated proteins from the <i>Psmc1^{fl/fl};CaMKIIα-Cre</i> cortex ..	85
Chapter 4: Proteomic investigation of the <i>Psmc1^{fl/fl};CaMKIIα-Cre</i> mouse cortex reveals differential expression of cytoskeletal, antioxidant and mitochondrial proteins.....	89
4.1 Introduction.....	90
4.2. Results.....	93
4.2.1. Differential expression of proteins in the <i>Psmc1^{fl/fl};CaMKIIα-Cre</i> cortex ...	93
4.2.2. Proteins spots identified by MALDI-TOF-MS.....	97
4.2.3 Protein validation by Western blot	100
4.2.3.1 Glial fibrillary acidic protein (GFAP) is increased and post translationally modified in <i>Psmc1^{fl/fl};CaMKIIα-Cre</i> mouse cortex.....	100
4.2.3.2 Vimentin (VIME) is up-regulated in <i>Psmc1^{fl/fl};CaMKIIα-Cre</i> mouse cortex.....	103
4.2.3.3 Up-regulation of peroxiredoxin-6 (PRDX-6) in <i>Psmc1^{fl/fl};CaMKIIα-Cre</i> mouse cortex	103
4.2.3.4 Stathmin-1 (STMN-1) is down-regulated in the <i>Psmc1^{fl/fl};CaMKIIα-Cre</i> mouse cortex	104
4.2.3.5 Mitochondrial fumarate hydratase (mFUMH) is down-regulated in <i>Psmc1^{fl/fl};CaMKIIα-Cre</i> mouse cortex.....	104
4.2.3.6 Neurogranin (NEUG) is down-regulated in <i>Psmc1^{fl/fl};CaMKIIα-Cre</i> mouse cortex	105

4.2.3.7 Differentially expressed Proteins identified by 2D-DIGE -MS, but not validated by Western blotting	108
4.2.4 Immunohistochemical investigations of differentially-expressed proteins ..	111
4.2.4.1 GFAP and VIME are expressed in astrocytes.....	111
4.2.4.2 Preoxidoredoxin-6 is expressed in astrocytes.	111
4.3 Discussion	115
4.3.1 Upregulation of GFAP in <i>Psmc1^{fl/fl};CaMKIIα-Cre</i> mouse cortex indicates reactive astrogliosis.....	115
4.3.2 VIME upregulation supports reactive astrogliosis.....	117
4.3.3 Upregulation PRDX-6 indicates oxidative stress.....	117
4.3.4 Downregulation of STMN-1 suggests dysregulation of the cytoskeleton	119
4.3.5 Downregulation of mFUMH suggests mitochondrial dysfunction in <i>Psmc1^{fl/fl};CaMKIIα-Cre</i> mouse cortex	121
4.3.6 Downregulation of neurogranin (NEUG) may cause postsynaptic impairment	122
4.3.7 Limitations of Proteomics in <i>Psmc1^{fl/fl};CaMKIIα-Cre</i> brain cortex mice	123
Chapter 5: Changes in redox homeostasis and PLA₂ activity in <i>Psmc1^{fl/fl};CaMKIIα-Cre</i> mouse cortex	124
5.1 Introduction.....	125
5.2 Results.....	126
5.2.1 Malondialdehyde levels are increased in <i>Psmc1^{fl/fl};CaMKIIα-Cre</i> cortices .	126
5.2.2 Measurement of protein carbonyl group in <i>Psmc1^{fl/fl};CaMKIIα-Cre</i> cortex showed no change compared to control.....	129
5.2.3 Increased nitro-tyrsoinated proteins in <i>Psmc1^{fl/fl};CaMKIIα-Cre</i> cortex	130
5.2.4 Reactive oxygen species decline with increasing age in the cortex of <i>Psmc1^{fl/fl};CaMKIIα-Cre</i> mouse.....	133
5.2.5 PRDX-6 expression increases with age in <i>Psmc1^{fl/fl};CaMKIIα-Cre</i> cortex	136
5.2.6 Modification of PRDX-6 in the <i>Psmc1^{fl/fl};CaMKIIα-Cre</i> mouse cortex	141

5.2.7 Phospholipase A2 enzyme activity is increased the <i>Psmc1^{fl/fl};CaMKIIα-Cre</i> cortex	143
5.3 Discussion.....	146
Chapter 6: General discussion and conclusion.....	152
Conclusion	154
Future work.....	155
Bibliography	156
Appendix I	174
Appendix II	177

List of Figures

Figure number	Page.
Figure 1.1 Schematic representation of the 20S core particle.....	7
Figure 1.2 Schematic representation of the 19S regulatory particle.....	8
Figure 1.3 Protein ubiquitination and degradation by the ubiquitin 26S proteasome system	11
Figure 1.4 Lipid peroxidation cascade.....	20
Figure 1.5 Extensive cortical neurodegeneration in <i>Psmc1^{fl/fl};CaMKIIα-Cre</i> mouse cortex.....	25
Figure 1.6 Lewy-like intraneuronal inclusion pathology in <i>Psmc1^{fl/fl};CaMKIIα-Cre</i> mouse cortical neurones at 6 weeks of age	26
Figure 2.1 Representative image of <i>Psmc1</i> and Cre genotyping.....	31
Figure 2.2 Representative standard curve of MDA.....	54
Figure 2.3 Representative standard curves for PLA ₂ activity.....	60
Figure 3.1 Anti-ubiquitin Western blot analysis of control and <i>Psmc1^{fl/fl};CaMKIIα-Cre</i> cortex samples from mice at 2, 3, 4, and 6 weeks ages.....	65
Figure 3.2 Coomassie Blue-stained SDS-PAGE gel showing immobilized GST ZNF216 fusion proteins and their thrombin cleavage.....	67
Figure 3.3 Schematic representation for the production of recombinant ZNF216 proteins.....	68
Figure 3.4 Binding of ZNF216 proteins to CNBr activated Sepharose beads.....	70
Figure 3.5 Schematic representation of the capture of ubiquitinated proteins using ZNF216 affinity matrices.....	72
Figure 3.6 Capture of ubiquitinated proteins from mouse brain.....	73
Figure 3.7 Evaluation of the binding capacity of ZNF216-Wt affinity matrices.....	75
Figure 3.8 Schematic representation of deubiquitination using USP2.....	77
Figure 3.9 Ubiquitin Western blot showing deubiquitination of captured polyubiquitinated proteins using USP2 DUB enzyme.....	78

Figure number	Page.
Figure 3.10 Two dimensional gel electrophoresis protein profiles following elution of ubiquitinated proteins from ZNF216-Wt and ZNF216-mutant affinity matrices.....	80
Figure 3.11 One dimensional gel electrophoresis protein profiles following elution of ubiquitinated proteins from ZNF216-Wt and ZNF216-mutant affinity matrices.....	82
Figure 3.12 The results of STRING software analysis of proteins identified.....	88
Figure 4.1 False-colored images of the gels following 2-D DIGE analysis.....	94
Figure 4.2 (A) A representative silver staining following 2D-DIGE of a pooled Cy2-labeled sample.....	95
Figure 4.2 (B) Preparative 2DG electrophoresis visualized with colloidal Coomassie stain.....	95
Figure 4.3 Master image of the 2-D DIGE analysis produced by the Samespots software.....	96
Figure 4.4 2-D Western blotting for GFAP of control and <i>Psmc1^{fl/fl};CaMKIIα-Cre</i> mice cortices samples.....	102
Figure 4.5 GFAP, VIME and PRDX-6 are up-regulated in <i>Psmc1^{fl/fl};CaMKIIα-Cre</i> cortex.....	106
Figure 4.6 STMN-1 and mFUMH are decreased in <i>Psmc1^{fl/fl};CaMKIIα-Cre</i> cortex.....	107
Figure 4.7 GAPDH, COX5A, HSP7C, SNAB and SEPT-7 do not show differential expression in control and <i>Psmc1^{fl/fl};CaMKIIα-Cre</i> mice cortices.....	110
Figure 4.8 Astrocytic expression of GFAP and VIME.....	112
Figure 4.9 PRDX-6 is expressed in astrocytes.....	113
Figure 4.10 PRDX-6 is not expressed in the neurones	114
Figure 5.1 Cortical MDA concentrations in <i>Psmc1^{fl/fl};CaMKIIα-Cre</i> and control mice at 4, 5 and 6 weeks of ages.....	128
Figure 5.2 The level of protein carbonyl groups in <i>Psmc1^{fl/fl};CaMKIIα-Cre</i> and control moice cortices at 6 weeks age.....	129
Figure 5.3 Representative Western blot analysis of nitrated proteins.....	131

Figure 5.4 Densitometry analyses of nitrated proteins.....	132
Figure 5.5 Fluorescent intensities produced by ROS in control and <i>Psmc1^{fl/fl};CaMKIIα-Cre</i> mice cortices.....	134
Figure 5.6 Correlation and regression analysis of ROS levels with age.....	135
Figure 5.7 Western blots of cortical homogenates from control and <i>Psmc1^{fl/fl};CaMKIIα-Cre</i> mice for PRDX-6 at 2, 3, 4, 5 and 6 weeks of age.....	137
Figure 5.8 Relative PRDX-6 expression levels in <i>Psmc1^{fl/fl};CaMKIIα-Cre</i> mice compared to controls at different ages.....	138
Figure 5.9 Correlation analysis of PRDX-6 expression and age in <i>Psmc1^{fl/fl};CaMKIIα-Cre</i> mouse cortex.....	139
Figure 5.10 Inverse relationships between % increase of PRDX-6 expression and % decrease of ROS in <i>Psmc1^{fl/fl};CaMKIIα-Cre</i> mouse cortex	140
Figure 5.11 2DG PRDX-6 Western blotting of control and <i>Psmc1^{fl/fl};CaMKIIα-Cre</i> cortices.....	142
Figure 5.12 PLA ₂ enzyme activities in control and <i>Psmc1^{fl/fl};CaMKIIα-Cre</i> mice cortices at 4, 5 and 6 weeks age.....	144
Figure 5.13 PLA ₂ enzyme activities in control and <i>Psmc1^{fl/fl};CaMKIIα-Cre</i> mice cortices at 6 weeks of age in the presence and absence of MJ33	145
Figure 5.14 Eicosanoid biosynthesis pathway.....	147

List of Tables

Table number	Page
Table 1.1 Examples of proteinopathies.....	3
Table 2.1 volumes and concentration of compounds used to prepare SDS-PAGE, mini gel.....	41
Table 2.2 Experimental design for 2D-DIGE analysis.....	47
Table 2.3 Volumes of TMOP for MDA standard curve.....	52
Table 3.1 Proteins identified by MALDI-TOF-MS.....	83
Table 4.1 Differentially expressed proteins in <i>Psmc1^{fl/fl};CaMKIIα-Cre</i> mice brain cortex.....	99

CHAPTER 1

The Introduction

1.1 Introduction

Neurodegenerative diseases are characterized by the progressive loss of neurones in specific regions of the nervous system and formation of protein inclusions in surviving neurones. These diseases are proteinopathies which affect protein homeostasis. Examples of proteinopathies and their associated abnormal proteins are given in Table 1.1, including major human neurodegenerative diseases such as Parkinson's disease (PD), dementia with Lewy bodies (DLB) and Alzheimer disease (AD). Mitochondrial impairment, oxidative stress and dysfunction of protein degradation are key hypotheses in disease cause and progression. However, the mechanisms involved in neurodegeneration and inclusion body formation in different regions of the brain remain unclear.

The ubiquitin proteasome system (UPS) is the major pathway for degradation of unwanted soluble intracellular proteins (Ciechanover, 1994; Hochstrasser, 1996). Dysfunction of the UPS has been implicated in the pathogenesis of neurodegenerative diseases for over two decades (Lowe et al., 1993) and is supported by cellular and animal models (Bedford et al., 2008; Gavilan et al., 2009; Romero-Granados et al., 2011).

Animal models provide a tool to investigate the mechanisms involved in neurodegenerative diseases as well as evaluate new treatment strategies. A recently developed mouse model showing neurodegeneration and the formation of protein inclusions provided direct evidence for the importance of proteasomal dysfunction in neurodegenerative disease (Bedford et al., 2008). This was achieved by conditional genetic depletion of the 26S proteasome in mouse cortex (*Psmc1^{fl/fl};CaMKII α -Cre*).

This thesis is divided into 3 main areas of study that carried out on *Psmc1^{fl/fl};CaMKII α -Cre* mouse cortex and include;(1) investigations of the brain ubiquitome using bio-affinity chromatography (see chapter 3), (2) investigation of changes in the brain proteome in response to neuronal 26S proteasomal depletion using two dimensional fluorescence difference in-gel electrophoresis (2D-DIGE) (see chapter 4) and (3) investigations of oxidative stress and peroxiredoxin-6 (see chapter 5). The overall aim is to identify mechanisms involved in neurodegeneration and inclusion formation that may be translated to human disease.

Table 1.1 Examples of proteinopathies

Disease Name	Abnormal protein	References
Parkinson's disease	α -synuclein ubiquitinated proteins	(Mayer, 2003; Stefanis, 2012)
Lewy body dementia	α -synuclein ubiquitinated proteins	(Mayer, 2003; Puschmann et al., 2012)
Alzheimer's disease	Amyloid- β Tau	(Musiek and Holtzman, 2012; Gilbert, 2013)
Huntington's disease	Huntingtin	(Hoffner and Djian, 2002)
Familial amyotrophic lateral sclerosis	Superoxide dismutase	(Chattopadhyay and Valentine, 2009)
Frontotemporal dementia	Tau	(Gasparini et al., 2007)
Multiple systemic atrophy	α -synuclein	(Yoshida, 2007)
Creutzfeldt-Jacob disease	Prion	(Head and Ironside, 2012)
Progressive supranuclear palsy	Tau protein	(Kaat et al., 2011)
Spinocerebellar ataxia	Ataxin	(Orr, 2012)
Corticobasal degeneration	Tau	(Kouri et al., 2011)
Familial encephalopathy with neuroserpin inclusion	Neuroserpin	(Davis et al., 2002)

1.2 The ubiquitin 26S proteasome system

1.2.1 The 26S proteasome

The 26S proteasome is a multi-protein complex present in the nucleus and cytosol of eukaryotic cells. It is an essential and abundant complex, constituting up to 1% of the intracellular protein content. The 26S proteasome performs proteolysis of unwanted proteins that are tagged with ubiquitin (ubiquitinated) as a signal for their degradation (see section 1.2.6). The 26S proteasome is made up of two sub-complexes; a barrel-shaped 20S proteolytic core particle (CP) and a 19S regulatory particle (RP), which recognizes ubiquitinated proteins for degradation (Glickman et al., 1998; Lam et al., 2002; da Fonseca and Morris, 2008). A 19S RP caps either end of the 20S CP to form the 26S proteasome that is essential for the ubiquitin proteasome system (UPS) (Wang et al., 1997; da Fonseca and Morris, 2008).

1.2.2 The 20S core particle

The structure and enzymatic activity of the 20S CP of the 26S proteasome have been described. The CP is a barrel-shaped elongated hollow cylinder with narrow constrictions at both ends of a central cavity (Smith et al., 2007). The CP consists of four stacked heptameric rings made up of α_1 /PSMA1 – α_7 /PSMA7 and β_1 /PSMB1- β_7 /PSMB7 protein subunits, on the basis of their sequence similarity (Figure 1.1). The α /PSMA subunits form the outer rings of the 20S CP and the β /PSMB subunits form two inner rings (Coux et al., 1996). The N-terminal tails of the α /PSMA subunits gate entry into the 20S proteolytic CP, preventing unregulated access of substrates (Unno et al., 2002). Opening of the 20S CP is controlled by binding of the 19S RP (Glickman et al., 1998; Lam et al., 2002; Chen et al., 2008). The β /PSMB subunits are responsible for the proteolytic functions of the 20S proteasome; β_1 /PSMB1, β_2 /PSMB2 and β_5 /PSMB5 exhibit chymotrypsin-like, trypsin-like and peptidyl-glutamyl peptide hydrolyzing activities respectively (Groll et al., 1997; Glickman and Ciechanover, 2002). The remaining β /PSMB subunits may form the scaffold structure of the proteasome barrel (Baldovino et al., 2006).

1.2.3 The 19S regulatory particle

The 19S RP is made up of at least eighteen different subunit proteins divided into base and lid arrangements (Glickman et al., 1998; Chen et al., 2008). Figure 1.2 shows the arrangement of the 19S RP. In the base, there are six non-redundant ATPases subunits that join to the 20S CP as well as three non-ATPase subunits (Glickman et al., 1998; Chen et al., 2008; Hendil et al., 2009; Kaneko et al., 2009). The lid is composed of eight non-ATPase subunits. Rpn10/S5a/PSMD4 is assumed to sit at the interface of the base and lid, interacting with Rpn2/S1/PSMD1 (base) and Rpn11/S13/PSMD14 (lid) subunits (Hendil et al., 2009; Kaneko et al., 2009). The RP has several roles as part of the 26S proteasome, including substrate recognition, deubiquitination, unfolding and translocation into the 20S CP. The subunits of the RP have specific roles. In the base, Rpt2/S4/PSMC1 controls substrate entry into the 20S CP by opening the pore gated by the 20S α /PSMA subunits (Köhler et al., 2001; Gillette et al., 2008). The Rpt5/S6a/PSMC3 subunit can recognize and bind polyubiquitinated proteins (Lam et al., 2002; Gillette et al., 2008). Rpn1/S2/PSMD2 and Rpn2/S1/PSMD1 direct substrate recruitment and translocation into the proteolytic chamber of CP (Rosenzweig et al., 2008). In the lid complex, Rpn11/S13/PSMD14 has deubiquitination (DUB) activity that facilitates degradation of ubiquitinated proteins (Koulich et al., 2008). Rpn13/ADRM1 is a ubiquitin receptor (Husnjak et al., 2008).

1.2.4 Proteasome assembly

The 20S proteasome behaves as a platform onto which the 19S RP can bind, forming the active 26S proteasome (Hendil et al., 2009). The biogenesis of the 20S CP is initiated by the formation of a pre-20S subcomplex; the α_1 /PSMA1 - α_7 /PSMA7 ring is formed by the action of proteasome-specific chaperones (Hirano et al., 2005; Hirano et al., 2006). This is followed by stepwise incorporation of the β /PSMB subunits, forming a half-proteasome (one α_1 /PSMA1 - α_7 /PSMA7 ring bound to one β_1 /PSMB1 - β_7 /PSMB7 ring). Two half-proteasomes combine to form a mature 20S CP (Hirano et al., 2006; Fricke et al., 2007; Le Tallec B, 2007; Hirano et al., 2008).

The base and lid of the 19S RP are assembled independently. For the base, assembly is initiated by association of Rpt3/S6b/PSMC4, Rpt6/S8/PSMC5 and Rpn1/S7/PSMC2, Rpt2/S4/PSMC1, Rpn1/S2/PSMD2 subcomplexes, followed by

incorporation of Rpt4/S10b/PSMC6, Rpt5/S6a/PSMC3 and Rpn2/S1/PSMD1 (Kaneko et al., 2009; Murata et al., 2009).

There are also two lid subcomplexes; Rpn6/S9/PSMD11, Rpn8/S12/PSMD7, Rpn9/S11/PSMD13, Rpn11/S13/PSMD14 and Rpn3/S3/PSMD3, Rpn7/S10a/PSMD6, Rpn12/S14/PSMD8, Rpn7/S10a/PSMD6 which combine together and ultimately with the base through the Rpn10/S5a/PSMD4 subunit (Murata et al., 2009).

The assembly of the 26S proteasome is achieved through specific interaction between 20S CP and 19S RP subunits: Rpt6/S8/PSMC5 is known to interact with α_2 /PSMA2, Rpt2/S4/PSMC1 binds to α_7 /PSMA7, Rpt5/S6a PSMC3 can bind to α_4 /PSMA4 and Rpn2/S1/PSMD1 joins to the α /PSMA ring of the 20S CP (Sato et al., 2001; Gillette et al., 2008; Rosenzweig et al., 2008).

Figure 1.1

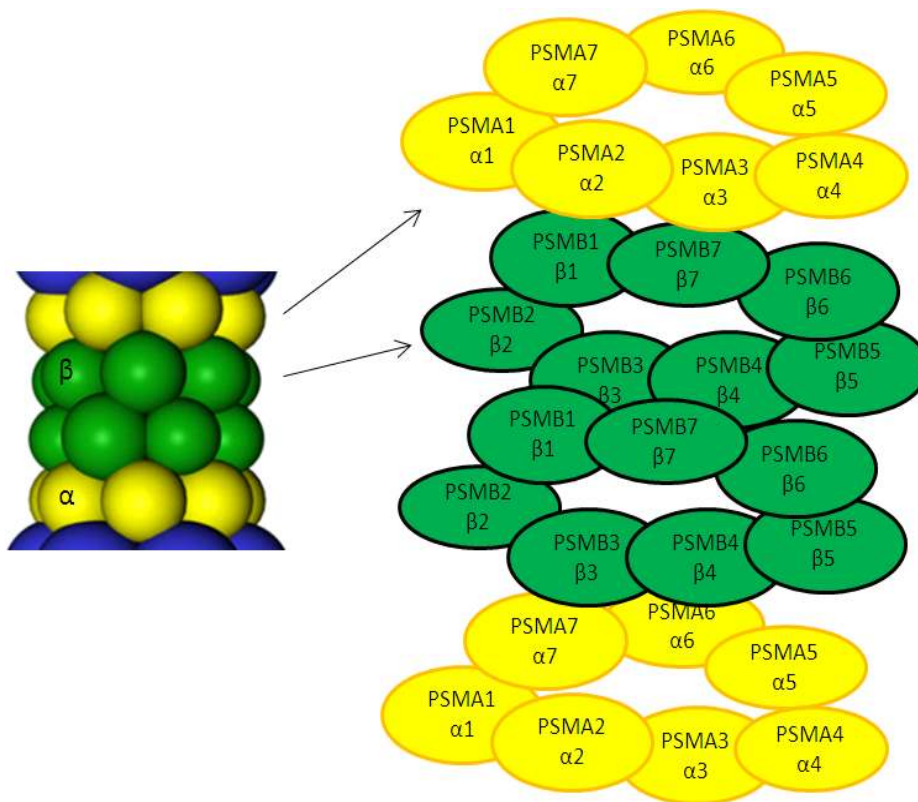


Figure 1.1 Schematic representation of the 20S core particle. The α /PSMA subunits form the outer rings of 20S CP; and β /PSMB subunits form two inner rings. *Abbreviations:* PSMA, PSMB: proteasomal subunits of mammalian subunits A or B.

Figure 1.2

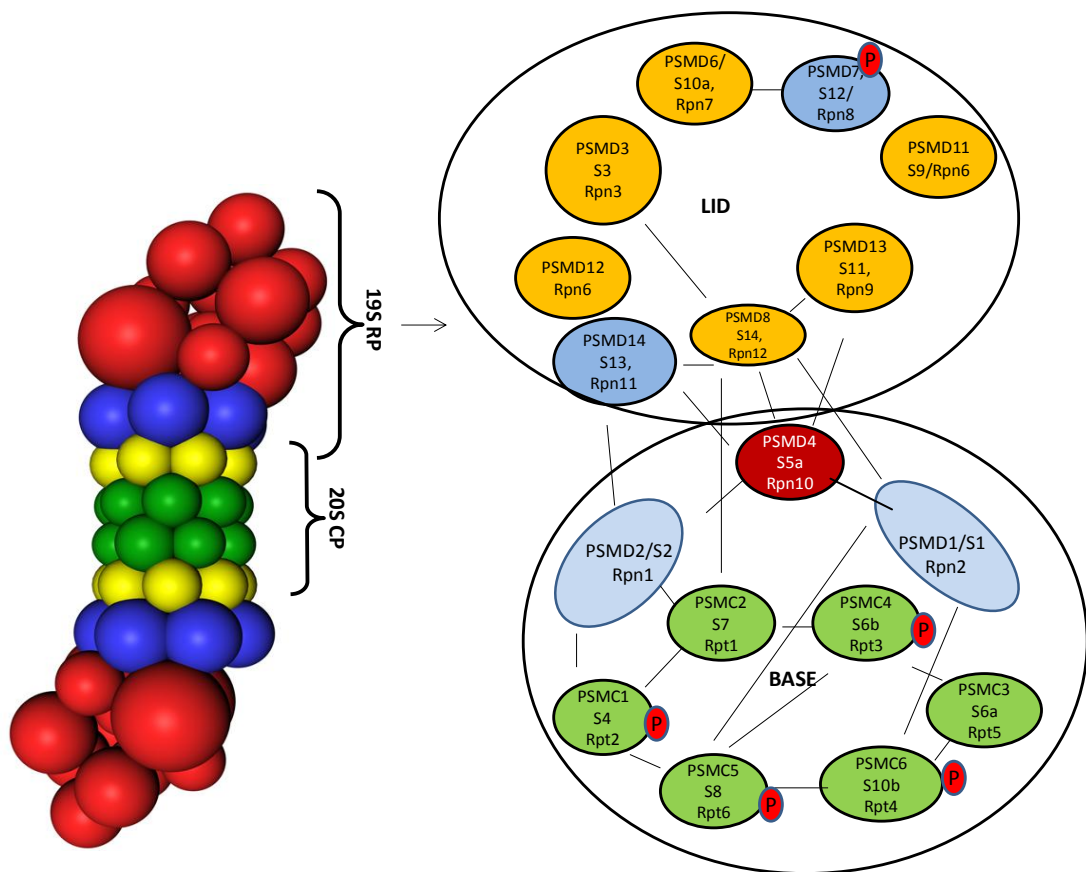


Figure 1.2 Schematic representation of the 19S regulatory particle. Deletion of the base subunit ATPase PSMC1 causes failure in the formation of 26S proteasome, which is the basis for creation of *Psmc1^{fl/fl};CaMKII α -Cre* mouse model of neurodegeneration. *Abbreviations:* PSMC, PSMD: proteasomal subunits of mammalian subunits C or D; S: proteasome subunits for *Saccharomyces cerevisiae*; Rpn: non ATPase regulatory particles; Rpt: ATPase regulatory particles.

1.2.5 Ubiquitin

Ubiquitin is a 76 amino acid protein with a molecular weight of 8.5 kDa. Ubiquitin is expressed in all eukaryotic cells by four genes; Rps27A and Uba52 both produce a single copy of ubiquitin fused with ribosomal protein (S27a and L40 respectively), while Ubb and Ubc are polyubiquitin encoding genes. The products of these genes are ubiquitin precursors, which are deubiquitinated to release ubiquitin monomers (Wiborg et al., 1985; Baker and Board, 1987a, b; Redman and Rechsteiner, 1989).

Post-translational modification by ubiquitin involves different topologies; a single ubiquitin molecule (mono-ubiquitinated), several mono-ubiquitins (multiple mono-ubiquitination) or polyubiquitination via the diverse lysine residues in ubiquitin. Ubiquitin has seven lysine residues; lys6, lys11, lys27, lys29, lys33, lys48, and lys63 as well as N-terminal tail that are involved in ubiquitination allowing the formation of diverse polyubiquitin chains (Weissman, 2001; Passmore and Barford, 2004). Ubiquitin modifications are decoded by ubiquitin receptors or ubiquitin binding domains (UBD) that interact non-covalently with the ubiquitin signals. Taken together, the combination of ubiquitin modifications and UBDs leads to a wide range of signals that have been shown to be involved in a variety of intracellular biological processes, such as DNA repair, endocytosis, autophagy, inflammation and proteasomal degradation (Husnjak and Dikic, 2012).

1.2.6 Ubiquitination

The post-translational modification of a protein substrate, with ubiquitin is called ubiquitination. It is thought that proteins targeted for 26S proteasomal degradation are tagged with at least four ubiquitins in a polyubiquitin chain linked through lysine 48 (Chau et al., 1989). However, recently it was shown that all the ubiquitin linkage-types with the exception of lysine 63 may facilitate proteasomal degradation (Xu et al., 2009).

Ubiquitination is a multistep process (Figure 1.3). An ubiquitin-activating enzyme (E1) activates and binds to ubiquitin through the formation of a thiol-ester bond with the C-terminal glycine (Gly76) residue of ubiquitin molecule in an ATP-dependent step. The activated ubiquitin is transferred to a cysteine group of a second enzyme; an ubiquitin-conjugating enzyme (E2). The ubiquitin molecule is then transferred to the substrate by the action of an ubiquitin ligase enzyme (E3). This sequence of events

leads to the formation of an isopeptide bond between a lysine residue of the substrate protein and the C-terminal glycine of ubiquitin. This may be followed by the sequential addition of ubiquitin to a lysine residue in the substrate bound ubiquitin, forming a lysine-specific polyubiquitin chains (Ciechanover, 1994; Pickart, 2001; Glickman and Ciechanover, 2002; Johnston and Madura, 2004). Subunits of the 26S proteasome recognize lysine 48-tagged unwanted proteins as a signal for degradation. These are bound, deubiquitinated, unfolded and translocated into the 20S CP for degradation into short peptides; ubiquitin molecules are recycled for further signalling (Liu and Jacobson, 2012).

1.2.6.1 The ubiquitin activation enzyme (E1): It is the product of a single gene that facilitates the activation of ubiquitin by an ATP-dependent process. It has a reactive cysteine residue that can bind to the ubiquitin molecule through a thiol-ester bond. The E1 enzyme carries activated ubiquitin to the E2 ubiquitin conjugating enzyme (Pickart, 2001; Johnston and Madura, 2004).

1.2.6.2 The ubiquitin conjugating enzyme (E2): It is a family of proteins designated Ubc for *S.cerevisiae* or UBCH for human. The E2 has a reactive cysteine residue that can form a thiol-ester bond with the ubiquitin molecule transferred from E1 in another ATP dependent step (Jentsch et al., 1990). The E2 can also interact with the E3 ubiquitin ligase (see section 1.2.6.3) to enhance ubiquitin-substrate binding (Johnston and Madura, 2004). Several E2 isozymes have been identified that may have specific functions. For example, Ubc1 can mediate lysine 48-linked polyubiquitin chains of unwanted substrates for 26S proteasome degradation (Rodrigo-Brenni and Morgan, 2007), while Ubc13 mediates lysine 63-linked polyubiquitin chains involved in cell signalling (Hofmann and Pickart, 1999; Deng et al., 2000).

1.2.6.3 The ubiquitin ligase enzyme (E3): There are two families; one containing proteins with a HECT (homologous to E6-AP C-terminus) domain and the other with a RING (Really Interesting New Gene) finger domain. Both domains, in association with other proteins found in the E3 complex, can bind to the E2 and facilitate substrate recognition and ubiquitination.

Figure 1.3

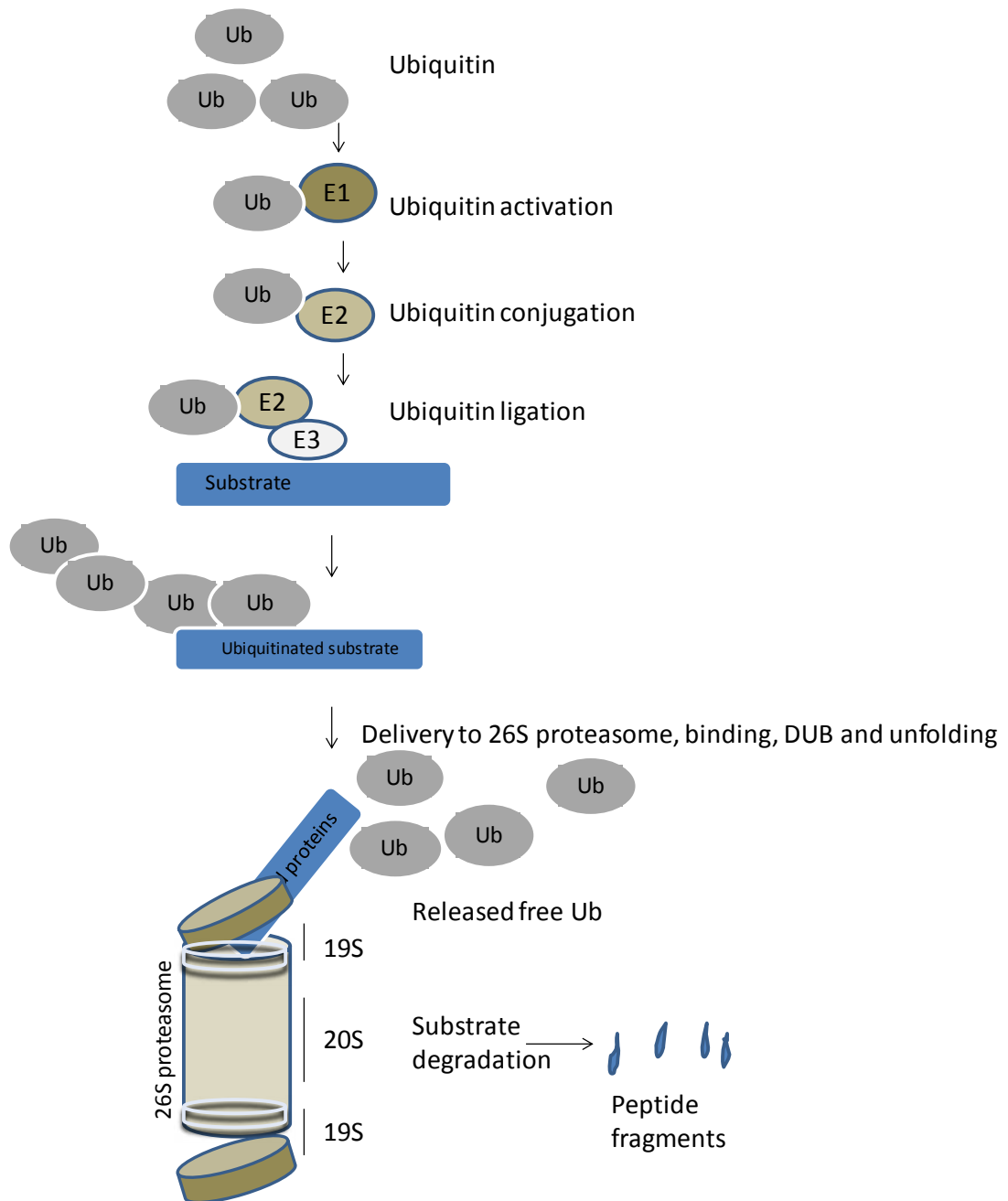


Figure 1.3 Protein ubiquitination and degradation by the ubiquitin 26S proteasome system

1.2.7 Unanchored polyubiquitin chains

Unanchored polyubiquitin chains ('free') are not attached to a substrate protein. In early studies, these chains were chemically synthesized; the chain length was between two to eight ubiquitin molecules (Piotrowski et al., 1997). However, the detection of Ubp14 in yeast supported the presence of unanchored ubiquitin chains. Ubp14 disassembles unanchored polyubiquitin chains *in vitro* (Amerik et al., 1997). In human cells, knockdown of isopeptidase T (Iso-T), a specific deubiquitinase for unanchored polyubiquitin chains, causes increased levels of free polyubiquitin chains that may compete with polyubiquitinated protein substrates for proteasome binding (Dayal et al., 2009). Few studies have investigated the physiological function of unanchored polyubiquitin chains, but a recent study suggested lysine 63-linked free chains may be involved in activating kinases *in vitro* (Xia et al., 2009) and in innate immunity (Zeng et al., 2010).

1.2.8 Ubiquitin specific peptidases (deubiquitinating enzymes)

Deubiquitinating enzymes (DUBs) are a large family of proteases that are specific for ubiquitin. They are also known as ubiquitin hydrolases. They are categorized into two main families; ubiquitin carboxy-terminal hydrolases (UCH) and ubiquitin-specific proteases (USP) (Reyes-Turcu et al., 2009). DUBs release ubiquitin from its fusion proteins or polyubiquitin chains during proteasomal degradation. This provides an essential pool of mono-ubiquitin for signalling. Moreover, DUBs can reverse the ubiquitination of target substrate proteins and generate mono-ubiquitin from unanchored polyubiquitin chains (Dayal et al., 2009). DUBs are important enzymes in intracellular ubiquitin homeostasis.

1.2.9 Ubiquitin binding proteins

Ubiquitin binding proteins (UBP) are a family of proteins that bind non-covalently to ubiquitin and ubiquitinated proteins via their ubiquitin binding domains (UBD), which depends on the ubiquitin chain length and linkage-type. UBDs bind to ubiquitin mainly through isoleucine-44, aspartate-58 and C-terminal (Gly-Gly) residues (Husnjak and Dikic, 2012). UBPs have different structures and functions. For example, the zinc finger UBD is present in DUB enzymes such as isopeptidase T (Iso-T or USP5), which has ability to bind and deubiquitinate unanchored polyubiquitin chains (Reyes-Turcu et al., 2009). The UBD of ubiquitin conjugating enzymes (E2)

has an essential role in the processes of protein substrate ubiquitination as described in section 1.2.6.2. The radiation sensitivity abnormal 23 protein (Rad23) contains two UBDs and may shuttle ubiquitinated proteins for proteasomal degradation (Kang et al., 2006). UBPs have also been identified in endocytosis and NF- κ B signalling (Dikic et al., 2009). Importantly, some of these proteins are now used in bio-affinity chromatography techniques to pull-down ubiquitinated proteins from crude tissue homogenates for the purpose of their subsequent identification. Examples of these proteins are proteasomal subunit Rpn10/S5a/PSMD4 (Layfield et al., 2001) and zinc finger proteins-ZNF216 (Strachan et al., 2012). The identification of ubiquitinated protein substrates would significantly contribute to our understanding of the UPS and its functions *in vivo*.

1.3 Protein homeostasis and neurodegenerative diseases

Protein homeostasis involves protein synthesis as well as degradation and is essential for survival (Balch et al., 2008; Douglas and Dillin, 2010). The pathological hallmarks of neurodegenerative diseases are selective progressive neuronal loss and the formation of protein inclusions in surviving neurones. Changes in protein homeostasis have been implicated in a number of neurodegenerative diseases characterized by the accumulation of proteins in inclusions, e.g. Lewy bodies (LB).

1.3.1 Lewy body diseases

LB are the hallmark of a spectrum of neurodegenerative diseases known as the synucleinopathies because the major component of LB is the pre-synaptic protein α -synuclein (Spillantini et al., 1998). Parkinson's disease (PD) and dementia with Lewy bodies (DLB) are examples of LB diseases, but these abnormal protein inclusions are a common feature of Alzheimer's disease (AD). The symptoms of the disease depend on the anatomical region of the brain affected by the formation of LB and neurodegeneration, e.g. brain stem and forebrain in PD and DLB patients respectively (Nussbaum and Polymeropoulos, 1997; Thomas, 2006). Therefore, although they are defined neurodegenerative diseases, they share common neuropathological features and may involve similar molecular mechanisms of disease cause and/or progression.

1.3.2 The Lewy body

Histological studies reveal the formation of eosinophilic cytoplasmic inclusions in surviving neurones in neurodegenerative diseases; LB (Dunnett and Björklund, 1999; Mattila et al., 2000). There are two morphological types of LB. The classical LB has a dense core surrounded by a halo and is found in brain stem regions associated with PD. The cortical LB is less defined and without a halo; found in cortical regions associated with Parkinson's disease with dementia (PDD) and DLB (Sakamoto et al., 2002). There is also the Pale body (PB), which is considered a LB precursor (Hayashida et al., 1993).

Compartmentalization of aggregated proteins may prevent potentially toxic proteins affecting normal neuronal function. It is also possible that the protein inclusions cause cellular damage. However, the role of protein inclusions in promoting neurodegeneration or neuroprotection is the subject of debate. Several studies have suggested LB formation is integral to the progression of neurodegeneration, showing reduced protein aggregation is neuroprotective (Trojanowski et al., 1998 ; Zhang et al., 2005 ; Pan et al., 2008; Gavilan et al., 2009). Interestingly, LB are absent in some cases of familial PD and are present in the aging asymptomatic population (Harrower et al., 2005). The mechanisms involved in protein inclusion formation remain elusive, including the role of ubiquitin.

1.3.3 Parkinson's disease

PD was first described by the English physician, James Parkinson, as a shaking palsy (Parkinson, 2002). The disease is the most common movement disorder resulting primarily from an impairment of the basal ganglia that regulate voluntary movement (Jankovic, 2008). This is caused by loss of dopaminergic neurones in the substantia nigra pars compacta that project to the basal ganglia (putamen and caudate nuclei) leading to a decrease in dopamine signalling and alterations in the activity of the neuronal circuits within the basal ganglia (Bartels and Leenders, 2009). The motor dysfunction often co-presents with other non-motor symptoms, including autonomic dysfunction and a behavioural phenotype. In the later stages of disease dementia is also common, which may be associated with prevalent LB in the neocortex as in PDD (Stein, 1990; Braak et al., 2003; Jankovic, 2008).

The symptoms of PD can be treated by various drugs, which aim to increase dopaminergic activity in the brain, such as the dopamine precursor levodopa (L-DOPA /carbidopa) and dopamine agonists. In the early stages of L-DOPA/carbidopa treatment, symptoms are reduced and patients well-treated. However, with long-term therapy tolerance develops leading to motor fluctuation with dyskinesia (Sujith and Lane, 2009). Dopamine agonists include lisuride, pergolide, pramipexole ropinirole and rotigotine are used to treat the motor symptoms of PD (Müller, 2012). These also are associated with side effects and some have been withdrawn from use. Monoamine oxidase inhibitors, such as rasagiline and selegiline, which act to decrease dopamine metabolism are also used as mono-therapy in early PD and provide mild symptomatic benefits (Lang and Lees, 2002; Schapira, 2005). Catechol-o-methyltransferase inhibitors tolcapone and entacapone have been used in adjunctive therapy with L-DOPA/carbidopa to inhibit dopamine degradation and decrease tolerance effects due to continuous dopamine therapy. However, their use has been restricted to specific cases (Bonifacio et al., 2007). There are several non-pharmacological treatments for PD, including stem cell therapy, but this is still far from clinical testing and has only shown limited effectiveness in animal models of PD (Glavaski-Joksimovic and Bohn, 2013). Neurosurgical intervention by deep brain stimulation (DBS) has shown increased interest due to the adverse effects of drug treatment. DBS of the subthalamic nucleus (STN) and the globus pallidus internus (GPi) has been documented to improve the L-DOPA response in PD. There are specific criteria for this type of treatment, including the presence of disability and absence of cognitive dysfunction which limits its therapeutic use (deSouza et al., 2013). This summarizes several of the treatment options for PD, which only provide symptomatic relief, and highlights the need to develop treatments to prevent and slow progression of this disease.

1.3.4 Dementia with Lewy bodies

Dementia is a condition of progressive loss of cognitive ability. The main symptoms of dementia are loss of memory, confusion, difficulty with speech and understanding, changes in personality and behavior often with visual hallucinations and parkinsonism (Galasko, 2001). There are many different types of dementia. AD is the most common dementia and neurodegenerative disease. DLB is the second most common cause of cognitive impairment in the elderly after AD (Zaccai et al., 2005). DLB may occur in

a 'pure' form, but it is increasingly recognized that this occurs in conjunction with PD in the condition of PDD (Horimoto et al., 2003).

The pharmacological treatment of DLB is mainly aimed at reducing disease symptoms. Dysfunction of cholinergic activity in the forebrain is thought to be the predominant patho-physiological mechanism in the development of DLB and PDD and the nucleus of Meynert is frequently affected by LB (Whitehouse et al., 1983). However, widespread distribution of LB has been described, including the cerebral cortex, midbrain, brainstem nuclei, basal forebrain nuclei and limbic cortical region (Braak et al., 2003; Neef and Walling, 2006). Since the disease presents with low levels of acetylcholine in the brain, treatment includes the use of acetylcholinesterase inhibitors (Gomez-Tortosa et al., 1998). Rivastigmine, donepezil and galanthamine have been used for treatment of dementia (O'Brien and Burns, 2011; Osona-Nunez et al., 2011). Although these drugs may improve cognitive function in PDD, they can worsen the symptoms of parkinsonism (Almaraz et al., 2009). Importantly, similar to other neurodegenerative diseases, current treatments do not delay dementia progression (Masoodi, 2013).

1.3.5 Dysfunction of the UPS and neurodegenerative disease

Interestingly, ubiquitinated and UPS proteins are a consistent feature of the inclusion bodies present in surviving neurones of the major neurodegenerative diseases, including PD, AD and DLB (Mayer et al., 1989). This observation suggests impairment of the UPS is involved in disease cause and/or progression. Several studies have been reported to support this hypothesis. The proteolytic activity of the 20S proteasome was shown to be impaired in patients with sporadic PD (McNaught et al., 2003). The use of pharmacological inhibitors of the 20S proteasome has been controversial. However, an important study using conditional genetic depletion of 26S proteasomes in mouse brain neurones showed 26S proteasomal dysfunction caused neurodegeneration and the formation of inclusions resembling human pale bodies (Bedford et al., 2008). Neurodegenerative diseases are age-related and accumulation of ubiquitinated proteins was detected in aged drosophila, associated with a decline in the assembly of 19S RP and 20S CP (Tonoki et al., 2009). These studies suggest that removal of unwanted proteins is important to maintain cellular proteostasis and survival.

The presence of ubiquitinated α -synuclein in LB inclusions implicates dysfunction of their degradation. The UPS is the major pathway for the degradation of α -synuclein under normal conditions (Bennett et al., 1999) suggesting dysfunction of this system may lead to the accumulation of α -synuclein in inclusions. Mutations in α -synuclein have been described in PD and DLB (Zarranz et al., 2004). Further support for the involvement of the UPS in neurodegenerative disease progression includes mutations in the genes encoding DUB ubiquitin carboxyl-terminal esterase L1 (UCHL1) and E3 ubiquitin ligase Parkin associated with familial cases of PD (Leroy et al., 1998). Reduced levels of UCHL1 have been described in patients with DLB (Barrachina et al., 2006). Taken together, these studies suggested that the role of the UPS in disease cause and/or progression needs to be further investigated and will form part of this aims of this thesis.

1.4 Oxidative stress and neurodegeneration

Oxidative stress is one of the key hypotheses implicated in the pathogenesis of several neurodegenerative diseases. A relationship between proteasomal dysfunction and oxidative stress has been described that may be relevant to human disease.

The superoxide anion (O_2^-), hydrogen peroxide (H_2O_2) and hydroxyl radical ($HO\bullet$) are collectively known as reactive oxygen species (ROS). They are mainly generated from the mitochondria during the process of oxidative phosphorylation (OXPHOS). Superoxide radicals formed during this process are converted to hydrogen peroxide. Hydrogen peroxide can be further converted to water and oxygen by peroxidases or partially reduced to form further harmful molecules such as the hydroxyl radical (Murphy, 2009). Another source of ROS in the cell is the enzyme nicotinamide adenine dinucleotide phosphate (NADPH) oxidase, which generates the superoxide radical as part of the electron transfer from NADPH to oxygen. Studies have suggested that this enzyme is the major source of ROS in the brain and that NADPH oxidase enzyme activity is increased in neurodegenerative disease (Shimohama et al., 2000). Another form of reactive species is reactive nitrogen species (RNS) such as nitric oxide (NO) and peroxynitrite ($ONOO^-$). Nitric oxide may be generated during normal cellular metabolic processes; in neurones it is generated from L-arginine by the enzyme neuronal nitric oxide synthase for normal signalling in learning and memory (Jacoby et al., 2001; Sadeghian et al., 2011). Therefore, reactive species are continuously produced during normal cellular activities and must be tightly controlled to protect the cell from oxidative stress.

Reactive species are tightly controlled by specific antioxidant enzymes, e.g. catalase, superoxide dismutase, glutathione peroxidase and other peroxidase, as well as antioxidant compounds such as reduced glutathione (GSH), vitamin C and E. Failure of the cellular antioxidant protection or increased levels of reactive species will lead to oxidative and/or nitrative stress, which oxidizes critical cellular constituents (Pryor and Stanley, 1975; Shacter, 2000).

Oxidative stress has been implicated in the brains of patients with PD and DLB associated with changes in protein homeostasis such as α -synuclein aggregation (Castellani et al., 1996; Giasson et al., 2000; Yan et al., 2012). Mitochondrial

dysfunction is a key hypothesis in neurodegenerative disease pathogenesis and a source of ROS (Onyango, 2008; Shadrina and Slominskii, 2008; Moran et al., 2012). Exogenous exposure of cells to herbicides compound such as Paraquat that can produce reactive species has been reported to cause neurodegeneration (Miller, 2007; Sun et al., 2010). Failure of antioxidant enzymes can also cause neurodegeneration. Superoxide dismutase detoxifies superoxide radicals to hydrogen peroxide, which is a less reactive species. Mutations in superoxide dismutase cause a fatal neurodegenerative disorder called familial amyotrophic lateral sclerosis (FALS) (Deng et al., 1993). A mouse model of AD has been created by deletion of superoxide dismutase; this mouse showed increased oxidative stress with accumulation and oligomerization of β -amyloid protein and cognitive impairment (Murakami et al., 2011).

Peroxiredoxins are a group of enzymes with peroxidase activity that facilitate the reduction of hydrogen peroxide, lipid peroxides and peroxynitrite (Wood et al., 2003). A transgenic mouse overexpressing peroxiredoxin-2 was shown to tolerate neuronal injury caused by ischemia (Gan et al., 2012), a condition usually followed by increased production of ROS as result of increased utilization of oxygen for compensation.

1.4.1 Lipid peroxidation

Membrane phospholipids are the most vulnerable cellular component to oxidation. Lipid peroxidation is a well-known mechanism of cellular damage. Polyunsaturated fatty acids can be oxidized by ROS/RNS. Figure 1.4 shows the lipid peroxidation cascade. The reactive species extracts a hydrogen atom from their structural backbone, leaving behind a carbon radical. This has the ability to combine with oxygen to make a peroxy radical. The peroxy radical, in turn, can start a cascade of hydrogen abstraction from neighboring backbones, splitting the carbon backbone to form unstable lipid hydroperoxides that are ultimately converted to stable end products such as malondialdehyde (MDA) and / or 4-Hydroxynonenal (HNE) (Byun et al., 1999; Rodenas et al., 2000). MDA levels have been used extensively as an indicator of oxidative stress in the biological milieu. Lipid peroxidation may lead to inhibition of membrane function, destroying its barrier properties (Stadelmann-Inggrand et al., 2004).

Figure 1.4

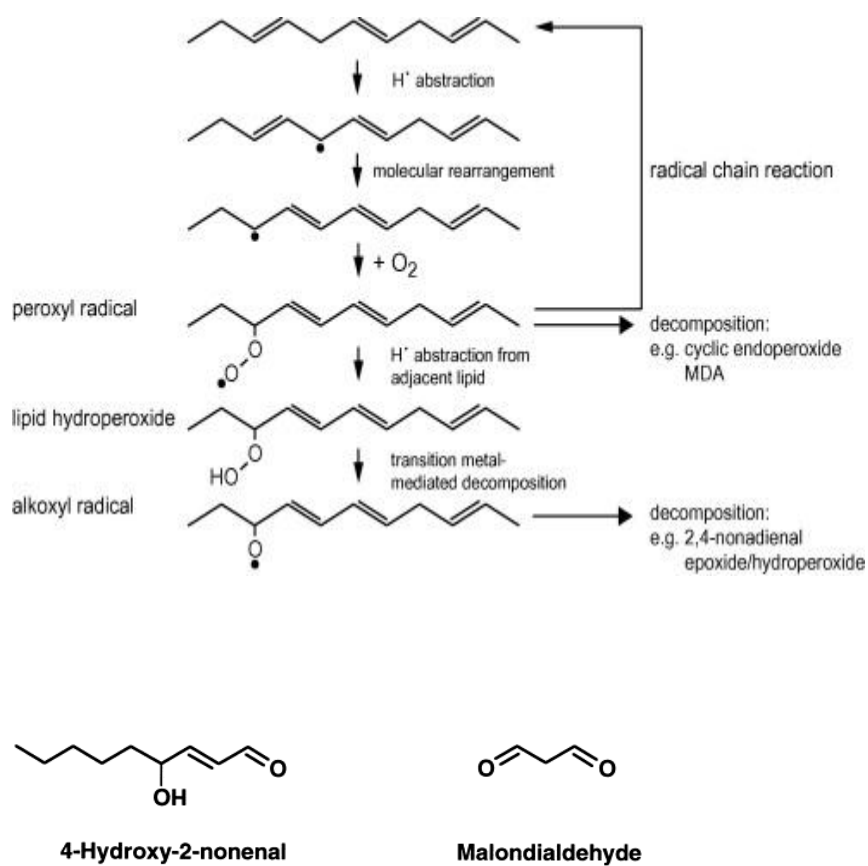


Figure 1.4 Lipid peroxidation cascade. Lipid peroxidation is initiated by hydrogen (H) abstraction, propagation and decomposition to carbonyl products such as aldehydes, e.g. malondialdehyde (MDA) and 4-Hydroxynonenal (HNE). Diagram taken from (Conrad et al., 2013).

1.4.2 Protein oxidation

Proteins are also a target of ROS/RNS and their oxidation leads to covalent modification of proteins to form reactive aldehydes or ketones. Several amino acid acyl side chains can be oxidized into carbonyls, e.g. lysine, arginine, proline and threonine, whereas others such as Tyrosine undergo to nitration by peroxynitrite (Shacter, 2000). Oxidative damage to proteins causes loss of function and hydrophobicity. This could potentially lead to increased aggregation, which has been shown in AD brain tissue together with the accumulation of ubiquitinated proteins (Dasuri et al., 2010). Protein nitration may also facilitate protein aggregation associated with neurodegenerative disease; nitrated α -synuclein has been reported to aggregate (Giasson et al., 2000). The proteasome is vulnerable to oxidative modification and proteasomal proteins are targets of ROS/RNS, which causes inhibition of proteasomal activity (Glockzin et al., 1999; Osna et al., 2004). In particular, the Rpt5/S6a/PSMC3 ATPase subunit of 26S proteasome has been shown to undergo oxidation modification (Ishii et al., 2005). Further components of the UPS may be oxidatively modified; this has been shown for UCHL1, which was associated with increased aggregation of proteins in AD and PD (Choi et al., 2004). Proteasomal dysfunction and oxidative stress are implicated in the pathogenesis of several neurodegenerative diseases, but their relationship with each other requires further investigation.

1.5 Reactivation of astrocytes in neurodegenerative diseases

Astrocytes are ubiquitously expressed star-shaped glial cells present in most regions of the central nervous system. They have extensive finely branched processes that make physical contact with the neuron's dendrites and synapses (Halassa et al., 2007). Astrocytes also contact cerebral blood vessels and control cerebral blood flow (Parri and Crunelli, 2003) through the release of nitric oxide, arachidonic acid and prostaglandins (Haydon and Carmignoto, 2006; Iadecola and Nedergaard, 2007). The astrocytes therefore connect neuronal cells, providing structural integrity and control brain blood supply. Increased reactivity and number of astrocytes has been documented in several neurodegeneration diseases (Pekny and Nilsson, 2005; Sofroniew and Vinters, 2010; Yata K, 2011). The 26S proteasome-depleted mouse model showed evidence of extensive astrocytic gliosis in the affected brain regions (Figure 1.5) (Bedford et al., 2008). Therefore, we will briefly review the role of astrocytes in physiology and pathology.

1.5.1 The role of astrocytes

In normal physiology, astrocytes can release the amino acid neurotransmitter glutamate to provoke signals in adjacent neurones and also express the glutamate transporter to remove glutamate from the synaptic space (Parpura and Haydon, 2000; Santello and Volterra, 2009). Therefore, astrocytes promote a role in synaptic transmission by regulating the extracellular levels of glutamate, providing protection from glutamate's excitotoxicity. Astrocytes have also been reported to take up increased extracellular potassium ions following neuronal activity via a potassium channel to maintain resting membrane potential (Walz, 2000). Metabolically, astrocytes can store glycogen and supply energy substrates to the neurones. They can perform glycolysis and release lactate into the extracellular space, which can be taken up by neurones (Choi et al., 2012). Astrocytes can provide neurones with protective antioxidants such as GSH (Sagara et al., 1996). In general, astrocytes are recognized to play an important role in the normal function of the central nervous tissue.

1.5.2 Reactive astrogliosis

Astrocytes respond to neurodegeneration by a process referred to as reactive astrogliosis. This involves changes in their morphology, function and number. These changes have been considered as one of pathological features of neurodegenerative brain pathology. In general, astrocytes reactivation is characterized by extensive proliferation and the formation of glial scar (Sofroniew, 2009). The intracellular changes include increased expression of glial fibrillary acidic protein (GFAP) with hypertrophy of the astrocytic cell body and processes. In severe reactivation these processes overlap forming a barrier around the dying neurones. This barrier may be neuroprotective against inflammatory cell migration, but may also prevent the local re-growth of nerve fibres (Bush et al., 1999).

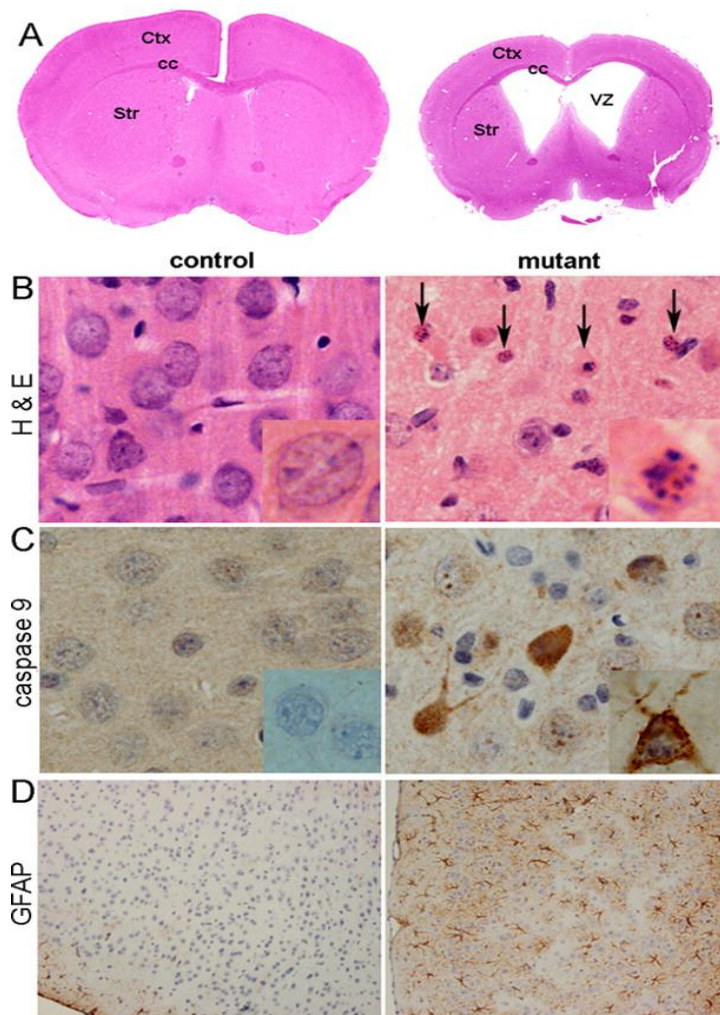
There are many intra- and inter-cellular signalling molecules involved in reactive astrogliosis. These include polypeptide growth factors such as tumor necrosis factor- α (TNF- α), interferon- γ (INF γ), cytokines such as interleukin 6 (IL-6), neurotransmitters such as glutamate, purines and reactive species such as nitric oxide as well as proteins associated with neurodegeneration such as β -amyloid (Hamby et al., 2008; Sofroniew, 2009). The antioxidant transcription factor, nuclear factor erythroid 2-related factor 2 (Nrf2), that controls the expression of antioxidant proteins has been reported to be activated in astrocytes and provided protection against neurotoxin, 1-methyl-4-phenyl-1, 2, 3, 6-tetrahydropyridine (MPTP)-induced toxicity in mice modeling PD (Chen et al., 2009).

1.6 26S proteasomal depletion mouse model; *Psmc1*^{fl/fl}; *CaMKII α -Cre*

To increase understanding of the contribution of the UPS to neurodegenerative disease, a conditional genetic mouse model causing specifically 26S proteasomal depletion in neurones was created. Using Cre recombinase/loxP conditional gene targeting, inactivation of an essential subunit of the 19 RP, ATPase *Psmc1* (see section 1.2.4), lead to depletion of 26S proteasomes in forebrain neurones (Bedford et al., 2008). The floxed *Psmc1* gene was inactivated by calcium calmodulin-dependent protein kinase II α promoter-driven Cre recombinase. This strategy did not affect the formation and activity of the ubiquitin-independent 20S proteasome.

Neuropathological studies of the mouse cortical brain tissue showed that 26S proteasomal depletion caused the formation of intraneuronal Lewy-like inclusions and neurodegeneration. Figure 1.5 shown extensive cortical neurodegeneration in 26S proteasome-depleted mouse cortex. The intraneuronal lewy-like protein inclusions were similar to human PB, containing ubiquitin, α -synuclein mitochondria (Figure 1.6). The 26S proteasomal depletion mouse model also showed evidence of extensive gliosis in regions of neurodegeneration as indicated by changed morphology of astrocytes and increased number (Figure 1.5). Behavioural studies demonstrated a deficit in learning and memory in the Morris water maze test. The mice also showed growth retardation and premature death before 12 weeks of age. The neuropathological as well as behavioural changes in *Psmc1^{fl/fl};CaMKII α -Cre* mice make it a useful model to study mechanisms of neurodegeneration. This model is unique, leading to accumulation of ubiquitinated proteins and α -synuclein resembling pale bodies of human synucleinopathies and neurodegeneration. Other models of PD include α -synuclein transgenic and parkin knockout mice; genes associated with the familial disease. Although these mice show evidence of behavioural and biochemical changes related to PD, but not to PDD or DLB, importantly, they do not display extensive neurodegeneration as seen in human disease (Periquet et al., 2005). In addition, aggregates of α -synuclein in these models do not resemble paranuclear LB like the *Psmc1^{fl/fl};CaMKII α -Cre* mice.

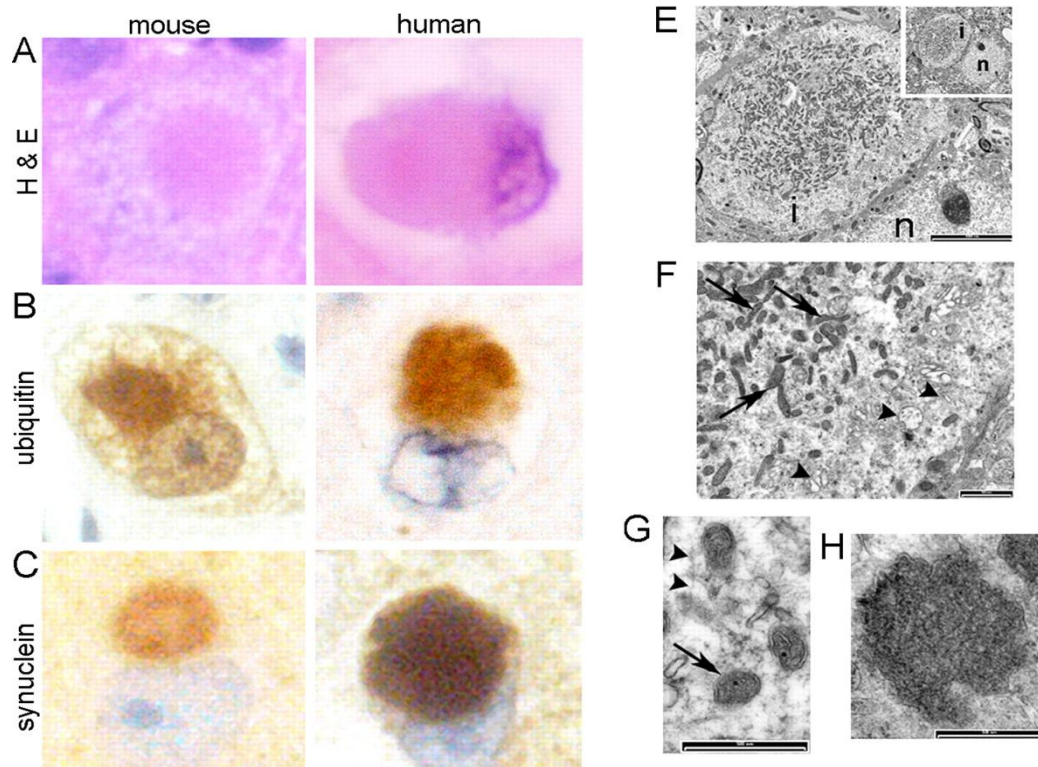
Figure 1.5



Bedford, l et al., 2008, J Neurosci 28, 8189-98

Figure 1.5 Extensive cortical neurodegeneration in *Psmc1^{fl/fl};CaMKII α -Cre* mouse cortex. Histological examination of coronal brain sections from control and *Psmc1^{fl/fl};CaMKII α -Cre* (mutant) mice. *A*, hematoxylin and eosin (H&E)-stained whole brain sections, and *B*, at higher magnification. The arrows indicate pyknotic nuclei in the *Psmc1^{fl/fl};CaMKII α -Cre* cortex. Immunohistochemistry with cleaved caspase 9 (*C*) and glial acidic fibrillary protein (GFAP) (*D*).

Figure 1.6



Bedford, l et al., 2008, J Neurosci 28, 8189-98

Figure 1.6 Lewy-like intraneuronal inclusion pathology in *Psmc1^{fl/fl};CaMKII α -Cre* mouse cortical neurons at 6 weeks of age. A-C, show mouse (left-hand side) and human (right-hand side) inclusions stained with H&E, ubiquitin and α -synuclein respectively. E-G, show ultrastructure of mouse Lewy-like inclusions. E, shows the paranuclear inclusion (n, nucleus; i, inclusion), G and F show mitochondria (arrows), and H, shows autophagosome-like dense bodies.

Aim

Together, the investigations in this thesis aim to identify mechanisms involved in neurodegeneration and inclusion formation that may be translated to human disease. There are limited studies investigating the ubiquitome in mouse brain *in vivo*. One of the aims of this thesis was to identify novel ubiquitinated proteins in mouse brain neurones that further studies would investigate their function. These proteins may be new proteasomal substrates or involved in the formation of LB and associated with neurodegeneration. The *Psmc1^{fl/fl};CaMKII α -Cre* mouse displays extensive accumulation of ubiquitinated protein in the mouse forebrain making it an ideal model for this aim. The use of bioaffinity chromatography with immobilized ubiquitin binding domain (UBD) attached to solid beads (matrices) was chosen to capture polyubiquitinated proteins from tissue homogenate (Strachan et al., 2012). This study used ZNF216 protein which contains an N-terminal ZnF A20 UBD to capture ubiquitinated proteins (Hishiya et al., 2006).

In addition to the ubiquitome study, which is specific for one protein category, we aimed to investigate the global proteome in *Psmc1^{fl/fl};CaMKII α -Cre* mouse cortex. To our knowledge this is novel; there are limited proteomic studies associated with accumulation of ubiquitinated proteins *in vivo*. We chose to use 2-dimensional fluorescence difference in-gel electrophoresis (2-D DIGE) introduced by *Unlu et al.* (1997) (Unlü, 1997). This is a sensitive proteomics technique that can visualize thousands of proteins spots following two-dimensional protein analysis gel electrophoresis (2-D PAGE) and has been used in basic research as well as clinical studies (Jesse et al., 2012; Wang, 2010). Differential protein expression identified in the *Psmc1^{fl/fl};CaMKII α -Cre* compared to control cortices may lead to the identification of novel proteins involved in neurodegeneration that can be translated to human disease, i.e. biomarkers, protective and /or detrimental signalling. We aimed to understand the mechanisms of neurodegeneration associated with 26 proteasome dysfunction in mammalian brain tissue. The proteins identified will be further investigated using biochemical approaches and immunohistochemistry.

CHAPTER 2

Materials and Methods

2.1 Experimental animals

2.1.1 Generation of *Psmc1^{fl/fl};CaMKII α -Cre* Mice

Mice were generated by conditional Cre/loxP gene targeting. A key subunit of the 26S proteasome, ATPase *Psmc1*, was inactivated by crossing floxed *Psmc1* mice (*Psmc1^{fl/fl}*) with mice expressing Cre recombinase from the calcium calmodulin-dependent protein kinase II α promoter (*CaMKII α -Cre*) (Bedford et al., 2008). This leads to the inactivation of *Psmc1* in forebrain neurones (*Psmc1^{fl/fl};CaMKII α -Cre*) at approximately postnatal week two. *Psmc1^{fl/fl};CaMKII α -Wt* and *Psmc1^{fl/wt};CaMKII α -Wt* littermates were used as controls. Mice were housed under constant conditions of 12 /12 h light-dark cycle and 21 ± 2 °C room temperature. Food and water were accessible ad libitum. All experiments were carried out in accordance with the Home Office Animals (Scientific Procedures) Act 1986, under the Home Office project license number 40/3394 and personal license 70/14272.

2.1.2 Extraction of genomic DNA from mouse tissues

2.1.2.1 Reagents

- 1) Tissue lysis buffer: 100 mM Tris-HCL pH 8.5, 5 mM Na-EDTA, 0.2 % SDS and 200 mM NaCl.
- 2) Proteinase K (10 mg /ml).
- 3) Isopropanol.
- 4) 70 % ethanol.

2.1.2.2 Protocol

Mouse tail or ear notches were used for extraction of genomic DNA (gDNA). Samples were placed in a 1.5 ml eppendorf tube and incubated overnight (12-24 hrs) at 55 °C in tissue lysis buffer (700 μ l for tail or 500 μ l for ear notches) containing a final concentration of 0.5 mg /ml proteinase K. The samples were vortexed and then centrifuged at 9300 x *g* for 10 minutes at room temperature. The supernatant was transferred into a new eppendorf tube with an equal volume of isopropanol to precipitate the gDNA. The tubes were shaken vigorously followed by centrifugation at 16100 x *g* for 10 minutes at room temperature. The supernatant was discarded and 500 μ l of 70 % ethanol added to the gDNA pellet and again centrifuged at 16100 x *g*

for 10 minutes at room temperature. The 70 % ethanol was discarded and gDNA pellet air dried at room temperature. 50-150 µl of nuclease-free water was added to the pellet.

2.1.3 Polymerase Chain Reaction (PCR)

2.1.3.1 Reagents

- 1) Primers: 4 µM Cre (sense and antisense), 4 µM Psmc1-LB3 (sense), 4 µM Psmc1-D1360 (sense) and 4 µM Psmc1-X316 (antisense) (sequences are given in appendix I-A).
- 2) 10X PCR buffer containing 20 mM MgCl₂ (Fermentase).
- 3) DNA polymerase 5 U/µl (Fermentase).
- 4) 1 mM deoxynucleotide triphosphates (dNTPs).

2.1.3.2 Protocol

The final reaction volume for each PCR was 10 µl containing final concentrations: 0.5 µl of gDNA template. The PCR was performed in a thermo-cycle PCR (Master cycle-ependorf®) under the condition of 94°C for 3 minutes, and then for 30 cycle of 94°C for 1 minute, 60°C for 30 seconds and 72°C for 30 seconds.

2.1.4 Agarose gel electrophoresis

2.1.4.1 Reagents

- 1) Tris-acetate EDTA buffer (TAE): 40 mM Tris-acetate, 1 mM EDTA pH 8 with HCL.
- 2) 4 % agarose gel solution (4.5 g agarose in 150 ml TAE).
- 3) Ethidium bromide solution (1 % w/v in water).
- 4) 50-1350 bp DNA Ladder

2.1.4.2 Protocol

The 4 % agarose gel solution was melted using a microwave. 7 µl of ethidium bromide was added to the melted agarose once cooled to approximately 55°C. The gel was poured into a gel tray pre-fitted with combs. Once the gel was set, TAE buffer was poured into the gel apparatus to cover the gel. The PCR samples and DNA ladder were loaded. A constant voltage of 150 V was applied for electrophoresis. PCR bands were detected by using a UV trans-illuminator (Figure 2.1).

Figure 2.1

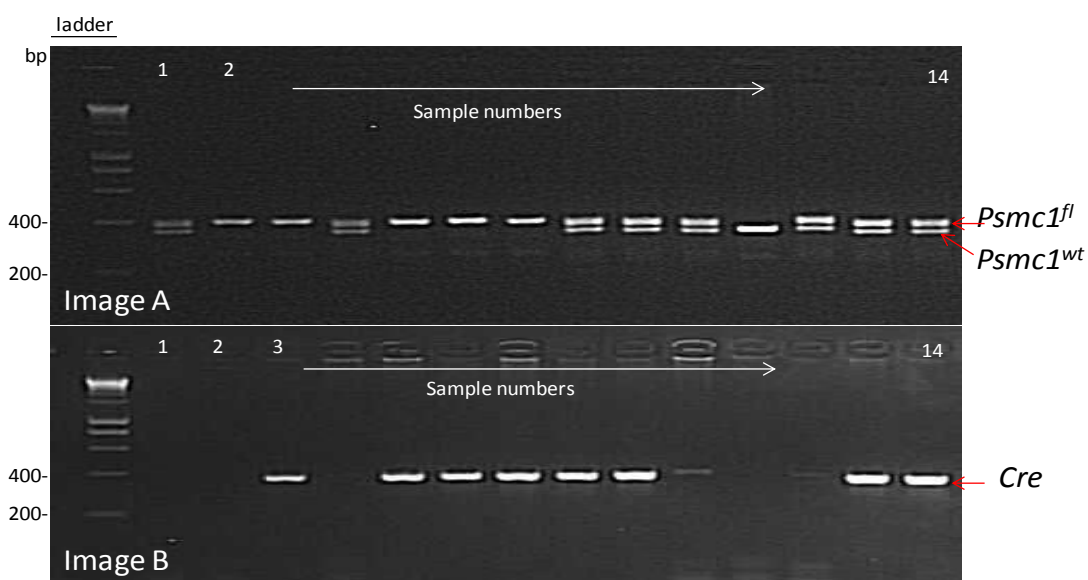


Figure 2.1 Representative image of *Psmc1* and *Cre* genotyping. PCR products for *Psmc1* (image A) and *Cre* (image B) following electrophoresis. Bands were detected using a UV trans-illuminator. *Psmc1^{fl}* 395 bp; *Psmc1^{wt}* 349 bp; *Cre*-recombinase as shown.

Examples of mouse genotypes:

Mouse number 1 is *Psmc1^{fl/wt}*; *CaMKII α -Wt* (control)

Mouse number 2 is *Psmc1^{fl/fl}*; *CaMKII α -Wt* (control)

Mouse number 3 is *Psmc1^{fl/fl}*; *CaMKII α -Cre* (mutant)

Mouse number 14 is *Psmc1^{fl/wt}*; *CaMKII α -Cre* (control)

2.2 Preparation of affinity chromatography matrices and capture of ubiquitinated proteins

2.2.1 Preparation of *E. coli* glycerol stock

2.2.1.1 Reagents

- 1) XL10-Gold® *Escherichia coli*: transformed with pGEX-4T-1 plasmid with GST-ZNF216 wild-type or GST-C30/33A ZNF216 mutant, containing β -Lactam antibiotic selection cassette (kindly provided by Dr Layfield).
- 2) 80 % (v/v) glycerol.
- 3) Luria Broth (LB, 25 g /L).
- 4) 2 ml Cryo tubes.

2.2.1.2 Protocol

1.5 ml of an overnight culture of *E. coli* transformed with either GST-ZNF216 wild-type or GST-C30/33A ZNF216 mutant was spun down at 3300 x g 4°C for 10 minutes and the supernatant discarded. Cell pellets were re-suspended in 425 μ l of LB plus 75 μ l of 80 % (v/v) glycerol, transferred to a Cryo Tube and snapped frozen in liquid nitrogen. Bacterial glycerol stocks were stored at -80°C.

2.2.2 Plasmid purification for sequencing

2.2.2.1 Reagents

- 1) 1.5 ml overnight cultures of GST-ZNF216 wild-type and GST-C30/33A ZNF216 mutant *E. coli*.
- 2) QIAprep Spin Mini-prep Kit for plasmid purification (Qiagen®).

2.2.2.2 Protocol

Plasmids were purified from overnight bacterial cultures of 1.5 ml. The protocol was performed as described in the QIAprep Spin Mini-prep Kit. The plasmids were quantified using a Thermo Scientific NanoDrop® ND-1000 spectrophotometer. 15 μ l of 95 ng/ μ l plasmid was submitted for sequencing.

The DNA sequencing results from both plasmids (GST-ZNF216 wild-type and GST-C30/33A ZNF216 mutant) were blasted against each other for comparison using <http://blast.ncbi.nlm.nih.gov/Blast>. The DNA sequences were translated into

corresponding amino acid sequences using <http://web.expasy.org/translate/>. The comparative sequencing is presented in Appendix I-B and C.

2.2.3 Preparation of 20 ml overnight *E. coli* culture

2.2.3.1 Reagents

- 1) Antibiotic stock solution (80 mg /ml ampicillin plus 20 mg /ml oxacillin).
- 2) LB (25 g /L).
- 3) Bacto-agar (15 g /L).

2.2.3.2 Protocol

LB-agar plates for *E. coli* expressing GST-ZNF216 wild-type and GST-C30/33A ZNF216 mutant were prepared using the reagents described. This mixture was autoclaved for sterilization, cooled and the antibiotic added to a final concentration of 80 µg /ml ampicillin and 20 µg /ml oxacillin. From the bacterial glycerol stocks (Section 2.2.1) cells were streaking onto LB-agar plates and incubated at 30°C overnight. A single colony from each plate was inoculated into 20 ml LB media containing antibiotics at a final concentration of 80 µg /ml ampicillin and 20 µg /ml oxacillin. The cultures were incubated overnight at 37°C with shaking.

2.2.4 Bacterial expression of recombinant proteins

2.2.4.1 Reagents

- 1) 500 ml of LB (25 g /L).
- 2) 200 mM isopropyl-β-D-thiogalactopyranosid (200 mM IPTG stock).
- 3) Tris-buffered saline (TBS) with 1% Triton-100 pH 7.5 (TBST-100): 10 mM Tris, 150 mM sodium chloride and 0.1 % (v/v) Triton-x 100.
- 4) Spectrophotometer for OD₆₀₀ (BioPhotometer- eppendorf[®])

2.2.4.2 Protocol

20 ml overnight cultures (Section 2.2.3) were diluted into 500 ml of LB containing antibiotics and grown for 3 hours with shaking at 37 °C and 190 rpm until OD₆₀₀ = 0.6-0.8 (growth phase). GST-recombinant protein expression was induced by adding

0.5 ml of stock IPTG an incubated for a further 3 hours with shaking. The culture was spun down at 4000 x g 4°C for 30 minutes. Supernatants were discarded and the resultant pellets re-suspended in 5-10 ml TBST-100 and stored at -20°C until required for protein purification.

2.2.5 Purification of GST-ZNF216 recombinant proteins

2.2.5.1 Reagents

- 1) Chromatography columns - 10 ml and 50 ml capacity (*BIORAD*).
- 2) Glutathione Sepharose 4B (GSH) beads (GE Healthcare).
- 3) Tris-buffered saline (TBS) with 1 % Triton-100 pH 7.5 (TBST-100): 10 mM Tris, 150 mM sodium chloride and 0.1 % (v/v) Triton-x 100.

2.2.5.2 Protocol

The bacterial pellets prepared in Section 2.2.4 were thawed and sonicated on ice at ~ 6 microns for 15 seconds 7 times. The bacterial was then spun down for 30 minutes at 43000 x g 4°C (Avanti JA 25.5 rotor type). The supernatant-1 was collected and kept on ice. An aliquot from the supernatant was kept for SDS-PAGE to visualize expression of recombinant proteins (see section 3.2.2). The pellets were discarded.

A separate chromatography column was set up for each type of recombinant protein (GST-ZNF216 wild-type and GST-C30/33A ZNF216 mutant). A 10 ml or 50 ml column was used depending on the volume of recombinant protein. One volume (usually 1 ml) of ethanol pre-soaked glutathione (GSH) beads was added to each column and the ethanol storage buffer allowed running through. The GSH beads were washed with 5-10 volumes of TBST-100. Supernatant-1 was then added to the column and kept for 3 hours gently rotating in the cold room, allowing GSH bead-GST-recombinant protein binding. After incubation, the supernatant-1 was allowed to run through and GSH beads washed three times with 5-10 volumes of TBST-100. A sample of the beads was kept for SDS-PAGE to check the binding to recombinant protein. The beads were washed twice with Thrombin Cleavage Buffer (TCB) to equilibrate before adding thrombin for GST-recombinant protein cleavage.

2.2.6 Thrombin cleavage of GST-recombinant proteins

2.2.6.1 Reagents

- 1) 0.5 U / μ l thrombin (Sigma).
- 2) Thrombin Cleavage Buffer (TCB); 20 mM Tris, 150 mM sodium chloride and 2.5 mM calcium chloride dehydrate, pH 8.4 adjusted with HCL.

2.2.6.2 Protocol

One volume of thrombin-TCB solution (5 U Thrombin /1 ml TCB) was added to one volume containing GSH beads bound to recombinant protein. The columns were then rotated overnight in the cold room. The column flow through was collected and kept on ice. A further one volume of TCB was added to each column and incubated in the cold room for 1 hour to collect any residual recombinant proteins. This flow though was collected and pooled with the first overnight flow though (supernatant-2). An aliquot from the pooled supernatant-2 as well as of beads was kept for SDS-PAGE to characterize the cleavage of fusion protein by thrombin. The resultant supernatant-2 should be cleaved ZNF216 recombinant proteins and was stored at -20°C.

2.2.7 Coupling ZNF 216 purified proteins to Sepharose beads - preparation of ZNF216 affinity matrices

2.2.7.1 Reagents

- 1) Cyanogen bromide activated – Sepharose-4B (CNBr) (GE Healthcare).
- 2) Coupling buffer: 100 mM sodium hydrogen carbonate, 500 mM sodium chloride, pH 8.3.
- 3) 1 mM hydrochloric acid.
- 4) 1 M ethanolamine pH 8.
- 5) Washing buffer 1: 100 mM sodium acetate, 500 mM sodium chloride, pH 4.
- 6) Washing buffer 2: 100 mM Tris-HCl, 500 mM sodium chloride, pH 8.
- 7) Column storage buffer: 50 % TBS, 50 % glycerol, 1 mM DTT, sodium azide, pH 7.4.

2.2.7.2 Protocol

CNBr Sepharose beads were hydrated by incubation with 1mM hydrochloric acid (1 g /3.5 ml) for 15 minutes on a rocking platform. The Sepharose beads-HCl suspension was placed in the column and the hydrochloric acid allowed running through. The beads were washed twice with 5-10 volumes of coupling buffer. Supernatant-2 (see section 2.2.6) was thawed and protein concentration determined. A sample was kept for SDS-PAGE analysis. Supernatant-2 was added to the column of activated CNBr Sepharose (1 ml solid beads volume to 1- 4 mg ZNF216 protein) and incubated for 3 hours rotating in a cold room to allow CNBr beads-ZNF216 protein binding. After incubation, the buffer was allowed to run through and a sample was kept for SDS-PAGE analysis to check the unbound protein. Sepharose beads were washed twice with 5-10 ml ethanolamine; a further similar volume of ethanolamine was added and the columns incubated overnight rotating in the cold room to block nonspecific binding site in the sepharose beads. The ethanolamine was allowed to run through the column and the beads were washed with 5-10 bead volumes of coupling buffer followed by washing 4 times alternating between washing buffers 1 and 2. These ZNF216 affinity matrices were then washed and stored with 5 volumes of storage buffer. Matrices used immediately were kept in TBS only. ZNF216 affinity matrices were kept at 4°C.

2.2.8 Capture of ubiquitinated proteins from brain tissue homogenate

2.2.8.1 Reagents

- 1) Washing buffer (TBS-NP40): 10 mM Tris, 150 mM sodium chloride, Nonidet P- 40, 1 mM DTT, pH 7.4.
- 2) Protease inhibitor cocktail (Sigma-Aldrich).
- 3) N-ethylmaleimide (NEM).
- 4) Phenylmethane sulfonyl fluoride (PMSF).
- 5) Homogenizing buffer: TBS-NP40, protease inhibitor cocktail (1:100), 5 mM NEM, 1 mM phenylmethane sulfonyl fluoride (PMSF), and pH 7.4.
- 6) 1 M DTT.

2.2.8.2 Protocol

Mouse brain cortices were homogenized using a Dounce glass homogenizer in cold homogenizing buffer. Each brain cortex was homogenized in 2-2.5 ml homogenizing buffer. Homogenates were clarified by centrifugation at 30800 x g for 20 minutes. The supernatants were incubated with 10 mM DTT for 15 minutes to remove the NEM in homogenizing buffer. Protein concentration was determined by Bradford. Equal amounts of protein in a similar volume of supernatant were incubated with the pre-washed ZNF216 affinity matrices (see 2.2.7) in a column for 3 hours rotating in the cold room. The column flow through was then collected and a sample from this kept for Western blot analysis of the unbound fraction. The affinity matrices were washed 3 times for 10 minutes, and stored in TBS-NP40 (1 ml beads to 1 ml buffer; 50 % slurry). Samples from the bound matrices were collected to investigate the binding of ubiquitinated proteins by western blot analysis.

2.2.9 Capture of Lysine- 48 synthetic polyubiquitin chain

2.2.9.1 Reagents

- 1) Washing buffer (TBS-NP40): 10 mM Tris, 150 mM sodium chloride, Nonidet P-40, 1 mM DTT, pH 7.4.
- 2) Synthetic Lys48 polyubiquitin chain.

2.2.9.2 Protocol

An amount of 2 µg of Synthetic Lys48 polyubiquitin chain were dissolved in 800 µl TBS-NP40 buffer and incubated with the pre-washed 200 µl of 50 % slurry of ZNF216 affinity matrices (see 2.2.7) in an eppendorf tube for 3 hours rotating in the cold room. This was followed by centrifugation and the supernatant was then collected and a sample from this kept for Western blot analysis of the unbound fraction. The affinity matrices were washed 3 times for 10 minutes, and samples from the bound matrices were collected to investigate the binding of synthetic Lys48 polyubiquitin by Western blot analysis.

2.2.10 Deubiquitination using ubiquitin-specific protease (USP2) enzyme

2.2.10.1 Reagents

- 1) USP2 catalytic domain (0.5 µg /µl; UW9850 Enzo Life Sciences).
- 2) ZNF216 affinity matrices bound to ubiquitinated proteins (see section 2.2.8).
- 3) Deubiquitinase buffer (DUB buffer): 50 mM Tris-HCl, 1 mM DTT, pH 7.4.
- 4) TBS-NP40 (see section 2.2.8.1).
- 5) 2 ml eppendorfs.

2.2.10.2 Protocol

ZNF216 affinity matrices were washed 3 times for 10 minutes each time with TBS-NP40 in rotating columns. 50 % slurry of affinity matrices were transferred into 2 ml eppendorf tubes. USP2 was added (10 µg /0.4 ml 50 % slurry) and the affinity matrices were incubated at 37 °C rotating overnight. Matrices were centrifuged at 400 x g using a top bench centrifuge for 5 minutes at room temperature. The supernatants* were collected carefully and the beads were washed with DUB buffer. A 20 µl sample of the supernatant and 50 µl fraction of matrices was also collected for Western blotting analysis. The rest of the supernatant* following incubation with DUB actions was submitted for mass spectrometry. In an alternative approach, the supernatant* was filtered through a 5 kDa cut-off filter, involving centrifugation at 450 x g for 30 minutes (HARRIER 18 / 80 MSE centrifuge). This resulted in a reduction in the supernatant volume from original of 1-2 ml to approximately 60-50 µl. These samples were subjected to 2 dimensional gels (DG) or 1DG SDS-PAGE. The resultant protein spots or bands were excised from the silver stained gel trypsinated (see section 2.3.7 and 2.4.4) and submitted for mass spectrometry; Matrix – associated laser desorption ionization– time of flight (MALDI-TOF-MS) was used. The generated peptide mass fingerprints by MALDI-TOF-MS were analyzed by uploading the data into Mascot search engine (<http://www.matrixscience.com>); using the following parameters; “mus musculus” species, carbamidomethyl as a fixed modification, methionine oxidation as variable modification and Swiss-Prot as a database to compare candidate peptides.

2.3 Protein analysis

2.3.1 Bradford assay for protein quantitation

2.3.1.1 Reagents

- 1) Bradford reagent: 100 mg of Coomassie Brilliant Blue G2, 50 ml ethanol, 100 ml perchloric acid and 50 ml deionized water.
- 2) Bovine serum albumin (BSA) standard solution: 1 mg /ml water

2.3.1.2 Protocol

A known volume of protein sample was pipetted into a 96 well plate and made up to a volume of 50 μ l. A standard curve (0-50 μ g standard protein) was generated using the BSA solution. All samples and standards were analyzed in duplicate. 150 μ l of Bradford reagent (1:11 ml deionized water) was added into each sample and the standard. The resultant blue color was measured using a spectrophotometer at 595 nm (SPECTRA MAX 190) and the protein concentration determined from the standard curve.

2.3.2 One dimensional (1DG) sodium dodecyl sulphate polyacrylamide gel electrophoresis (SDS-PAGE) - large gradient gel (5-20 %)

2.3.2.1 Reagents

- 1) 30 % (w/v) acrylamide solution.
- 2) 10 % sodium dodecyl sulphate (SDS).
- 3) Buffer A: 1.1 M Tris, 0.1 % SDS and 30 % glycerol, pH 8.8.
- 4) Buffer B: 1.1 M Tris, 0.1 % SDS pH 8.8.
- 5) Electrode Buffer: 25 mM Tris, 190 mM Glycine and 0.1% SDS.
- 6) Stacking gel buffer: 150 mM Tris, 0.1% SDS, pH 6.8.
- 7) Gel application buffer (2x GAB): 150 mM Tris, 8 M Urea, 2.5 % SDS, 20 % Glycerol (v/v), 10% (v/v) 2-mercaptoethanol, 3% DTT (w/v) and bromophenol blue, pH 6.8.
- 8) Ammonium per-sulphate (AMPS): 10 % (w/v) AMPS solution.
- 9) N, N, N, N- Tetramethylene diamine (TEMED).
- 10) Stacking gel solution: 5 ml of stacking gel buffer, 1 ml acrylamide, 5 μ l TEMED and 100 μ l of AMPS.

11) Protein ladder: ColorPlus Prestained broad range (10-230 kDa).

12) Gel electrophoresis system.

2.3.2.2 Protocol

The gel solutions (5 % and 20 %) were prepared in a total volume of 10 ml each. The 5 % gel solution was prepared using 1.67 ml of acrylamide, 3.3 ml of buffer A and 5ml deionized water. The 20 % gel solution was prepared with 6.6 ml of acrylamide and 3.3 ml buffer B. 10 µl of TEMED and 100 µl of AMPS were added to the gel solutions just before use to facilitate gel polymerization. The gradient gel was poured with gentle agitation starting with the 20 % of gel solution and mixing in the 5 % solution. Using a Pasteur pipette, a water-saturated butanol solution was layer a top gel whilst the gel polymerized. After polymerization, the butanol layer was decanted. A stacking gel was poured on top of the gradient gel and a sample comb inserted. Once the stacking gel had polymerized, the comb was removed before loading the protein samples for separation. Protein samples for SDS-PAGE were treated with 2 x GAB and boiled for 5 minutes before loading. The samples were subjected to electrophoresis using electrode buffer at constant current 40mA supplied by an electrophoresis power pack. Once the proteins were separated the gel was ready for staining or Western blot analysis.

2.3.3 1DG SDS-PAGE - mini gradient (10-18%) and 12% gel

2.3.3.1 Protocol

Table 2.1 below shows the volume and solution concentrations used for mini gels. The 10-18 % gradient mini gel was prepared by using the gradient apparatus. The methods follow that described in section 2.3.2.2, using 5µl TEMED and 25 µl of AMPS. The stacking gel solution was prepared using 700 µl of water, 165 µl of 30 % acrylamide, 125 µl of 1.1 M Tris pH 8.8, 10 µl of 10 % SDS, 10 µl AMPS and 5 µl TEMED. The separation carried out at 200 mA using a Mini-protean (Bio-Rad) system.

Table 2.1 volumes and concentration of compounds used to prepare SDS-PAGE, mini gel

Solution	10 %	12 %	18 %
30 % acrylamide	1.5 ml	1.8 ml	2.7 ml
1.1 M Tris pH 8.8	1.5 ml	1.5 ml	-
1.1 M Tris, 30 % glycerol pH 8.8	-	-	1.5 ml
10 % (w/v) SDS	45 μ l	45 μ l	45 μ l
Water	1.455 ml	1.155 ml	0.255 ml

2.3.4 Two dimensional (2DG) gel electrophoresis

2.3.4.1 Reagents

- 1) Tissue homogenization buffer; 30 mM Tris, 8 M Urea, 4 % Chaps in Nanopure water, pH 8.8.
- 2) Isoelectric focusing sample buffer: Destreak rehydration solution (GE Healthcare).
- 3) Carrier Ampholytes in aqueous solution: IPG buffer, pH 3-10NL (GE Healthcare).
- 4) Immobilised non-linear pH 3-10 strip gel (Immobiline TM Dry Strip gel, pH gradient 3-10 NL, 7 cm length).
- 5) Equilibration base buffer I: 6 M urea, 2 % SDS, 20 % glycerol, 50 mM Tris-HCl pH 8.8, 2 % DTT, in Nanopure water.
- 6) Equilibration base buffer II: 6 M urea, 2 % SDS, 20 % glycerol, 50 mM Tris-HCl pH 8.8, 2.5 % iodoacetamide, in Nanopure water.
- 7) All components of SDS-PAGE (see section 2.3.2.1).
- 8) 0.5 % agarose with 0.1 (w/v) bromophenol blue
- 9) Mineral oil (Bio-Rad).
- 10) ColorPlus Prestained protein ladder (broad range 10-230 kDa).
- 11) PROTEAN IEF system (BIO-RAD)

2.3.4.2 Protocol

1) Sample preparation:

Mouse cortices were homogenized in cold homogenization buffer using ceramic beads (MPbio Lysing matrix D) and beads-beater twice at a setting of 6 m /sec for 20 seconds. The resulting homogenates were centrifuged at 4°C and 16100 x g for 10 minutes. The supernatants were transferred to fresh eppendorf tubes and protein concentrations determined by Bradford assay (see section 2.3.1).

2) First dimension isoelectric focusing (IEF)

Protein samples were made up to 65 µl with homogenizing buffer. 65 µl of destreak rehydration solution was mixed with 2 % ampholytes 3-10NL and added to the protein sample. Samples were vortexed and loaded into individual channels of a mini IEF tray (BIO-RAD PROTEAN IEF system). An IPG strip (NL 3-10) was laid into each channel gel side down with the acidic end toward the anode. The IPG strips were allowed to passively hydrate for 1 hour. The IPG strips were then covered with 1 ml of mineral oil and IEF was performed using the BGF (Bioassay Guided Fractionation) focusing program as indicted below:

- Step 1: 250V-LINEAR-20 min
- Step 2: 4000V-LINEAR-2hours
- Step 3: 4000V-RAPID-10000 V hours
- Step 4: 500V-RAPID-25 hour

3) Equilibration of IPG strips

The focused IPG strips were equilibrated with equilibrium buffer I then II. The focused IPG strips were placed in 1 ml of equilibrium buffer I (DTT) and gently shaken for 15 minutes at room temperature. This was followed by a similar incubation with equilibrium buffer II (Iodoacetamide).

4) Second dimension electrophoresis

The 12 % or 10-18 % SDS-PAGE gel was prepared as described in the section 2.3.3 up to the point of the resolving gel. The focused and equilibrated IPG strip was then placed on the top of the resolving gel. 5 µl of protein ladder was applied to paper wicks and placed at the acidic end of the IPG focused strip. The strips were covered

with 5 % melted agarose. Electrophoresis was run using Mini-protean (Bio-Rad) supplied with 200 mA and 135 V. Following separation, the gel was either stained with Coomassie Blue stain or silver nitrite or the gel was processed to Western blotting.

2.3.5 Coomassie Blue staining

2.3.5.1 Reagents

- 1) Coomassie Blue stain: 50 % Methanol, 20 % Acetic Acid, 0.12 % (w/v) Coomassie Brilliant Blue in water.
- 2) Coomassie Blue de-stain: 10 % Methanol and 10 % Acetic Acid in water.

2.3.5.2 Protocol

Immerse gel for 1-2 hours in Coomassie stain on a rocking platform. De-stain with several changes of solution until the non-specific background becomes clear.

2.3.6 Colloidal Coomassie staining

2.3.6.1 Reagents

- 1) CooBlue Max stain
- 2) 7 % (v/v) glacial acetic acid.

2.3.6.2 Protocol

This stain was compatible with mass spectrometry. The gel was placed in a tray and washed with 7 % glacial acetic acid for 15-20 minutes with gentle shaking. The gel was then immersed in 20 ml of CooBlue Max stain for 1-2 hours with gentle shaking. The stained gel was washed with an excess of ultra-pure water to remove any background.

2.3.7 Silver staining

2.3.7.1 Reagents

- 1) Plus One Silver Staining kit, protein (GE Healthcare).
- 2) Fixing solution (30 % (v/v) ethanol, 10 % (v/v) glacial acetic acid).
- 3) Sensitizing solution (30 % ethanol, 5 % (w/v) sodium thiosulphate, 6 % (w/v) sodium acetate).
- 4) Staining solution (2.5 % (w/v) silver nitrate).
- 5) Developing solution (2.5 % (w/v) sodium carbonate, 24 μ l from 5 % (w/v) sodium thiosulphate and 150 μ l from 35 % (v/v) formaldehyde).
- 6) Stopping solution (12 % acetic acid).

2.3.7.2 Protocol

All steps were performed as indicated in the manufacturer's protocol using gentle shaking for incubation and nanopure water.

First the gels were incubated in fixing solution for 60 minutes twice. This was followed by incubation for 2 hours in sensitizing solution. The sensitizing solution was removed and gels washed with excess water for 5 x 8 minutes. Silver reaction was performed by incubating the gels with the silver staining solution for 60 minutes. The gel was washed with water four times for one minute each time. Developing solution was added and left for 2-5 minutes or until the protein spots reached the desired intensity. The gels were then immediately transferred into stopping solution for 45 minutes. Gels were washed with water for 2 x 30 minutes.

2.3.8 Western blotting analysis

2.3.8.1 Reagents

- 1) Western transfer buffer: 25 mM Tris-HCl, 190 mM glycine, 20 % methanol (v/v) in deionized water.
- 2) Electrophoretic transfer apparatus (Bio-Rad).
- 3) Nitrocellulose membrane (Hybond-C)
- 4) TBST: Tris buffered saline, 0.1 % (v/v) Tween.
- 5) PBST: Phosphate buffered saline, 0.1 % (v/v) Tween.
- 6) 4 % (w/v) non-fat dry milk solution (Marvel[®]) in TBST or PBST.

- 7) Primary antibodies and secondary antibody conjugated to Horseradish Peroxidase (HRP).
- 8) Chemiluminescent substrate (ECL).
- 9) X-ray film; Lumi- Film Chemiluminescent detection film.
- 10) Developing solution (Calumet Photograph LTD 757314).
- 11) Fixative solution (Calumet Photograph LTD 2000RT).

2.3.8.2 Protocol

Following separation of proteins by SDS-PAGE (described in section 2.3.2) the gel was placed onto nitrocellulose membrane that had been soaked in transfer buffer. This was placed between two sheets of Whatman 3 mm filter paper and transferred into cassettes for protein transfer, which was performed at 10 V and 40 mA overnight. After transfer, the membranes were blocked with 4 % (w/v) Marvel in TBS-T or PBS-T for 1 hour with gentle shaking. The membrane was then incubated with primary antibody in 4 % (w/v) Marvel either for 1 hour at room temperature or overnight at 4°C. The membrane was then washed with TBS-T or PBS-T three times for 10 minutes each. Primary antibodies and their concentrations are detailed in Appendix I. The secondary antibody was used at 1:3000 in 4 % (w/v) Marvel for 1 hour, followed by washing with TBS-T or PBS-T three times for 10 minutes each. Immunoreactivity was detected using ECL according to the manufacturer's protocol and the chemiluminescence signal was detected using X-ray film. For densitometry analyses of band signal intensity the X-ray films were scanned and ScnImage software used. Immunoreactivity for all blots was normalized to β -actin as a protein loading control.

2.3.9 Striping of antibody from the nitrocellulose membrane

2.3.9.1 Reagents

Stripping buffer: 0.5 M Tris-HCl, pH 6.8, 10 % SDS (w/v), 0.8 % 2-mercaptoethanol (v/v).

2.3.9.2 Protocol

The membrane was washed with TBST or PBST and then incubated in stripping buffer at 55°C for 30-45 minutes on a rocking platform. The membrane was washed several times with TBS-T or PBS-T.

2.4 Two-dimensional fluorescence difference in-gel electrophoresis (2D-DIGE)

2.4.1 Reagents

For reagents see section 2.3.4 (2D PAGE) and as follows:

- 1) CyDye™ DIGE for protein labeling (0.2 mM N-hydroxy succinimide ester of the fluorescent cyanine dyes Cy2, Cy3 and Cy5).
- 2) Tissue homogenizing buffer: 30 mM Tris, 8 M Urea, 4 % Chaps in Nanopure water, pH 8.8.
- 3) 10 mM lysine.

2.4.2 Protocol

2.4.2.1 Sample preparation

Cortices from control and *Psmc1^{fl/fl};CaMKII α -Cre* mouse brains aged 6 weeks were involved in this study (n = 4). Cortices were homogenized in pre-cooled homogenizing buffer as described in section 2.4.1. Protein concentration was determined using Bradford assay.

2.4.2.2 Experimental design and CyDye labeling

The cyanine dyes (Cy2, Cy3 and Cy5) used for 2D-DIGE contain N-hydroxysuccinimide ester derivatives which bind to the ϵ -amino group of lysine residue in proteins. Because of the distinct excitation and emission fluorescent spectra of each CyDye, the labeled samples and internal standard are mixed and run together on one gel. This minimizes gel-to-gel variability, allowing easy protein spot-matching and accurate quantitative analysis of spot pixel volume. This method also decreases the number of gels used compared to conventional 2D-PAGE.

To avoid any labeling bias arising from the fluorescent dyes, a dye-swap with Cy3 and Cy5 was incorporated in the experiment. Cy2 was used to label the internal standard. Table 2.2 summarizes the CyDye labeling and experimental design.

For CyDye labeling, 15 μ g of each protein sample was incubated individually with 120 pmol of Cy3, Cy5 or Cy2 for 30 minutes on ice in the dark. Following this

incubation, the reaction was stopped by adding 1µl of 10 mM lysine and incubating for a further 10 minutes in the dark. After this labeling, one control (15 µg) and one *Psmc1^{fl/fl};CaMKIIα-Cre* (15 µg) sample and 15 µg of pooled internal standard were combined together in an eppendorf tube. These samples were subjected to first dimensional IEF.

*All steps involved in 2D-DIGE were performed in the dark.

Table 2.2 Experimental design for 2D-DIGE analysis

Gel No.	Cy2 (internal standard)	Cy3	Cy5
1	All sample mixture	control sample 1	<i>Psmc1^{fl/fl}; CaMKIIα-Cre</i> sample 5
2	All sample mixture	control sample 2	<i>Psmc1^{fl/fl}; CaMKIIα-Cre</i> sample 6
3	All sample mixture	<i>Psmc1^{fl/fl}; CaMKIIα-Cre</i> sample 7	control sample 3
4	All sample mixture	<i>Psmc1^{fl/fl}; CaMKIIα-Cre</i> sample 8	control sample 4

2.4.2.3 First dimension isoelectric focusing (IEF)

The volume of each pre-labeled combined sample (45 µg) was made up to 65 µl with homogenizing buffer. IEF was performed as described in section 2.3.4.

2.4.2.4 Equilibration of IPG strips

The focused IPG strips were equilibrated with equilibration buffers I and II as described in section 2.3.4.

2.4.2.5 Second dimension electrophoresis

A 10-18 % gradient SDS-PAGE was used and electrophoresis was carried out as described in section 2.3.4

2.4.2.6 Gel imaging

Following second dimension electrophoresis, the gels were removed from the glass plates, rinsed with deionized water and scanned using a Fujifilm scanner (FLA-5100 imager scanner) at 50 µm resolution. Each gel was scanned at the three different wavelengths for the fluorescent CyDyes. Cy2 images were scanned at 473 nm, Cy3

at 532 nm and Cy5 at 635 nm. Therefore, three fluorescence images were produced for each gel. All images were saved for analysis. Two gels were randomly selected and stained with silver nitrite.

2.4.2.7 Analysis of 2D-DIGE images to identify differential abundant spots

Progenesis SameSpot software (Nonlinear Dynamics - version 4.0) was used for analysis of the CyDye 2D-DIGE images. In brief, the 3 images from each gel were grouped; one of the images was selected as a reference; all the images were then carefully aligned and the pixel density of each spot was normalized to the internal control. The results of image analysis were given as fold-change between control and *Psmc1^{fl/fl};CaMKII α -Cre* samples using ANOVA ($p < 0.05$) and 1.2 fold changes.

2.4.3 Preparative 2DG and spot picking

Preparative 2DG gels stained with colloidal Coomassie were used for protein spot identification by mass spectroscopy. This used a pooled cortical sample from control and *Psmc1^{fl/fl};CaMKII α -Cre* mice. 2DG separation was performed as described in section 2.3.4. Gels were stained and the differentially expressed protein spots identified using Progenesis Samespot visually matched and selected for picking. Spots were picked using cut micropipette tips and the gel plug transferred into eppendorf tubes for protein extractions.

2.4.4 Protein extraction for MALDI-TOF-MS

2.4.4.1 Reagents

- 1) 10 mM DTT
- 2) 50 mM iodoacetamide
- 3) Acetonitrile (HPLC grade)
- 4) 25 mM ammonium bicarbonate
- 5) 12.5 ng / μ l trypsin (sequencing grade)

2.4.4.2 Protocol

Protein in the gel plugs from section 2.4.3 was reduced with 10 mM DTT and alkylated with 50 mM iodoacetamide. The plugs were then dehydrated in 50 μ l of

acetonitrile and 25 mM ammonium bicarbonate solution (2:1) for 15 minutes. This solution was discarded and the gel plug rehydrated using 50 μ l of 25 mM ammonium bicarbonate solution for 10 minutes. This dehydration / rehydration cycle was repeated once and gel plugs were dried up for 15 minutes. For protein extraction, gel plugs were incubated with 4 μ l of 12.5 ng / μ l of trypsin in 25 mM ammonium bicarbonate solution for 30 minutes. The trypsin solution was discarded and gel plugs were covered with 10 μ l of 25 mM ammonium bicarbonate solution and incubated at 37°C for 4 hours. The tubes were placed on vigorous shaker for 20 minutes, and the supernatants were transferred to new eppendorf tubes and retained. This was followed by addition of 10 μ l of acetonitrile: water mixture (20:80) and allowed to rehydrate plugs for 15 minutes. The supernatants containing the peptide digest were removed and combined with the previously retained fraction and submitted for protein identification by MALDI-TOF-MS (see section 2.2.10.2).

2.4.5 Protein validation following MALDI-TOF-MS

Proteins selected for validation following identification by MALDI-TOF-MS were based on antibody availability. Western blot analysis was performed as described in section 2.3.8 using 12 % one dimensional mini SDS-PAGE. 2DG Western blots were also performed. A minimum of three control and *Psmc1^{fl/fl}*; *CaMKII α -Cre* mice were used for validation. Samples were homogenized in the same buffer as for 2D-DIGE. Immunoreactivity for all blots was normalized to protein loaded using β -actin.

2.5 Histological studies of brain sections - protein localization

Coronal histological sections of cerebral cortices of brain mice were prepped in Pathology department- Clinical School; The University of Nottingham. The tissues sections were provided as paraffin embedded sections.

2.5.1 Double immunofluorescent

2.5.1.1 Material and reagents

- 1) Coronal histological sections of cerebral cortices.
- 2) Xylene
- 3) Ethanol, 100 %, 95 % and 70 % dilutions
- 4) Coplin jar (for slide washing)
- 5) Antigen retrieval buffer solution: 10 mM sodium citrate buffer containing 0.05 % Tween, pH 6
- 6) MOM TM kit; for detection of mouse primary antibody on mouse tissue (VECTOR Lab, Inc.)
- 7) 10 % goat serum (VECTASTAIN Elite rabbit IgG, ABC kit)
- 8) Secondary fluorescent antibodies: Rhodamine Red gout anti mouse IgG; Alexa Flour gout anti rabbit IgG (Invitrogen).
- 9) Hoechst 33342 stock
- 10) PBS

2.5.1.2 Protocol

Brain cortices sections were deparaffinized by immersion the slides in xylene for 10 minutes, and gradually rehydrated by ethanol, using three consecutive 10 minutes incubation of sections with 100 %, 95 % and finally in 70 %. The slides were then placed in a beaker under gentle running tap water for 10 minutes. They were transferred into another beaker containing a heated retrieval buffer solution at 100 °C, and heated for further 20 minutes. The beaker was placed on shaker platform for 20 minutes with gentle shaking, and slides were washed gently in running water for 10 minutes.

For blocking of nonspecific binding sites on tissue cortex, sections were covered with 70 μ l of blocking reagents and incubated for 1 hour in humid chamber; we used MOM Ig blocking solution for mouse antibody (1 drop of stock solution in 1.25 ml PBS) and 10 % goat serum were used for rabbit antibodies. The sections were then washed in three changes with PBS for 5-10 minutes each.

For labeling procedure, MOM diluent was used for mouse primary antibody and its corresponding secondary (80 μ l of concentrated protein in 1 ml PBS). For rabbit primary, PBS was used as diluents. Antibodies solutions of 65 μ l were covered brain section within a frame. The sections were covered and incubated in humid chamber for overnight at 4°C. They were washed in the PBS for 3x10 minutes each. Corresponding secondary antibody were applied and sections were incubated for 1 hour in the dark humid chamber. A control sections were included which prepared in the similar way except no primary antibodies were used.

The brain sections were then washed with PBS for 3x10minutes, and the second labeling for marker protein was performed using cell specific marker for astrocytes or neurones. The section were washed in PBS and counterstained to visualize nuclei by Hoechst in a concentration of 1:5000 in PBS. The sections were incubated in the dark for 15 minutes followed by 3 washing and cover slip with fluorescence mounting medium. Slides were kept at 4°C and in the dark until investigated by fluorescent microscope.

2.6 Measures of oxidative stress markers

2.6.1 Determination of Malondialdehyde (MDA)

2.6.1.1 Reagents and solutions

- 1) N-methyl-2-phenylindol (MPD).
- 2) HCL 12 M.
- 3) MDA-standard. 1, 1, 3, 3-tetramethoxypropane (TMOP).
- 4) Butylated hydroxytoluene (BHT).
- 5) Acetonitrile
- 6) Methanol
- 7) 10 mM Tris-HCL buffer pH 7.0
- 8) PBS pH 7.4

2.6.1.2 Preparation of stock solutions

- 1) Reacting reagent (R1) was prepared by dissolving 0.28 g of MPD in 100 ml of acetonitrile. From this stock 18 ml was mixed with 6 ml methanol, to end up with working concentration of 10.3 mM and 24 ml of reacting reagent (R2). This was prepared just before the experiment.
- 2) 10 mM of TMOP for MDA standard stock was prepared by adding 82.5 μ l of TMOP to 50 ml Tris-HCL buffer.
- 3) BHT stock of 0.5 M was prepared by dissolving 0.56 g of BHT in 5 ml of acetonitrile.

All these stocks were preserved in fridges at 4°C.

2.6.1.3 Preparation of MDA Standard Curve.

10 mM of TMOP stock was diluted to 20 μ M (1:500-v/v) in water just prior to use. This was then used to prepare a serial dilution for standard curve. The table below indicated the volumes of TMOP and water used to give 120 μ l as a final volume.

Table 2.3 Volumes of TMOP for MDA standard curve

Standard	S1	S2	S3	S4	S5	S6	S7	S8
Volume of 20 μ M TMOP, (μ l)	0	3.75	7.5	15	30	60	90	120
Volume of water (μ l)	120	116.25	112.5	105	90	60	30	0
Final conc. (μ M)	0	0.125	0.25	0.5	1.0	2.0	3.0	4.0

2.6.1.4 Sample Preparation for MDA Measurement.

Brain cortices from control and *Psmc1^{fl/fl};CaMKII α -Cre* mice were placed in 500 μ l pre-cooled phosphate buffer, pH 7.4. A volume of 5 μ l of 0.5M BHT was added to each tube to prevent sample auto oxidation. Ceramic beads (MP bio Lysing matrix D) and beads-beater at setting of 5 m/sec for 15 seconds were used for homogenization and this was repeated once. The homogenates were then centrifuged at 4°C and 16100 x g for 10 minutes using top bench centrifuge, and the clear supernatant fractions were transferred to a new eppendorf tubes. The protein concentrations were determined using Bradford assay.

Samples were adjusted to the same concentration of protein (9.5 μ g / μ l). To measure total MDA, hydrolysis step was performed by adding 1.5-2.5 μ l of HCL to sample and blank to bring their pH upto 1-2 (using litmus paper), then they were heated at 60 °C for 80 minutes.

2.6.1.5 Assay procedure for MDA measurement

A sample volume of 60 μ l was transferred to a labeled eppendorf; the test was carried out by using duplicate sample as well as blank for each individual brain cortex. A volume of 190 μ l from R1 reagent was added to each sample, alternatively for sample blank 1:3 mixture of methanol: acetonitrile was used, all tubes were vortexed. Blank was included for each sample to correct any absorbance A_{586} data due to sample inherent color. A volume of 45 μ l HCL was added; tubes were vortexed vigorously and incubated at 45 °C for 1hour. Then after they were centrifuged at 16100 x g for 10 minutes, clear supernatants were separated carefully from the rest of the precipitate and transferred into a new eppendorf. A reactant volume of 150 μ l from sample or blank was transferred to 96- micro-well plate and the absorbance was measured at 586 nm using spectrophotometer (SPECTRA MAX 190).

Figure 2.2

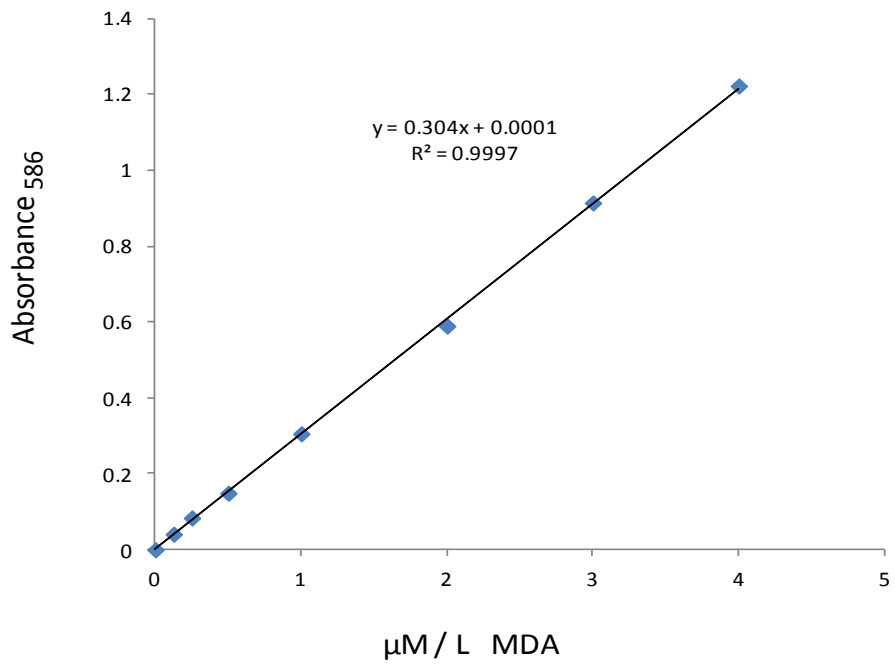


Figure 2.2 Representative standard curve of MDA.

2.6.2 Estimation of protein carbonyl group

2.6.2.1 Reagents and solutions

- 1- 50 mM Tris-HCl
- 2- 10 mM 2,4- dinitrophenylhydrazine (DNPH) in 2.5 M HCl
- 3- 6 M Guanidine HCl in water.
- 4- 10 % and 20 % Trichloroacetic acid-TCA (w/v) in water
- 5- Ethanol : Ethyl acetate solution 1:1 (v/v)
- 6- 2.5 M HCl

2.6.2.2 Protocol

Mice brain cortices were placed in tubes containing 500 μ l pre-cooled phosphate buffer, pH 7.4. The samples were prepared as described in section 2.6.1.4; and protein concentration was determined using Bradford assay.

Samples of 200 μ l with similar protein concentration (2.5 μ g / μ l) were used in duplicate with a blank for each one. 800 μ l of DNPH was added to the sample, whereas sample blank was mixed with 800 μ l of 2.5 M HCl. These were incubated in the dark at room temperature for 1 hour, while they were vortexed every 15 minutes. A volume of 1 ml of 20 % TCA was added; tubes were vortexed and incubated on ice for 5 minutes. They were centrifuged at 16100 x g for 10 minutes at 4°C and the supernatants were discarded. The resultant pellets were re-suspended in 1 ml of 10 % TCA with vigorous vortex, incubated on ice for 5 minutes and centrifuged as mentioned above. The supernatants were discarded and pellets were re-suspended in ethanol: ethyl acetate mixture, small spatula and vortex were used to facilitate pellets solubilization. These were centrifuged at 16100 x g for 10 minutes at 4 °C and pellets were re-suspended in 500 μ l 6 M guanidine-HCl with vortex. Debris not soluble was removed by centrifugation at 16100 x g for 10 minutes, and the reactant volume of 220 μ l of supernatants was transferred into 96- micro-well plate. The absorbance was measured at 370 nm using SPECTRA MAX 190 plat reader.

The average sample absorbance was subtracted from average sample blank to give corrected absorbance (CA). The concentration of carbonyl group was calculated by using the following equation:

$$\text{Protein carbonyl (nM / ml)} = [(CA) / (* 0.011)] (500 \mu\text{l} / 200 \mu\text{l})$$

* is an actual extinction coefficient for DNPH. This value has been adjusted for the path length of the solution in the well.

500 μl is the volume used for last pellet re-suspension.

200 μl is the original volume of sample used for the assay.

2.6.3 Determination of nitrated proteins

This were measured using Western blot analysis using mouse anti- nitrotyrosine antibody and performed as described in section 2.3.8

2.6.3.1 Reagents and solutions

- 1- Radioimmunoprecipitation assay buffer (RIPA); 50 mM Tris-HCl pH7.4, 150 mM sodium chloride, 0.5 % Sodium deoxycholate, 1 % NP-40 and 0.1% SDS.
- 2- Gel application buffer (2x GAB): 150 mM Tris, 2.5 % SDS, 20 % Glycerol (v/v), 10 % 2-mercaptoethanol (v/v), DTT (3 % w/v) and bromophenol Blue, pH 6.8 adjusted with HCL.
- 3- 12 % SDS-PAGE
- 4- Anti- nitrotyrosine antibody
- 5- Ingredient for preparation of peroxyxynitrite solution; 0.6 M sodium nitrate, 0.6 M hydrochloric acid / 1.2 M hydrogen peroxide solution, 0.9 M sodium hydroxide, manganese oxide (solid) , 0.45 M sodium hydroxide.

2.6.3.2 Preparation of peroxyxynitrite solution

This was synthesized by sodium nitrate and acidic hydrogen peroxide using method described by Koppenol et al., 1996. Equal volumes (usually 5 ml) of ice cold 0.6 M sodium nitrate and 0.6 M hydrochloric acid / 1.2 M hydrogen peroxide solution were mixed and vortexed. 10 ml of 0.9 M sodium hydroxide was added immediately to

preserve the peroxyxynitrite. 1 gram of manganese oxide was added to this solution and stirred in fume cupboard until the rising bubbles disappears. The solution was filtered and incubated for 3 hours at -80°C. The resulted liquid fraction of the upper layer was collected and diluted in 0.45 M sodium hydroxide. Typically 80-100 mM peroxyxynitrite was obtained from this solution. The solution can be additionally diluted in 0.45 M sodium hydroxide to prepare the required concentrations.

2.6.3.3 Preparation of positive control of nitrated proteins

This was produced by incubating sample from mouse brain cortex with peroxyxynitrite solution prepared previously (see section 2.6.3.2), to obtain a positive control for anti-tyrosine Western blotting. 10 µl of protein sample in RIPA buffer was mixed with diluted peroxyxynitrite solution (0.1-1 mM), this was treated with GAB and heated for 5 minutes in boiling water bath.

2.6.4 Measurement of reactive oxygen species (ROS) in cortical tissue

2.6.4.1 Reagents and solutions

Cellular reactive oxygen species detection assay kit (DCFDA)-MitoSciences, ab113851 was used. This contain reactant reagent of 20 mM 2, 7-dichlororfluorescein diacetate, ROS inducer for positive control (55 mM tert-butyl hydrogen peroxide, TBHP) and buffer. A concentration of 40 µM DCFDA was used to give a final concentration of 20 µM in sample mixture.

2.6.4.2 Protocol

Samples from mice cortices were prepared as described in section 2.6.1.4, using the provided buffer for homogenization and protein concentration was determined using Bradford assay. A sample volume of 100 µl (4 µg / µl) was transferred into a black 96-micro-well plates and mixed with 100 µl of 40 µM DCFDA. A sample negative control which contains no DCFDA as well as a positive control which is a sample pretreated with 1 µl 55 mM TBHP and DCFDA were included. This strategy was applied for normal and test tissues. The positive control was to ensure if the enzymatic system and redox potential of both samples (wild and mutant) were efficient. The well plate was incubated at 37°C for 30 minutes and fluorescence detected at 485 nm of excitation and 520 emission spectra using Pherastar FS -BMG lab tech.

2.7 Assay of total phospholipase activity (PLA₂)

2.7.1 Reagents and solutions

EnzChek[®] Phospholipase A₂ Assay Kit, Catalog Number: E10217 (Invitrogen). This kit contains the following reagents:

- 1) PLA₂ substrate (Red / Green BODIPY[®] PC-A₂)
- 2) Dioleoylphosphatidylcholine (DOPC).
- 3) Dioleoylphosphatidylglycerol (DOPG).
- 4) Phospholipase A₂, enzyme from honey bee venom.
- 5) Dimethylsulfoxide (DMSO).
- 6) 5 x PLA₂ reaction buffer.

The solutions preparation and assay method were performed as recommended by the manufacturer.

2.7.1.1 Preparation of solutions

- 1) 1 mM PLA₂ substrate: one vial of this substrate was allowed to warm to room temperature and dissolved in 40 µl of DMSO. This was aliquoted and stored at -20°C until needed.
- 2) 1x reaction buffer: 1 ml of 10 x reaction buffer was diluted to 1x in deionized water, and stored at 4°C.
- 3) 10 mM of DOPC solution was prepared by dissolving the content of one DOPC vial in 100 µl of ethanol and stored at -20°C.
- 4) 10 mM of DOPG solution was prepared by dissolving the content of one DOPG vial in 100 µl of ethanol and this was stored at -20°C.
- 5) 500 Units / ml PLA₂ enzyme: this stock solution of the enzyme was prepared by dissolving one vial of PLA₂ enzyme into 80 µl of 1x reaction buffer.

2.7.1.2 Preparation of sample

Brain micel cortices were placed in 500 µl pre-cooled 1x reaction buffer provided. They were homogenized as described in section 2.6.1.4, the supernatant protein concentrations were determined using Bradford assay.

2.7.2 Protocol

Serial dilutions from PLA₂ enzyme (500 U / ml) were prepared for standard curve. They were ranging from 0-10 U / ml using 1x reaction buffer as a diluent. These all were prepared in a volume of 50 µl in each assigned well of black 96-micro-well plate.

A volume of 10 µl from 10 mM DOPC, 10 mM DOPG and 1 mM of PLA₂ substrate were mixed together, vortexed, and kept protected from light. This 30 µl of lipid mixture was injected slowly into 5 ml beaker containing 2.5 ml 1x reaction buffer, while vortex is formed for 1 minute. This gave a substrate-liposome mix which was kept protected from light.

Supernatants from brain cortex homogenate in a volume of 50 µl and 2 µg / µl proteins concentration were added to each assigned microplate well in duplicated similar volume of each sample was included for sample blank. To both standard and test sample, a volume 50 µl of substrate-liposome mix was added, and similar volume of 1x buffer was added to sample blank. The plate was protected from light and incubated at room temperature for 10 minutes. A Fluorescent measures were recorded at 485 nm excitation and 520 nm emission using Pherastar FS -BMG lab tech. Following this first measure, several times point was recorded.

The standard curve was built up from serial dilution of PLA₂ enzyme stock. Each reading for test sample was subtracted from the sample blank, this was to correct for background fluorescence. For each time point, an independent standard curve for PLA₂ activity was constructed and used for calculation of sample PLA₂ activities.

Figure 2.3

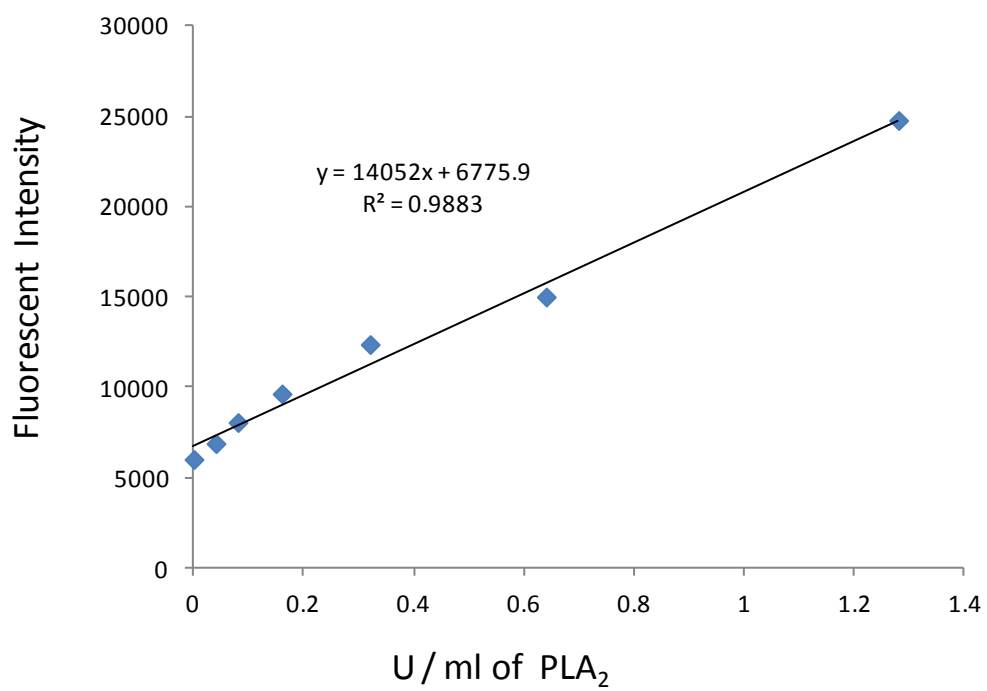


Figure 2.3 Representative standard curves for PLA₂ activity

CHAPTER 3

Investigation into ubiquitinated proteins in the
Psmc1^{fl/fl};CaMKII α -Cre mouse cortex

3.1 Introduction

Accumulation of ubiquitinated proteins associated with ubiquitin-positive protein inclusions is a consistent neuropathological feature of the major human neurodegenerative diseases (Lowe et al., 1993). Ubiquitin-positive protein inclusions and accumulation of ubiquitinated proteins are evident in the *Psmc1^{fl/fl};CaMKII α -Cre* mouse cortex following 26S proteasomal depletion making this a useful model to investigate ubiquitinated proteins in neurones *in vivo* (Bedford et al., 2008). Interestingly, Lewy bodies in PD and DLB contain lysine 48-specific ubiquitinated α -synuclein, suggesting impairment of the ubiquitin 26S proteasome system (Gorbatyuk et al., 2008).

Since protein ubiquitination is a dynamic process involving ubiquitination and deubiquitination, it is difficult to study ubiquitinated proteins without enrichment such as by proteasome inhibition. Therefore, a study of the *Psmc1^{fl/fl};CaMKII α -Cre* mouse cortex following 26S proteasomal depletion in neurones will be a valuable *in vivo* contribution to the current literature. Numerous large-scale proteomic studies investigating ubiquitinated proteins have been reported *in vitro* (Kirkpatrick et al., 2005; Jeon et al., 2007; Zhou et al., 2007; Bazile et al., 2008; Meierhofer et al., 2008). In these studies, cells were transfected with tagged ubiquitin, e.g. histidine-tagged ubiquitin, and ubiquitinated proteins were captured using ion metal affinity chromatography. These approaches have proved to be a useful research tool, but the ability to investigate ubiquitinated proteins in their physiological context *in vivo* such as in the mouse brain without overexpression or tagging would expand this data.

To our knowledge there are limited studies investigating the ubiquitome *in vivo* in the mouse brain. This study used affinity chromatography with immobilized ZNF216 protein. The rat ZNF216 protein sequence is 213 amino acid residues. It contains an N-terminal ZnF A20 ubiquitin binding domain (UBD) between amino acids 11-35 and a C-terminal ZnF AN1 domain between amino acids 154-191 (Huang et al., 2004a). Point mutation of the cysteine residues at positions 30 and 33 by alanine substitution (C30A/C33A) abrogates the ubiquitin binding of the A20 domain of ZNF216 protein (Hishiya et al., 2006). We have used ZNF216 affinity matrices to capture ubiquitinated proteins from the *Psmc1^{fl/fl};CaMKII α -Cre* cortex.

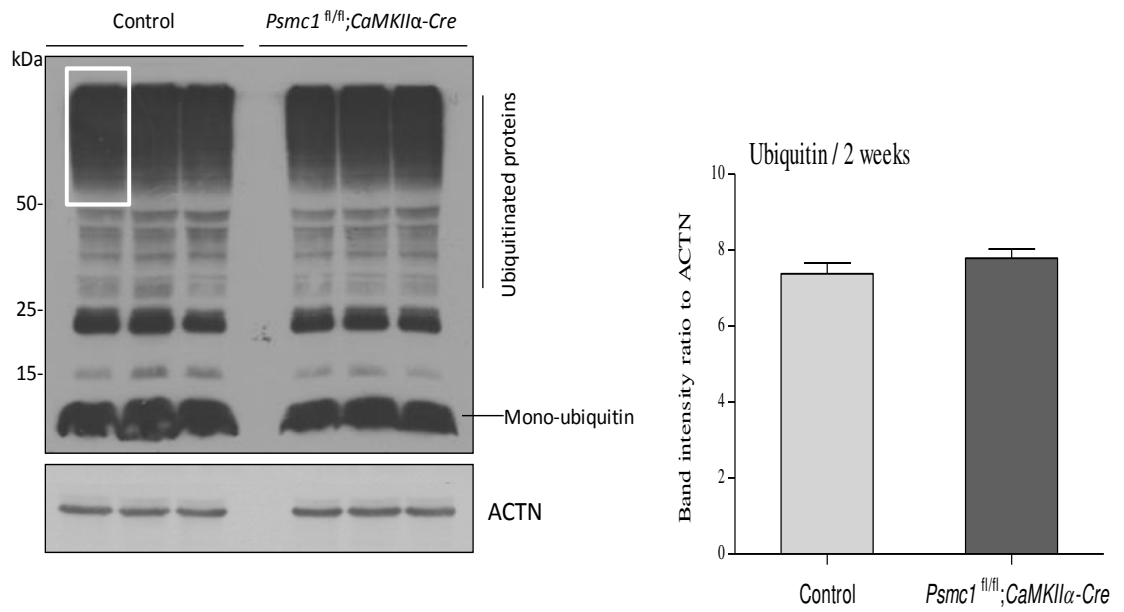
3.2. Results

3.2.1. Accumulation of polyubiquitinated proteins in *Psmc1^{fl/fl};CaMKII α -Cre* mouse cortex

Control and *Psmc1^{fl/fl};CaMKII α -Cre* mouse cortices were homogenized in urea homogenizing buffer and separated by 12 % SDS-PAGE. This was followed by overnight protein transfer to nitrocellulose membrane and Western blot analysis carried out using an in-house anti-ubiquitin rabbit polyclonal antibody. Cortical samples were investigated at 2, 3, 4 and 6 weeks of age. High molecular weight polyubiquitinated proteins increased with age (Figure 3.1A-D). Quantitation of the ubiquitin smear above 50 kDa showed a significant difference at 3, 4 and 6 weeks between *Psmc1^{fl/fl};CaMKII α -Cre* and control cortices ($p < 0.05$). The most significant difference was at 6 weeks of age. Therefore we decided to use 6 week-old mice for the investigations in this chapter. We also noted the presence of polyubiquitin chains in the *Psmc1^{fl/fl};CaMKII α -Cre* cortex which migrate similarly to the synthetic Lys48-specific polyubiquitin chains, suggesting the accumulation of free unanchored polyubiquitin in the *Psmc1^{fl/fl};CaMKII α -Cre* cortex compared to the control (Figure 3.1D).

Figure 3.1

A-2 weeks age



B-3 weeks age

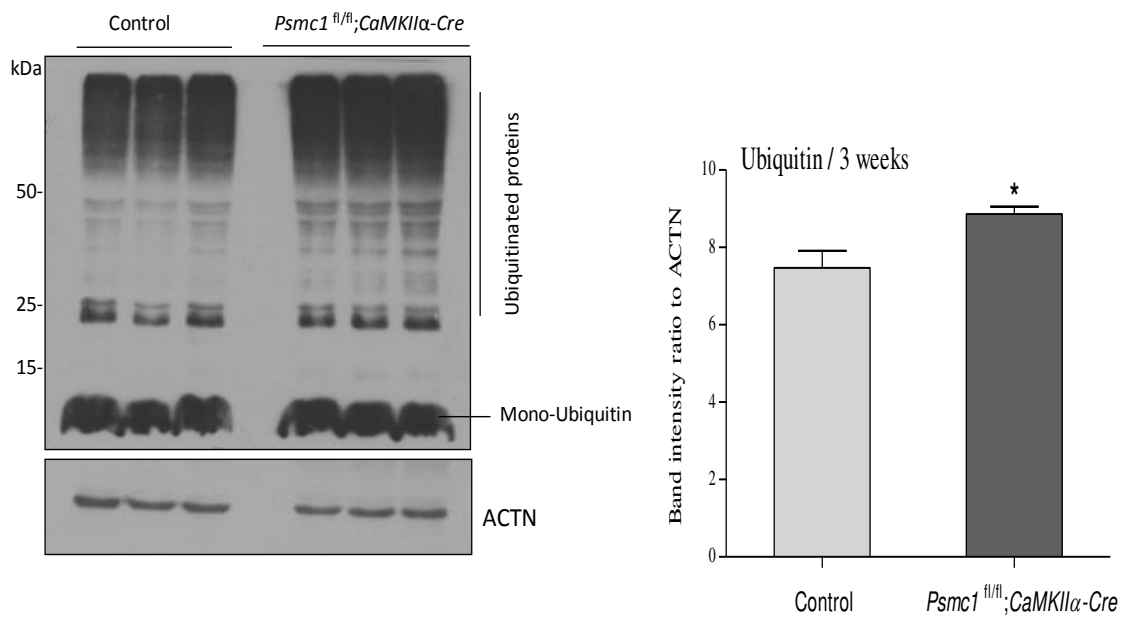
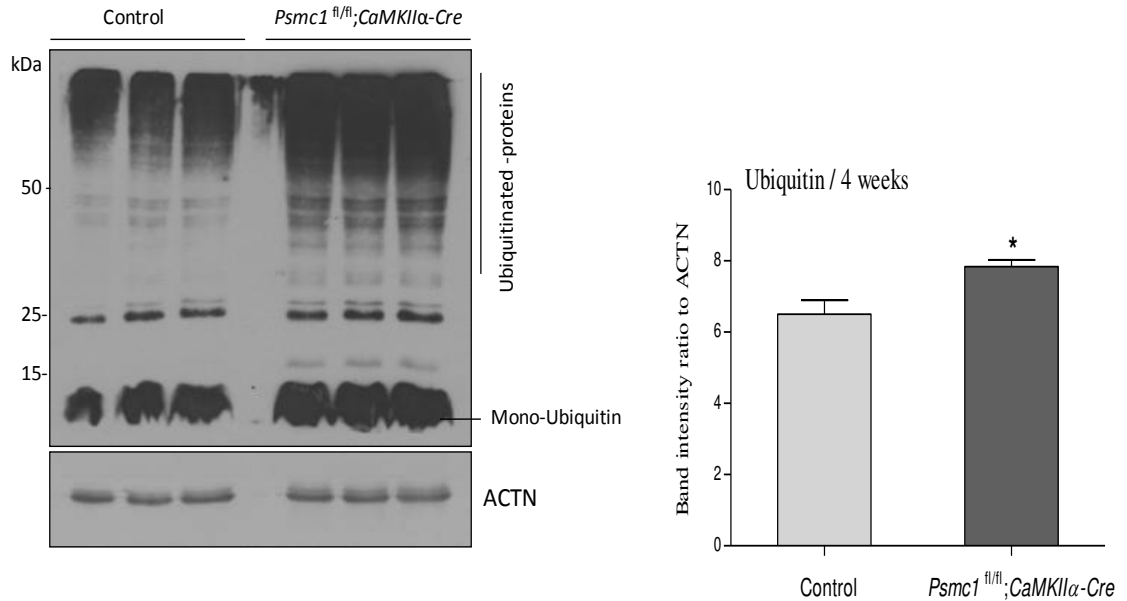


Figure 3.1 continued.

C- 4 weeks age



D-6 weeks age

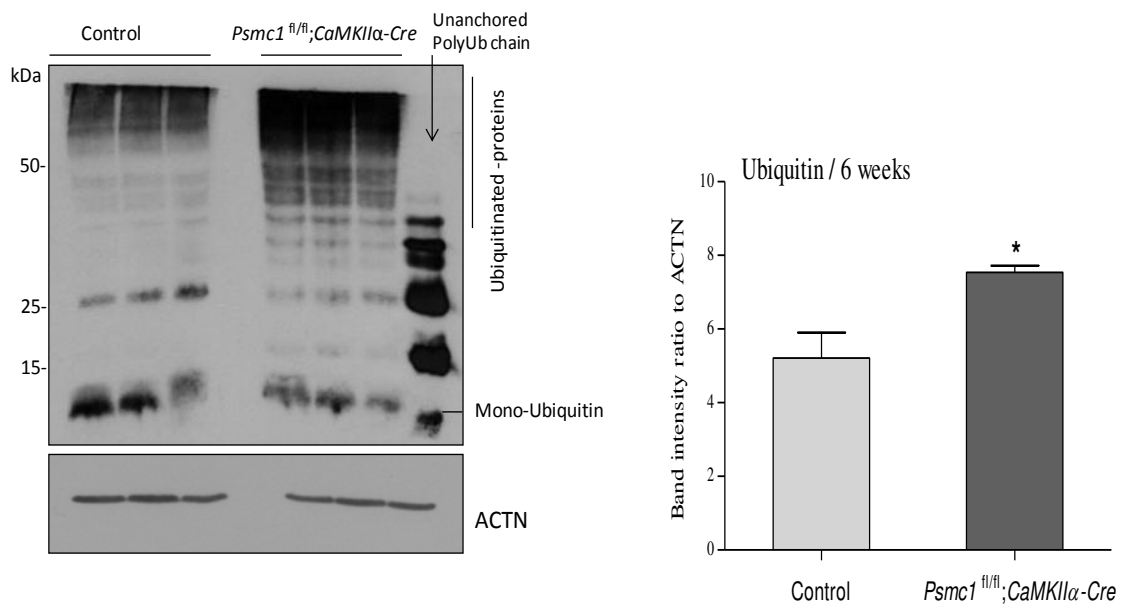


Figure 3.1 Anti-ubiquitin Western blot analysis of control and *Psmc1^{fl/fl};CaMKII α -Cre* cortex samples from mice at 2 (A), 3 (B), 4(C) and 6 (D) weeks of age. The left panel shows a representative Western blot image (50 μ g protein). The blot was stripped and re-probed with β -actin (ACTN) for normalization of protein loading. The right panel shows quantitation of the corresponding Western blot using densitometry (> 50 kDa; boxed region shown in A) normalized to β -actin. Data were analyzed versus control mice using unpaired student *t*-test and presented as mean \pm SEM (n = 3) **p* < 0.05.

3.2.2 Purification of ZNF216 recombinant proteins

This was carried out to prepare recombinant ZNF216 proteins for affinity matrices for the capture of ubiquitinated proteins. Wild-type and mutant GST-ZNF216 fusion proteins were expressed in *E.coli* cultures from plasmids encoding the corresponding GST-tagged ZNF216 proteins. Following growth ($OD_{600} = 0.6 - 0.8$), bacterial cells were lysed by sonication in TBS-Triton and clarified by centrifugation. The clarified supernatant was then incubated with glutathione (GSH)-Sepharose beads to purify the GST-fusion proteins. Figure 3.2A shows capture of the ZNF216-GST fusion proteins on GSH beads at approximately 52 kDa. The GSH beads-GST fusion proteins were then incubated with thrombin to cleave the ZNF216 proteins from their GST-tag. The GST-tag contains a sequence of six amino acids (Leu-Val-Pro-Arg-Gly-Ser) that are recognized by thrombin. Following cleavage ZNF216 proteins were collected in the flow from chromatography columns. The GST-tag remains bound to GSH beads. Cleaved ZNF216 wild-type and mutant proteins migrated at approximately at 34 and 32 kDa respectively on SDS-PAGE as shown in Figure 3.2B. We expect that both ZNF216 wild-type and mutant proteins have the same molecular weight, but the mutation causes them to migrate differently on SDS-PAGE. Figure 3.3 shows a schematic diagram representing the steps described in this section. The purified ZNF216 proteins were then immobilized onto another chromatographic solid phase (Cyanogen bromide activated sepharose beads) for affinity purification of ubiquitinated proteins (see section 3.2.3).

Figure 3.2

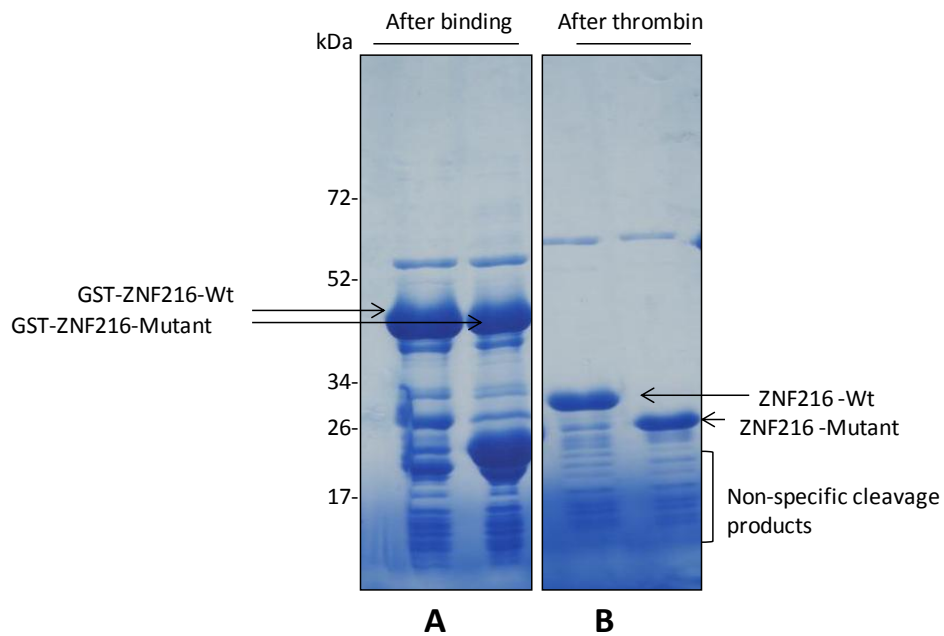


Figure 3.2 Coomassie Blue-stained SDS-PAGE gel showing immobilized GST ZNF216 fusion proteins and their thrombin cleavage. (A) Binding of GST ZNF216 fusion proteins to GSH beads as indicated by the arrows. The fusion proteins are approximately 52 kDa. (B) ZNF216 proteins following thrombin cleavage. ZNF216 wild-type (Wt) and mutant (C30/33A) migrated at approximately 34 kDa 32 kDa respectively.

Figure 3.3

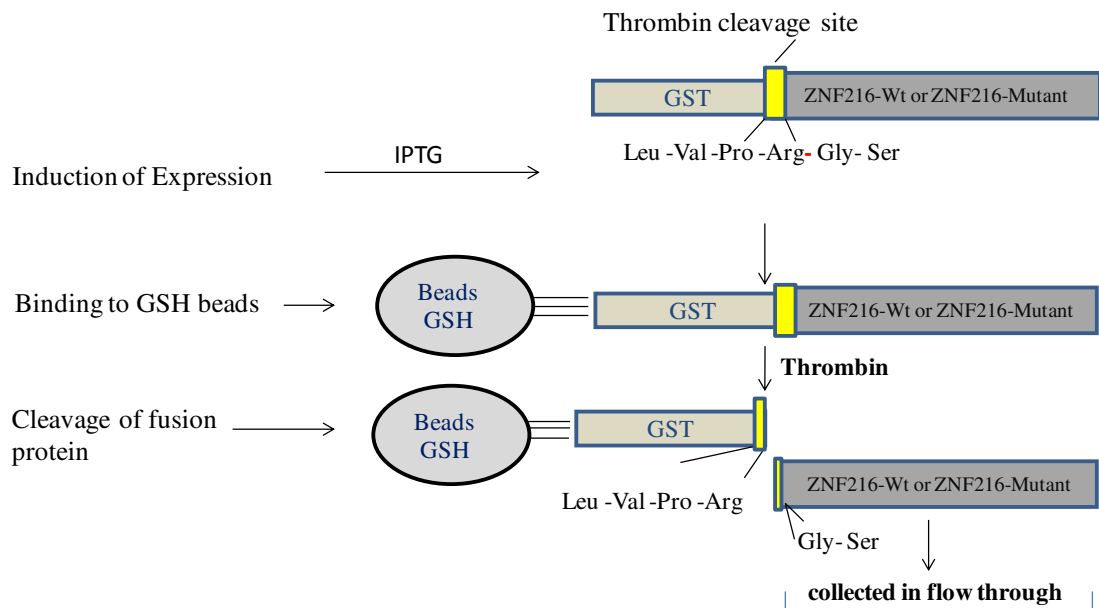


Figure 3.3 Schematic representation for the production of recombinant ZNF216 proteins. The expression of GST-ZNF216 recombinant proteins was induced in bacterial *E.coli* cultures with IPTG (isopropylthio- β -galactoside). This was followed by cell lysis and incubation of the clarified bacterial lysate with glutathione (GSH)-Sepharose beads in chromatographic columns. Following binding between GSH beads and GST-ZNF216 fusion proteins, thrombin was added to the column and incubated overnight at 4°C for cleavage of the ZNF216 fusion proteins. The flow through from the column containing the ZNF216 proteins was collected and kept for preparing ZNF216 affinity matrices. Samples from the GSH beads-GST ZNF216 fusion proteins and from the flow through were taken for SDS-PAGE analysis and are shown in Figure 3.2.

3.2.3 Preparation of ZNF216 affinity matrices for the capture of ubiquitinated proteins

Cyanogen bromide activated sepharose beads (CNBr beads) were used to immobilize purified ZNF216 recombinant proteins to provide a chromatography stationary phase (affinity matrices) for the capture of ubiquitinated proteins. CNBr beads have an imido-carbonate group that can bind to primary amines of proteins. Therefore, ZNF216 protein binds to CNBr beads through an amide bond.

Figure 3.4 shows the binding of purified recombinant ZNF216 proteins from section 3.2.2 with CNBr beads. We investigated two CNBr beads: ZNF216 protein ratios (1:1 and 1:4) to determine the optimal concentration of ZNF216 protein for preparing affinity matrices. The results show that both ratios investigated resulted in immobilizing ZNF216 proteins and we decided to use 1:4 for the preparation of affinity matrices.

Following binding of ZNF216 proteins to CNBr beads, the affinity matrices were washed and incubated with ethanolamine to block any remaining active sites. The ZNF216 affinity matrices were prepared in TBS to yield 50 % slurry (this slurry contains 50 % solid beads and 50 % buffer) and stored at 4°C.

Figure 3.4

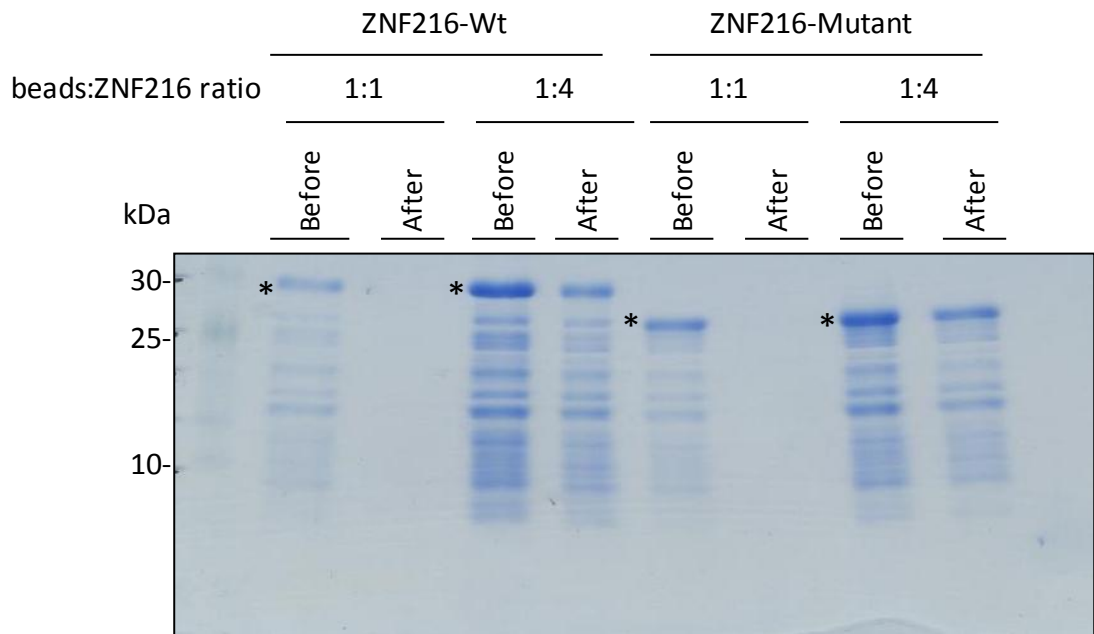


Figure 3.4 Binding of ZNF216 proteins to CNBr activated Sepharose beads. A Coomassie Blue-stained gel showing before (Before) and after (After) binding using two ratios: 1:1 and 1:4 beads: protein (μg protein: μl of beads volume). ZNF216 proteins are indicated by the *. Note that the lower molecular weight bands may be degradation products.

3.2.4 Binding of ubiquitinated proteins to ZNF216 affinity matrices

Cortical mouse tissue from control and *Psmc1^{fl/fl};CaMKII α -Cre* mice was homogenized in TBS-NP40 buffer using a glass dounce homogenizer. This results in detergent-soluble proteins for investigation. The buffer contained the cysteine protease inhibitor N-ethylmaleimide to inhibit deubiquitination as well as a protease inhibitor cocktail to inhibit trypsin-like activity in the mouse cortical homogenates.

Figure 3.5 shows a schematic representation for the capture of ubiquitinated proteins using ZNF216 affinity matrices. Previous studies have shown in mammalian cells *in vitro* that the ZNF216-Wt protein has the ability to bind ubiquitinated proteins, but that the ZNF216-mutant does not (Hishiya et al., 2006). Furthermore, the ZnF A20 ubiquitin binding domain of ZNF216 was used for affinity purification of endogenous polyubiquitin chains from skeletal muscle homogenates (Strachan et al., 2012).

Solubilized protein from brain tissue homogenates of the control and *Psmc1^{fl/fl};CaMKII α -Cre* mice were incubated with ZNF216-Wt or ZNF216-mutant affinity matrices. Capture of ubiquitinated proteins was investigated by Western blot analysis using an in-house anti-ubiquitin polyclonal rabbit antibody. The unbound fraction was also investigated by collecting the flow-through from the chromatographic column following incubation.

The results in Figure 3.6 show that ZNF216-Wt can capture ubiquitinated proteins (Figure 3.6; lanes 1 and 5), while the ZNF216-mutant does not (Figure 3.6; lanes 3 and 7). We sometimes note a very low ubiquitin signal in the ZNF216-mutant affinity matrix, but this is not significant compared to the ZNF216-Wt (Figure 3.6; lanes 5 and 7). We also note that the affinity matrices had no affinity for mono-ubiquitin. ZNF216-Wt affinity matrices capture mostly high molecular weight ubiquitinated proteins (Figure 3.6). We were interested in the identity of these ubiquitinated proteins and these were significantly increased in the *Psmc1^{fl/fl};CaMKII α -Cre* cortex (Figure 3.6; lanes 1 and 5). The ZNF216-mutant affinity matrix is a suitable control for any false positive proteins bound to the ZNF216 protein via a domain other than the ubiquitin binding domain.

Figure 3.5

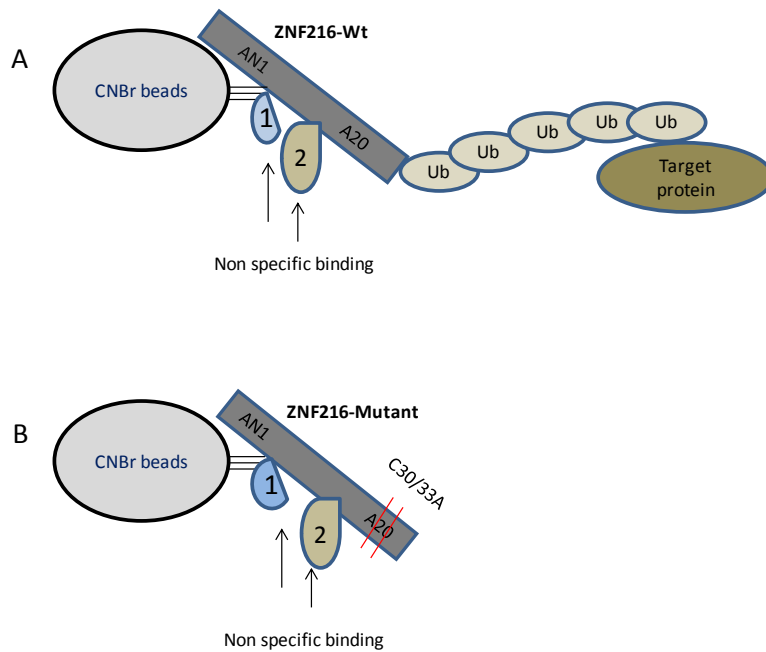


Figure 3.5 Schematic representation of the capture of ubiquitinated proteins using ZNF216 affinity matrices. Purified ZNF216-Wt (A) and ZNF216-mutant (B) were coupled to CNBr beads to produce affinity matrices. Affinity matrices were incubated with clarified homogenates from mouse brain cortex. The ZNF216-Wt affinity matrix should capture ubiquitinated proteins, whilst the ZNF216-mutant affinity matrix should not. The ZNF216-mutant is used as a control for proteins that bind to ZNF216 through domains other than the A20 ubiquitin binding domain, e.g. 1 and 2.

Figure 3.6

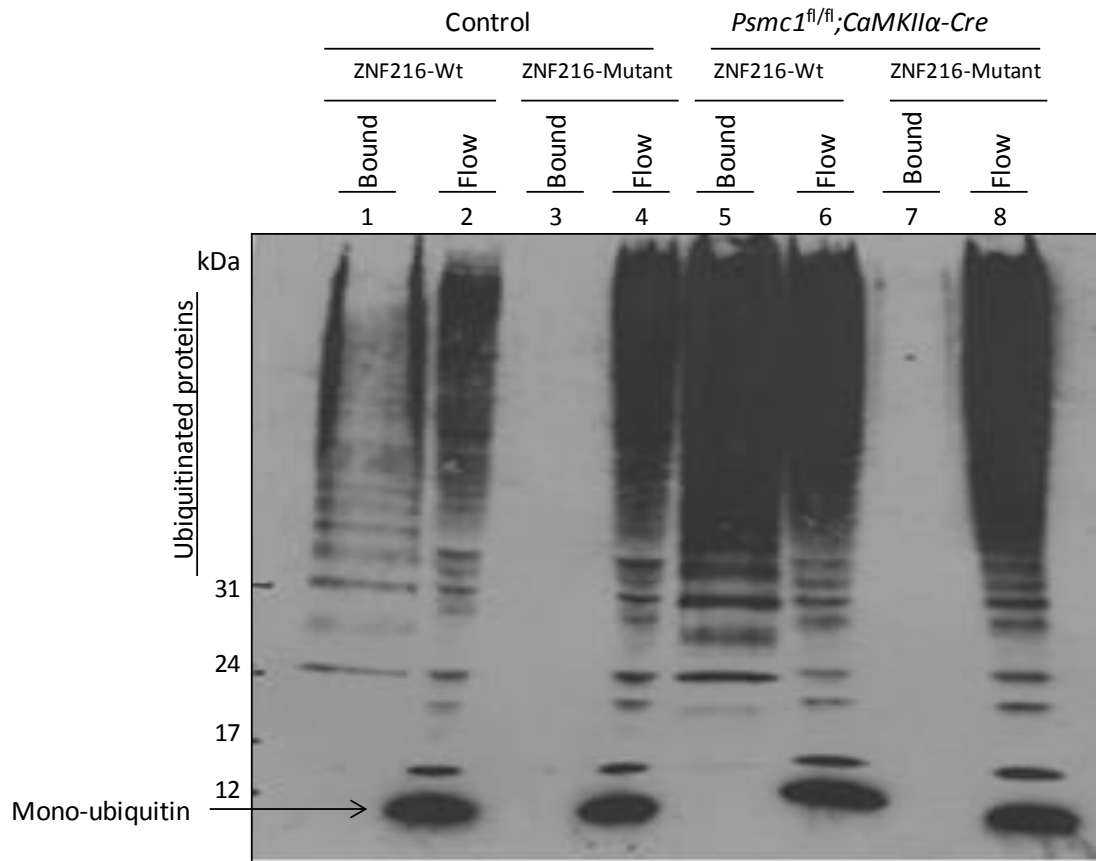


Figure 3.6 Capture of ubiquitinated proteins from mouse brain. Anti-ubiquitin Western blot following incubation of ZNF216-Wt and ZNF216-mutant affinity matrices with cortical homogenates from control and *Psmc1^{fl/fl};CaMKII α -Cre* mice at 6 weeks-old. Ubiquitinated proteins appear as a high molecular weight smear. ZNF216-Wt matrices capture ubiquitinated proteins (lanes 1 and 5) whilst the ZNF216-mutant do not (lanes 3 and 7). The Western blot shows the captured ubiquitinated proteins (bound) as well as a sample of the flow-through following binding (flow).

3.2.5 Evaluation of the binding capacity of ZNF216-Wt affinity matrices

We sought to evaluate the binding capacity of ZNF216-Wt affinity matrices. This was to determine the protein concentration required for optimal capture of ubiquitinated proteins. The aim was to capture sufficient ubiquitinated proteins for subsequent identification by mass spectrometry.

The binding capacity was evaluated using a constant amount of matrices (50 μ l of 50 % slurry) with increasing amounts of protein homogenate from *Psmc1*^{fl/fl}; *CaMKII α -Cre* mouse cortex (50-200 μ g). Figure 3.7 shows that high molecular weight ubiquitinated proteins consistently bound to ZNF216-Wt matrices and this increased with the increasing amounts of cortical protein homogenate.

Figure 3.7

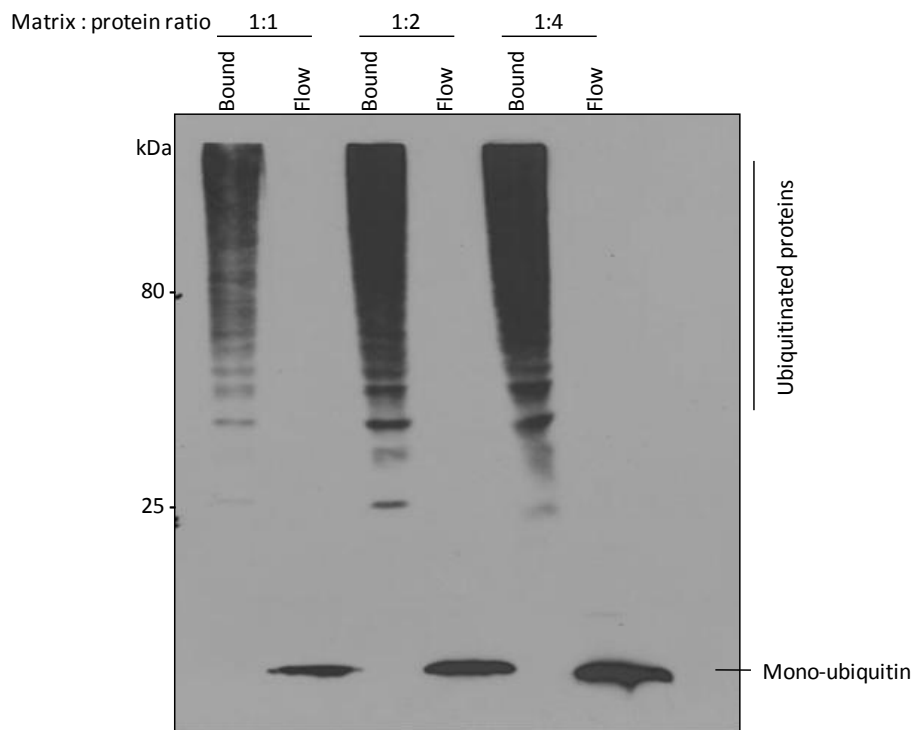


Figure 3.7 Evaluation of the binding capacity of ZNF216-Wt affinity matrices. An anti-ubiquitin Western blot following incubation of 50 μ l of affinity matrices with 50 (1:1), 100 (1:2) and 200 (1:4) μ g of protein from *Psmc1^{fl/fl};CaMKII α -Cre* brain cortex at 6 weeks of age.

3.2.6 Deubiquitination of captured ubiquitinated proteins using ubiquitin specific protease 2

Using a commercially available deubiquitinase (DUB) enzyme with ubiquitin specific protease activity (USP2), the ubiquitinated proteins captured by ZNF216 affinity matrices were deubiquitinated, releasing the proteins from the matrices for further identification. USP2 has been shown *in vitro* to trim ubiquitinated proteins and unanchored polyubiquitin chains bound to affinity matrices (Shahnawaz et al., 2007). Figure 3.8 shows a schematic representation of the deubiquitination of captured polyubiquitinated proteins on ZNF216-Wt affinity matrices using USP2. Target proteins captured via the A20 ubiquitin binding domain are released into the soluble phase that can be used for target protein identification by mass spectrometry.

The deubiquitination activity of USP2 was investigated by ubiquitin Western blotting using ZNF216-Wt affinity matrices bound to cortical homogenate as well as synthetic Lysine-48 unanchored polyubiquitin chains. Figure 3.9 shows that USP2 deubiquitinated the captured polyubiquitinated proteins on ZNF216-Wt affinity matrices. The high molecular weight ubiquitin smear or synthetic polyubiquitin chain changed to mono-ubiquitin and some di-ubiquitin (Ub₂) after incubation with DUB enzyme.

Following elution of proteins from the ZNF216 matrices, the elute was subjected to in-solution digestion followed by Liquid chromatography–mass spectrometry (LC/MS-MS) in Biomedical Sciences, University of Nottingham. However, the protein identification using this method of analysis was limited. Candidate proteins were identified with low mascot scores and number of peptides. It is possible that the amount of protein captured by the affinity matrices was too low for this method of identification and further experiments were carried out to optimize the results.

Figure 3.8

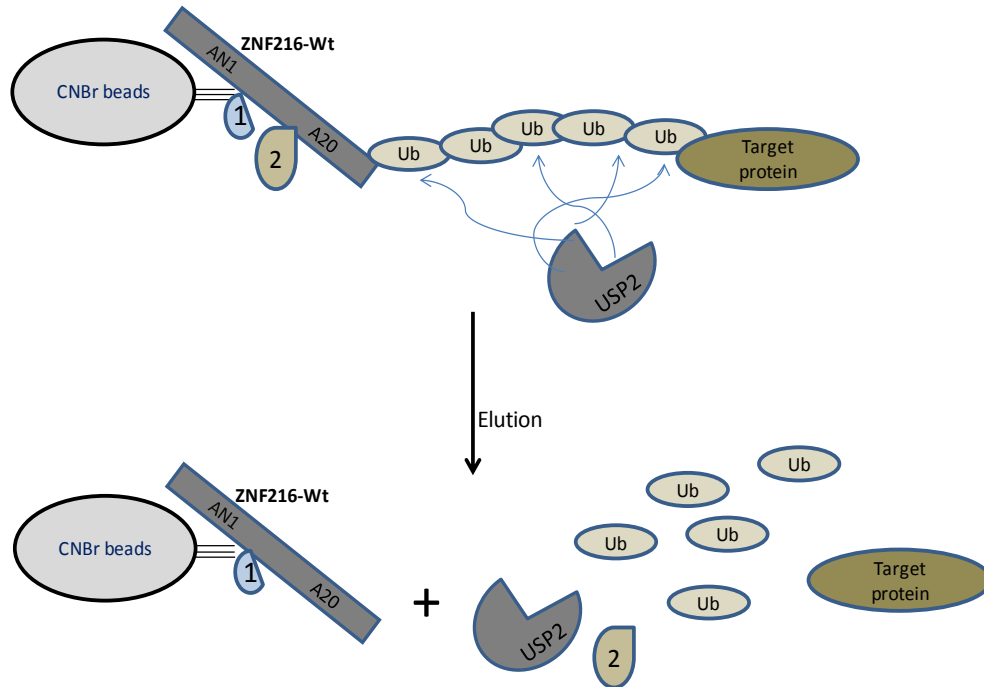


Figure 3.8 Schematic representation of deubiquitination using USP2. Target proteins captured via the A20 ubiquitin binding domain are released into the soluble phase by incubation with ubiquitin specific protease 2 (USP2). The elute was collected for target protein identification by mass spectrometry. Proteins identified in the ZNF216-Wt, but not in the ZNF216-Mutant will be considered as ubiquitinated proteins. Proteins also identified in the ZNF216-Mutant will be non-specific, e.g. protein 2.

Figure 3.9

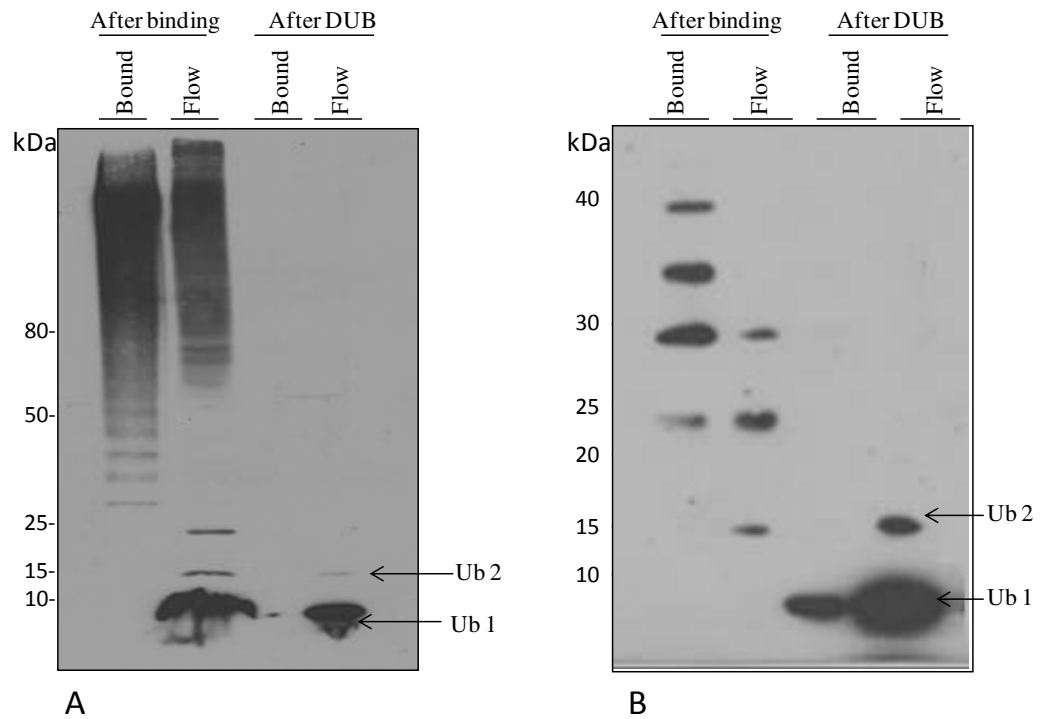


Figure 3.9 Ubiquitin Western blot showing deubiquitination of captured polyubiquitinated proteins using USP2 DUB enzyme. (A) ZNF216-Wt affinity matrices bound to proteins from cortical mouse brain homogenate (bound). (B) ZNF216-Wt affinity matrices bound to synthetic Lysine -48 polyubiquitin chains (bound). DUB enzyme action results in the loss of the high molecular weight ubiquitin smear associated with the matrices and the appearance of mono-ubiquitin in addition to some di-ubiquitin in the flow-through (flow). Ub1, mono ubiquitin; Ub2, di-ubiquitin.

3.2.7 Two dimensional profile of proteins bound to ZNF216 affinity matrices

To optimize the identification of target proteins captured using ZNF216 affinity matrices, we used 2-dimensional gel (2-DG) electrophoresis in addition to the in-solution digestion for mass spectrometry described in section 3.2.6. Two modifications were made to this experiment: (1) a 4-fold increase (10 mg) of *Psmc1^{fl/fl};CaMKII α -Cre* cortical homogenate was used; and (2) following protein elution from ZNF216 affinity matrices, the elute was filtered through a 5 kDa filter to concentrate the protein before mass spectrometry. The concentrated protein samples were subjected to 2DG electrophoresis as described in the section 2.3.4, and stained with silver nitrite compatible with mass spectrometry.

Figure 3.10 shows the 2DG profile of proteins eluted from ZNF216-Wt and ZNF-Mutant affinity matrices. The arrows show a small number of spots were detected in the ZNF216-Wt sample (Figure 3.10A). These spots were visible in the stained gel above a light box and 8 spots were excised from the gel and prepared for mass spectrometry. These spots were submitted for identification by MALDI-TOF-MS. These spots were not detected in the ZNF216-Mutant 2DG (Figure 3.10B).

This approach only identified one protein (Figure 3.10A; ubiquitin). This was most likely due to the low protein abundance in the spots for identification by the mass spectrometry approach. The identified spot at approximately 10 kDa was identified as ubiquitin (Figure 3.10A). This had a mascot score of 132 (a significant score for mascot is > 55) and 52% peptide coverage of the candidate protein.

Figure 3.10

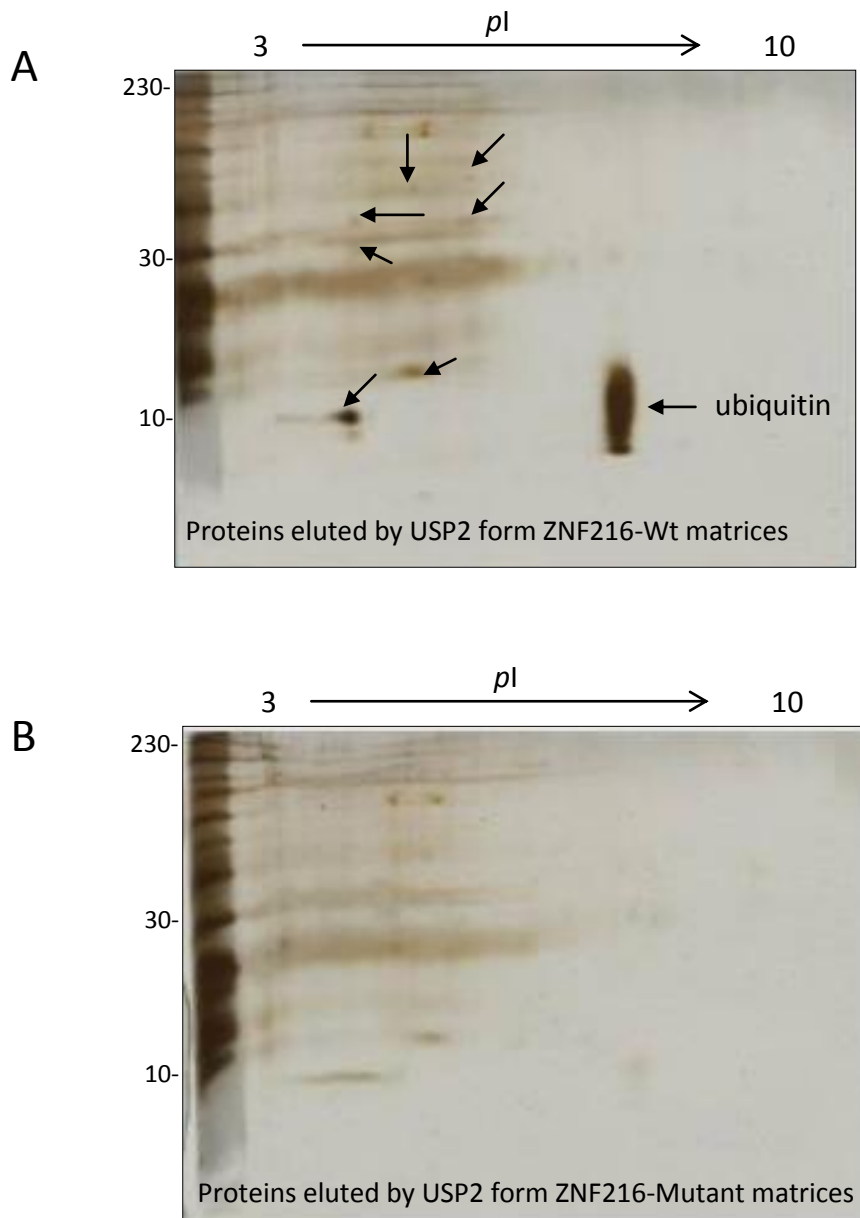


Figure 3.10 Two dimensional gel electrophoresis protein profiles following elution of ubiquitinated proteins from ZNF216-Wt (A) and ZNF216-Mutant (B) affinity matrices. Proteins were captured using ZNF216 affinity matrices from 6 weeks of age *Psmc1^{fl/fl};CaMKII α -Cre* cortical tissue and eluted with DUB enzyme. The eluted proteins were subjected to 2DG electrophoresis and silver staining. Arrows indicate spots that were excised and processed for MADLI-TOF mass spectrometry protein identification.

3.2.8 One dimensional profile of proteins bound to ZNF216 affinity matrices

The 2DG electrophoresis approach was unsuccessful (see section 3.2.7); therefore we used one dimensional gel (1DG) separation following concentration of the eluted target proteins as described in section 3.2.7. This approach minimizes any loss of sample as a consequence of the IEF. Figure 3.11 shows several discreet protein bands in the ZNF216-Wt sample that are not evident in the ZNF216-Mutant. Twenty one bands were excised from the ZNF216-Wt lane and prepared for MALDI -TOF-MS identification. Table 3.1 shows the proteins that were identified. Although two proteins had a mascot score below 55, they were included as potential ubiquitin-bound proteins because multiple peptides were identified.

The proteins bands denoted by asterisks in Figure 3.11 were present in both ZNF216-Wt as well as ZNF216-Mutant eluted fractions. However, they were more abundant in the ZNF216-Wt sample. Band 3* was identified as Tryptophanyl-tRNA synthetase -1, cytoplasmic. Bands 1* and 2* were ubiquitin. This suggests that the ZNF216-Mutant may associate with low levels of ubiquitin or there is some non-specific binding when using relatively high cortical protein concentrations.

Figure 3.11

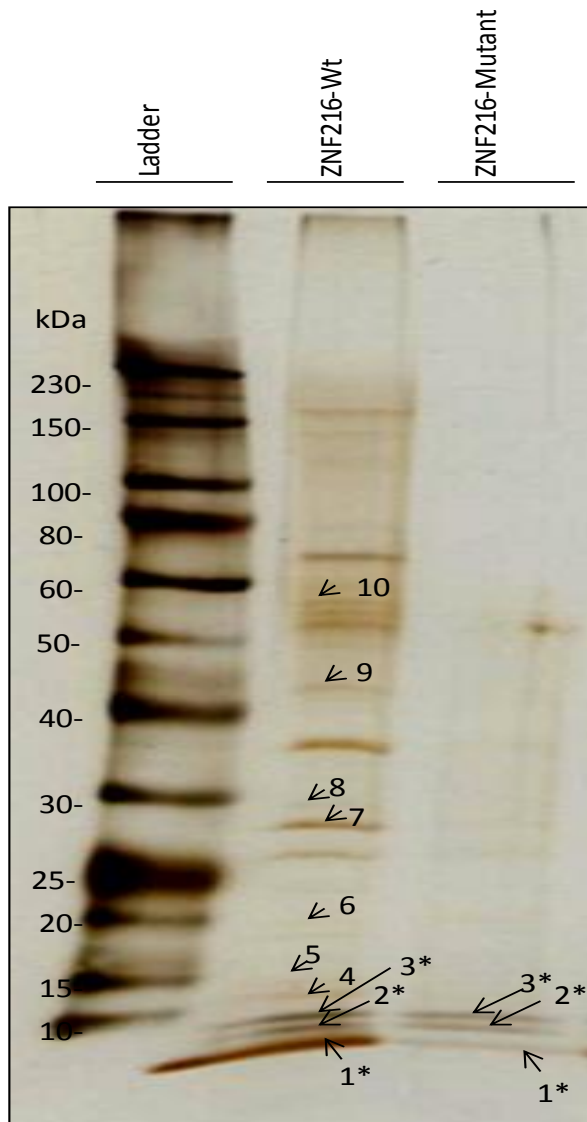


Figure 3.11 One dimensional gel electrophoresis protein profiles following elution of ubiquitinated proteins from ZNF216-Wt and ZNF216-Mutant affinity matrices. Proteins were captured using ZNF216 affinity matrices from 6 weeks of age of *Psmc1^{fl/fl};CaMKII α -Cre* cortical tissue and eluted with DUB enzyme. The eluted proteins were subjected to 1DG electrophoresis and silver staining. The labeled bands correspond to Table 3.1.

Table 3.1 Proteins identified by MALDI-TOF mass spectrometry. The table corresponds to Figure 3.11.

Band number	NCBI-Gene ID	Uni Prot Accession code	STRING Accession code	Protein ID	Mascot Score ⁱⁱ	Matched peptides ^γ	Sequence coverage (%) ^φ
1*	22186	RL40_MOUSE	Uba52/ Ubc/ Ubb	Ubiquitin-60S ribosomal protein L40 (Ub peptides)	122	10	52
2*	22186	RL40_MOUSE	Uba52/ Ubc/ Ubb	Ubiquitin-60S ribosomal protein L40 (Ub peptides)	77	6	35
3*	7453	SYWC_MOUSE	Wars	Tryptophanyl-tRNA synthetase	64	9	22
4	68972	TATD3_MOUSE	Tatdn3	Putative deoxyribonuclease	61	6	16
	22186	RL40_MOUSE		Ubiquitin-60S ribosomal protein L40 (Ub peptides)	58	8	54
5	14569	GDIB_MOUSE	Gdi2	Rab GDP dissociation inhibitor beta	56	10	32
6	53379	ROA2_MOUSE	Hnrnpa2b1	Heterogeneous nuclear ribonucleoproteins A2/B1	149	15	24
7	227682	TRUB2_MOUSE	Trub2	Probable tRNA pseudouridine	83	13	42
8	871	SERPH_MOUSE	Serpinh1	Serpin H1	51 ⁺	7	29
9	60	ACTB_MOUSE	Actb	Actin- cytoplasmic 1	79	10	43
10	7257	TSNAX_MOUSE	Tsnax	Translin-associated protein X	52 ⁺	11	37

* represents ubiquitin peptides.

ⁱⁱ Mascot score is a statistical score for how well the experimental data (peptide masses) match the database sequence. A score value of 55 or more represents significant values ($p < 0.05$). ⁺Lower values can be considered if matched protein appears at the top of the hit list of the resultant identified proteins.

^γ Matched peptides are the number of peptides identified as matching the database sequence of candidate protein.

^φ Sequence coverage is the percentage of the database protein sequence covered by matching peptides from the experimental data. The larger the sequence coverage the more certain is the identification.

3.3 Discussion

3.3.1 Age-related accumulation of polyubiquitinated proteins and unanchored polyubiquitin chains

Ubiquitinated proteins are a consistent feature of the major human neurodegenerative diseases (Lowe et al., 1993). Therefore, it is of considerable interest to identify proteins that are targeted for ubiquitination in neurones to understand physiological as well as pathological cellular pathways associated with the UPS. Our mouse with neuronal 26S proteasomal depletion (*Psmc1^{fl/fl};CaMKII α -Cre*) provides a novel model in which ubiquitinated proteins can be investigated *in vivo*.

This study showed an age-related increase in polyubiquitinated proteins between two and six weeks of age in *Psmc1^{fl/fl};CaMKII α -Cre* compared to control mice cortex. Previously, we reported that 26S proteasomal depletion in cortical neurones caused neurodegeneration and the formation of ubiquitin-positive intraneuronal inclusions resembling human pale bodies at 6 weeks of age (Bedford et al., 2008). Components of the UPS have recently been linked to the quality control system for aberrant proteins (Pegoraro et al., 2012; Chhangani et al., 2013).

Interestingly we note the possibility of increased unanchored polyubiquitin chains following 26S proteasomal depletion in the *Psmc1^{fl/fl};CaMKII α -Cre* cortex. Figure 3.1 D shows ubiquitin bands on Western blot at 6 weeks of age corresponding to the synthetic unanchored lysine-48 polyubiquitin. Classically, the 26S proteasome has been associated with the degradation of polyubiquitinated proteins (Liu and Jacobson, 2012). However, our observation suggests that the proteasome may also be involved in the degradation of free polyubiquitin chains and further investigations in this model will be valuable. For example, it will be interesting to study whether free unanchored polyubiquitin accumulated within the ubiquitinated inclusion bodies following 26S proteasomal depletion in mouse neurones.

Lysine-48 and lysine-11 linked unanchored polyubiquitin have been identified in rat skeletal muscle (Strachan et al., 2012). Interestingly, evidence suggests that unanchored polyubiquitin chains can be metabolised by specific enzymes, supporting an important physiological role in the cell. USP5 enzyme has been shown to specifically trim unanchored lysine-48 chains in mammalian cells (Dayal et al., 2009).

In addition, unanchored Lysine-63 polyubiquitin chains have been investigated as a signal to activate innate immunity against viruses (Zeng et al., 2010).

In our study, the increase in unanchored polyubiquitin chains may represent the cellular activation of enzymes that release polyubiquitin chains from conjugated proteins or the expression of ubiquitin may be increased to compensate for 26S proteasome failure. The latter possibility is not supported because the levels of mono-ubiquitin in *Psmc1^{fl/fl};CaMKII α -Cre* cortex were not significantly different from controls (Figure 3.1). A previous study has shown the release of unanchored polyubiquitin chains from the ubiquitinated proteins by the action of DUB enzymes such as ataxin 3 following chemical inhibition of the 20S proteasome by MG132 (Ouyang et al., 2011).

3.3.2 Capture of ubiquitinated proteins from the *Psmc1^{fl/fl};CaMKII α -Cre* cortex

Previous studies have shown that ubiquitin binding domains (UBD) can be used for the capture of ubiquitinated proteins from protein homogenate (Ventadour et al., 2007). The A20 UBD of ZNF216 has been shown to behave as a shuttle protein for the proteasome (Hishiya et al., 2006). The A20 ZnF domain binds to a polar patch on ubiquitin molecules at Aspartate-58 (Hurley et al., 2006). In our study we have used the ZNF216 protein to produce affinity matrices for the capture of ubiquitinated proteins from mouse brain. The ZNF216-Wt affinity matrices captured ubiquitinated proteins, but not mono-ubiquitin. A previous study showed that diverse polyubiquitin chains accumulated following 26S proteasomal depletion in the mouse brain (Bedford et al., 2011) that may be captured in this study. A ZNF216-mutant in the A20 domain was used as a control that did not capture ubiquitinated proteins.

The aim was to use the ZNF216 affinity matrices to capture ubiquitinated proteins for subsequent identification by mass spectrometry. The major disadvantage of our approaches was the low abundance of proteins for identification. It is possible that these were below the detection limits of the mass spectrometry available for this study.

Using 2DG electrophoresis, only ubiquitin was identified and would be the most abundant protein in the sample of captured polyubiquitinated proteins. The 1DG

electrophoresis approach proved to be more informative leading to the identification of 8 potential target proteins in *Psmc1^{fl/fl};CaMKII α -Cre* cortex. Further explanations for the low target identification in this study are described. It is possible that the target proteins are ubiquitinated with extensive polyubiquitin chains, including branched chains, which would skew the identification of the lower abundance target protein. Alternatively, a large proportion of the sample may be unanchored polyubiquitin chains and therefore not attached to target proteins. This would lead to the identification of ubiquitin.

Overall, we identified a relatively low number of target proteins. Increasing the amount of cortical protein homogenate may improve these results together with the use of a more sensitive mass spectrometry such as the Orbi-trap.

The candidate proteins identified in this study were investigated to identify cellular pathways that might be affected in the brain of *Psmc1^{fl/fl};CaMKII α -Cre* mouse cortex following proteasomal dysfunction using software such as STRING (<http://string-db.org>) and UniProt (<http://www.uniprot.org>). An example of the results from STRING is shown in Figure 3.12. Experimental studies have shown an interaction between ubiquitin and the Translin-associated protein X. Also, there is literature to suggest an interaction between ubiquitin and actin.

The proteins identified in this study function in gene expression and regulation. The heterogeneous nuclear ribonucleoproteins A2/B1 are RNA binding proteins involved in the processing of primary mRNA transcripts to yield functional mRNA and transport to the cytoplasm (Dreyfuss et al., 1993). Translin-associated protein X is post-translationally modified by sumoylation by small ubiquitin-like modifier protein (SUMO) which is not for proteasomal degradation. It is thought to act with the RNA and DNA binding protein Translin in DNA damage response, RNA transport and translational control (Jaendling and McFarlane, 2010). The tryptophanyl-tRNA synthetase protein catalyzes tryptophanyl-tRNA^{trp} formation. This protein is abundant in brain tissue and post-translationally modified by phosphorylation. The protein activates signal transduction such as extracellular signal-regulated kinases pathways. tRNA pseudouridine functions in RNA processing such as splicing and production of mature RNA. Putative deoxyribonuclease has a role in DNA hydrolysis and the guanosine diphosphate (GDP) dissociation inhibitor beta regulates the

GDP/GTP exchange. Serpin H1 (47 kDa heat shock protein or serine (or cysteine) peptidase inhibitor) may behave as a chaperone in the collagen biosynthetic pathway. Serpins are a superfamily that share the same well-conserved structure, but differ in their function (Silverman et al., 2001). Inclusions containing neuro-serpin (one of the serpin family) aggregates have been described in brain sections from familial dementia patients. This was confirmed by a Western blotting study and indicated to be due to amino acid substitutions leading to protein conformational changes and aggregation (Davis et al., 2002). Actin is a cytoskeletal protein that has been shown to be post-translationally modified by ubiquitin, supporting our findings. The proteins identified in this study, except for actin, have not previously been reported as targets for ubiquitination. These results may suggest a feedback between systems controlling protein synthesis and degradation.

Although potential ubiquitinated proteins were identified in this study, the use of a more sensitive mass spectrometer may significantly improve the results.

Figure 3.12

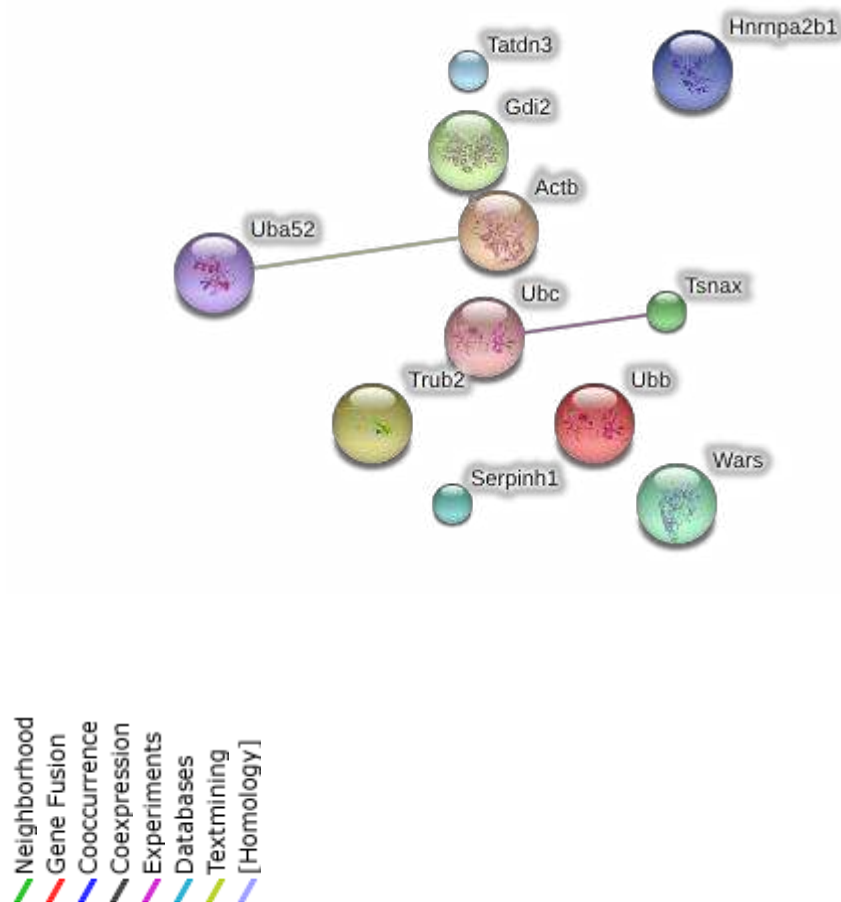


Figure 3.12 The results of STRING software analysis of proteins identified in Table 3.1.

STRING is a database of known protein interactions or association (functional) sourced from genomic context, high-throughput experiments and previous knowledge from Pubmed. Different line colours represent the interaction type and association.

- Experiments line; indicates interaction detected by experimental work (high score of interaction);
- Textmining line represents the association of two protein in publications (low score)

Uba52 and Ubc, Ubiquitin; Wars, tryptophanyl-tRNA synthase; Tatdn3, Putative deoxyribonuclease; Gdi2, Rab GDP dissociation inhibitor beta; Hnmpa2b1, Heterogeneous nuclear ribonucleoproteins A2/B1; Trub2, Probable tRNA pseudouridine; Serpinh1, Serpin H1; Actb, Actin-cytoplasmic 1; TsnaX, Translin-associated protein X.

CHAPTER 4

Proteomic investigation of the *Psmc1^{fl/fl};CaMKII α -Cre* mouse cortex reveals differential expression of cytoskeletal, antioxidant and mitochondrial proteins

4.1 Introduction

Proteomic studies have been used to investigate protein networks involved in several disease states, including neurodegeneration. These studies include the analysis of protein expression levels, protein-protein interactions and post-translational modifications. Differential protein expression between normal and diseased samples may lead to the discovery of early potential biomarkers for specific disease states, decipher mechanisms involved in disease progression and identify pharmacological targets.

Proteome investigations are based on the understanding that proteins mediate an important part of the biological actions in the cell. Although mRNA is the molecule for protein synthesis, numerous factors can prevent the linear association between mRNA and protein expression level, including post-transcriptional changes in mRNA and post-translational protein modifications which might affect protein function (Anderson and Seilhamer, 1997; Gygi SP, 1999).

Global profiling of protein expression based on 2-dimensional fluorescence difference in-gel electrophoresis (2-D DIGE) was introduced by Unlu *et al* in 1997 (Unlü M, 1997). This is a sensitive technique to resolve and visualize thousands of proteins spots following two-dimensional protein analysis gel electrophoresis (2-D PAGE). The 2-D DIGE has now been extensively used in research, including investigations of animal models and clinical research. The 2-D DIGE method depends on minimal labeling of the protein sample by fluorescent dyes called cyanine dyes (CyDyes: Cy2, Cy3, and Cy5). These dyes carrying N-hydroxysuccinimidyl ester group can covalently bind to the ϵ -amino groups of lysine residues of proteins. They have a matched charge and mass and therefore do not cause differences in protein migration. Normally, Cy3 and Cy5 are used for sample labeling (control and diseased) and Cy2 for labeling a pooled mixture from all samples to be analyzed (internal standard). Because of the distinct excitation and emission spectra of each CyDye, the labeled samples and internal standard are mixed and run together on a single 2-D PAGE gel. This technique minimizes gel-to-gel variability, allowing easily protein spot matching for analysis. In general, the separation of proteins by 2-D electrophoresis, according to their *pI* and molecular weight, is crucial for investigating protein isoforms and post-translational modifications. 2-D electrophoresis is usually coupled to mass

spectrometry for identification of proteins spots of interest. Previous studies have shown 2-D DIGE to be a sensitive and reproducible technique for differential protein expression analysis (Gharbi et al., 2002; Kurz et al., 2012).

2-D DIGE of the striatum from a Parkinson's disease mouse model over-expressing α -synuclein (A53T-SNCA) coupled to mass spectrometry identified differentially expressed proteins associated with pre-synaptic dysfunction, bioenergetics failure and dysregulation of cytoskeletal proteins (Kurz et al., 2012). A similar study in the cortex and striatum of a Parkin knockout mouse showing behavioural and biochemical changes related to PD revealed dysregulation of proteins involved in energy metabolism, stress, protein folding and degradation by the UPS (Periquet et al., 2005). 2-D DIGE has also been used in the clinical research field to search for disease biomarkers. Investigations of the proteome of CSF from normal, PD and PDD showed changes in the levels of specific proteins that may be promising biomarkers for PD and dementia developed in PD (Jesse et al., 2012; Wang E-S, 2010). These studies involving animal models as well as clinical research support the use of 2-D DIGE coupled to mass spectrometry for a comprehensive proteomic study into neurodegeneration presented here.

The conditional deletion of $Psmc1^{fl/fl};CaMKII\alpha-Cre$ expressing neurones of mouse brain was associated with neuropathological changes resembling human dementia with Lewy bodies (DLB), i.e. neurodegeneration and the formation of Lewy-like inclusions in surviving neurones of the cortex. Immunohistochemical staining also showed significant gliosis as indicated by glial fibrillary acidic protein (GFAP) as well as expression of p53 and cleaved caspase 9 (Bedford et al., 2008). An *in vitro* model of $Psmc1$ -KO in mouse embryonic fibroblasts further revealed changes in genes linked to apoptosis such as Bcl2 (Bedford et al., 2008). The $Psmc1^{fl/fl};CaMKII\alpha-Cre$ mouse is a unique *in vivo* model to investigate global protein profile changes that accompany neurodegeneration and Lewy-like inclusions formation in mouse cortical neurones following 26S proteasomal dysfunction. This investigation is important for understanding the mechanisms leading to neurodegeneration and may be relevant to human disease.

In this chapter we aimed to identify differentially expressed proteins in 6 week old $Psmc1^{fl/fl};CaMKII\alpha-Cre$ mouse cortex. This age was chosen because there were

extensive neuropathological changes following *Psmc1* inactivation (Bedford et al., 2008). We used 2-D DIGE coupled to MALDI-TOF mass spectrometry for protein identifications. We identified 17 proteins that were differentially regulated in the cortex of *Psmc1^{fl/fl};CaMKII α -Cre* mouse. The analysis revealed up-regulation of cytoskeletal astrocytic proteins, the glial acid fibrillary protein and vimentin, as well as another astrocyte-specific protein related to the oxidative homeostasis, peroxiredoxin-6. Several proteins were identified that were down-regulated; mitochondrial fumarate hydratase and stathmin-1, related to the tricarboxylic acid cycle and cytoskeletal microtubule dynamics respectively. Overall, the data presented here will increase our knowledge of pathways associated with neuronal loss following 26S proteasomal depletion and be important in understanding mechanisms involved in neurodegeneration diseases such as DLB.

4.2. Results

Differential protein expression in the *Psmc1^{fl/fl};CaMKII α -Cre* mouse brain cortex following depletion of 26S proteasome was investigated using 2-D DIGE coupled to mass spectrometry (MADLI-TOF). Identified proteins were validated by Western blotting.

4.2.1. Differential expression of proteins in the *Psmc1^{fl/fl};CaMKII α -Cre* cortex

Four cortical samples from control and *Psmc1^{fl/fl};CaMKII α -Cre* mice were used in this analysis. A dye swap was also incorporated where control and *Psmc1^{fl/fl};CaMKII α -Cre* samples are labeled with both Cy3 and Cy5 to limit any dye bias. Cy2 was used for the pooled internal standard. The labeled samples were resolved on four 2-D DIGE gels as described in methods section 2.4. Each gel was scanned at the three wavelengths corresponding to the Cy dyes (Cy2 images were scanned at 473 nm, Cy3 at 532 nm and for Cy5, 635 nm). This produced 12 images for analysis as shown in Figure 4.1. The images show scattered protein spots between relative molecular mass of 10 – 150 kDa, and approximately *pI* 4-8. After fluorescent imaging, a randomly selected gel was further silver stained to reveal the spot pattern and is shown in Figure 4.2A.

2-D DIGE images were analyzed for differences in protein expression using SameSpots image analysis software (Progenesis). This software generates a list of statistically significant differentially expressed spots (Appendix II). 24 spots showed differential abundance in the *Psmc1^{fl/fl};CaMKII α -Cre* cortex; identified by an ID number, fold-change (*Psmc1^{fl/fl};CaMKII α -Cre* versus control) and average normalized volume of each spot. Spots were selected as significant for protein identification with a *p* value < 0.05 and fold change of ≥ 1.2 . The master image generated by SameSpot software shows the location of each spot to be identified (Fig. 4.3). A preparative gel stained with colloidal Coomassie stain is used to match and excise the protein spots of interest for identification by mass spectrometry (Fig. 4.2B).

Figure 4.1

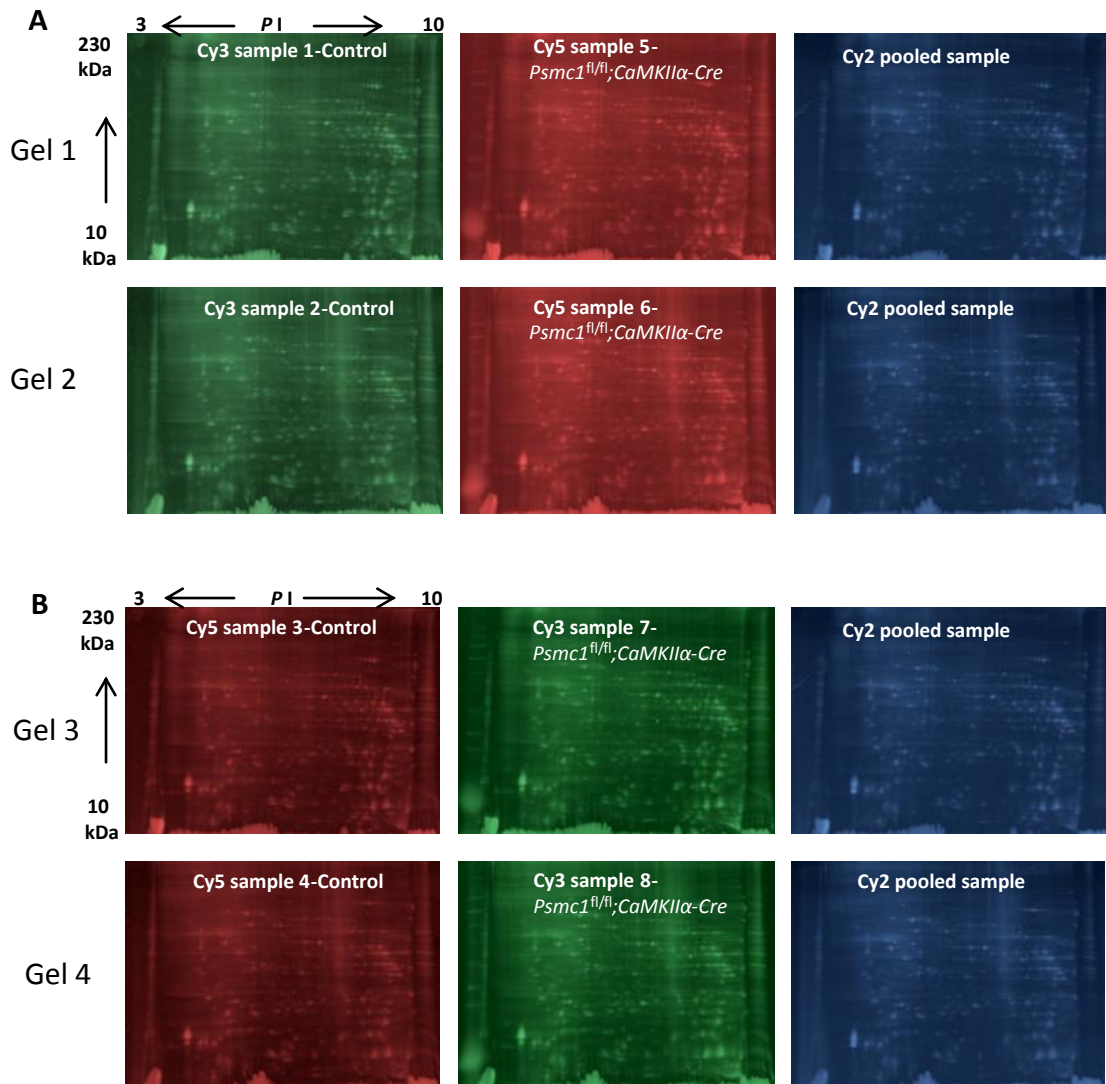


Figure 4.1 False-colored images of the gels following 2-D DIGE analysis (n = 4). Samples were from control, *Psmc1^{fl/fl};CaMKIIα-Cre* or a pooled (control plus *Psmc1^{fl/fl};CaMKIIα-Cre*) mixture. (A) Images for Cy3-labeled control and Cy5-labeled *Psmc1^{fl/fl};CaMKIIα-Cre*. (B) Images for dye swap labeling; Cy5-labeled control and Cy3-labeled *Psmc1^{fl/fl};CaMKIIα-Cre*. Pooled samples were labeled with Cy2 and used as an internal reference of protein loading for normalization.

Figure 4.2

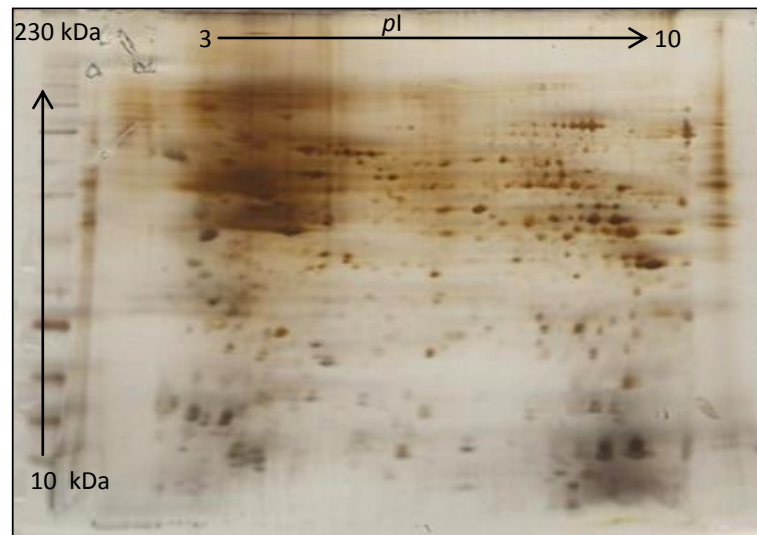


Figure 4.2 (A) A representative silver staining following 2-D DIGE of a pooled Cy2-labeled sample.

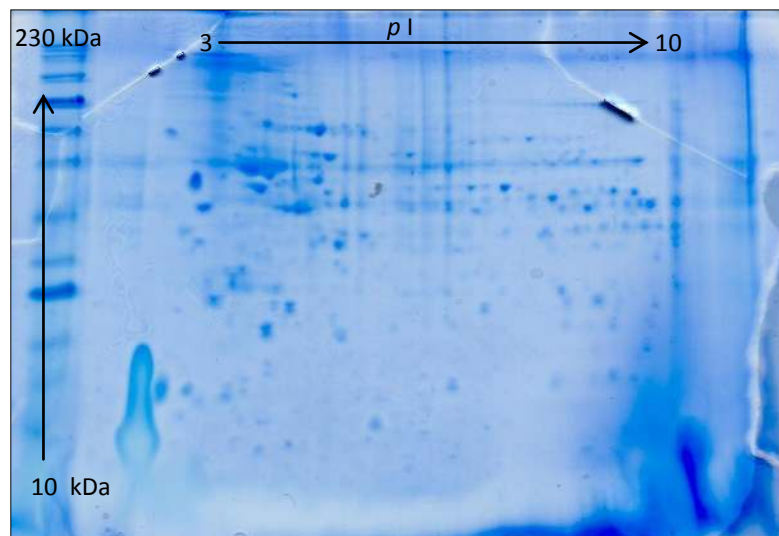


Figure 4.2 (B) Preparative 2DG electrophoresis visualized with colloidal Coomassie stain. Differentially expressed spots from the master gel shown in Figure 4.3 were matched with this gel, excised and identified by MALDI-TOF-MS.

Figure 4.3

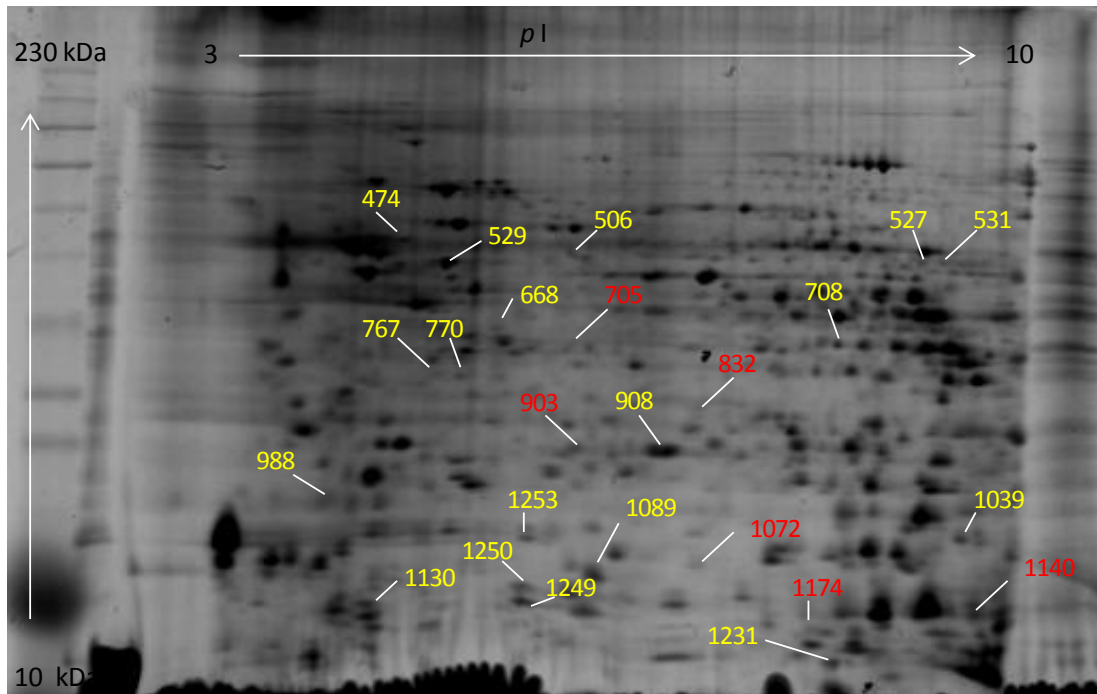


Figure 4.3 Master image of the 2-D DIGE analysis produced by the Samespots software. Differentially expressed spots in the *Psmc1^{fl/fl};CaMKII α -Cre* cortex are indicated by ID numbers. These spots were > 1.2 fold change in protein abundance between control and *Psmc1^{fl/fl};CaMKII α -Cre*, and $p < 0.05$ (ANOVA). The spots labeled in yellow were identified by MALDI-TOF-MS and are listed in table 4.1. The spots labeled in red were not identified due to low expression levels.

4.2.2. Proteins spots identified by MALDI-TOF-MS

To identify the differentially expressed protein spots from the 2-D DIGE, a pooled protein sample from *Psmc1^{fl/fl};CaMKII α -Cre* and control mouse brain cortices was focused and resolved on a preparative 2-D gel and stained with colloidal Coomassie stain (Figure 4.2B). The location of the spots from the Samespots Master image was visually matched to spots on the preparative gel. 18 of the 24 spots were recognized (Figure 4.3, yellow labels), but it was not possible to confidently locate the remaining 6 spots (Figure 4.3, red labels).

The located spots were excised from the preparative gel and prepared for MALDI-TOF-MS as described in the methods section 2.4.4, mass spectrometer analysis was carried out at Nottingham Trent University, Nottingham UK. MS analysis was accompanied by a Mascot database search for protein identification (ID). According to the Mascot algorithm criterion; peptides matching the internal sequence of a theoretical candidate protein with a score greater than 55, were considered significant ($p < 0.05$).

All of the identified proteins are listed in Table 4.1. The table summarizes the protein accession code (UniProt Accession code), gene ID, protein name, fold change, percentage of identified sequence coverage, molecular mass, *pI* value and mascot score. It is noted that several spots (474, 668, 708, 770, 988, and 1130) were found to contain more than one protein. This leads to difficulty in identifying the protein displaying change. This could result from similar migration patterns of these proteins on the IPG strip, protein post-translational modifications, and protein cleavage or the presence of protein isoforms. Appendix II illustrates the results of the peptide data and Mascot search relating to protein identification.

Table 4.1 Differentially expressed proteins in *Psmc1^{fl/fl};CaMKII α -Cre* mice brain cortex

<i>2DIGE image analysis</i>			<i>Protein identified by MALDI-TOF-MS and MASCOT</i>							
Spot No.	Fold change	<i>p</i> -value	NCBI-Gene ID	Uniprot Accession code	Protein ID	MW	<i>pI</i>	Mascot Score ⁱⁱ	Matched peptides ^γ	Sequence Coverage % ^φ
474	1.4	0.003	22352	VIME_MOUSE	Vimentin	53	5.06	165	32	69
			227613	TBB2C_MOUSE	Tubulin beta-2C chain	50	4.79	187	37	68
506	-1.3	0.023	11947	ATPB_MOUSE	ATP synthase subunit beta, mitochondrial.	56	5.19	115	18	41
527	-1.3	0.022	14194	FUMH_MOUSE	Fumarate hydratase, Mitochondrial	54	9.12	83	13	26
529	3.2	1.02E-04	14580	GFAP_MOUSE	Glial fibrillary acidic protein	50	5.27	407	65	82
531	-1.4	0.043	235072	SEPT7_MOUSE	Septin-7	50	8.73	107	15	46
668	1.6	1.76E-04	22151	TBB2A_MOUSE	Tubulin beta-2A chain	50	4.78	108	18	43
			22142	TBA1A_MOUSE	Tubulin alpha-1A chain	50	4.49	53 ⁺	9	32
			15481	HSP7C_MOUSE	Heat shock cognate 71	71	5.37	48 ⁺	11	23
708	1.2	9.77E-004	26876	AK1A1_MOUSE	Alcohol dehydrogenase [NADP+]	36	6.9	369	31	71
			14447	G3P_MOUSE	Glyceraldehyde-3-phosphate dehydrogenase	36	8.44	158	20	61
767	-1.2	0.025	17957	SNAB_MOUSE	Beta-soluble NSF attachment protein	33	5.52	74	8	32
770	1.7	0.005	14580	GFAP_MOUSE	Glial fibrillary acidic protein	50	5.27	141	28	47
			11816	APOE_MOUSE	Apolipoprotein E	36	5.56	66	18	48

Table 4.1 continued.

<i>2DIGE image analysis</i>			<i>Protein identified by MALDI-TOF-MS and MASCOT</i>							
Spot No.	Fold change	<i>p</i> -value	NCBI-Gene ID	Uniprot Accession code	Protein ID	MW	<i>pI</i>	Mascot Score ⁱⁱ	Matched peptides ^γ	Sequence Coverage % ^φ
908	1.4	0.006	11758	PRDX6_MOUSE	Peroxiredoxin-6	26	5.71	177	25	84
988	-1.2	0.019	16396 227613	ITCH_MOUSE TBB2C_MOUSE	E3 ubiquitin-protein ligase Itchy Tubulin beta-2C chain	9.96 50.2	5.93 4.79	60 54 ⁺	15 13	24 21
1039	1.3	4.17E-004	22195	UB2L3_MOUSE	Ubiquitin-conjugating enzyme E2 L3	18	8.68	157	16	79
1089	-1.2	0.003	12859	COX5B_MOUSE	Cytochrome c oxidase subunit 5B, mitochondrial	14	8.68	80	8	56
1130	1.2	0.008	12858	COX5A_MOUSE PHP14_MOUSE	Cytochrome c oxidase subunit 5A, mitochondrial 14 kDa phosphohistidine phosphatase	16.3 14.1	6.08 5.26	143 79	9 8	65 70
1231	1.3	0.046	78330	NDUV3_MOUSE	NADH dehydrogenase [ubiquinone] flavoprotein 3, mitochondrial	11.8	9.34	58	4	40
1249 1250	-1.4 -1.4	0.008 0.002	64011	NEUG_MOUSE	Neurogranin	7.7	6.57	144 131	5 5	57 58
1253	-1.2	0.023	16765	STMN1_MOUSE	Stathmin-1	17.2	5.76	111	12	77

ⁱⁱ Mascot score is a statistical score for how well the experimental data (peptide masses) match the database sequence. A score value of 55 or more represents significant values ($p < 0.05$). ⁺Lower values can be considered if matched protein appears at the top of the hit list of the resultant identified proteins.

^γ Matched peptides are the number of peptides identified as matching the database sequence of candidate protein.

^φ Sequence coverage is the percentage of the database protein sequence covered by matching peptides from the experimental data. The larger the sequence coverage the more certain is the identification.

4.2.3 Protein validation by Western blot

In order to validate the proteins identified by 2-D DIGE and MALDI-TOF-MS, 1-Dimensional (1-D) Western blotting was performed. 50-100 µg protein were extracted from control and *Psmc1^{fl/fl};CaMKIIα-Cre* cortices (n = 4) using the same urea lysis buffer used for 2-D DIGE. Proteins were resolved using 12% SDS-PAGE and transferred onto nitrocellulose membrane. The membrane was probed with an antibody for the protein of interest and then re-probed with an actin antibody for normalization. The protein levels were quantified using densitometry analysis (ScnImage software) of the bands developed on the autograph following western blotting. Data was statistically analyzed using Graph Pad prism 5. Western validation was performed at least twice for each protein and representative images are shown.

4.2.3.1 Glial fibrillary acidic protein (GFAP) is increased and post translationally modified in *Psmc1^{fl/fl};CaMKIIα-Cre* mouse cortex

GFAP is a classical astrocytic protein marker. GFAP is a 50 kDa (432 amino acid residues) type III intermediate filament protein. Its coiled-coil domains provide mechanical strength for the formation of firm bundles fibers. In this study GFAP was identified in two protein spots; 529 and 770 (Figure 4.3 and Table 4.1). These spots showed 3.2- and 1.7-fold increase respectively in *Psmc1^{fl/fl};CaMKIIα-Cre* versus control cortex. The ApoE protein was identified in addition to GFAP in spot 770.

1-D Western blot analysis of GFAP showed a 4-fold increase ($P < 0.01$) in GFAP expression in *Psmc1^{fl/fl};CaMKIIα-Cre* cortex compared to control (Figure 4.5A). Figure 4.5A also shows a high molecular weight smear above 50 kDa in the *Psmc1^{fl/fl};CaMKIIα-Cre* cortical samples.

Upregulation of GFAP in this study confirms the extensive astrocytic gliosis revealed by cortical immunohistochemistry, accompanying neurodegeneration (Bedford et al., 2008) and is supported by other neurodegenerative disease models showing increased GFAP expression. 2D-DIGE global proteome analysis of striatal tissue from the A53T α -synuclein PD mouse model showed a 3-fold increase in GFAP versus controls (Kurz et al., 2012). Moreover, a 220 % increase in GFAP expression was reported in the striatum of an MPTP (1-methyl-4-phenyl-1,2,3,6-tetrahydropyridine) neurotoxin model of PD (Muroyama et al.).

Upregulation of GFAP expression is not confined to animal models of neurodegeneration. Increased expression of GFAP has also been detected in the entorhinal cortex of postmortem brain samples from patients affected by neurodegeneration such as AD (Porchet et al., 2003). Although neurodegeneration has been associated with astrocytic gliosis in animal models and human studies, there is limited data specifically connecting astrocytic activation with cortical Lewy body disease (DLB).

GFAP was identified in two differentially-expressed protein spots. To further investigate GFAP expression we performed 2-D PAGE followed by Western blotting for GFAP (Figure 4.4). Interestingly, comparison of control versus *Psmc1^{fl/fl};CaMKII α -Cre* cortical samples showed a different protein expression pattern with additional GFAP protein spots in the *Psmc1^{fl/fl};CaMKII α -Cre* sample that were absent from the control sample (spot number 1,2, 5 and 6). Two spots were approximately 30 kDa and may match spot ID 770 identified in 2-D DIGE containing both GFAP and ApoE (Table 4.1). Therefore, we suggest that the 1.7-fold change is at least partly related to GFAP in this spot. However, this does not exclude changes in ApoE which have not been investigated. Interestingly, ApoE is also expressed in astrocytes (Bachoo et al., 2004).

The major form of GFAP is 50 kDa. Therefore, the low molecular weight protein spot ID 770 may represent accumulation of GFAP isoform or fragments as a consequence of degradation in *Psmc1^{fl/fl};CaMKII α -Cre* mouse cortex. The mascot search results for peptide matched for GFAP from spot 529 (regular from-at 50 kDa) showed 70 % of peptide identified from total protein, while GFAP identified from spot 770 (at lower kDa) showed 47 % of peptide matches.

In addition to the lower molecular weight spots, two additional GFAP spots are shown in Figure 4.4 (spot number 1 and 2) with a similar molecular weight to the normal GFAP (~ 50 kDa), but a shift toward acidic *pI*. These spots were not identified by the 2-D DIGE analysis. This may be due to sensitivity of Western blotting in addition to increased protein loading of these gels compared to 2-D DIGE. Protein phosphorylation can reduce a protein's *pI* value (Yamagata et al., 2002). GFAP may undergo posttranslational modification by phosphorylation (Inagaki et al., 1994) causing the shift toward acidic *pI* in *Psmc1^{fl/fl};CaMKII α -Cre* cortex.

Figure 4.4

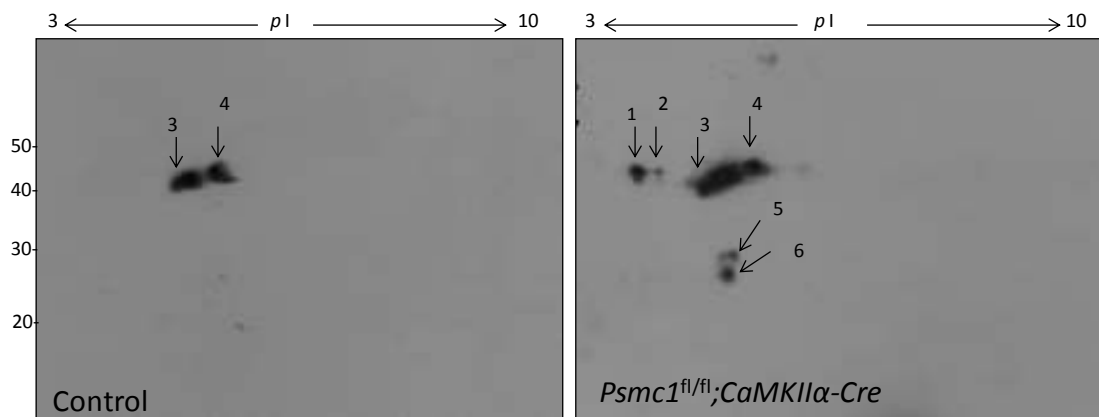


Figure 4.4 2-D Western blotting for GFAP of control and *Psmc1^{fl/fl};CaMKIIα-Cre* mice cortices samples. 300 μ g of protein was focusing on 3-10 NL IPG strips followed by second dimensional electrophoresis using 12% SDS-PAGE. The major GFAP spots are numbered 3 and 4, which are clearly increased in the *Psmc1^{fl/fl};CaMKIIα-Cre* cortex. Additional spots at \sim 45-50 kDa with lower pI (spot numbered 1 and 2) as well as lower molecular weight spots 5 and 6 (\sim 20 -30 kDa) are also evident in the *Psmc1^{fl/fl};CaMKIIα-Cre* cortex.

4.2.3.2 Vimentin (VIME) is up-regulated in *Psmc1^{fl/fl}*; *CaMKII α -Cre* mouse cortex

Vimentin was identified in protein spot 474. Vimentin is a 53 kDa (466 amino acid residues) type III intermediate filament protein of the cellular cytoskeleton. There was a 1.4-fold increase in this spot in the *Psmc1^{fl/fl}*; *CaMKII α -Cre* cortex sample compared to control (Table 4.1, $p = 0.003$). 1-D Western blotting showed vimentin was not expressed in control samples, but significantly up-regulated in the *Psmc1^{fl/fl}*; *CaMKII α -Cre* cortex (Figure 4.5B, $p < 0.01$). The absence of vimentin expression in control mouse brain cortex is supported by studies showing low vimentin levels in normal human subjects (Pekny and Nilsson, 2005). Increased vimentin is considered to be a marker of astrogliosis (Yamada et al., 1992; Porchet et al., 2003). Therefore, vimentin expression in the *Psmc1^{fl/fl}*; *CaMKII α -Cre* cortex is consistent with the increased GFAP expression and extensive astrocytic gliosis described in section 4.2.3.1. However, tubulin beta-2C, another cytoskeleton protein, was also identified in this spot. Tubulin beta-2C was not further investigated and we cannot exclude the possibility that this protein also increases in the *Psmc1^{fl/fl}*; *CaMKII α -Cre* cortex.

4.2.3.3 Up-regulation of peroxiredoxin-6 (PRDX-6) in *Psmc1^{fl/fl}*; *CaMKII α -Cre* mouse cortex

Peroxiredoxin-6 is a bifunctional enzyme with glutathione peroxidase and phospholipase A₂ activities (Chen et al., 2000). The protein had been called non-selenium GSH peroxidase (contains no selenium atom) to differentiate it from other subtypes of the peroxiredoxin class. PRDX-6 has a molecular weight of 26 kDa and the mouse protein has a predicted length of 224 residues. PRDX-6 has two active sites; cysteine-47 for the peroxidase activity and cysteine-32 associated with phospholipase activity. Its pI is ~ 5.1 , which may vary depending on the oxidation and/or phosphorylation of the protein (Power and Nicholas, 1999; Wu et al., 2009).

PRDX-6 was identified in spot 908, showing a 1.4-fold increase in expression in the *Psmc1^{fl/fl}*; *CaMKII α -Cre* cortex (Table 4.1, $p = 0.006$). Increased PRDX-6 expression was validated by 1-D Western blotting and densitometric analysis showed a 2-fold increase in expression in *Psmc1^{fl/fl}*; *CaMKII α -Cre* versus control mouse cortex (Figure 4.5C, $p < 0.001$).

Previous proteomic investigations in mouse models of neurodegenerative disease support our findings. Models of familial amyotrophic lateral sclerosis and Alzheimer's disease have shown up-regulation of PRDX-6 (Strey et al., 2004; Yata K, 2011). PRDX-6 up-regulation was also detected in postmortem AD, PD and PDD brain (Power et al., 2002; Power JH, 2008). Interestingly, these results suggest that the up-regulation of PRDX-6 is protective against oxidative stress.

4.2.3.4 Stathmin-1 (STMN-1) is down-regulated in the *Psmc1^{fl/fl};CaMKII α -Cre* mouse cortex

Stathmin-1 has a molecular weight of 18 kDa, corresponding to 149 amino acid residues. STMN-1 was identified in spot 1253, showing a 1.2-fold decrease in *Psmc1^{fl/fl};CaMKII α -Cre* cortex compared to controls (Table 4.1, $p = 0.02$). The significant decrease in STMN-1 expression was validated by 1-DG Western blotting followed by densitometry analysis (Figure 4.6 A, $p < 0.001$). This decrease in the expression of STMN-1 is more significant than suggested by the 2-D DIGE because STMN-1 expression is absent in *Psmc1^{fl/fl};CaMKII α -Cre* mice cortex as showed by Western blotting. Previous data has indicated STMN-1 down-regulation in frontal and temporal cortices of AD associated with neurodegeneration (Cheon et al., 2001). In addition, the STMN-1-KO mouse develops age-related axon pathology (Liedtke et al., 2002). The *Psmc1^{fl/fl};CaMKII α -Cre* mouse model is the first model of neurodegeneration to describe differential regulation of STMN-1 in cortical tissue associated with neurodegeneration and Lewy body pathology.

4.2.3.5 Mitochondrial fumarate hydratase (mFUMH) is down-regulated in *Psmc1^{fl/fl};CaMKII α -Cre* mouse cortex

Mitochondrial FUMH (mFUMH) is a nuclear encoded mitochondrial enzyme responsible for the reversible conversion of fumarate to malate in the citric acid cycle. mFUMH is a 54 kDa protein of 507 amino acid residues. This protein was identified in spot 527, showing a 1.3-fold decrease in expression (Table 4.1, $p = 0.02$). Decreased mFUMH expression was validated by 1-DG Western blotting and densitometric analysis, revealing 2-fold lower expression in *Psmc1^{fl/fl};CaMKII α -Cre* cortex compared to control (Figure 4.6B, $p = 0.03$). Data linking specifically mFUMH to neurodegeneration is limited; however, mitochondrial dysfunction is well documented in neurodegenerative diseases such as PD and PDD.

4.2.3.6 Neurogranin (NEUG) is down-regulated in *Psmc1^{fl/fl}*; *CaMKII α -Cre* mouse cortex

Neurogranin was identified in two spots in the 2-D DIGE analysis; 1249 and 1250, both showing a 1.4-fold fold decrease (Table 4.1, $p = 0.008$ and 0.002 respectively). It is ~ 8 kDa and 78 amino acid residues. This protein was not validated by 1-DG Western blotting as no suitable antibody was available. However, the identification of NEUG in two spots, demonstrating a high mascot score and high fold change in spot intensity (see tabel 4.1 and appendix II); can confirm its down-regulation in *Psmc1^{fl/fl}*; *CaMKII α -Cre* mouse cortex. NEUG is a tissue specific protein; it is found in the cell body of layer II-VI cerebral cortex neurones, and also in the apical and basal dendrites of pyramidal neurones. NEUG has been indicated to be lost in the neurodegeneration diseases (Reddy et al., 2005).

Figure 4.5

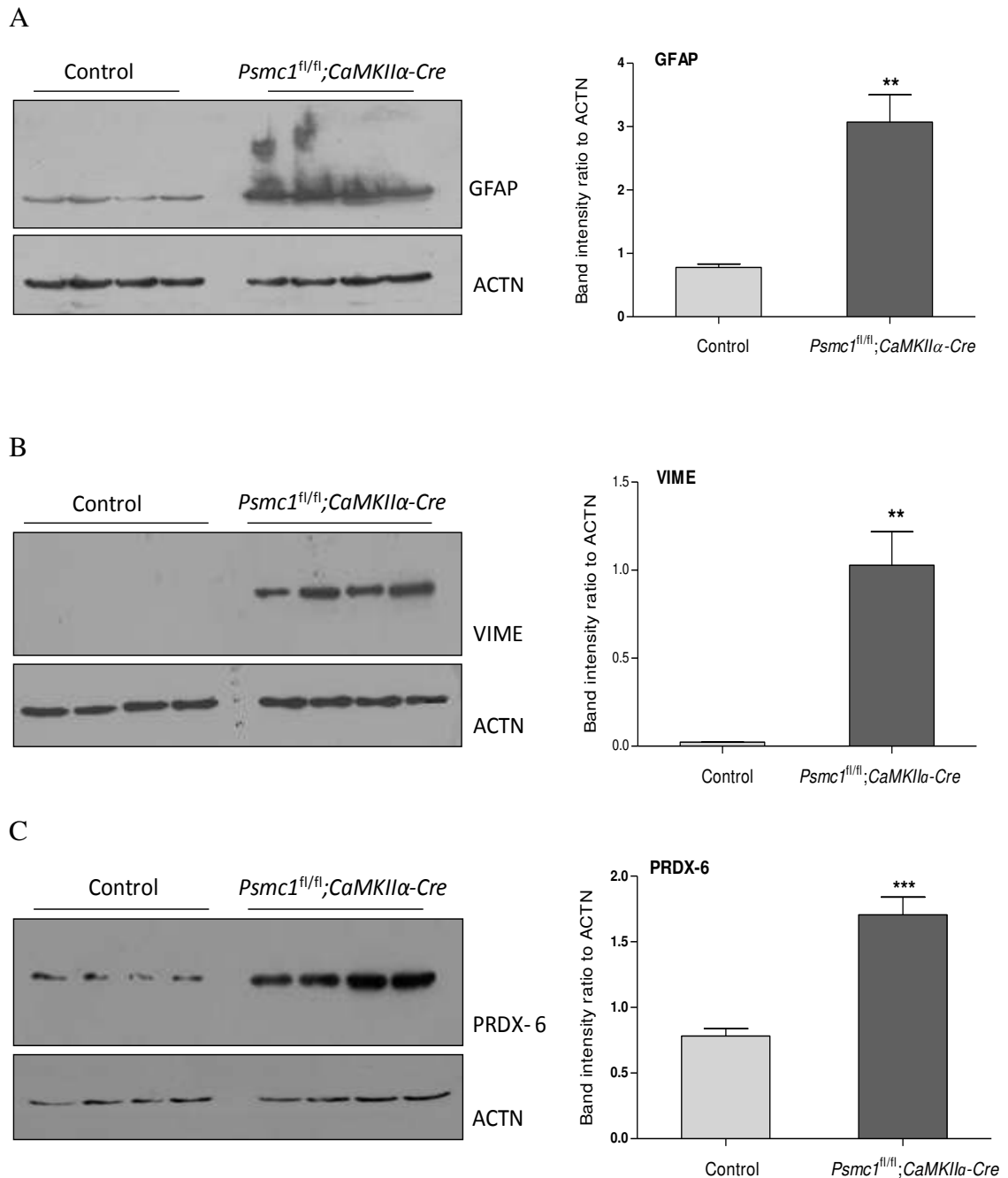


Figure 4.5 GFAP, VIME and PRDX-6 are up-regulated in *Psmc1^{fl/fl};CaMKIIα-Cre* cortex. Representative 1-DG Western blotting (left-hand-side) and densitometric analyses (right-hand-side) of cortical homogenates from control and *Psmc1^{fl/fl};CaMKIIα-Cre* mice for GFAP (A), VIME (B) and PRDX-6 (C). Each blot was probed with the antibody of interest and then stripped and re-probed with β -actin (ACTN). Graphs depict mean protein levels (optical density values) normalized to β -actin. Error bars indicate SEM, $n = 4$. ** $p < 0.01$; *** $p < 0.001$, Student's t -test.

Figure 4.6

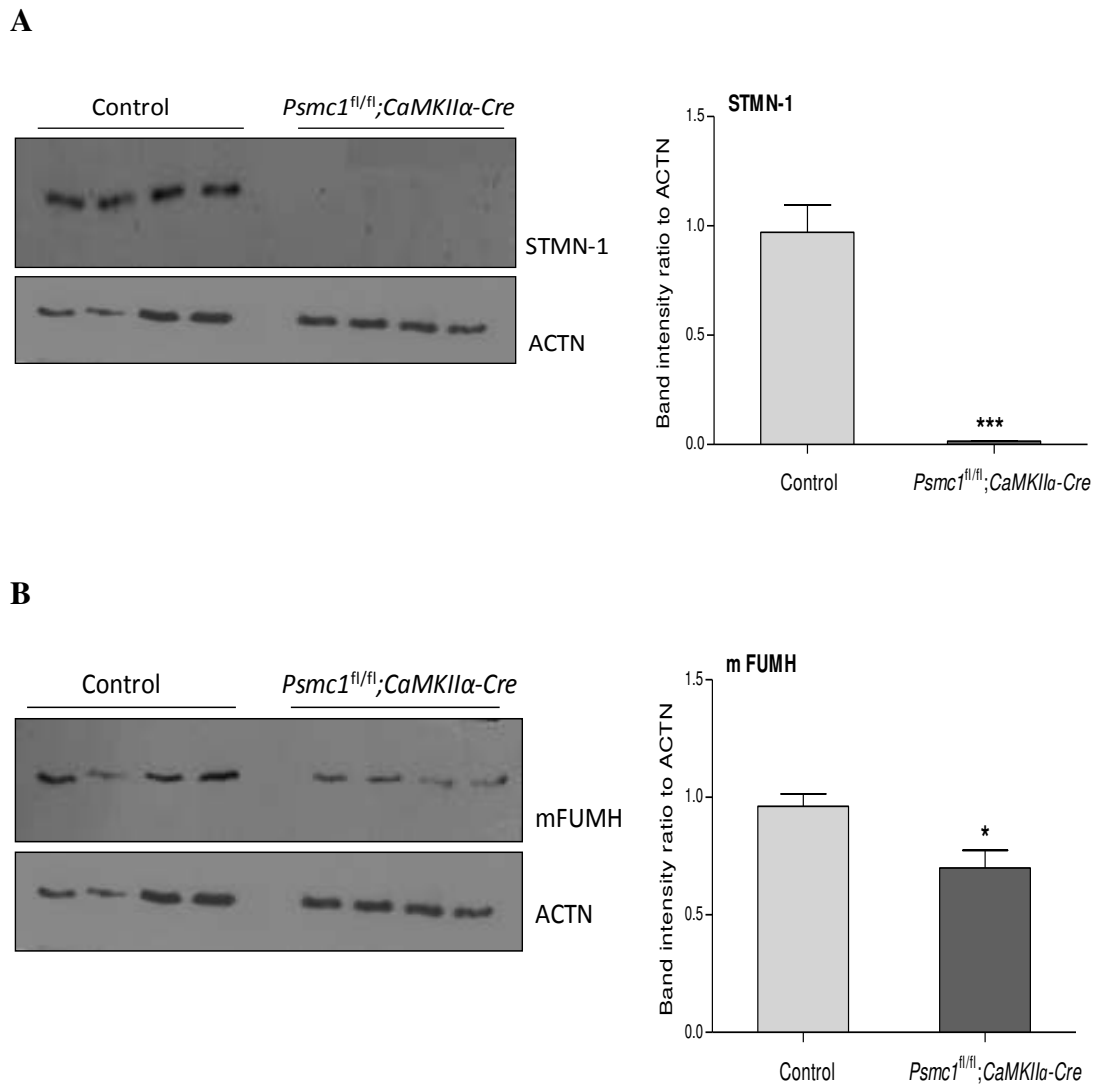


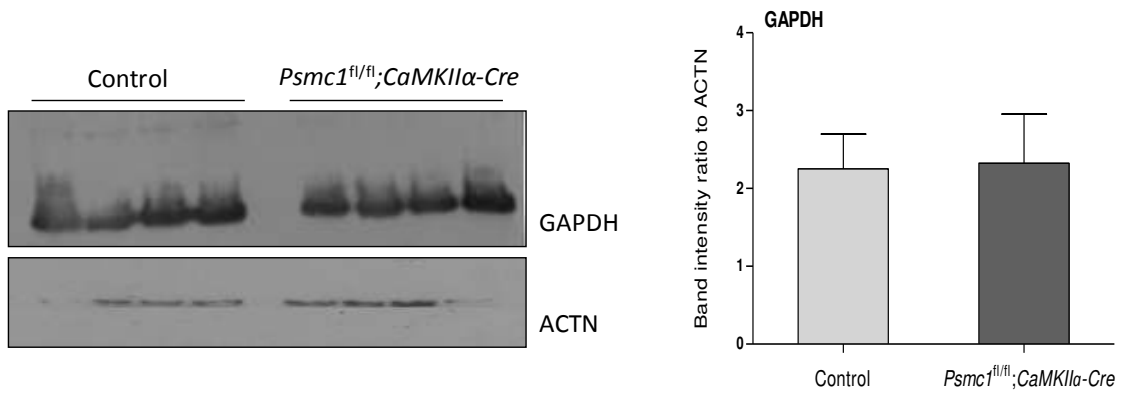
Figure 4.6 STMN-1 and mFUMH are decreased in *Psmc1^{fl/fl};CaMKIIα-Cre* cortex. Representative 1-DG Western blotting (left-hand-side) and densitometric analyses (right-hand-side) of cortical homogenates from control and *Psmc1^{fl/fl};CaMKIIα-Cre* mice for STMN-1 (A) and mFUMH (B). Each blot was probed with the antibody of interest and then stripped and re-probed with β -actin (ACTN). Graphs depict mean protein levels (optical density values) normalized to β -actin. Error bars indicate SEM, n = 4. ** $p < 0.01$; *** $p < 0.001$, Student's *t*-test.

4.2.3.7 Differentially expressed Proteins identified by 2D-DIGE -MS, but not validated by Western blotting

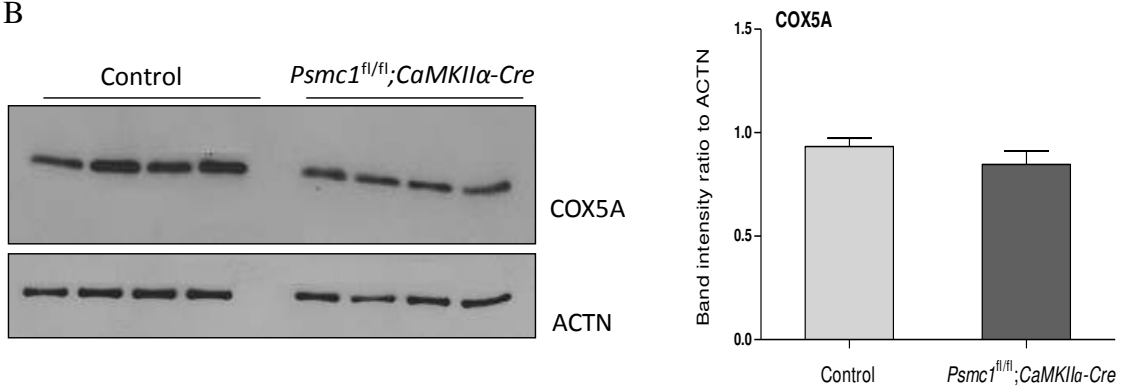
Several proteins identified by 2-D DIGE were not validated by 1-DG Western blotting. Figure 4.7 shows 1-DG Western blotting for Glyceraldehyde-3-phosphate dehydrogenase (GAPDH or G3P, spot 708); Cytochrome c oxidase subunit 5A, mitochondrial (COX5A, spot1130); Heat shock cognate 71 kDa protein (HSP7C spot 668), Beta-soluble NSF attachment protein (SNAB, spot 767); and Septin-7 (SEPT-7 spot 531). This may be due to differences in the sensitivity of the techniques used and/or protein expression levels in the total pool. A further explanation may be the identification of more than one protein in a spot, e.g. GAPDH, COX5A and HSP7C were identified in spots containing other proteins (Table 4.1). In these cases not all proteins identified were investigated and further work may reveal the differentially expressed protein in these spots.

Figure 4.7

A



B



C

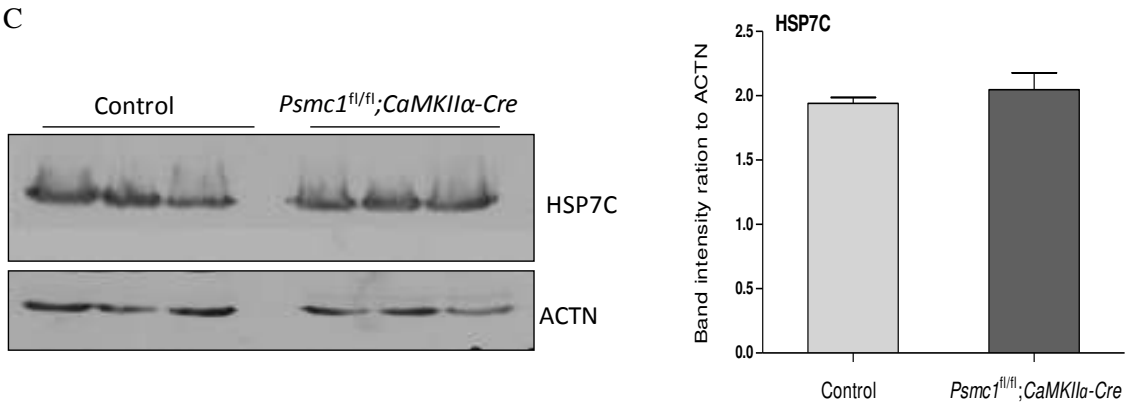


Figure 4.7 continued.

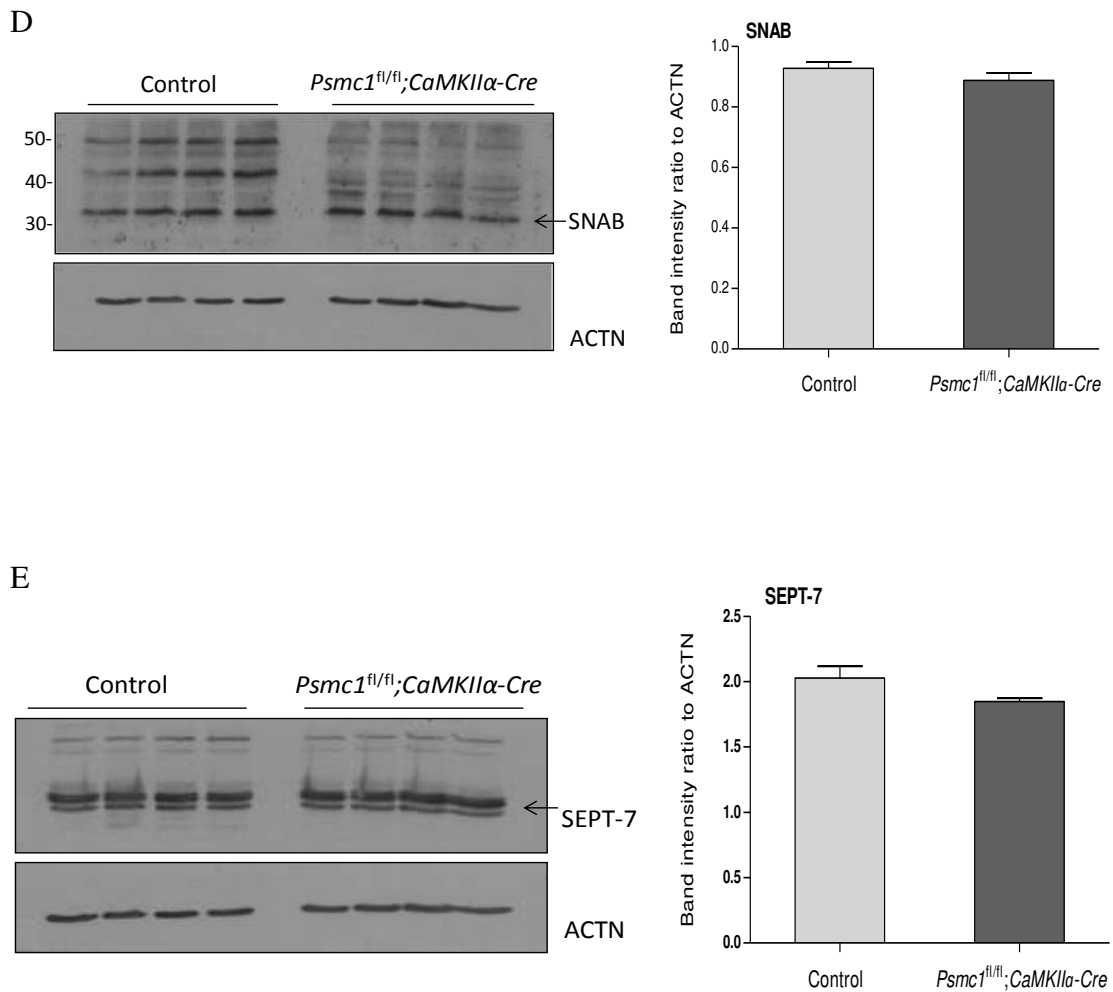


Figure 4.7 GAPDH, COX5A, HSP7C, SNAB and SEPT-7 do not show differential expression in *Psmc1^{fl/fl};CaMKIIα-Cre* mouse cortex. Representative 1-DG Western blotting (left-hand-side) and densitometric analyses (right-hand-side) of cortical homogenates from control and *Psmc1^{fl/fl};CaMKIIα-Cre* mice for GAPDH (A), COX5A (B), HSP7C (C), SNAB (D) and SEPT-7 (E). Each blot was probed with the antibody of interest and then stripped and re-probed with β -actin (ACTN). Graphs depict mean protein levels (optical density values) normalized to β -actin. Error bars indicate SEM. No significant difference, Student's *t*-test ($n = 4$).

4.2.4 Immunohistochemical investigations of differentially-expressed proteins

4.2.4.1 GFAP and VIME are expressed in astrocytes.

Immunohistochemistry of cortical brain sections from control and *Psmc1^{fl/fl};CaMKII α -Cre* mice was performed for GFAP and VIME proteins. GFAP is a well characterized marker of astrocytes (Jacque et al., 1978). Figure 4.8 shows increased GFAP and VIME-positive cells in the *Psmc1^{fl/fl};CaMKII α -Cre* cortical mouse brain sections. Double-immunofluorescent staining of sections with GFAP and VIME was unsuccessful. However, although GFAP staining is more extensive and showed branched astrocytes in the *Psmc1^{fl/fl};CaMKII α -Cre* cortex, the VIME-positive cells have some characteristic features of the GFAP-stained astrocytes. VIME is mostly in the astrocytic cell body rather than the end feet like GFAP. We suggest that VIME is most likely expressed in astrocytes. This is also supported by previous studies showing VIME co-localized with GFAP in astrocytes (Escartin et al., 2006; Seehusen et al., 2007).

4.2.4.2 Preoxidorexin-6 is expressed in astrocytes.

We investigated the cellular localization of PRDX-6 in cortical mouse brain sections using double immunofluorescent staining. GFAP and microtubule-associated proteins (MAP2) were used as markers of astrocytes and neurones respectively. Previous studies have shown extensive astrocytic gliosis in this mouse model (Bedford et al., 2008). Figures 4.9 and 4.10 show PRDX-6 is expressed in astrocytes and not neurones respectively. PRDX-6 is evident in control brain and we suggest that these are not reactive astrocytes and hence do not express GFAP, explaining the absence of co-localization. Figure 4.9 also shows the subcellular distribution of PRDX-6 is more focused around the cell body, whereas GFAP staining is in astrocytic processes. The absence of GFAP staining in control cortex differs from the Western blot analysis, showing GFAP expression. The reason behind this may be differences in the sensitivity between techniques. For example, the tissue lysis buffer used for Western blotting could make the GFAP protein more accessible for antibody binding. We suggest that the increase in PRDX-6 expression in *Psmc1^{fl/fl};CaMKII α -Cre* cortex is associated with reactive astrocytes and is consistent with previously reported studies (Jin et al., 2005).

Figure 4.8

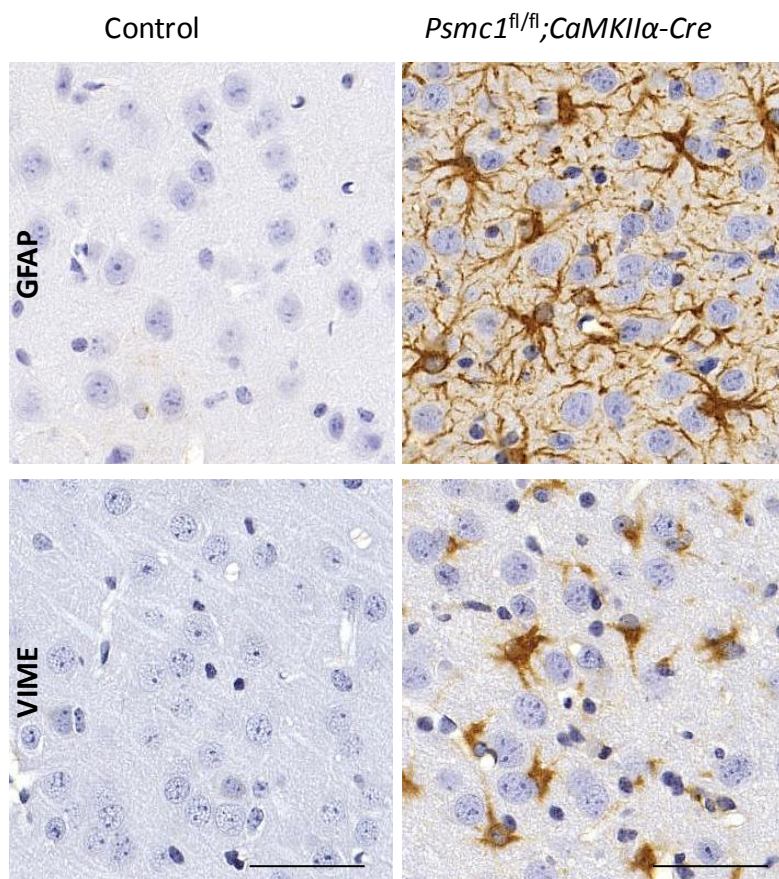


Figure 4.8 Astrocytic expression of GFAP and VIME. Immunohistochemical staining chromogenic brown for GFAP and VIME in control and *Psmc1^{fl/fl};CaMKIIα-Cre* mouse cortical sections (scale bar 50 μ m). Figure kindly provided by Dr L Bedford.

Figure 4.9

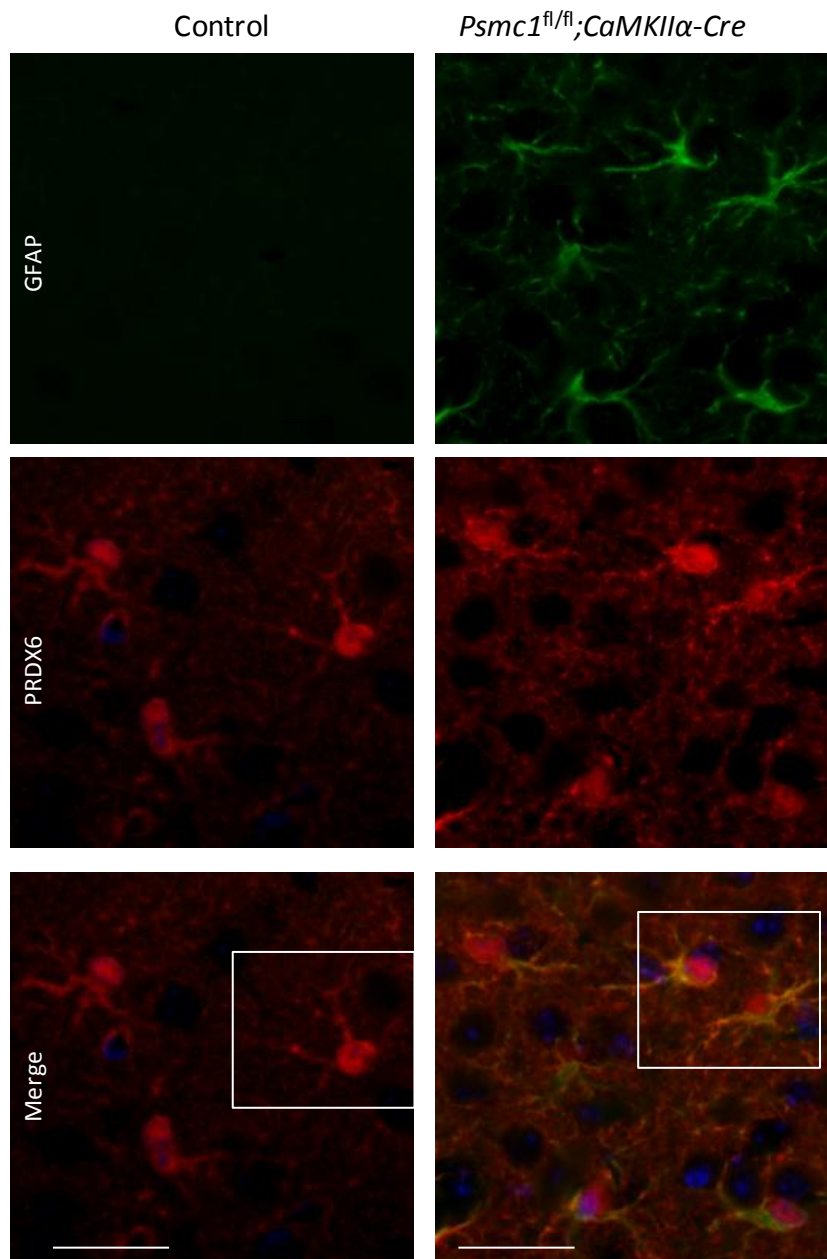


Figure 4.9 PRDX-6 is expressed in astrocytes. Double immunofluorescent staining for GFAP (astrocytes/green) and PRDX-6 (red) in control and *Psmc1^{fl/fl};CaMKIIα-Cre* mice cortical sections. The merged image shows co-localization of PRDX-6 in GFAP-positive astrocytes. Scale bar 50 μ m. Figure kindly provided by Dr L Bedford.

Figure 4.10

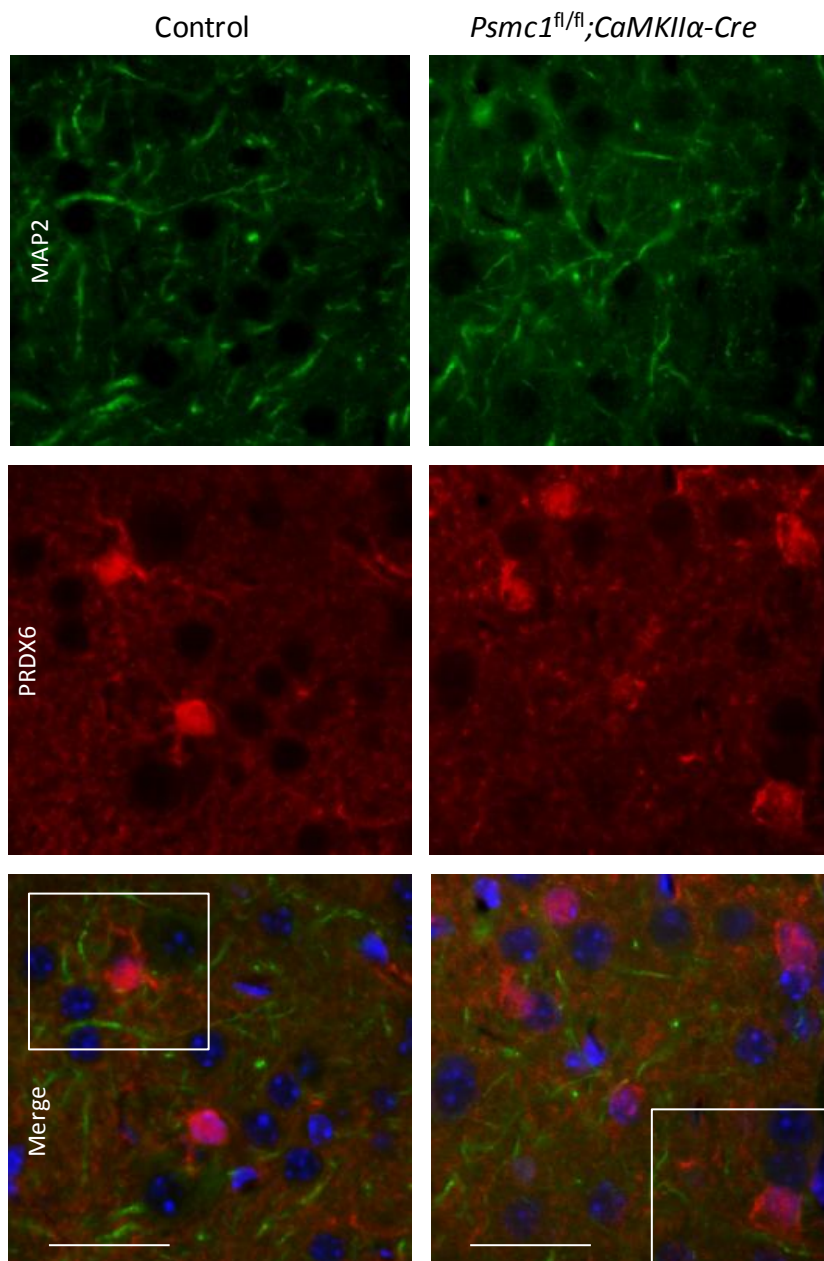


Figure 4.10 PRDX-6 is not expressed in the neurones. Double immunofluorescent staining for MAP2 (Neurones/green) and PRDX-6 (red) in control and *Psmc1^{fl/fl};CaMKIIα-Cre* mice cortical sections. The merged image shows no co-localization of PRDX-6 in MAP2-positive neurones. Scale bar 50 μ m. Figure kindly provided by Dr L Bedford.

4.3 Discussion

We have carried out a comparative proteomic study of mouse cortex following 26S proteasome deletion in CaMKII α -expressing neurones. Using 2-D DIGE we found 24 protein spots showing differential expression in the *Psmc1^{fl/fl};CaMKII α -Cre* cortex compared to controls. We were able to identify 18 of these spots by MS and went on to validate several proteins based on antibody availability by 1DG Western blotting. We have found significantly up-regulation of astrocytic proteins GFAP, VIME and PRDX-6. We also validated the down-regulation of mFUMH and STMN-1.

To our knowledge this is a unique proteomic study *in vivo* using in a mouse model of neurodegeneration caused by 26S proteasomal deletion. This offers the possibility to identify proteins that are involved in the neuropathological mechanisms of inclusion body formation and neurodegeneration and may be relevant to human disease.

4.3.1 Upregulation of GFAP in *Psmc1^{fl/fl};CaMKII α -Cre* mouse cortex indicates reactive astrogliosis

Upregulation of intermediate filament proteins GFAP and VIME is a characteristic feature of astrogliosis following brain injury and neurodegeneration (Yamada et al., 1992; Porchet et al., 2003). We previously reported astrogliosis accompanying neurodegeneration in *Psmc1^{fl/fl};CaMKII α -Cre* mice by GFAP immunohistochemical staining of cortical mouse brain sections (Bedford et al., 2008). Here we validate significantly increased expression of GFAP protein using proteomics approaches.

The control cortex showed limited GFAP expression. This does not indicate absence of astrocytes in the healthy brain, but that non-activated normal astrocytes express undetectable or very low levels of GFAP, which has been documented in previous studies (Sofroniew and Vinters, 2010; Marques et al., 2012).

GFAP knockout mice show a healthy brain and normal abundance of astrocytes indicated by S100 β staining, suggesting GFAP is not essential for the formation of astrocytes in healthy brain. However, the GFAP knockout mouse is susceptible to reactive gliosis following brain injury (Pekny et al., 1995). However, more recent studies have shown GFAP expression is associated with astrogliosis an important feature of the inflammatory response involving reactive astrocytes (Jardanhazi-Kurutz et al., 2011; Diaz et al., 2012).

The role of GFAP expression and astrogliosis during brain injury such as neurodegeneration is still unclear. In addition, whether astrocytes are protective or harmful is the subject of extensive debate. The expression of GFAP and reactive gliosis has been shown to be triggered by several molecules in the brain, including cytokines, growth factors, glutamate, nitric oxide and reactive oxygen species (Sofroniew, 2009). Interestingly, these molecules could be released from different neural cell types. Therefore, it is possible that reactive astrogliosis and increased GFAP expression in the *Psmc1^{fl/fl};CaMKII α -Cre* cortex is a consequence of pro-inflammatory mediators released from neurones. This is supported by the fact that 26S proteasomal deletion is conditionally targeted to neurones in the mouse model. Therefore, astrogliosis is a consequence of neuronal changes.

Although we have clearly shown a significant increase in GFAP protein expression by proteomics and immunohistochemistry, using 2-DG Western blotting we have identified variant forms of GFAP in the *Psmc1^{fl/fl};CaMKII α -Cre* cortex that are not evident in the control brain. These could reflect post-translational modification, splice variants and/or degradation products.

Lower molecular weight GFAP spots were detected, approximately at 30 kDa. A GFAP protein of similar size has been described in the entorhinal cortex of normal elderly and associated with neurodegeneration. The authors suggested this was a degradative form (Porchet et al., 2003). Interestingly, it has also been suggested that the more acidic form of GFAP is more vulnerable to degradation (Porchet et al., 2003), which is increased in the *Psmc1^{fl/fl};CaMKII α -Cre* cortex and discussed below. Therefore, it is possible that the lower molecular weight forms of GFAP we see are degradation products. However, GFAP splice variants have also been described that show differential expression patterns in the human brain. The low molecular weight GFAP identified on our 2DG Western blot is similar in size to the reported Gfap Δ Ex6 isoform (Kamphuis, 2012). To our knowledge this isoform has not been described in the mouse brain (Kamphuis, 2012).

In 2-DG Western blotting, we also show an acidic shift in the GFAP protein in *Psmc1^{fl/fl};CaMKII α -Cre* cortex that is not found in the control. GFAP phosphorylation is known to make the protein more acidic, changing its focus on 2-DG toward acidic pI, but at the same molecular weight (Bigbee and Eng, 1982; Inagaki et al., 1994).

It was suggested that this was involved in astrocytes frameworks remodeling during mitosis (Inagaki et al., 1994). Therefore, in the *Psmc1^{fl/fl};CaMKII α -Cre* cortex it is possible that GFAP is phosphorylated to mediate extensive astrocytes proliferation. However, the effect of GFAP phosphorylation was unclear.

4.3.2 VIME upregulation supports reactive astrogliosis

Vimentin is the major astrocyte-specific intermediate filament protein in the neonatal brain, it expressed in immature astrocytes and it is the natural partner of GFAP for maintaining cell integrity. We have shown significantly increased expression of VIME in *Psmc1^{fl/fl};CaMKII α -Cre* cortex following 26S proteasomal deletion as well as VIME-positive astrocyte staining focused in the cell body. Upregulation of VIME has been associated with several neurodegeneration diseases, such as Alzheimer's disease, Pick's disease, amyotrophic lateral sclerosis and PD (Yamada et al., 1992). VIME is essential for formation of intermediate filaments (IF) normal structure, in VIME deficient astrocytes it was indicated to be necessary for GFAP stabilization and consequently the IF network creation (Galou et al., 1996). Glial cells can impair nerve regeneration due to its scar formation, where those devoid of GFAP and VIME showed less scar formation. It has been suggested that therapeutic suppression of IF upregulation in reactive glial cells may assist neuroregeneration (Lu et al., 2011). Therefore, increased expression of VIME can support reactive gliosis in the *Psmc1^{fl/fl};CaMKII α -Cre* mouse brain, and this might have a role in the neurodegeneration.

4.3.3 Upregulation PRDX-6 indicates oxidative stress

In addition to the increased expression of GFAP and VIME, we identified peroxiredoxin-6 as a significantly increased protein in the *Psmc1^{fl/fl};CaMKII α -Cre* cortex. Interestingly we and others show this is an astrocyte-specific protein. PRDX-6 is a bifunctional enzyme with peroxidase and phospholipase A₂ (PLA₂) activities, acting as an antioxidant and in phospholipid hydrolysis respectively (Fisher et al., 1999). PRDX-6 is expressed in the control cortex in cells with astrocytic morphology. We consider these to be non-reactive astrocytes in the normal brain because they do

not express GFAP. Our results demonstrate that PRDX-6 is expressed in both non-reactive as well as reactive astrocytes and its up-regulation is most likely associated with the astrogliosis as a consequence of neurodegeneration in the *Psmc1^{fl/fl};CaMKII α -Cre* mouse brain.

The astrocytic-specific expression of PRDX-6 is supported by previous studies. Jin et al. found that astrocytes, but not neurones, in normal mouse brain express PRDX-6 (Jin et al., 2005). In human AD frontal cortex tissue, astrocytes were significantly increased and overexpressed PRDX-6 (Power et al., 2002). A low level of neuronal expression was also detected in this study. A study performed on PD and DLB brain tissue showed that although the number of astrocytes in diseased cortical tissue varied and was not significantly increased, they expressed more PRDX-6 compared to controls (Power et al., 2002). Taken together, these studies support our finding that PRDX-6 is increased in astrocytes in a mouse model of neurodegeneration and inclusion body formation causing dementia. Interestingly, in consistent with our study, Power et al. (2002) also showed that α -synuclein positive LB in neurones stained with PRDX-6. Direct binding of PRDX-6 and α -synuclein was confirmed by immunoprecipitation and the authors proposed PRDX-6 may be involved in protecting neurones from oxidative stress caused by aggregated α -synuclein (Power et al., 2002). In our studies we did not detect co-localisation of PRDX-6 and neuronal marker MAP2 and did not detect PRDX-6 association with inclusion bodies in 26S proteasome-deleted neurones. It is still possible that astrocyte-specific PRDX-6 has a role in neuronal protection mechanisms in the *Psmc1^{fl/fl};CaMKII α -Cre* mouse cortex. Upregulation of PRDX-6 may be a general response to neuronal injury and neurodegeneration because this has been detected in different diseases as well as neural cell types.

Despite the general idea that PRDX-6 plays a protective role during neurodegeneration, studies involving PRDX-6 in different tissue and biological systems have been inconsistent. *In vivo*, PRDX-6 failed to protect ethanol-induced chronic liver intoxication mediated by oxidative stress in mice and exacerbated hepatic lipid accumulation, suggested an unknown function of PRDX-6 in lipid metabolism (Roede et al., 2009). Another study using the PRDX-6 knockout mouse challenged the lung with Lipopolysaccharides (LPS). This acute lung injury was exaggerated in PRDX-6 knockout mice compared to controls (Yang et al., 2011).

Investigations of neurodegeneration in the absence of PRDX-6 have not been reported, but would be interesting to investigate the antioxidant functions of PRDX-6 in neurodegeneration.

Regulation of the expression of PRDX-6 has been investigated in several biological systems and will be important in understanding its function. In an *in vitro* study performed in murine bone marrow derived macrophages the expression of PRDX-6 was induced by prostaglandins such as PGE2 and PGD2 through adenylate cyclase with the involvement of transcription factor Nrf2 (Erttmann et al., 2011). Nrf2 (Nuclear factor erythroid 2-related factor 2) is a redox-sensitive transcription factor which controls the expression of antioxidant proteins (Zhang, 2006). In human bronchial epithelial cells, PRDX-6 was protective against H₂O₂-induced apoptosis; through its cysteine-47 residue and mutation at this site reversed this protective effect (Kim et al., 2011). The PLA₂ activity of PRDX-6 can hydrolyze phospholipids (Fisher et al., 1999) and therefore can increase the release of arachidonic acid (AA) from phospholipid membranes and consequently increases the production of pro-inflammatory cytokine Interleukins, IL-1 β (Kim et al., 2011). Astrocytes can secrete IL-1 β *in vitro* (Akama and Van Eldik, 2000). These studies indicate PRDX-6 may play a role in inflammatory signalling through its PLA₂ activity, as well as an antioxidant action through peroxidase activity. We do not know at this time whether PRDX-6 is providing antioxidant and/or inflammatory function in the *Psmc1^{fl/fl};CaMKII α -Cre*.

4.3.4 Downregulation of STMN-1 suggests dysregulation of the cytoskeleton

We found that Stathmin-1 was significantly decreased to undetectable levels in the *Psmc1^{fl/fl};CaMKII α -Cre* brain cortex. In human brain tissue, double immunofluorescent staining has shown that STMN-1 co-localizes with neuronal marker MAP2, but not with GFAP, a marker of astrocytes, suggesting this protein is neuronal (Zhao et al., 2012). Therefore, we suggest that the STMN-1 decrease observed in *Psmc1^{fl/fl};CaMKII α -Cre* cortex is in neurones which are affected by 26S proteasomal deletion. This finding can place the question of whether STMN-1 expression is regulated by UPS; and dysfunction of this system can cause its downregulation, or this was consequences of ubiquitin pathology and

neurodegeneration which normally change protein homeostasis. To place a possible applicable answer for this question, it is necessary to come cross STMN-1 function and role in the normal and in the neurodegenerative system in relation to cytoskeleton regulation.

STMN-1 is an important regulatory protein involved in microtubule (MT) dynamics and therefore the cell's cytoskeleton. MTs are highly dynamic structures that continuously assemble and disassemble. MT dynamics must be controlled to maintain normal cell function and remodeling in response to the cell's needs (Feinstein and Wilson, 2005). STMN-1 interacts with tubulin dimers and its function described as a microtubule (MT) dynamic regulator (Belmont and Mitchison, 1996)

We would expect that the loss of STMN-1 in *Psmc1^{fl/fl};CaMKII α -Cre* cortex will disrupt MT dynamics. In neurones, the synaptic structure is reliant on regulated MT dynamics. Improper dynamics can reduce neuronal plasticity leading to cognitive impairment. Excessive plasticity can also cause neurological disorders such as seizures (Scharfman, 2002). Several studies implicate STMN-1 in neuronal plasticity. The STMN-1 null mouse shows age-dependent axonopathy and deficits in long term potentiation, suggested STMN-1 involvement in synaptic plasticity for learning and memory (Liedtke et al., 2002; Shumyatsky GP et al., 2005). Therefore, decreased STMN-1 in the *Psmc1^{fl/fl};CaMKII α -Cre* cortex may be involved in the learning and memory deficits previously reported in these mice (Bedford et al., 2008). However, a histological study in the temporal cortex of epileptic patient showed STMN-1 positive neurones associated with increased expression (Zhao et al., 2012)

Regulation of the expression of STMN-1 has been studied. It has been shown that STMN-1 mRNA levels were downregulated following p53 induction by apoptotic insults such as UV irradiation, temperature shift and doxorubicin treatment (Ahn et al., 1999). In addition, p53 negatively regulated STMN-1 expression at the level of both transcription and translation in a human cancer cell line. This study indicated transcriptional repression of STMN-1 by P53 (Johnsen et al., 2000). We previously reported that 26S proteasome deletion in the mouse brain causes upregulation of p53 (Bedford et al., 2008). Therefore, it is possible that STMN-1 downregulation is connected to increased expression of p53 and that this is part of a p53-regulated apoptotic signalling process controlled by p53 leading to neuronal loss.

4.3.5 Downregulation of mFUMH suggests mitochondrial dysfunction in *Psmc1^{fl/fl};CaMKII α -Cre* mouse cortex

Mitochondrial Fumarate hydratase (mFUMH) is an enzyme that catalyses the reversible conversion of fumarate to malate in the Krebs cycle. A mutant form has been identified that causes fumarase deficiency leading to encephalopathy (Zinn et al., 1986; Gellera et al., 1990). In *Psmc1^{fl/fl};CaMKII α -Cre* mouse cortex, mFUMH expression was decreased ~ 25 % compared to controls, indicating decreased mitochondria and/or mitochondrial dysfunction.

The mitochondrion is an essential energy-generating organelle; it produces ATP via the respiratory chain reaction and Krebs cycle. ATP is critical for high energy-requiring organs such as the brain. Mitochondrial dysfunction has been extensively implicated in neurodegenerative disease, particularly PD. It has been shown that inhibition of complex I of the respiratory chain by MPTP in the substantia nigra causes degeneration of dopaminergic neurones and acute models of Parkinsonism (Langston et al., 1983). Other PD-related proteins have been linked to mitochondrial function, including PINK1 (mitochondrial serine/threonine-protein kinase), Parkin (E3 ubiquitin ligase), DJ-1 (redox-sensitive chaperone) and LRRK2 (Leucine-rich repeat kinase 2, function in protein folding) (Onyango, 2008). To our knowledge there is no study investigating specifically mFUMH in PD, DLB, AD or related animal models. Therefore, we report a novel connection between neurodegeneration following 26S proteasomal deletion and decreased mFUMH expression that may be a consequence of mitochondrial dysfunction and energy metabolism impairment in *Psmc1^{fl/fl};CaMKII α -Cre* mouse cortex.

The major consequence of mFUMH deficiency is increased fumarate levels. This was detected in the CSF of patients with mFUMH deficiency (Deschauer et al., 2006) and in the cardiomyocytes of FUMH-M null mice (Ashrafian et al., 2012). In the latter study, fumarate increase was shown to be protective against ischemic-reperfusion injury; an injury causes oxidative stress, inducing the nuclear factor erythroid 2-related factor 2 (Nrf2) transcription factor associated with antioxidant pathways (Ashrafian et al., 2012). Nrf2 has been shown to be ubiquitinated for proteasomal degradation (Sekhar et al., 2002; Egger et al., 2009) indicating that the UPS may be involved in the regulation of Nrf2 and the antioxidant response. In general we can

conclude that *Psmc1^{fl/fl};CaMKII α -Cre* mice suffering from energy metabolism impairment in their cortices which probably affects other neuronal vital function.

4.3.6 Downregulation of neurogranin (NEUG) may cause postsynaptic impairment

Neurogranin is highly expressed in selective neurones of the mammalian cerebral cortex, hippocampus, and amygdala; areas known for their learning and memory tasks (Watson et al., 1990). NEUG is involved in the regulation of postsynaptic signalling. The absence of NEUG has been associated with altered Ca^{2+} dynamics in cortical neurones (Gerendasy and Sutcliffe, 1997; Vanden Hoek et al., 1997). We found that NEUG was ~ 30 % less in the mouse cortex following 26S proteasome deletion. We previously reported deficits in spatial learning and memory in these mice, which are consistent with the learning and memory deficits reported in NEUG knockout mice (Pak et al., 2000; Bedford et al., 2008). Therefore, it is possible that the learning and memory defects in *Psmc1^{fl/fl};CaMKII α -Cre* may be associated with downregulation of NEUG.

NEUG is a specific substrate for Protein Kinase C (PKC) (Baudier, 1991) and binds to calmodulin (CaM) (Huang et al., 2004b). Phosphorylation of NEUG by PKC can reduce its binding to the CaM protein, thereby increasing free Ca^{2+} . In addition, at the postsynaptic membrane, phosphorylated NEUG can stimulate G-protein coupled receptors of the phosphoinositide pathway leading to release of intercellular Ca^{2+} (Cohen et al., 1993). Therefore, NEUG phosphorylation by PKC can stimulate Ca^{2+} and Ca^{2+} /CaM-dependent enzymes involved in synaptic plasticity, learning and memory (Huang et al., 2004b). Since CaMKII α expressing neurones are targeted by 26S proteasomal depletion in the mouse model, this supports the decreased expression of NEUG. Studies have shown decreased post-synaptic NEUG in the frontal cortex of neurodegenerative disease patients, including AD (Reddy et al., 2005). Elevated NEUG was also shown in the CSF of patients with AD, suggested this was due to synaptic degeneration (Thorsell et al., 2010). Postsynaptic loss is also a feature of PD and DLB (Revuelta et al., 2008; Nikolaus et al., 2009).

Summary

26S proteasomal deletion in CaMKII α -expressing neurones of the mouse brain associated with neurodegeneration and inclusion body formation is accompanied by changes in several pathways, including inflammation, energy metabolism, synaptic plasticity and axonal integrity. 26S proteasomal deletion is conditionally targeted to neurones and therefore the astrogliosis must be a consequence of cross-talk between neural cells in the mouse brain as a consequence of neuronal changes leading to neurodegeneration. Increased expression of PRDX-6 is an indication of changes in cortical oxidative homeostasis and/or phospholipase activity and now merits further investigation (see chapter 5).

This is the first proteomics study of a mouse model of cortical inclusion body formation and neurodegeneration as a consequence of 26S proteasomal deletion. The proteins identified will need to be investigated in human samples from PD, DLB and PDD. However, the data so far has provided known and novel mechanisms for further investigation.

4.3.7 Limitations of Proteomics in *Psmc1^{fl/fl};CaMKII α -Cre* brain cortex mice

Although our 2-D DIGE study successfully identified differentially expressed proteins, a much higher number than 24 spots was expected to be identified. The fact that 26S proteasomal deletion is conditionally targeted to CaMKII α neurones means that this study is conducted in a mixed cell population containing targeted and non-targeted neural cells. This is further complicated by the increased number of astrocytes in the *Psmc1^{fl/fl};CaMKII α -Cre* cortex. Proteins with low abundance, even if they are differentially expressed, may not be detected using this approach. There may also be some inconsistency between 2-DG and 1-DG Western blotting as a result of different isoforms that cannot be resolved on 1-DG. In addition, basic proteins ($pI > 10$) as well as hydrophobic proteins with difficult solubility may not be best suited to this approach. In general, these are some inherent limitations of this technique.

CHAPTER 5

Changes in redox homeostasis and PLA₂ activity in
Psmc1^{fl/fl};CaMKII α -Cre mouse cortex

5.1 Introduction

The 2-D DIGE proteomic investigation described in Chapter 4 showed reactive astrogliosis in *Psmc1^{fl/fl};CaMKII α -Cre* cortex by upregulation of GFAP and VIME. Interestingly, the increased expression of antioxidant enzyme PRDX-6 was also associated with astrocytes. PRDX-6 has been reported to be associated with oxidative stress and neurodegeneration (Power et al., 2002; Boukhtouche et al., 2006; Yoon et al., 2009). Several studies have also shown oxidative stress as a result of changes in protein homeostasis in brain in PD and DLB (Castellani et al., 1996; Giasson et al., 2000; Yan et al., 2012). Since proteasomal dysfunction and oxidative stress are implicated in the pathogenesis of neurodegenerative disease, this chapter aimed to further investigate oxidative stress and PRDX-6 *in vivo* in the brain following 26S proteasomal depletion in cortical neurones. This was investigated at various ages following *Psmc1* deletion to provide a general picture of the changes occurring in the mouse brain associated with neurodegeneration, astrogliosis and PRDX-6.

PRDX-6 can reduce H₂O₂ as well as phospholipid hydroperoxides (Fisher et al., 1999). PRDX-6 upregulation in cortical tissue of *Psmc1^{fl/fl};CaMKII α -Cre* mice lead us to investigate whether 26S proteasomal depletion causes the production of reactive oxygen species (ROS) and a cascade of oxidative stress targeting lipids, protein as well as DNA.

Although the peroxidase activity of PRDX-6 is associated with antioxidant properties, PRDX-6 also has phospholipase A₂ (PLA₂) activity that may be associated with other beneficial and/or detrimental functions. Therefore, we further investigate this activity of PRDX-6 in this chapter.

5.2 Results

5.2.1 Malondialdehyde levels are increased in *Psmc1^{fl/fl};CaMKII α -Cre* cortices

The high polyunsaturated fatty acid content of the brain lipids makes it susceptible to oxidation. An increased concentration of malondialdehyde (MDA) is used as an index of lipid peroxidation *in vivo* and *in vitro* (Lazzarino et al., 1995). We measured the total amount of MDA in control and *Psmc1^{fl/fl};CaMKII α -Cre* mouse cortices at 4, 5 and 6 weeks of age. In this experiment, homogenization buffers contained the antioxidant butylated hydroxytoluene (BHT) that has been shown to prevent auto-oxidation of samples (Pikul and Leszczynski, 1986) was used. Importantly, in this experiment we measured total MDA. Since MDA can react and bind to proteins or DNA forming cross-linked products (Marnett, 1999; Rittie et al., 2002).

Figure 5.1 shows significantly increased MDA concentrations in *Psmc1^{fl/fl};CaMKII α -Cre* cortex at 5 and 6 weeks of age. At 6 weeks, the MDA concentration was 8.62 ± 0.42 nM / μ g in *Psmc1^{fl/fl};CaMKII α -Cre* cortex compared to 6.513 ± 0.55 nM / μ g in the control ($p < 0.01$). At 5 weeks of age, the MDA concentration was 18.25 ± 1.01 nM / μ g and 12.63 ± 0.56 nM / μ g in *Psmc1^{fl/fl};CaMKII α -Cre* and control cortices respectively ($p < 0.001$). The MDA levels were not significantly different between *Psmc1^{fl/fl};CaMKII α -Cre* and controls at 4 weeks of age. The increased MDA levels in *Psmc1^{fl/fl};CaMKII α -Cre* cortex following 26S proteasomal dysfunction are suggestive of increased lipid peroxidation (or abnormal lipid metabolism). In both *Psmc1^{fl/fl};CaMKII α -Cre* and control cortices, the level of MDA at 6 weeks was lower than at earlier ages. This may be explained by interassay variation. The assays at 6 weeks were measured on a different day to the other age groups.

MDA can be measured by different methods. Increased MDA-Lysine-modified α -synuclein was detected in the frontal cortex of PD and DLB patients by Western blotting with anti-MDA-Lysine antibody, indicating the ability of MDA to covalently modify to disease-associated proteins (Dalfo and Ferrer, 2008). Another study used the thiobarbituric acid assay to show increased MDA levels in the substantia nigra of a mouse model of PD induced by chemical toxin MPTP (Sun et al., 2010). These previous studies support our findings that increased MDA is associated with neurodegeneration.

In our study, the increased concentration of MDA was associated with reactive gliosis, since MDA was significantly elevated in *Psmc1^{fl/fl};CaMKII α -Cre* mice cortices at age of 5 weeks and reactive astrocytes was evident at 4 weeks in the *Psmc1^{fl/fl};CaMKII α -Cre* cortical mice tissue (Bedford et al., 2008).

Figure 5.1

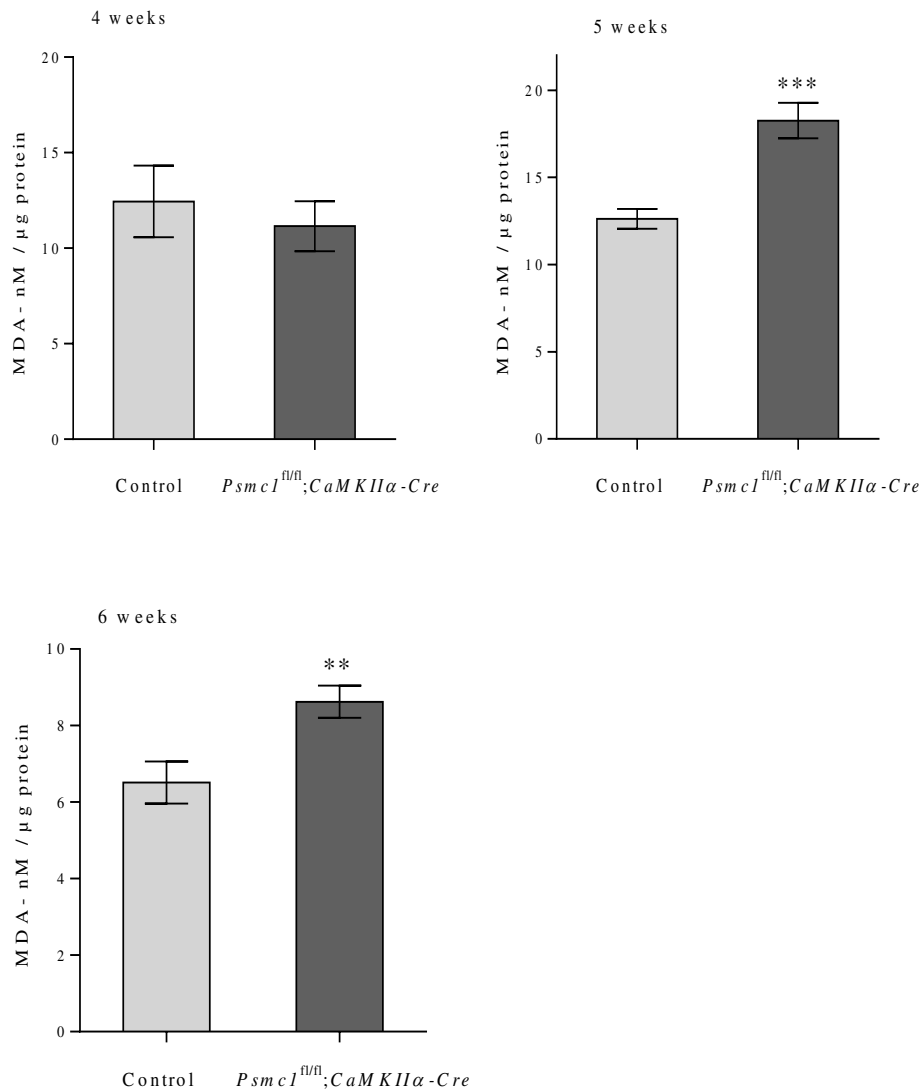


Figure 5.1 Cortical MDA concentrations in *Psmc1^{fl/fl};CaMKII α -Cre* and control mice at 4, 5 and 6 weeks of age. Data were statistically analyzed by unpaired Student's *t*-test and presented as mean \pm SEM. $n = 8$. ** $p < 0.01$, *** $p < 0.001$.

5.2.2 Measurement of protein carbonyl group in *Psmc1^{fl/fl};CaMKII α -Cre* cortex showed no change compared to control.

The protein carbonyl group is a hallmark of protein oxidation (Shacter, 2000). Several amino acid side chains can be oxidized, e.g. Lys, Arg, Pro, Thr, into carbonyl derivatives (Shacter, 2000). Figure 5.3 shows that protein carbonyl groups were not significantly different between *Psmc1^{fl/fl};CaMKII α -Cre* and control cortices at 6 weeks of age. Therefore, this investigation was not carried out with 4 and 5 week-old samples. This result suggests that neurodegeneration following 26S proteasomal depletion in mouse cortical neurones is not associated with protein oxidation.

Figure 5.2

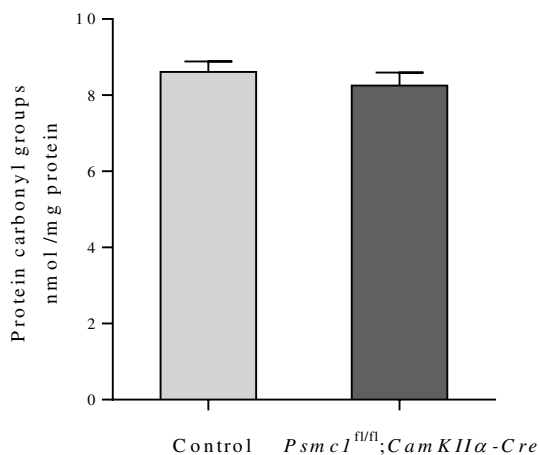


Figure 5.2 The level of protein carbonyl groups in *Psmc1^{fl/fl};CaMKII α -Cre* and control mice cortices at 6 weeks age. Data were statistically analyzed by Student's *t*-test and presented as mean \pm SEM. *n* = 10.

5.2.3 Increased nitro-tyrosinated proteins in *Psmc1^{fl/fl};CaMKII α -Cre* cortex

Although protein carbonyl groups were not changed in *Psmc1^{fl/fl};CaMKII α -Cre* cortex, we investigated nitrated proteins in *Psmc1^{fl/fl};CaMKII α -Cre* and control cortices. Reactive nitrogen species (RNS), such as peroxynitrite, are produced by the reaction of nitric oxide and superoxide radicals. Tyrosine residues in proteins can undergo nitration by peroxynitrate (Shacter, 2000).

In this experiment, we used Western blotting of 6 week-old *Psmc1^{fl/fl};CaMKII α -Cre* and control cortical protein samples homogenized in RIPA buffer with a nitro-tyrosine mouse monoclonal antibody. Figure 5.3 shows a representative Western blot image. A positive control for nitrated proteins was prepared with 1 mM peroxynitrite solution as described in the materials and methods (see section 2.6.3)

Four nitrated protein bands were detected in control and *Psmc1^{fl/fl};CaMKII α -Cre* cortices as indicated in Figure 5.3. These bands were subject to densitometry and statistical analysis as shown in Figure 5.4. Nitrosylated protein bands 2-4 were significantly increased in the *Psmc1^{fl/fl};CaMKII α -Cre* cortex compared to control ($p < 0.01$). This suggests the presence of nitrative stress following 26S proteasomal depletion in the mouse cortex.

Previous studies have shown that nitrative stress is a feature of neurodegeneration. Nitro-tyrosinylated proteins were observed in surviving neurones of the substantia nigra in PD and the Lewy body core immunolabeled with nitro-tyrosine antibody, which may correspond to nitrated neurofilament proteins (Good et al., 1998). In another postmortem study in a patient with acute multiple sclerosis, hypertrophic astrocytes stained positive with nitro-tyrosine antibody (Oleszak et al., 1998). *Psmc1^{fl/fl};CaMKII α -Cre* showed extensive astrogliosis and it would be interesting to investigate whether astrocytes are positive for nitro-tyrosine.

Figure 5.3

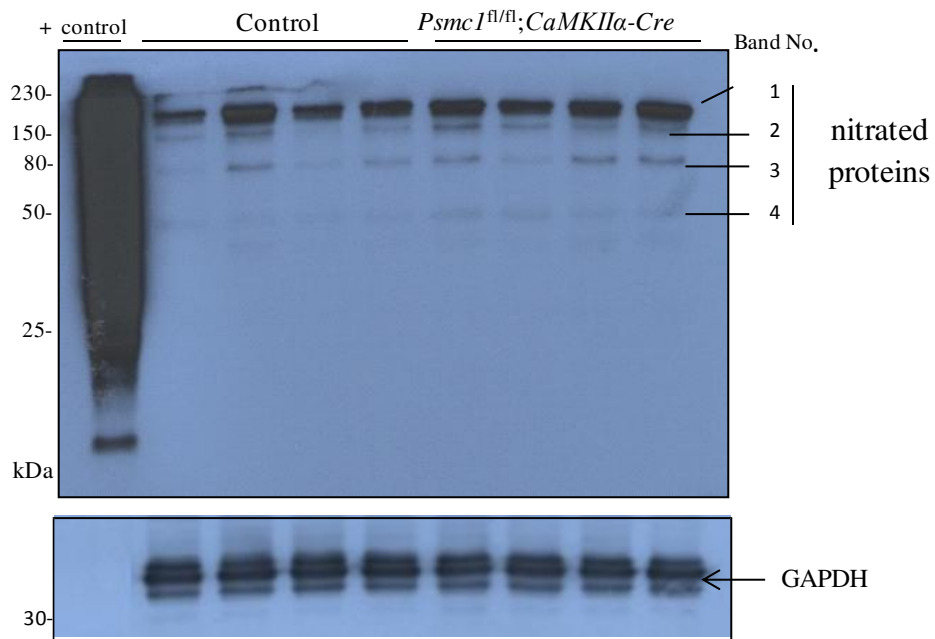


Figure 5.3 Representative Western blot analysis of nitrated proteins. The blot was re-probed with anti-GAPDH antibody as a protein loading control for normalization. Four nitrated protein bands were identified. A positive control (+ control) was included in the Western blot produced as described in section 2.6.3. The results of densitometry analysis are presented in Figure 5.4

Figure 5.4

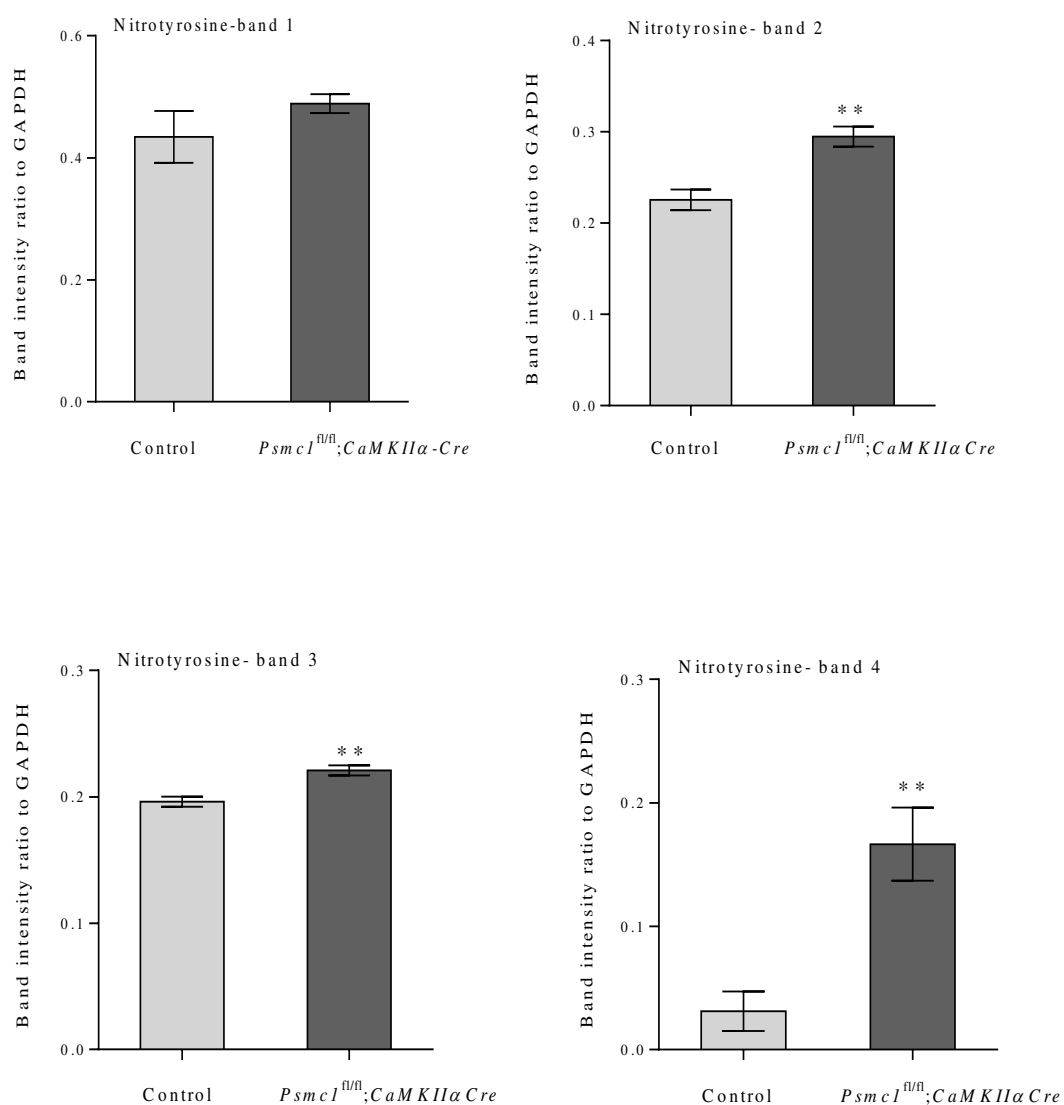


Figure 5.4 Densitometry analyses of nitrated proteins from Figure 5.3. Densitometry of the four bands was normalized to the corresponding GAPDH and analyzed using unpaired Student's *t*-test. The data are presented as mean \pm SEM. $n = 4$. ** $p < 0.01$.

5.2.4 Reactive oxygen species decline with increasing age in the cortex of *Psmc1^{fl/fl};CaMKII α -Cre* mouse

To further investigate changes in redox homeostasis, we measured reactive oxygen species (ROS) in *Psmc1^{fl/fl};CaMKII α -Cre* and control cortices. Since ROS trigger oxidative changes, we investigated time-points from *Psmc1* deletion at 2 weeks of age to allow correlation with our previous data on oxidative stress. We measured ROS in control and *Psmc1^{fl/fl};CaMKII α -Cre* cortical tissue at 17 days, 3, 4, and 6 weeks of age. Figure 5.5 shows the results of ROS analysis. In 17 day-old mice, there was a tendency for ROS to be increased, but this was not significant (Figure 5.5). No significant difference in ROS was found at 3 weeks of age, but interestingly, at 4 and 6 weeks of age ROS significantly decreased. Correlation analysis showed a statistically significant linear relationship between *Psmc1^{fl/fl};CaMKII α -Cre* mice age and change in ROS level ($p < 0.05$) (Figure 5.6). As expected, for control mice the data was not significant (Figure 5.6).

In general, ROS are diverse species, including superoxide, hydroxyl radicals and non-radical H₂O₂. The DCFDA kit; 2, 7-dichlorofluorescein diacetate (see section 2.7.3) used in our study detects hydroxyl and peroxy species. Other studies have shown DCFDA is not sensitive to the superoxide radical, but oxidized by the hydroxyl radical or H₂O₂ (Rothe and Valet, 1990; Vanden Hoek et al., 1997). In addition, we found tert-butyl hydrogen peroxide induced oxidative stress similarly in both *Psmc1^{fl/fl};CaMKII α -Cre* and control cortex homogenates. Since the hydroxyl radical has a very short half-life, particularly in a cell-free system, we suggest that we are measuring mostly measured H₂O₂ in cortical homogenates using DCFDA.

The decreased ROS in 4 and 6 week-old *Psmc1^{fl/fl};CaMKII α -Cre* mouse cortices is not consistent with the evidence of oxidative stress as indicated by increased lipid peroxidation and nitrated proteins as shown in sections 5.2.1 and 5.2.3 respectively. However, ROS may have triggered oxidative stress at an early time point. There was a tendency for increased ROS at 17 days old in 26S proteasome-depleted cortex that may have caused oxidative stress. Interestingly, lipid peroxidation is self-catalytic once initiated. Therefore, lipid oxidation may increase through these mechanisms despite evidence that hydroxyl and hydrogen peroxide species are decreased. This increases the complexity of observations made in the *Psmc1^{fl/fl};CamKII α -Cre* cortex associated with neurodegeneration.

Figure 5.5

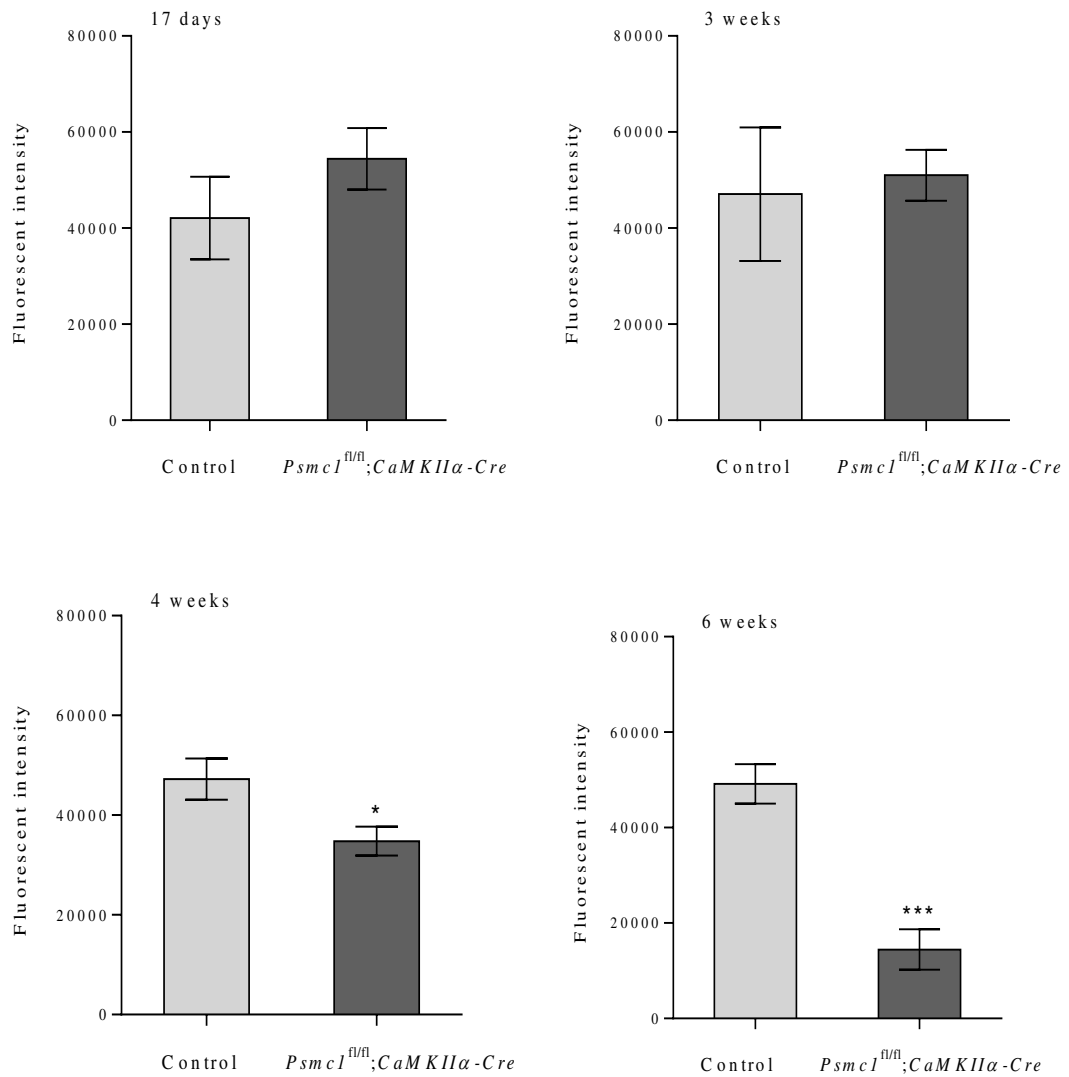


Figure 5.5 Fluorescent intensities produced by ROS in control and *Psmc1^{fl/fl}; CaMKIIα-Cre* mice cortices. Measurements were performed at different ages as indicated. The data are presented as mean \pm SEM. n = 5 for two weeks; n = 8 three weeks; n = 9 four weeks and n = 11 for six weeks. *** $p < 0.01$, * $p < 0.05$, Student's *t*-test.

Figure 5.6

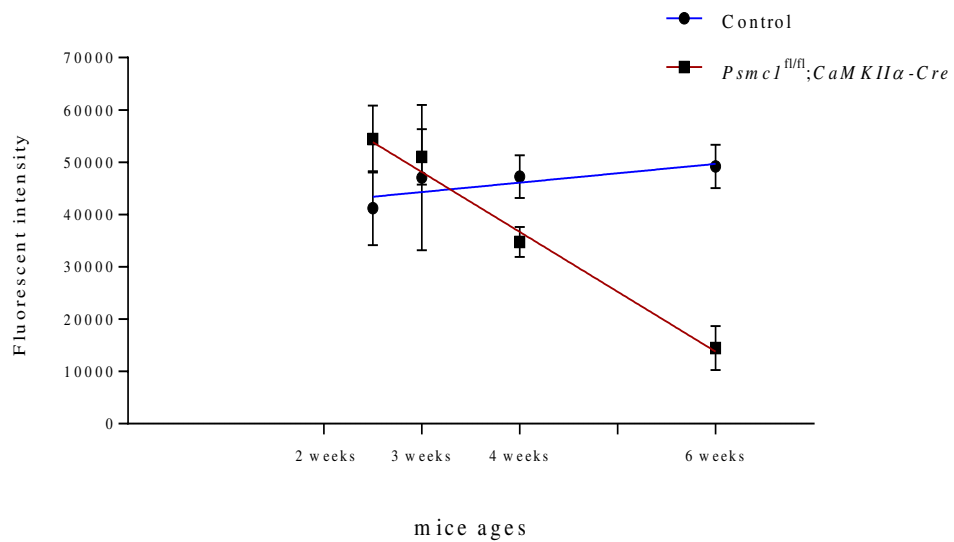


Figure 5.6 Correlation and regression analysis of ROS levels with age. The linear regression analysis was significant for *Psmc1*^{fl/fl}; *CaMKIIα-Cre* cortex ($p < 0.0001$) and $R^2 = 0.69$, but not control ($p = 0.36$) and $R^2 = 0.03$. There is significant inverse correlation between ROS and mice age in *Psmc1*^{fl/fl}; *CaMKIIα-Cre*, $R = 0.9$; but not for control. The data are represented as mean \pm SEM.

5.2.5 PRDX-6 expression increases with age in *Psmc1^{fl/fl};CaMKII α -Cre* cortex

To further investigate PRDX-6, identified in the 2-D DIGE proteomic study as significantly increased at 6 weeks of age, we investigated the expression of PRDX-6 from 2 weeks of age when *Psmc1* is deleted in cortical neurones initiating neurodegeneration. The results of Western blotting analysis are shown in Figure 5.7. Densitometry was used to quantitate PRDX-6 expression between control and *Psmc1^{fl/fl};CaMKII α -Cre* cortices, normalized to β -actin and is shown in Figure 5.8. The results were then analyzed by unpaired Student's *t*-test. PRDX-6 expression showed an increase at 5 weeks of age ($p = 0.07$), but was not statistically significant until 6 weeks of age ($p < 0.01$). Further statistical analysis showed a significant correlation between increased PRDX-6 expression and age ($p < 0.05$) (Figure 5.9).

This data indicates that an antioxidant system is activated in the brain following 26S proteasomal depletion in cortical neurones accompanying neurodegenerative changes. Analysis of the relationship between PRDX-6 and ROS in *Psmc1^{fl/fl};CaMKII α -Cre* mice showed an inverse correlation in Figure 5.10.

Figure 5.7

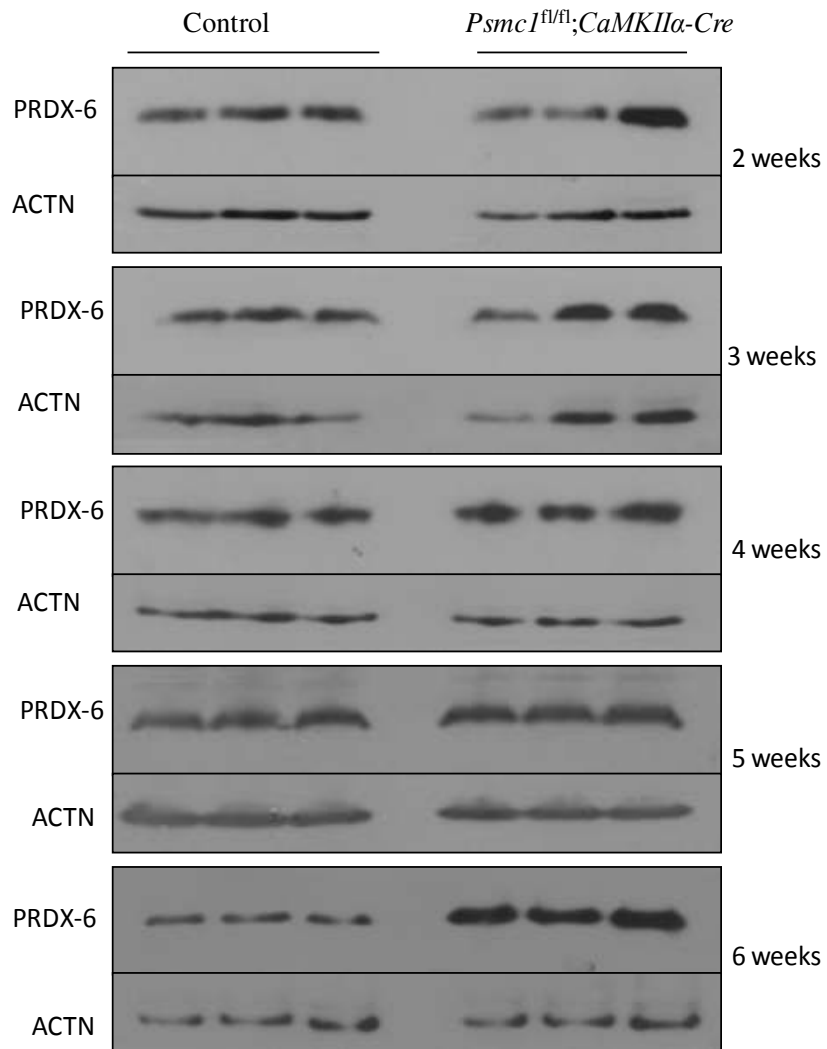


Figure 5.7 Western blots of cortical homogenates from control and *Psmc1^{fl/fl};CaMKIIα-Cre* mice for PRDX-6 at 2, 3, 4, 5 and 6 weeks of age. β -actin (ACTN) was used as a protein loading control. The band intensities from these images were measured by densitometry and the data statistically analyzed as shown in Figure 5.8.

Figure 5.8

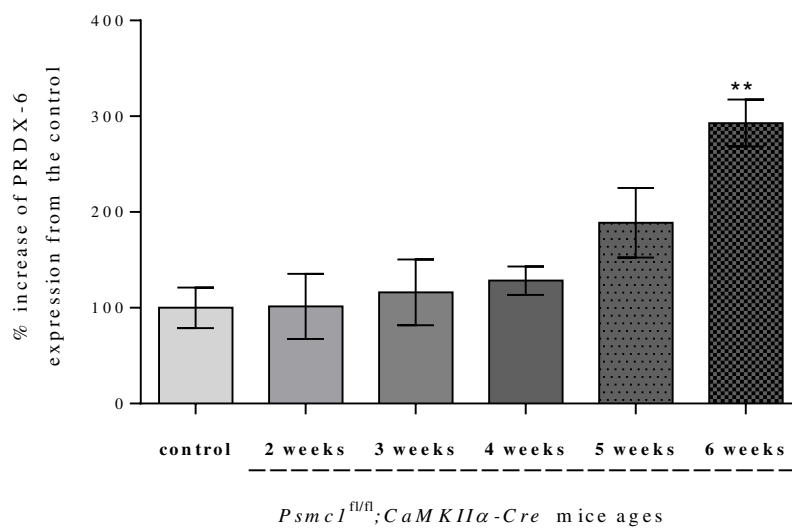


Figure 5.8 Relative PRDX-6 expression levels in *Psmc1^{fl/fl};CaMKII α -Cre* mice compared to controls at different ages. The data are presented as mean \pm SEM. n = 3. ** $p < 0.01$ versus control by using a *post hoc* Dunnett's Multiple Comparison Test.

Figure 5.9

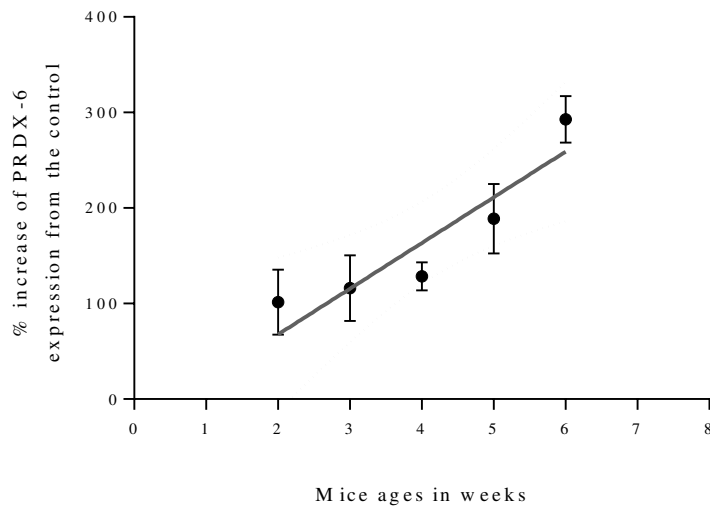


Figure 5.9 Correlation analysis of PRDX-6 expression and age in *Psmc1^{fl/fl};CaMKII α -Cre* mouse cortex. There is a positive correlation with $p < 0.05$ and $R = 0.84$. The data are represented as mean \pm SEM. Dotted lines show the 95 % confidence interval.

Figure 5.10

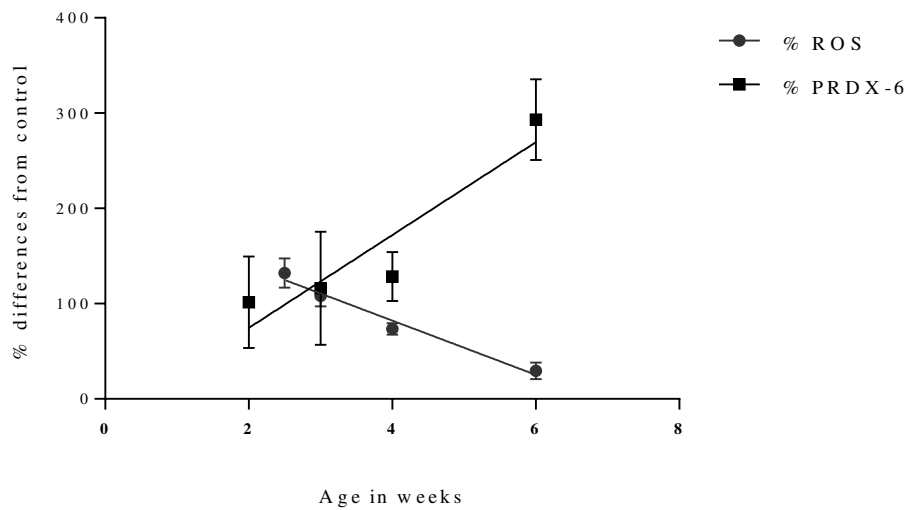


Figure 5.10 Inverse relationships between % increase of PRDX-6 expression and % decrease of ROS in *Psmc1^{fl/fl};CaMKII α -Cre* mouse cortex from the control ($p < 0.05$); $R = 0.9$, and $R = 0.84$ respectively. Values are presented as mean \pm S.E.M.

5.2.6 Modification of PRDX-6 in the *Psmc1^{fl/fl};CaMKII α -Cre* mouse cortex

We further investigated PRDX-6 expression profile at 6 weeks of age using 2DG electrophoresis followed by PRDX-6 Western blotting. We noted increased expression of the major PRDX-6 spot (Figure 5.11; spot 1) in *Psmc1^{fl/fl};CaMKII α -Cre* cortex compared to control. In addition, there was a more acidic minor PRDX-6 spot (Figure 5.11; spot 2) that was also increased in the *Psmc1^{fl/fl};CaMKII α -Cre* cortex.

A previous study reported oxidation of Cysteine-47 residue of PRDX-6 in the presence of H₂O₂ *in vitro* in melanoma cell line that would cause a similar acidic shift in 2DG analysis (Jeong et al., 2012). Therefore, PRDX-6 is known to undergo post-translational modifications, including oxidation.

Figure 5.11

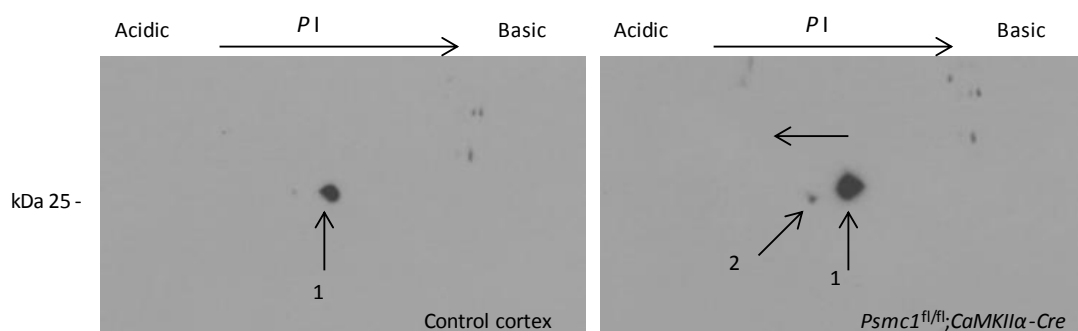


Figure 5.11 2D PRDX-6 Western blotting of control and *Psmc1^{fl/fl};CaMKIIα-Cre* cortices. Two PRDX-6 spots were identified as indicated. Spot 1 is the major spot identified by 2-D DIGE analysis. Spot 2 represents an acidic shift (arrow) that may be a post-translational modification such as oxidation.

5.2.7 Phospholipase A2 enzyme activity is increased the *Psmc1^{fl/fl};CaMKII α -Cre* cortex

PRDX-6 is a bifunctional enzyme with peroxidase and phospholipase A₂ (PLA₂) activities (Fisher et al., 1999). Therefore, we decided to investigate PLA₂ activity in control and *Psmc1^{fl/fl};CaMKII α -Cre* mouse cortex.

PLA₂ activity was measured in control and *Psmc1^{fl/fl};CaMKII α -Cre* cortices at 4, 5 and 6 weeks of age (Figure 5.12). The results show that PLA₂ activity was significantly increased in *Psmc1^{fl/fl};CaMKII α -Cre* (1.472 ± 0.1247 U/ml/mg protein) compared to control (0.8145 ± 0.1274 U/ml/mg protein) mice at 6 weeks of age ($p < 0.01$). The increase at 5 weeks of age was also reaching significance ($p = 0.07$).

These results show PLA₂ activity is increased in *Psmc1^{fl/fl};CaMKII α -Cre* cortices. Since, the phospholipase enzymes are a superfamily, we then investigated whether this increased activity was due to PRDX-6. 1-Hexadecyl-3-trifluoroethylglycero-sn-2-phosphomethanol (MJ33) is a fluorinated phospholipid analogue that can inhibit the PLA₂ activity of PRDX-6 (Chatterjee et al., 2011). Therefore, MJ33 was incubated with the cortical homogenate prior to PLA₂ activity measurement. Figure 5.13 shows significant inhibition of PLA₂ activity in *Psmc1^{fl/fl};CaMKII α -Cre* mouse cortices. Inhibition of enzyme activity was also evident in the control cortex, but the levels of PLA₂ activity in general were low and therefore inhibition was not significant. Therefore, we suggest that at least some of the increased PLA₂ activity is due to increased expression of PRDX-6 in the *Psmc1^{fl/fl};CaMKII α -Cre* mouse cortex.

Figure 5.12

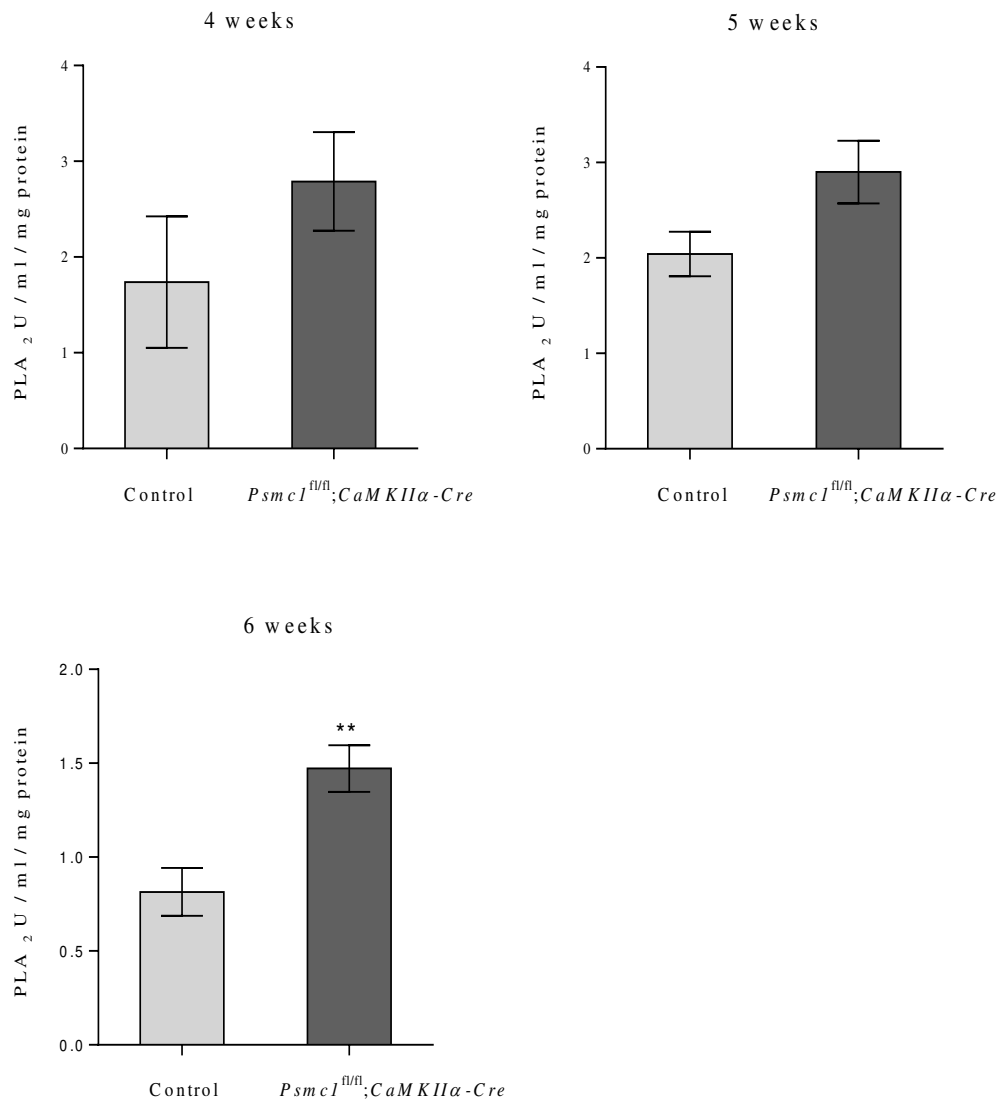


Figure 5.12 PLA₂ enzyme activities in control and *Psmc1^{fl/fl};CaMKIIα-Cre* mice cortices at 4, 5 and 6 weeks of age. The data was analyzed by unpaired Student's *t*-test (n = 4). Values are presented as mean ± S.E.M. ** *p* < 0.01.

Figure 5.13

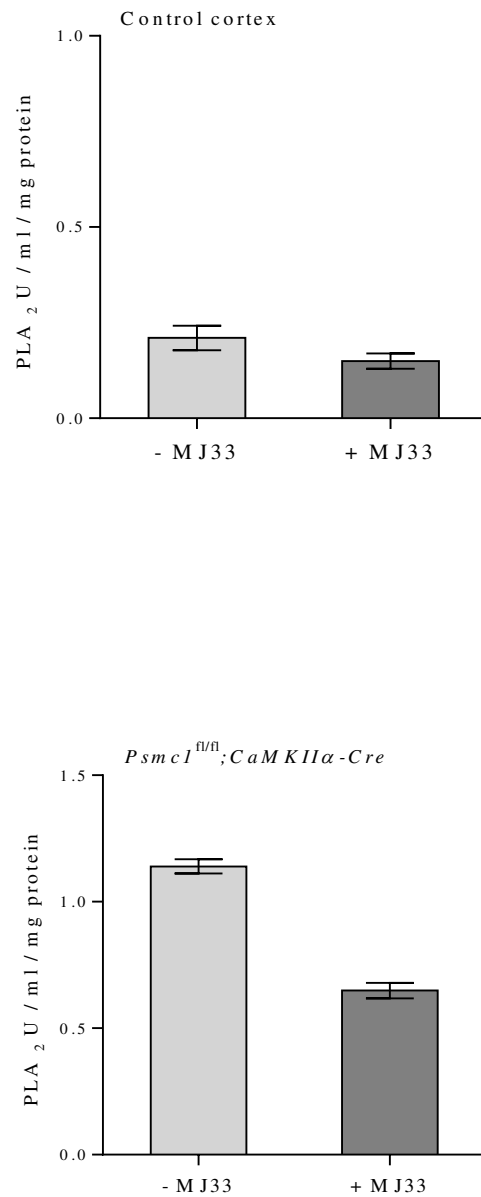


Figure 5.13 PLA₂ enzyme activities in control and *Psmc1^{fl/fl};CaMKIIα-Cre* mice cortices at 6 weeks of age in the presence and absence of MJ33 inhibitor. The data was analyzed by unpaired Student's *t*-test (n = 4). Values are presented as mean ± S.E.M. *** *p* < 0.001.

5.3 Discussion

Oxidative stress has been implicated in the pathogenesis of neurodegenerative disease (Dalfo et al., 2005; Gironi et al., 2011). We have shown here changes in oxidative homeostasis in the cortex following 26S proteasomal depletion in cortical neurones. Markers of lipid peroxidation and nitrated proteins were increased in *Psmc1^{fl/fl};CaMKII α -Cre* brain compared to controls. Interestingly, these changes were associated with decreased levels of ROS at similar ages. Furthermore, the PLA₂ activity of PRDX-6 was increased that may be associated with a change in oxidative homeostasis and/or phospholipid metabolism. This complex scenario in the *Psmc1^{fl/fl};CaMKII α -Cre* brain provides interesting data related neurodegenerative changes as a consequence of 26S proteasome depletion.

One of the significant biochemical changes observed in the *Psmc1^{fl/fl};CaMKII α -Cre* cortex was increased PLA₂ activity associated with increased PRDX-6. We found PRDX-6 expression in astrocytes as part of the extensive astrogliosis accompanying neurodegeneration in this mouse model. In general, the phospholipase enzymes facilitate membrane phospholipid remodeling and synthesis of some eicosanoids (Figure 5.14).

Previous studies have suggested that increased phospholipase activity may be harmful. In PC12 cells, increased PLA₂ activity was shown to have a significant role in hypoxic nuclear shrinkage; a feature of pyknosis (Shahnawaz et al., 2007). Hyperoxidation of PRDX-6 by H₂O₂ was associated with increased PLA₂ activity and cell cycle arrest in HeLa cells (Kim et al., 2008). *In vivo*, inhibition of PLA₂ activity decreased MPTP-induced dopamine loss in the PD mouse model of neurodegeneration (Tariq et al., 2001). Therefore, the increased PLA₂ activity in astrocytes in the *Psmc1^{fl/fl};CaMKII α -Cre* cortex may be involved in harmful rather than protective mechanisms during neurodegeneration. For example, this may be involved in inflammatory signalling by astrocytes, possibly through activation of eicosanoid pathway. However, upregulation of PRDX-6 was also correlated with significantly decreased ROS levels in *Psmc1^{fl/fl};CaMKII α -Cre* cortex, suggesting protective actions for PRDX-6, possibly associated with its peroxidase activity, in addition to mechanisms involving PLA₂ activity.

Figure 5.14

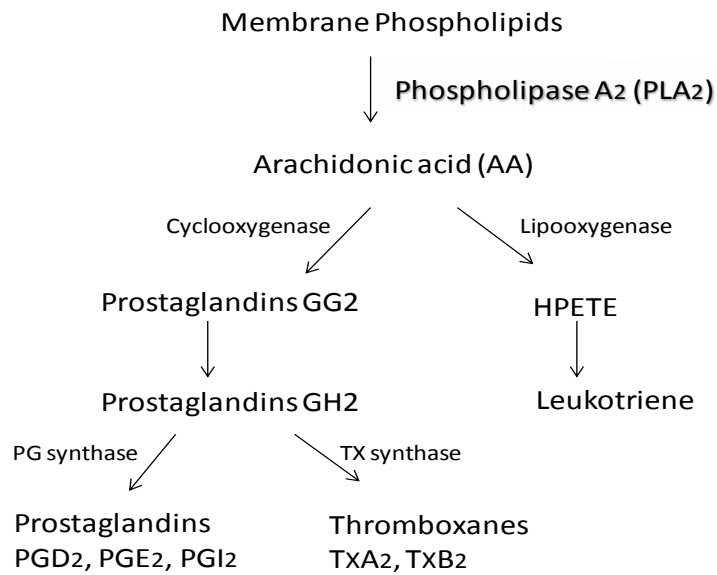


Figure 5.14 Eicosanoid biosynthesis pathway.
Abbreviations: HPETE, hydroperoxyeicosatetraenoic acid; Tx, Thromboxane; PG, Prostaglandines.

Changes in the expression of antioxidant enzymes are considered an indirect biomarker of oxidative stress (Kamsler et al., 2001; Harish et al., 2013). In addition to increased expression of the antioxidant enzyme PRDX-6, we found evidence of increased lipid peroxidation and nitrated proteins, indicative of oxidative stress. However, the levels of ROS decreased in the *Psmc1^{fl/fl};CaMKII α -Cre* cortex. There was an inverse correlation between PRDX-6 expression and ROS levels suggesting PRDX-6 may detoxify ROS in the *Psmc1^{fl/fl};CaMKII α -Cre* cortex in an antioxidant protective mechanism. PRDX-6 has recently been shown to have peroxidase activity against H₂O₂ (Kim et al., 2008; Kim et al., 2011). Increased ROS could have occurred at an earlier time point before significant upregulation of PRDX-6 was detected. The results suggest that this may be between 2 and 3 weeks of age around the time when *Psmc1* is deleted in cortical neurones. Alternatively, it is possible that we did not detect all ROS with the kit used in this study. In addition, lipid peroxidation is self-catalytic and PRDX-6 is unique in its ability to reduce phospholipid hydroperoxides further supporting a role of increased PRDX-6 in protection against lipid peroxidation. Interestingly, we showed an acidic shift in PRDX-6 by 2DG Western blotting suggestive of its oxidative modification (Jeong et al., 2012). This oxidation might support the conversion of H₂O₂ to water and hence detoxification. PRDX-6 has a conserved cysteine residue (Cys⁴⁷) that oxidizes to sulfonic acid upon reduction with peroxide substrates (Wood et al., 2003).

A possible source of ROS is mitochondria. The mitochondrial electron transport chain has several redox complexes. Dysfunction of these complexes has the potential to leak electrons to oxygen forming superoxide radicals. Complex I (NADH dehydrogenase) has been shown to be the primary source of ROS in PD (Kushnareva, 2002 ; Trojanowski, 2003). Mitochondrial function is under investigation in the *Psmc1^{fl/fl};CaMKII α -Cre*. However, we know that the Lewy-like inclusions in surviving neurones following 26S proteasomal depletion contain morphologically abnormal mitochondria with disrupted cristea (Paine et al., 2013). Moreover, in this work mitochondrial fumarate hydratase was significantly decreased in the *Psmc1^{fl/fl};CaMKII α -Cre* cortex.

In several neurodegeneration diseases, proteins have been shown to undergo oxidation and nitration causing their aggregation (Martinez et al., 2010). The detection of increased nitrated protein in the *Psmc1^{fl/fl};CaMKII α -Cre* cortex is suggestive of

nitritative stress in the brain following neuronal 26S proteasomal depletion. Abnormal protein nitration can cause protein dysfunction. Nitration of α -synuclein causes the formation of a fibrillar form that resembles α -synuclein isolated from PD brains and the formation of stable intracellular α -synuclein inclusions requires tyrosine residues (Norris et al., 2003). Nitric oxide (NO) is a small, highly diffusible and reactive molecule; it can be generated by the action of nitric oxide synthase (NOS) on amino acid L-arginine (Alderton et al., 2001). There are three types of NOS; neuronal, endothelial and inducible (nNOS, eNOS and iNOS). In general, NOS can generate NO and superoxide radicals. If these radicals are not scavenged by antioxidants, they can react together to form the peroxynitrite radical; a powerful oxidant (Beckman and Koppenol, 1996; Pou et al., 1999). The peroxynitrite radical is very diffusible within cellular layers and can oxidize cellular constituents causing lipid peroxidation and protein nitration (Pacher et al., 2007). A study performed on postmortem brain tissue from PD showed iNOS expressed in astrocytes can produce high levels of NO (Hunot et al., 1996). Further histopathological studies have shown nitro-tyrosine-positive hypertrophic astrocytes and nitrated α -synuclein in classical and cortical Lewy bodies in patients with dementia (Oleszak et al., 1998, Giasson et al., 2000, Gomez-Tortosa et al., 2002). Nitric oxide was also identified in the CSF and plasma of a patient suffering from DLB and it was suggested that excessive NO production may be related to the pathogenesis of this disorder (Molina et al., 2002). These previous studies support our data that nitritative stress may be involved in the mechanisms of neurodegeneration. Interestingly, studies have indicated an involvement of NOS and the UPS; nNOS and iNOS are targets of ubiquitination and degradation by the 26S proteasome (Bender et al., 2000; Dunbar et al., 2004). Further investigations in the *Psmc1^{fl/fl};CaMKII α -Cre* cortex should include these enzyme activities.

In general, MDA is considered to be an index of lipid peroxidation resulting from the attack of ROS on membrane phospholipids (Lazzarino et al., 1995). However, MDA can be generated through the metabolism of arachidonic acid (Hecker and Ullrich, 1989). MDA is a reactive molecule that has been shown to cause lipid, protein and DNA damage. Lipid peroxidation may inhibit membrane function, destroying its barrier properties and ultimately lead to cell death (Stadelmann-Ingrand et al., 2004). Interestingly pyknotic nuclei are evident in the *Psmc1^{fl/fl};CaMKII α -Cre* cortex at 6 weeks of age (Bedford et al., 2008). Given that MDA levels are increased following

the extensive astrogliosis and neuropathological changes, it is unlikely that MDA toxicity itself initiates these processes, but more likely MDA is a product of lipid peroxidation or phospholipid metabolism. Additionally, we suggest there is a relationship between gliosis and increased MDA concentration, where astrocytic activation preceded increasing MDA raises another question that MDA may be a result of inflammatory processes associated with reactive astrocytes.

The idea that increased MDA may be a consequence of increased phospholipid metabolism cannot be excluded in this study. MDA can be generated through the action of PLA₂ on membrane phospholipids through the eicosanoid pathway. In this pathway, for example, thromboxane synthase can convert prostaglandin H₂ to thromboxane A₂ and fragmentation into MDA, and also prostaglandin G₂ can be transformed to MDA (Hecker et al., 1987; Hecker and Ullrich, 1989). To support this data, anti-inflammatory drugs such as acetylsalicylic acid and indomethacin can inhibit the formation of MDA from arachidonic acid in rat platelets rich plasma through inhibition of the cyclo-oxygenase enzyme (de Gaetano et al., 1980). Others have confirmed that PRDX-6 has PLA₂ activity (Kim et al., 2008; Wu et al., 2009; Chatterjee et al., 2011) and can release arachidonic acid from lipid membranes (Ho et al., 2010; Kim et al., 2011). It is possible that increased phospholipase activity of PRDX-6 increases the concentration of MDA through changes in eicosanoid synthesis, indicating an inflammatory response following 26S proteasome depletion in the mouse cortex. 26S proteasome depletion has been described previously to cause inflammation *in vitro* (Rockwell et al., 2000).

Protein carbonylation is another form of protein oxidation caused by oxidative stress. This did not increase in the *Psmc1^{fl/fl};CaMKII α -Cre* cortex. It is possible that the method used to detect protein carbonyls may not be of sufficient sensitivity to detect protein carbonylation in the mixed cell population of the brain. The concept of protein decarbonylation has been accepted via activation of the thioredoxin pathway (Wong et al., 2008). This is a pathway regulating cellular redox balance and alleviated damage caused by ROS.

The precise role of PRDX-6 upregulation in the *Psmc1^{fl/fl};CaMKII α -Cre* cortex is unclear. Whether this is associated with antioxidant protection and/or lipid metabolism associated with deleterious activities required further investigation.

Increased PRDX-6 may be involved in decreasing ROS or increasing the MDA concentration through its bifunctional enzymatic activities. Deleterious effects of the astrocytic expression of PRDX-6 will affect neurones that are not targeted by 26S proteasomal depletion. We show novel evidence that 26S proteasomal depletion in cortical neurones leads to evidence of oxidative stress by increased lipid peroxidation and nitrated proteins. The observations of ROS levels are interesting and it may be necessary to investigate alternative methods for the measurement of these species to clarify the results.

CHAPTER 6

General discussion and conclusion

The depletion of 26S proteasomal in neurones leads to the significant accumulation of ubiquitinated proteins, but our investigations into the ubiquitome were challenging. Ubiquitinated proteins were captured by bioaffinity chromatography using UBDs, which was optimized for the brain in this study and identified several potential ubiquitinated proteins. These were mostly associated with gene regulation and expression. The identification of ubiquitinated proteins requires their intracellular enrichment and careful sample preservation. It is possible that the mixed cell population and extensive gliosis in the brain following 26S proteasomal dysfunction limits the identification of ubiquitinated proteins accumulating in targeted neurones. The accumulation of ubiquitinated proteins in neurones may play a role in degeneration since recent evidence suggests intracellular protein accumulation is involved in pathological events leading to neuronal death (Huang and Figueiredo-Pereira, 2010).

The 2D-DIGE investigation of the 26S proteasome-depleted mouse cortex identified several differentially expressed proteins associated with neurodegeneration and inclusion formation. Several of these proteins were validated by 1D Western blotting. Decreased expression of mitochondrial fumarate hydratase, which is essential for the Krebs's cycle, suggests defects in energy metabolism following 26S proteasomal depletion. In humans, a deficiency in this enzyme is characterized by progressive neurological abnormalities (Pagon et al., 2006). Downregulation of the postsynaptic protein neurogranin and stathmin 1 suggest impairment of neuronal plasticity and may be associated with the previously reported spatial and learning deficits in these mice (Bedford et al., 2008). Neurogranin is a postsynaptic protein indicative of postsynaptic function impairment added evidence of dysfunction in the neuronal plasticity. This indicated a complex proteomic feature linked 26S depletion with toxicity of accumulated proteins possible impairment in mitochondria, and axonal disease leading to neuron die.

Neurodegeneration in this model was associated with activation of astrocytes. Upregulation of GFAP and VIME was identified in the 2D-DIGE proteomics study, indicative reactive astrogliosis. The activation of astrocytes may be triggered by many intracellular signalling molecules such as IL-6, TNF- α and NO (Sofroniew and Vinters, 2010). Increased expression of the astrocytic antioxidant enzyme PRDX-6 was indicative of oxidative stress involvement following 26S proteasomal depletion.

This is the first evidence *in vivo* in the mammalian brain that 26S proteasomal dysfunction directly causes oxidative stress.

Further biochemical studies of oxidative and nitrative stress were carried out in the *Psmc1^{fl/fl};CaMKII α -Cre* cortex. The lipid peroxidation marker MDA and protein nitration were increased. However, protein carbonyl groups were not significantly different between control and 26S proteasome depleted cortical tissue. Interestingly, ROS levels were dramatically decreased. Taken together, we have identified changes in oxidative homeostasis caused by 26S proteasomal depletion in neurones. PRDX-6 may be involved in neuroprotection against ROS, indicated by the inverse relationship between levels of PRDX-6 and ROS.

It is possible that MDA may originate from the inflammatory processes. Increased phospholipase A₂ activity was present in the 26S proteasome-depleted cortex, correlating with increased expression of PRDX-6. Whether the PLA₂ activity is beneficial or detrimental in the progression of neuronal death is unknown. PLA₂ activity has been implicated in the neurodegeneration disease (Allyson and Massicotte, 2011; Lee et al., 2011), but studies also suggest this may be a house keeping enzyme under basal conditions (Ong et al., 2010). Therefore, further investigations of this activity are necessary to further elucidate its role in the brain.

Conclusion

Our study has provided new information about the role of astrocytes in neurodegeneration. PRDX-6 may be an important antioxidant mechanism in the brain to limit oxidative stress. Dysfunction of proteasomal degradation and oxidative stress are both important hypotheses involved in neurodegenerative disease and this study has provided a potential novel insight into the interaction of these processes.

Future work

The 2D-DIGE experiment identified several differentially expressed proteins in *Psmc1^{fl/fl};CaMKII α -Cre* mouse cortical tissue. We focused the studies in this thesis on the most abundant identified proteins; GFAP, VIME and PRDX-6 which is the first *in vivo* evidence of oxidative stress as a direct consequence of 26S proteasome dysfunction. It may be possible to further these investigations and identify other protein changes by sub-cellular fractionation of the cortical tissue before 2D-DIGE analysis. Bernocco et al, (2008) used a detergent tissue pre-fractionation method to isolate sub-cellular fractions from primary culture neurones (Bernocco et al., 2008). We could perform a sequential protein solubilization of mouse cortical tissue using various detergents such as digitonin, Triton X-100 and Tween 40 using deoxycholate and urea buffers, producing sub-cellular tissue fractions according to protein solubility. This would reduce the complexity of proteins and may identify lower abundant protein changes. This future work would provide a more detailed map of the proteome changes in *Psmc1^{fl/fl};CaMKII α -Cre* mouse cortex and allow exploration of additional targets and biomarkers in neurodegenerative mechanisms.

Investigations into the consequences of increased PLA₂ activity in the mouse brain may be possible with the administration of MJ33 a PRDX6 inhibitor to mice as done in a recent study examining this activity in the mouse lung (Lee et al., 2013). This would involve intravenous administration of MJ33 using mixed unilamellar liposomes to ensure drug up-take into the brain tissue of *Psmc1^{fl/fl};CaMKII α -Cre* mice. The PLA₂ activity would then be determined at several time points (hours) after MJ33 administration. Measurements of ROS and MDA levels as well as immunohistochemical investigations of astrocytes would be carried out. These studies may indicate the relationship between these parameters, PLA₂ activity, astrocyte activation and neurodegeneration.

Bibliography

- Ahn J, Murphy M, Kratowicz S, Wang A, Levine AJ, George DL (1999) Down-regulation of the stathmin/Op18 and FKBP25 genes following p53 induction. *Oncogene* 18:5954-5958.
- Akama KT, Van Eldik LJ (2000) Beta-amyloid stimulation of inducible nitric-oxide synthase in astrocytes is interleukin-1beta- and tumor necrosis factor-alpha (TNFalpha)-dependent, and involves a TNFalpha receptor-associated factor- and NFkappaB-inducing kinase-dependent signaling mechanism. *J Biol Chem* 275:7918-7924.
- Alderton WK, Cooper CE, Knowles RG (2001) Nitric oxide synthases: structure, function and inhibition. *Biochem J* 357:593-615.
- Allyson J, Massicotte G (2011) Neuropathological Disorders and Calcium Independent Forms of Phospholipase A2 Activities in the Brain. InTech, 307:-485-486.
- Almaraz AC, Driver-Dunckley ED, Woodruff BK, Wellik KE, Caselli RJ, Demaerschalk BM, Adler CH, Caviness JN, Wingerchuk DM (2009) Efficacy of rivastigmine for cognitive symptoms in Parkinson disease with dementia. *Neurologist* 15:234-237.
- Amerik A, Swaminathan S, Krantz BA, Wilkinson KD, Hochstrasser M (1997) In vivo disassembly of free polyubiquitin chains by yeast Ubp14 modulates rates of protein degradation by the proteasome. *EMBO J* 16:4826-4838.
- Anderson L, Seilhamer J (1997) A comparison of selected mRNA and protein abundances in human liver. *Electrophoresis* 18:533-537.
- Ashrafian H, Czibik G, Bellahcene M, Aksentijevic D, Smith C. A, Mitchell, J. S, Dodd S. M, Kirwan J, Byrne J. J, Ludwig C (2012) Fumarate is cardioprotective via activation of the Nrf2 antioxidant pathway. *Cell metabolism* 15:361-371.
- Bachoo RM, Kim RS, Ligon KL, Maher EA, Brennan C, Billings N, Chan S, Li C, Rowitch DH, Wong WH, DePinho RA (2004) Molecular diversity of astrocytes with implications for neurological disorders. *Proc Natl Acad Sci U S A* 101:8384-8389.
- Baker RT, Board PG (1987a) Nucleotide sequence of a human ubiquitin Ub B processed pseudogene. *Nucleic Acids Res* 15:4352.
- Baker RT, Board PG (1987b) The human ubiquitin gene family: structure of a gene and pseudogenes from the Ub B subfamily. *Nucleic Acids Res* 15:443-463.
- Balch WE, Morimoto RI, Dillin A, Kelly JW (2008) Adapting proteostasis for disease intervention. *Science* 319:916-919.
- Baldovino S, Piccinini M, Anselmino A, Ramondetti C, Rinaudo MT, Costanzo P, Sena LM, Roccatello D (2006) Structural and functional properties of proteasomes purified from the human kidney. *J Nephrol* 19:710-716.
- Barrachina M, Castano E, Dalfo E, Maes T, Buesa C, Ferrer I (2006) Reduced ubiquitin C-terminal hydrolase-1 expression levels in dementia with Lewy bodies. *Neurobiol Dis* 22:265-273.
- Bartels AL, Leenders KL (2009) Parkinson's disease: the syndrome, the pathogenesis and pathophysiology. *Cortex* 45:915-921.

- Baudier J, Deloulme, J.C., Van Dorsselaer A., Black D., Matthes H.W. (1991) Purification and characterization of a brain-specific protein kinase C substrate, neurogranin (p17). Identification of a consensus amino acid sequence between neurogranin and neuromodulin (GAP43) that corresponds to the protein kinase C phosphorylation site and the calmodulin-binding domain. *J Biol Chem* 266:229-237.
- Bazile F, Gagne^l• JP, Mercier G, Lo KS, Pascal A, Vasilescu J, Figeys D, Poirier GG, Kubiak JZ, Chesnel F (2008) Differential proteomic screen to evidence proteins ubiquitinated upon mitotic exit in cell-free extract of *Xenopus laevis* embryos. *Journal of proteome research* 7:4701-4714.
- Beckman JS, Koppenol WH (1996) Nitric oxide, superoxide, and peroxynitrite: the good, the bad, and ugly. *Am J Physiol* 271:C1424-1437.
- Bedford L, Layfield R, Mayer RJ, Peng J, Xu P (2011) Diverse polyubiquitin chains accumulate following 26S proteasomal dysfunction in mammalian neurones. *Neurosci Lett* 491:44-47.
- Bedford L, Hay D, Devoy A, Paine S, Powe DG, Seth R, Gray T, Topham I, Fone K, Rezvani N, Mee M, Soane T, Layfield R, Sheppard PW, Ebendal T, Usoskin D, Lowe J, Mayer RJ (2008) Depletion of 26S proteasomes in mouse brain neurons causes neurodegeneration and Lewy-like inclusions resembling human pale bodies. *J Neurosci* 28:8189-8198.
- Belmont LD, Mitchison TJ (1996) Identification of a protein that interacts with tubulin dimers and increases the catastrophe rate of microtubules. *Cell* 84:623-631.
- Bender AT, Demady DR, Osawa Y (2000) Ubiquitination of neuronal nitric-oxide synthase in vitro and in vivo. *J Biol Chem* 275:17407-17411.
- Bennett MC, Bishop JF, Leng Y, Chock PB, Chase TN, Mouradian MM (1999) Degradation of alpha-synuclein by proteasome. *J Biol Chem* 274:33855-33858.
- Bernocco S, Fondelli C, Matteoni S, Magnoni L, Gotta S, Terstappen GC, Raggiaschi R (2008) Sequential detergent fractionation of primary neurons for proteomics studies. *Proteomics* 8:930-938.
- Bigbee JW, Eng LF (1982) Analysis and comparison of in vitro synthesized glial fibrillary acidic protein with rat CNS intermediate filament proteins. *J Neurochem* 38:130-134.
- Bonifacio MJ, Palma PN, Almeida L, Soares-da-Silva P (2007) Catechol-O-methyltransferase and Its Inhibitors in Parkinson's Disease. *CNS drug reviews* 13:352-379.
- Boukhtouche F, Vodjdani G, Jarvis CI, Bakouche J, Staels B, Mallet J, Mariani J, Lemaigre-Dubreuil Y, Brugg B (2006) Human retinoic acid receptor-related orphan receptor alpha1 overexpression protects neurones against oxidative stress-induced apoptosis. *J Neurochem* 96:1778-1789.
- Braak H, Del Tredici K, Rub U, de Vos RA, Jansen Steur EN, Braak E (2003) Staging of brain pathology related to sporadic Parkinson's disease. *Neurobiol Aging* 24:197-211.
- Bush TG, Puvanachandra N, Horner CH, Polito A, Ostefeld T, Svendsen CN, Mucke L, Johnson MH, Sofroniew MV (1999) Leukocyte infiltration, neuronal degeneration, and neurite outgrowth after ablation of scar-forming, reactive astrocytes in adult transgenic mice. *Neuron* 23:297-308.

- Byun J, Mueller DM, Fabjan JS, Heinecke JW (1999) Nitrogen dioxide radical generated by the myeloperoxidase-hydrogen peroxide-nitrite system promotes lipid peroxidation of low density lipoprotein. *FEBS Lett* 455:243-246.
- Castellani R, Smith MA, Richey PL, Perry G (1996) Glycooxidation and oxidative stress in Parkinson disease and diffuse Lewy body disease. *Brain Res* 737:195-200.
- Chatterjee S, Feinstein SI, Dodia C, Sorokina E, Lien YC, Nguyen S, Debolt K, Speicher D, Fisher AB (2011) Peroxiredoxin 6 phosphorylation and subsequent phospholipase A2 activity are required for agonist-mediated activation of NADPH oxidase in mouse pulmonary microvascular endothelium and alveolar macrophages. *J Biol Chem* 286:11696-11706.
- Chattopadhyay M, Valentine JS (2009) Aggregation of copper-zinc superoxide dismutase in familial and sporadic ALS. *Antioxidants & redox signaling* 11:1603-1614.
- Chau V, Tobias JW, Bachmair A, Marriott D, Ecker DJ, Gonda DK, Varshavsky A (1989) A multiubiquitin chain is confined to specific lysine in a targeted short-lived protein. *Science* 243:1576-1583.
- Chen C, Huang C, Chen S, Liang J, Lin W, Ke G, Zhang H, Wang B, Huang J, Han Z, Ma L, Huo K, Yang X, Yang P, He F, Tao T (2008) Subunit-subunit interactions in the human 26S proteasome. *Proteomics* 8:508-520.
- Chen JW, Dodia C, Feinstein SI, Jain MK, Fisher AB (2000) 1-Cys peroxiredoxin, a bifunctional enzyme with glutathione peroxidase and phospholipase A2 activities. *J Biol Chem* 275:28421-28427.
- Chen PC, Vargas MR, Pani AK, Smeyne RJ, Johnson DA, Kan YW, Johnson JA (2009) Nrf2-mediated neuroprotection in the MPTP mouse model of Parkinson's disease: Critical role for the astrocyte. *Proc Natl Acad Sci U S A* 106:2933-2938.
- Cheon MS, Fountoulakis M, Cairns NJ, Dierssen M, Herkner K, Lubec G (2001) Decreased protein levels of stathmin in adult brains with Down syndrome and Alzheimer's disease. *J Neural Transm Suppl*:281-288.
- Chhangani D, Jana NR, Mishra A (2013) Misfolded proteins recognition strategies of e3 ubiquitin ligases and neurodegenerative diseases. *Mol Neurobiol* 47:302-312.
- Choi HB, Gordon GRJ, Zhou N, Tai C, Rungta RL, Martinez J, Milner TA, Ryu JK, McLarnon JG, Tresguerres M (2012) Metabolic Communication between Astrocytes and Neurons via Bicarbonate-Responsive Soluble Adenylyl Cyclase. *Neuron* 75:1094-1104.
- Choi J, Levey AI, Weintraub ST, Rees HD, Gearing M, Chin LS, Li L (2004) Oxidative modifications and down-regulation of ubiquitin carboxyl-terminal hydrolase L1 associated with idiopathic Parkinson's and Alzheimer's diseases. *J Biol Chem* 279:13256-13264.
- Ciechanover A (1994) The ubiquitin-mediated proteolytic pathway: mechanisms of action and cellular physiology. *Biol Chem Hoppe Seyler* 375:565-581.
- Cohen RW, Margulies JE, Coulter PM, 2nd, Watson JB (1993) Functional consequences of expression of the neuron-specific, protein kinase C substrate RC3 (neurogranin) in *Xenopus* oocytes. *Brain Res* 627:147-152.
- Conrad M, Schick J, Angeli JPF (2013) Glutathione and thioredoxin dependent systems in neurodegenerative disease: What can be learned from reverse genetics in mice. *Neurochemistry international* in press.

- Coux O, Tanaka K, Goldberg AL (1996) Structure and functions of the 20S and 26S proteasomes. *Annu Rev Biochem* 65:801-847.
- da Fonseca PC, Morris EP (2008) Structure of the human 26S proteasome: subunit radial displacements open the gate into the proteolytic core. *J Biol Chem* 283:23305-23314.
- Dalfo E, Ferrer I (2008) Early alpha-synuclein lipoxidation in neocortex in Lewy body diseases. *Neurobiol Aging* 29:408-417.
- Dalfo E, Portero-Otin M, Ayala V, Martinez A, Pamplona R, Ferrer I (2005) Evidence of oxidative stress in the neocortex in incidental Lewy body disease. *J Neuropathol Exp Neurol* 64:816-830.
- Dasuri K, Ebenezer P, Zhang L, Fernandez-Kim SO, Bruce-Keller AJ, Markesbery WR, Keller JN (2010) Increased protein hydrophobicity in response to aging and Alzheimer disease. *Free Radic Biol Med* 48:1330-1337.
- Davis RL, Shrimpton AE, Carrell RW, Lomas DA, Gerhard L, Baumann B, Lawrence DA, Yepes M, Kim TS, Ghetti B (2002) Association between conformational mutations in neuroserpin and onset and severity of dementia. *The Lancet* 359:2242-2247.
- Dayal S, Sparks A, Jacob J, Allende-Vega N, Lane DP, Saville MK (2009) Suppression of the deubiquitinating enzyme USP5 causes the accumulation of unanchored polyubiquitin and the activation of p53. *Journal of Biological Chemistry* 284:5030-5041.
- de Gaetano G, Rajtar G, Livio M, Merino J (1980) Arachidonic acid-induced malondialdehyde formation in rat platelets. Kinetic aspects and inhibition by acetylsalicylic acid and indomethacin. *Naunyn Schmiedeberg's Arch Pharmacol* 312:85-89.
- Deng H-X, Hentati A, Tainer JA, Iqbal Z, Cayabyab A, Hung W-Y, Getzoff ED, Hu P, Herzfeldt B, Roos RP (1993) Amyotrophic lateral sclerosis and structural defects in Cu, Zn superoxide dismutase. *Science* 261:1047-1051.
- Deng L, Wang C, Spencer E, Yang L, Braun A, You J, Slaughter C, Pickart C, Chen ZJ (2000) Activation of the I κ B kinase complex by TRAF6 requires a dimeric ubiquitin-conjugating enzyme complex and a unique polyubiquitin chain. *Cell* 103:351-361.
- Deschauer M, Gizatullina Z, Schulze A, Pritsch M, Knoppel C, Knape M, Zierz S, Gellerich FN (2006) Molecular and biochemical investigations in fumarase deficiency. *Mol Genet Metab* 88:146-152.
- deSouza R-M, Moro E, Lang AE, Schapira AHV (2013) Timing of deep brain stimulation in Parkinson disease: A need for reappraisal? *Annals of neurology* 73:565-575.
- Diaz A, Limon D, ChÃ¡vez RI, Zenteno E, Guevara J (2012) A β 25-35 Injection into the Temporal Cortex Induces Chronic Inflammation that Contributes to Neurodegeneration and Spatial Memory Impairment in Rats. *Journal of Alzheimer's Disease* 30:505-522.
- Dikic I, Wakatsuki S, Walters KJ (2009) Ubiquitin-binding domains - from structures to functions. *Nat Rev Mol Cell Biol* 10:659-671.
- Douglas PM, Dillin A (2010) Protein homeostasis and aging in neurodegeneration. *J Cell Biol* 190:719-729.
- Dreyfuss G, Matunis MJ, Pinol-Roma S, Burd CG (1993) hnRNP proteins and the biogenesis of mRNA. *Annu Rev Biochem* 62:289-321.

- Dunbar AY, Kamada Y, Jenkins GJ, Lowe ER, Billecke SS, Osawa Y (2004) Ubiquitination and degradation of neuronal nitric-oxide synthase in vitro: dimer stabilization protects the enzyme from proteolysis. *Mol Pharmacol* 66:964-969.
- Dunnett SB, Björklund A (1999) Prospects for new restorative and neuroprotective treatments in Parkinson's disease. *Nature* 399:A32-A39.
- Eggler, AL, Small E, Hannink M, AD. M (2009) Cul3-mediated Nrf2 ubiquitination and antioxidant response element (ARE) activation are dependent on the partial molar volume at position 151 of Keap1. *Biochem J* 422:171-180.
- Erttmann SF, Bast A, Seidel J, Breitbach K, Walther R, Steinmetz I (2011) PGD2 and PGE2 regulate gene expression of Prx 6 in primary macrophages via Nrf2. *Free Radic Biol Med* 51:626-640.
- Escartin C, Brouillet E, Gubellini P, Trioulier YI, Jacquard C, Smadja C, Knott GW, Kerkerian-Le Goff L, Deglon N, Hantraye P (2006) Ciliary neurotrophic factor activates astrocytes, redistributes their glutamate transporters GLAST and GLT-1 to raft microdomains, and improves glutamate handling in vivo. *The Journal of neuroscience* 26:5978-5989.
- Feinstein SC, Wilson L (2005) Inability of tau to properly regulate neuronal microtubule dynamics: a loss-of-function mechanism by which tau might mediate neuronal cell death. *Biochim Biophys Acta* 1739:268-279.
- Fisher AB, Dodia C, Manevich Y, Chen JW, Feinstein SI (1999) Phospholipid hydroperoxides are substrates for non-selenium glutathione peroxidase. *J Biol Chem* 274:21326-21334.
- Fricke B, Heink S, Steffen J, Kloetzel P-M, Kruger E (2007) The proteasome maturation protein POMP facilitates major steps of 20S proteasome formation at the endoplasmic reticulum. *EMBO reports* 8:1170-1175.
- Galasko D (2001) Lewy bodies and dementia. *Curr Neurol Neurosci Rep* 1:435-441.
- Galou M, Colucci-Guyon E, Ensergueix D, Ridet JL, Gimenez y Ribotta M, Privat A, Babinet C, Dupouey P (1996) Disrupted glial fibrillary acidic protein network in astrocytes from vimentin knockout mice. *J Cell Biol* 133:853-863.
- Gan Y, Ji X, Hu X, Luo Y, Zhang L, Li P, Liu X, Yan F, Vosler P, Gao Y, Stetler RA, Chen J (2012) Transgenic overexpression of peroxiredoxin-2 attenuates ischemic neuronal injury via suppression of a redox-sensitive pro-death signaling pathway. *Antioxid Redox Signal* 17:719-732.
- Gasparini L, Terni B, Spillantini MG (2007) Frontotemporal dementia with tau pathology. *Neurodegenerative Diseases* 4:236-253.
- Gavilan MP, Pintado C, Gavilan E, Jimenez S, Rios RM, Vitorica J, Castano A, Ruano D (2009) Dysfunction of the unfolded protein response increases neurodegeneration in aged rat hippocampus following proteasome inhibition. *Aging Cell* 8:654-665.
- Gellera C, Uziel G, Rimoldi M, Zeviani M, Laverda A, Carrara F, DiDonato S (1990) Fumarase deficiency is an autosomal recessive encephalopathy affecting both the mitochondrial and the cytosolic enzymes. *Neurology* 40:495-495.
- Gerendasy DD, Sutcliffe JG (1997) RC3/neurogranin, a postsynaptic calpacitin for setting the response threshold to calcium influxes. *Mol Neurobiol* 15:131-163.
- Gharbi S, Gaffney P, Yang A, Zvelebil MJ, Cramer R, Waterfield MD, Timms JF (2002) Evaluation of two-dimensional differential gel electrophoresis for proteomic expression analysis of a model breast cancer cell system. *Mol Cell Proteomics* 1:91-98.

- Giasson BI, Duda JE, Murray IV, Chen Q, Souza JM, Hurtig HI, Ischiropoulos H, Trojanowski JQ, Lee VM (2000) Oxidative damage linked to neurodegeneration by selective alpha-synuclein nitration in synucleinopathy lesions. *Science* 290:985-989.
- Gilbert BJ (2013) The role of amyloid beta in the pathogenesis of Alzheimer's disease. *J Clin Pathol* 66:362-366.
- Gillette TG, Kumar B, Thompson D, Slaughter CA, DeMartino GN (2008) Differential roles of the COOH termini of AAA subunits of PA700 (19 S regulator) in asymmetric assembly and activation of the 26 S proteasome. *Journal of Biological Chemistry* 283:31813-31822.
- Gironi M, Bianchi A, Russo A, Alberoni M, Ceresa L, Angelini A, Cursano C, Mariani E, Nemni R, Kullmann C, Farina E, Martinelli Boneschi F (2011) Oxidative imbalance in different neurodegenerative diseases with memory impairment. *Neurodegener Dis* 8:129-137.
- Glavaski-Joksimovic A, Bohn MC (2013) Mesenchymal stem cells and neuroregeneration in Parkinson's disease. *Experimental neurology*.
- Glickman MH, Ciechanover A (2002) The ubiquitin-proteasome proteolytic pathway: destruction for the sake of construction. *Physiol Rev* 82:373-428.
- Glickman MH, Rubin DM, Coux O, Wefes I, Pfeifer Gn, Cjeka Z, Baumeister W, Fried VA, Finley D (1998) A subcomplex of the proteasome regulatory particle required for ubiquitin-conjugate degradation and related to the COP9-signalosome and eIF3. *Cell* 94:615-623.
- Glockzin S, von Knethen A, Scheffner M, Brune B (1999) Activation of the cell death program by nitric oxide involves inhibition of the proteasome. *J Biol Chem* 274:19581-19586.
- Gomez-Tortosa E, Ingraham AO, Irizarry MC, Hyman BT (1998) Dementia with Lewy bodies. *J Am Geriatr Soc* 46:1449-1458.
- Good PF, Hsu A, Werner P, Perl DP, Olanow CW (1998) Protein nitration in Parkinson's disease. *Journal of neuropathology and experimental neurology* 57:338.
- Gorbatyuk OS, Li S, Sullivan LF, Chen W, Kondrikova G, Manfredsson FP, Mandel RJ, Muzyczka N (2008) The phosphorylation state of Ser-129 in human alpha-synuclein determines neurodegeneration in a rat model of Parkinson disease. *Proceedings of the National Academy of Sciences* 105:763-768.
- Groll M, Ditzel L, Lowe J, Stock D, Bochtler M, Bartunik HD, Huber R (1997) Structure of 20S proteasome from yeast at 2.4 Å resolution. *NATURE-LONDON* 393:463-471.
- Gygi SP, Ryzhanskiy Y, Franza BR, Aebersold R (1999) Correlation between protein and mRNA abundance in yeast. *Mol Cell Biol* 19:1720-1730.
- Halassa MM, Fellin T, Takano H, Dong J-H, Haydon PG (2007) Synaptic islands defined by the territory of a single astrocyte. *The Journal of neuroscience* 27:6473-6477.
- Hamby ME, Gragnolati AR, Hewett SJ, Hewett JA (2008) TGFβ1 and TNFα potentiate nitric oxide production in astrocyte cultures by recruiting distinct subpopulations of cells to express NOS-2. *Neurochemistry international* 52:962-971.
- Harish, G, Mahadevan A, Srinivas Bharath MM, SK. S (2013) Alteration in Glutathione Content and Associated Enzyme Activities in the Synaptic Terminals but not in the Non-synaptic Mitochondria from the Frontal Cortex of Parkinson's Disease Brains. *Neurochem Res* 38:186-200.

- Harrower TP, Michell AW, Barker RA (2005) Lewy bodies in Parkinson's disease: protectors or perpetrators? *Exp Neurol* 195:1-6.
- Hayashida K, Oyanagi S, Mizutani Y, Yokochi M (1993) An early cytoplasmic change before Lewy body maturation: an ultrastructural study of the substantia nigra from an autopsy case of juvenile parkinsonism. *Acta neuropathologica* 85:445-448.
- Haydon PG, Carmignoto G (2006) Astrocyte control of synaptic transmission and neurovascular coupling. *Physiol Rev* 86:1009-1031.
- Head MW, Ironside JW (2012) Review: Creutzfeldt-Jakob disease: prion protein type, disease phenotype and agent strain. *Neuropathology and applied neurobiology* 38:296-310.
- Hecker M, Ullrich V (1989) On the mechanism of prostacyclin and thromboxane A2 biosynthesis. *J Biol Chem* 264:141-150.
- Hecker M, Haurand M, Ullrich V, Diczfalusy U, Hammarstrom S (1987) Products, kinetics, and substrate specificity of homogeneous thromboxane synthase from human platelets: development of a novel enzyme assay. *Arch Biochem Biophys* 254:124-135.
- Hendil KB, Kriegenburg F, Tanaka K, Murata S, Lauridsen A-MB, Johnsen AH, Hartmann-Petersen R (2009) The 20S proteasome as an assembly platform for the 19S regulatory complex. *Journal of molecular biology* 394:320-328.
- Hirano Y, Hendil KB, Yashiroda H, Iemura S-i, Nagane R, Hioki Y, Natsume T, Tanaka K, Murata S (2005) A heterodimeric complex that promotes the assembly of mammalian 20S proteasomes. *Nature* 437:1381-1385.
- Hirano Y, Kaneko T, Okamoto K, Bai M, Yashiroda H, Furuyama K, Kato K, Tanaka K, Murata S (2008) Dissecting beta-ring assembly pathway of the mammalian 20S proteasome. *The EMBO journal* 27:2204-2213.
- Hirano Y, Hayashi H, Iemura S-i, Hendil KB, Niwa S-i, Kishimoto T, Kasahara M, Natsume T, Tanaka K, Murata S (2006) Cooperation of multiple chaperones required for the assembly of mammalian 20S proteasomes. *Molecular cell* 24:977-984.
- Hishiya A, Iemura S, Natsume T, Takayama S, Ikeda K, Watanabe K (2006) A novel ubiquitin-binding protein ZNF216 functioning in muscle atrophy. *EMBO J* 25:554-564.
- Ho JN, Lee SB, Lee SS, Yoon SH, Kang GY, Hwang SG, Um HD (2010) Phospholipase A2 activity of peroxiredoxin 6 promotes invasion and metastasis of lung cancer cells. *Mol Cancer Ther* 9:825-832.
- Hochstrasser M (1996) Ubiquitin-dependent protein degradation. *Annu Rev Genet* 30:405-439.
- Hoffner G, Djian P (2002) Protein aggregation in Huntington's disease. *Biochimie* 84:273-278.
- Hofmann RM, Pickart CM (1999) Noncanonical MMS2-encoded ubiquitin-conjugating enzyme functions in assembly of novel polyubiquitin chains for DNA repair. *Cell* 96:645-653.
- Horimoto Y, Matsumoto M, Akatsu H, Ikari H, Kojima K, Yamamoto T, Otsuka Y, Ojika K, Ueda R, Kosaka K (2003) Autonomic dysfunctions in dementia with Lewy bodies. *J Neurol* 250:530-533.
- Huang J, Teng L, Li L, Liu T, Chen D, Xu LG, Zhai Z, Shu HB (2004a) ZNF216 is an A20-like and IkappaB kinase gamma-interacting inhibitor of NFkappaB activation. *Journal of Biological Chemistry* 279:16847-16853.

- Huang KP, Huang FL, Jager T, Li J, Reymann KG, Balschun D (2004b) Neurogranin/RC3 enhances long-term potentiation and learning by promoting calcium-mediated signaling. *J Neurosci* 24:10660-10669.
- Huang Q, Figueiredo-Pereira ME (2010) Ubiquitin/proteasome pathway impairment in neurodegeneration: therapeutic implications. *Apoptosis* 15:1292-1311.
- Hunot S, Boissiere F, Faucheux B, Brugg B, Mouatt-Prigent A, Agid Y, Hirsch EC (1996) Nitric oxide synthase and neuronal vulnerability in Parkinson's disease. *Neuroscience* 72:355-363.
- Hurley JH, Lee S, Prag G (2006) Ubiquitin-binding domains. *Biochem J* 399:361-372.
- Husnjak K, Dikic I (2012) Ubiquitin-binding proteins: decoders of ubiquitin-mediated cellular functions. *Annu Rev Biochem* 81:291-322.
- Husnjak K, Elsasser S, Zhang N, Chen X, Randles L, Shi Y, Hofmann K, Walters KJ, Finley D, Dikic I (2008) Proteasome subunit Rpn13 is a novel ubiquitin receptor. *Nature* 453:481-488.
- Iadecola C, Nedergaard M (2007) Glial regulation of the cerebral microvasculature. *Nat Neurosci* 10:1369-1376.
- Inagaki M, Nakamura Y, Takeda M, Nishimura T, Inagaki N (1994) Glial fibrillary acidic protein: dynamic property and regulation by phosphorylation. *Brain Pathol* 4:239-243.
- Ishii T, Sakurai T, Usami H, Uchida K (2005) Oxidative modification of proteasome: identification of an oxidation-sensitive subunit in 26 S proteasome. *Biochemistry* 44:13893-13901.
- Jacoby S, Sims RE, Hartell NA (2001) Nitric oxide is required for the induction and heterosynaptic spread of long-term potentiation in rat cerebellar slices. *The Journal of physiology* 535:825-839.
- Jacque CM, Vinner C, Kujas M, Raoul M, Racadot J, Baumann NA (1978) Determination of glial fibrillary acidic protein (GFAP) in human brain tumors. *J Neurol Sci* 35:147-155.
- Jaendling A, McFarlane RJ (2010) Biological roles of translin and translin-associated factor-X: RNA metabolism comes to the fore. *Biochem J* 429:225-234.
- Jankovic J (2008) Parkinson's disease: clinical features and diagnosis. *J Neurol Neurosurg Psychiatry* 79:368-376.
- Jardanhazi-Kurutz D, Kummer MP, Terwel D, Vogel K, Thiele A, Heneka MT (2011) Distinct adrenergic system changes and neuroinflammation in response to induced locus ceruleus degeneration in APP/PS1 transgenic mice. *Neuroscience* 176:396-407.
- Jentsch S, Seufert W, Sommer T, Reins H-A (1990) Ubiquitin-conjugating enzymes: novel regulators of eukaryotic cells. *Trends in Biochemical Sciences* 15:195-198.
- Jeon HB, Choi ES, Yoon JH, Hwang JH, Chang JW, Lee EK, Choi HW, Park ZY, Yoo YJ (2007) A proteomics approach to identify the ubiquitinated proteins in mouse heart. *Biochem Biophys Res Commun* 357:731-736.
- Jeong J, Kim Y, Kyung Seong J, Lee KJ (2012) Comprehensive identification of novel post-translational modifications in cellular peroxiredoxin 6. *Proteomics* 12:1452-1462.

- Jesse S, Lehnert S, Jahn O, Parnetti L, Soininen H, Herukka SK, Steinacker P, Tawfik S, Tumani H, von Arnim CA, Neumann M, Kretzschmar HA, Kulaksiz H, Lenter M, Wiltfang J, Ferger B, Hengerer B, Otto M (2012) Differential Sialylation of Serpin A1 in the Early Diagnosis of Parkinson's Disease Dementia. *PLoS One* 7:e48783.
- Jin MH, Lee YH, Kim JM, Sun HN, Moon EY, Shong MH, Kim SU, Lee SH, Lee TH, Yu DY, Lee DS (2005) Characterization of neural cell types expressing peroxiredoxins in mouse brain. *Neurosci Lett* 381:252-257.
- Johnsen JI, Aurelio ON, Kwaja Z, Jörgensen GE, Pellegata NS, Plattner R, Stanbridge EJ, Cajot J-F (2000) p53-mediated negative regulation of stathmin/Op18 expression is associated with G2/M cell-cycle arrest. *International journal of cancer* 88:685-691.
- Johnston JA, Madura K (2004) Rings, chains and ladders: ubiquitin goes to work in the neuron. *Prog Neurobiol* 73:227-257.
- Kaat D, Chiu W, Boon A, Swieten Jv (2011) Recent advances in progressive supranuclear palsy: a review. *Current Alzheimer Research* 8:295-302.
- Kamphuis WM, C.Moeton, M.Kooijman, L.Sluijs, J. A.Jansen, A. H.Verveer, M.de Groot, L. R.Smith, V. D.Rangarajan, S.Rodriguez, J. J.Orre, M.Hol, E. M. (2012) GFAP isoforms in adult mouse brain with a focus on neurogenic astrocytes and reactive astrogliosis in mouse models of Alzheimer disease. *PLoS One* 7:e42823.
- Kamsler A, Daily D, Hochman A, Stern N, Shiloh Y, Rotman G, Barzilai A (2001) Increased oxidative stress in ataxia telangiectasia evidenced by alterations in redox state of brains from Atm-deficient mice. *Cancer Res* 61:1849-1854.
- Kaneko T, Hamazaki J, Iemura S-i, Sasaki K, Furuyama K, Natsume T, Tanaka K, Murata S (2009) Assembly pathway of the Mammalian proteasome base subcomplex is mediated by multiple specific chaperones. *Cell* 137:914-925.
- Kang Y, Vossler RA, Diaz-Martinez LA, Winter NS, Clarke DJ, Walters KJ (2006) UBL/UBA ubiquitin receptor proteins bind a common tetraubiquitin chain. *Journal of molecular biology* 356:1027-1035.
- Kim SY, Chun E, Lee KY (2011) Phospholipase A2 of peroxiredoxin 6 has a critical role in tumor necrosis factor-induced apoptosis. *Cell Death & Differentiation*.
- Kim SY, Jo HY, Kim MH, Cha YY, Choi SW, Shim JH, Kim TJ, Lee KY (2008) H₂O₂-dependent hyperoxidation of peroxiredoxin 6 (Prdx6) plays a role in cellular toxicity via up-regulation of iPLA2 activity. *J Biol Chem* 283:33563-33568.
- Kirkpatrick DS, Weldon SF, Tsapralis G, Liebler DC, Gandolfi AJ (2005) Proteomic identification of ubiquitinated proteins from human cells expressing His-tagged ubiquitin. *Proteomics* 5:2104-2111.
- Köhler A, Cascio P, Leggett DS, Woo KM, Goldberg AL, Finley D (2001) The axial channel of the proteasome core particle is gated by the Rpt2 ATPase and controls both substrate entry and product release. *Molecular cell* 7:1143-1152.
- Koulich, Elena, Li, Xiaohua, DeMartino, N. G (2008) Relative structural and functional roles of multiple deubiquitylating proteins associated with mammalian 26S proteasome. *Molecular biology of the cell* 19:1072-1082.
- Kouri N, Whitwell JL, Josephs KA, Rademakers R, Dickson DW (2011) Corticobasal degeneration: a pathologically distinct 4R tauopathy. *Nature Reviews Neurology* 7:263-272.

- Kurz A, May C, Schmidt O, Muller T, Stephan C, Meyer HE, Gispert S, Auburger G, Marcus K (2012) A53T-alpha-synuclein-overexpression in the mouse nigrostriatal pathway leads to early increase of 14-3-3 epsilon and late increase of GFAP. *J Neural Transm* 119:297-312.
- Kushnareva Y, Murphy, A.N., Andreyev, A. (2002) Complex I-mediated reactive oxygen species generation: modulation by cytochrome c and NAD(P)⁺ oxidation-reduction state. *Biochem J* 368:545-553.
- Lam YA, Lawson TG, Velayutham M, Zweier JL, Pickart CM (2002) A proteasomal ATPase subunit recognizes the polyubiquitin degradation signal. *Nature* 416:763-767.
- Lang AE, Lees A (2002) Management of Parkinson's disease: an evidence-based review. *Mov Disord* 17:S1-S166.
- Langston JW, Ballard P, Tetrud JW, Irwin I (1983) Chronic parkinsonism in humans due to a product of meperidine-analog synthesis. *Science (New York, NY)* 219:979.
- Layfield R, Tooth D, Landon M, Dawson S, Mayer J, Alban A (2001) Purification of poly-ubiquitinated proteins by S5a-affinity chromatography. *Proteomics* 1:773-777.
- Lazzarino G, Tavazzi B, Di Pierro D, Vagnozzi R, Penco M, Giardina B (1995) The relevance of malondialdehyde as a biochemical index of lipid peroxidation of postischemic tissues in the rat and human beings. *Biological trace element research* 47:165-170.
- Le Tallec B BM, Courbeyrette R, Guérois R, Marsolier-Kergoat MC, Peyroche A. (2007) 20S proteasome assembly is orchestrated by two distinct pairs of chaperones in yeast and in mammals. *Molecular cell* 27:660-674.
- Lee I, Dodia C, Chatterjee S, Zagorski J, Mesaros C, Blair IA, Feinstein SI, Jain M, Fisher AB (2013) A novel non-toxic inhibitor of the activation of NADPH oxidase (NOX2) reduces reactive oxygen species production in mouse lung. *J Pharmacol Exp Ther.* 345:284-296
- Lee JC, Simonyi A, Sun AY, Sun GY (2011) Phospholipases A2 and neural membrane dynamics: implications for Alzheimer's disease. *J Neurochem* 116:813-819.
- Leroy E, Boyer R, Auburger G, Leube B, Ulm G, Mezey E, Harta G, Brownstein MJ, Jonnalagada S, Chernova T, Dehejia A, Lavedan C, Gasser T, Steinbach PJ, Wilkinson KD, Polymeropoulos MH (1998) The ubiquitin pathway in Parkinson's disease. *Nature* 395:451-452.
- Liedtke W, Leman EE, Fyffe RE, Raine CS, Schubart UK (2002) Stathmin-deficient mice develop an age-dependent axonopathy of the central and peripheral nervous systems. *Am J Pathol* 160:469-480.
- Liu CW, Jacobson AD (2012) Functions of the 19S complex in proteasomal degradation. *Trends Biochem Sci.*
- Lowe J, Mayer RJ, Landon M (1993) Ubiquitin in neurodegenerative diseases. *Brain Pathology* 3:55-65.
- Lu YB, Iandiev I, Hollborn M, Korber N, Ulbricht E, Hirrlinger PG, Pannicke T, Wei EQ, Bringmann A, Wolburg H, Wilhelmsson U, Pekny M, Wiedemann P, Reichenbach A, Kas JA (2011) Reactive glial cells: increased stiffness correlates with increased intermediate filament expression. *FASEB J* 25:624-631.
- Marnett LJ (1999) Lipid peroxidation-DNA damage by malondialdehyde. *Mutat Res* 424:83-95.

- Marques F, Mesquita SD, Sousa JoC, Coppola G, Gao F, Geschwind DH, Columba-Cabezas S, Aloisi F, Degn M, Cerqueira JoJ (2012) Lipocalin 2 is present in the EAE brain and is modulated by natalizumab. *Frontiers in Cellular Neuroscience* 6:1-10.
- Martinez A, Portero-Otin M, Pamplona R, Ferrer I (2010) Protein targets of oxidative damage in human neurodegenerative diseases with abnormal protein aggregates. *Brain Pathol* 20:281-297.
- Masoodi N (2013) Review: Cholinesterase inhibitors do not reduce progression to dementia from mild cognitive impairment. *Annals of internal medicine* 158:JC2.
- Mattila PM, Rinne JO, Helenius H, Dickson DW, Roytta M (2000) Alpha-synuclein-immunoreactive cortical Lewy bodies are associated with cognitive impairment in Parkinson's disease. *Acta Neuropathol* 100:285-290.
- Mayer RJ (2003) From neurodegeneration to neurohomeostasis: the role of ubiquitin. *Drug News Perspect* 16:103-108.
- Mayer RJ, Lowe J, Lennox G, Doherty F, Landon M (1989) Intermediate filaments and ubiquitin: a new thread in the understanding of chronic neurodegenerative diseases. *Prog Clin Biol Res* 317:809-818.
- McNaught KS, Belizaire R, Isacson O, Jenner P, Olanow CW (2003) Altered proteasomal function in sporadic Parkinson's disease. *Exp Neurol* 179:38-46.
- Meierhofer D, Wang X, Huang L, Kaiser P (2008) Quantitative analysis of global ubiquitination in HeLa cells by mass spectrometry. *J Proteome Res* 7:4566-4576.
- Miller GW (2007) Paraquat: the red herring of Parkinson's disease research. *Toxicol Sci* 100:1-2.
- Molina JA, Leza JC, Ortiz S, Moro MA, Perez S, Lizasoain I, Uriguen L, Oliva JM, Manzanares J (2002) Cerebrospinal fluid and plasma concentrations of nitric oxide metabolites are increased in dementia with Lewy bodies. *Neurosci Lett* 333:151-153.
- Moran M, Moreno-Lastres D, Marin-Buera L, Arenas J, Martin MA, Ugalde C (2012) Mitochondrial respiratory chain dysfunction: implications in neurodegeneration. *Free Radic Biol Med* 53:595-609.
- Müller T (2012) Drug therapy in patients with Parkinson's disease. *Translational neurodegeneration* 1:10.
- Murakami K, Murata N, Noda Y, Tahara S, Kaneko T, Kinoshita N, Hatsuta H, Murayama S, Barnham KJ, Irie K, Shirasawa T, Shimizu T (2011) SOD1 (copper/zinc superoxide dismutase) deficiency drives amyloid beta protein oligomerization and memory loss in mouse model of Alzheimer disease. *J Biol Chem* 286:44557-44568.
- Murata S, Yashiroda H, Tanaka K (2009) Molecular mechanisms of proteasome assembly. *Nature Reviews Molecular Cell Biology* 10:104-115.
- Muroyama A, Fujita A, Lv C, Kobayashi S, Fukuyama Y, Mitsumoto Y (2012) Magnolol Protects against MPTP/MPP(+)-Induced Toxicity via Inhibition of Oxidative Stress in In Vivo and In Vitro Models of Parkinson's Disease. *Parkinsons Dis* 2012:985157.
- Murphy MP (2009) How mitochondria produce reactive oxygen species. *Biochemical Journal* 417:1.

- Musiek ES, Holtzman DM (2012) Origins of Alzheimer's disease: reconciling cerebrospinal fluid biomarker and neuropathology data regarding the temporal sequence of amyloid-beta and tau involvement. *Current opinion in neurology* 25:715-720.
- Neef D, Walling AD (2006) Dementia with Lewy bodies: an emerging disease. *Am Fam Physician* 73:1223-1229.
- Nikolaus S, Antke C, Muller HW (2009) In vivo imaging of synaptic function in the central nervous system: I. Movement disorders and dementia. *Behav Brain Res* 204:1-31.
- Norris EH, Giasson BI, Ischiropoulos H, Lee VM (2003) Effects of oxidative and nitrative challenges on alpha-synuclein fibrillogenesis involve distinct mechanisms of protein modifications. *J Biol Chem* 278:27230-27240.
- Nussbaum RL, Polymeropoulos MH (1997) Genetics of Parkinson's disease. *Hum Mol Genet* 6:1687-1691.
- O'Brien JT, Burns A (2011) Clinical practice with anti-dementia drugs: a revised (second) consensus statement from the British Association for Psychopharmacology. *J Psychopharmacol* 25:997-1019.
- Oleszak, L. E, Zaczynska, Ewa, Bhattacharjee, Meena, Butunoi, Catalin, Legido, Agustin, Katsetos, D. C (1998) Inducible nitric oxide synthase and nitrotyrosine are found in monocytes/macrophages and/or astrocytes in acute, but not in chronic, multiple sclerosis. *Clinical and diagnostic laboratory immunology* 5:438-445.
- Ong WY, Farooqui T, Farooqui AA (2010) Involvement of cytosolic phospholipase A(2), calcium independent phospholipase A(2) and plasmalogen selective phospholipase A(2) in neurodegenerative and neuropsychiatric conditions. *Curr Med Chem* 17:2746-2763.
- Onyango IG (2008) Mitochondrial dysfunction and oxidative stress in Parkinson's disease. *Neurochem Res* 33:589-597.
- Orr HT (2012) Cell biology of spinocerebellar ataxia. *The Journal of cell biology* 197:167-177.
- Osna NA, Haorah J, Krutik VM, Donohue TM, Jr. (2004) Peroxynitrite alters the catalytic activity of rodent liver proteasome in vitro and in vivo. *Hepatology* 40:574-582.
- Osona-Nunez L, Guisado-Macias JA, Pons M (2011) Cognition and Lewy body disease. *Actas Esp Psiquiatr* 39:267-270.
- Ouyang H, Ali YO, Ravichandran M, Dong A, Qiu W, MacKenzie F, Dhe-Paganon S, Arrowsmith CH, Zhai RG (2011) Protein aggregates are recruited to aggresome by histone deacetylase 6 via unanchored ubiquitin C termini. *J Biol Chem* 287:2317-2327.
- Pacher P, Beckman JS, Liaudet L (2007) Nitric oxide and peroxynitrite in health and disease. *Physiol Rev* 87:315-424.
- Pagon RA, Bird TD, Dolan CR, Stephens K, Adam MP, Shih VE, Mandell R (2006) Fumarate Hydratase Deficiency. PMID: 20301679.
- Paine SM, Anderson G, Bedford K, Lawler K, Mayer RJ, Lowe J, Bedford L (2013) Pale Body-Like Inclusion Formation and Neurodegeneration following Depletion of 26S Proteasomes in Mouse Brain Neurones are Independent of alpha-Synuclein. *PLoS One* 8:e54711.

- Pak JH, Huang FL, Li J, Balschun D, Reymann KG, Chiang C, Westphal H, Huang KP (2000) Involvement of neurogranin in the modulation of calcium/calmodulin-dependent protein kinase II, synaptic plasticity, and spatial learning: a study with knockout mice. *Proc Natl Acad Sci U S A* 97:11232-11237.
- Pan T, Kondo S, Zhu W, Xie W, Jankovic J, Le W (2008) Neuroprotection of rapamycin in lactacystin-induced neurodegeneration via autophagy enhancement. *Neurobiol Dis* 32:16-25.
- Parkinson J (2002) An Essay on the Shaking Palsy. Classic article. In *J Neuropsychiatry Clin Neurosci* 14:223-236.
- Parpura V, Haydon PG (2000) Physiological astrocytic calcium levels stimulate glutamate release to modulate adjacent neurons. *Proc Natl Acad Sci U S A* 97:8629-8634.
- Parri R, Crunelli V (2003) An astrocyte bridge from synapse to blood flow. *Nat Neurosci* 6:5-6.
- Passmore LA, Barford D (2004) Getting into position: the catalytic mechanisms of protein ubiquitylation. *Biochem J* 379:513-525.
- Pegoraro G, Voss TC, Martin SE, Tuzmen P, Guha R, Misteli T (2012) Identification of mammalian protein quality control factors by high-throughput cellular imaging. *PLoS One* 7:e31684.
- Pekny M, Nilsson M (2005) Astrocyte activation and reactive gliosis. *Glia* 50:427-434.
- Pekny M, Leveen P, Pekna M, Eliasson C, Berthold CH, Westermark B, Betsholtz C (1995) Mice lacking glial fibrillary acidic protein display astrocytes devoid of intermediate filaments but develop and reproduce normally. *EMBO J* 14:1590-1598.
- Periquet M, Corti O, Jacquier S, Brice A (2005) Proteomic analysis of parkin knockout mice: alterations in energy metabolism, protein handling and synaptic function. *J Neurochem* 95:1259-1276.
- Pickart CM (2001) Mechanisms underlying ubiquitination. *Annu Rev Biochem* 70:503-533.
- Pikul J, Leszczynski DE (1986) Butylated hydroxytoluene addition improves the thiobarbituric acid assay for malonaldehyde from chicken plasma fat. *Nahrung* 30:673-678.
- Piotrowski J, Beal R, Hoffman L, Wilkinson KD, Cohen RE, Pickart CM (1997) Inhibition of the 26 S proteasome by polyubiquitin chains synthesized to have defined lengths. *Journal of Biological Chemistry* 272:23712-23721.
- Porchet R, Probst A, Bouras C, Draberova E, Draber P, Riederer BM (2003) Analysis of glial acidic fibrillary protein in the human entorhinal cortex during aging and in Alzheimer's disease. *Proteomics* 3:1476-1485.
- Pou S, Keaton L, Surichamorn W, Rosen GM (1999) Mechanism of superoxide generation by neuronal nitric-oxide synthase. *J Biol Chem* 274:9573-9580.
- Power JH, Nicholas TE (1999) Immunohistochemical localization and characterization of a rat Clara cell 26-kDa protein (CC26) with similarities to glutathione peroxidase and phospholipase A2. *Exp Lung Res* 25:379-392.
- Power JH, Shannon JM, Blumbergs PC, Gai WP (2002) Nonselenium glutathione peroxidase in human brain : elevated levels in Parkinson's disease and dementia with lewy bodies. *Am J Pathol* 161:885-894.

- Power JH AS, Chataway TK, Chegini F, Manavis J, Temlett JA, Jensen PH, Blumbergs PC, Gai WP. (2008) Peroxiredoxin 6 in human brain: molecular forms, cellular distribution and association with Alzheimer's disease pathology. *Acta Neuropathol* 115:611-622.
- Pryor WA, Stanley JP (1975) Letter: A suggested mechanism for the production of malonaldehyde during the autoxidation of polyunsaturated fatty acids. Nonenzymatic production of prostaglandin endoperoxides during autoxidation. *J Org Chem* 40:3615-3617.
- Puschmann A, Bhidayasiri R, Weiner WJ (2012) Synucleinopathies from bench to bedside. *Parkinsonism Relat Disord* 18 Suppl 1:S24-27.
- Reddy PH, Mani G, Park BS, Jacques J, Murdoch G, Whetsell W, Jr., Kaye J, Manczak M (2005) Differential loss of synaptic proteins in Alzheimer's disease: implications for synaptic dysfunction. *J Alzheimers Dis* 7:103-117; discussion 173-180.
- Redman KL, Rechsteiner M (1989) Identification of the long ubiquitin extension as ribosomal protein S27a. *Nature* 338:438-440.
- Revuelta GJ, Rosso A, Lippa CF (2008) Neuritic pathology as a correlate of synaptic loss in dementia with Lewy bodies. *American journal of Alzheimer's disease and other dementias* 23:97-102.
- Reyes-Turcu FE, Ventii KH, Wilkinson KD (2009) Regulation and cellular roles of ubiquitin-specific deubiquitinating enzymes. *Annu Rev Biochem* 78:363-397.
- Rittie L, Monboisse JC, Gorisse MC, Gillery P (2002) Malondialdehyde binding to proteins dramatically alters fibroblast functions. *J Cell Physiol* 191:227-236.
- Rockwell P, Yuan H, Magnusson R, Figueiredo-Pereira ME (2000) Proteasome Inhibition in Neuronal Cells Induces a Proinflammatory Response Manifested by Upregulation of Cyclooxygenase-2, its accumulation as ubiquitin conjugates, and production of the prostaglandin PGE(2). *Archives of biochemistry and biophysics* 374:325-333.
- Rodenas J, Carbonell T, Mitjavila MT (2000) Different roles for nitrogen monoxide and peroxynitrite in lipid peroxidation induced by activated neutrophils. *Free Radic Biol Med* 28:374-380.
- Rodrigo-Brenni MC, Morgan DO (2007) Sequential E2s drive polyubiquitin chain assembly on APC targets. *Cell* 130:127-139.
- Roede JR, Orlicky DJ, Fisher AB, Petersen DR (2009) Overexpression of peroxiredoxin 6 does not prevent ethanol-mediated oxidative stress and may play a role in hepatic lipid accumulation. *Journal of Pharmacology and Experimental Therapeutics* 330:79-88.
- Romero-Granados R, Fontan-Lozano A, Aguilar-Montilla FJ, Carrion AM (2011) Postnatal proteasome inhibition induces neurodegeneration and cognitive deficiencies in adult mice: a new model of neurodevelopment syndrome. *PLoS One* 6:e28927.
- Rosenzweig R, Osmulski PA, Gaczynska M, Glickman MH (2008) The central unit within the 19S regulatory particle of the proteasome. *Nature structural & molecular biology* 15:573-580.
- Rothe G, Valet G (1990) Flow cytometric analysis of respiratory burst activity in phagocytes with hydroethidine and 2',7'-dichlorofluorescein. *J Leukoc Biol* 47:440-448.

- Sadeghian R, Fereidoni M, Soukhtanloo M, Azizi-Malekabadi H, Hosseini M (2011) Decreased nitric oxide levels in the hippocampus may play a role in learning and memory deficits in ovariectomized rats treated by a high dose of estradiol. *Arquivos de neuro-psiquiatria* 70:874-879.
- Sagara J, Makino N, Bannai S (1996) Glutathione efflux from cultured astrocytes. *J Neurochem* 66:1876-1881.
- Sakamoto M, Uchihara T, Hayashi M, Nakamura A, Kikuchi E, Mizutani T, Mizusawa H, Hirai S (2002) Heterogeneity of nigral and cortical Lewy bodies differentiated by amplified triple-labeling for alpha-synuclein, ubiquitin, and thiazin red. *Exp Neurol* 177:88-94.
- Santello M, Volterra A (2009) Synaptic modulation by astrocytes via Ca²⁺-dependent glutamate release. *Neuroscience* 158:253-259.
- Satoh K, Sasajima H, Nyomura K-i, Yokosawa H, Sawada H (2001) Assembly of the 26S proteasome is regulated by phosphorylation of the p45/Rpt6 ATPase subunit. *Biochemistry* 40:314-319.
- Schapira AH (2005) Present and future drug treatment for Parkinson's disease. *J Neurol Neurosurg Psychiatry* 76:1472-1478.
- Scharfman HE (2002) Book review: Epilepsy as an example of neural plasticity. *The Neuroscientist* 8:154-173.
- Seehusen F, Orlando EA, Wewetzer K, Baumgartner W (2007) Vimentin-positive astrocytes in canine distemper: a target for canine distemper virus especially in chronic demyelinating lesions. *Acta neuropathologica* 114:597-608.
- Sekhar, KR, Yan XX, ML. F (2002) Nrf2 degradation by the ubiquitin proteasome pathway is inhibited by KIAA0132, the human homolog to INrf2. *Oncogene* 21:6829-6834.
- Shacter E (2000) Quantification and significance of protein oxidation in biological samples. *Drug Metab Rev* 32:307-326.
- Shadrina MI, Slominskii PA (2008) [Mitochondrial dysfunction and oxidative damages in the molecular pathology of Parkinson's disease]. *Mol Biol (Mosk)* 42:809-819.
- Shahnawaz M, Thapa A, Park I-S (2007) Stable activity of a deubiquitylating enzyme (Usp2-cc) in the presence of high concentrations of urea and its application to purify aggregation-prone peptides. *Biochemical and biophysical research communications* 359:801-805.
- Shimohama S, Tanino H, Kawakami N, Okamura N, Kodama H, Yamaguchi T, Hayakawa T, Nunomura A, Chiba S, Perry G, Smith MA, Fujimoto S (2000) Activation of NADPH oxidase in Alzheimer's disease brains. *Biochem Biophys Res Commun* 273:5-9.
- Shumyatsky GP, Malleret G, Shin RM, Takizawa S, Tully K, Tsvetkov E, Zakharenko SS, Joseph J, Vronskaya S, Yin D, Schubart UK, Kandel ER, VY. B (2005) stathmin, a gene enriched in the amygdala, controls both learned and innate fear. *Cell* 18.:697-709.
- Silverman GA, Bird PI, Carrell RW, Church FC, Coughlin PB, Gettins PGW, Irving JA, Lomas DA, Luke CJ, Moyer RW (2001) The serpins are an expanding superfamily of structurally similar but functionally diverse proteins evolution, mechanism of inhibition, novel functions, and a revised nomenclature. *Journal of Biological Chemistry* 276:33293-33296.
- Smith DM, Chang SC, Park S, Finley D, Cheng Y, Goldberg AL (2007) Docking of the proteasomal ATPases' carboxyl termini in the 20S proteasome's alpha ring opens the gate for substrate entry. *Mol Cell* 27:731-744.

- Sofroniew MV (2009) Molecular dissection of reactive astrogliosis and glial scar formation. *Trends Neurosci* 32:638-647.
- Sofroniew MV, Vinters HV (2010) Astrocytes: biology and pathology. *Acta neuropathologica* 119:7-35.
- Spillantini MG, Crowther RA, Jakes R, Hasegawa M, Goedert M (1998) alpha-Synuclein in filamentous inclusions of Lewy bodies from Parkinson's disease and dementia with lewy bodies. *Proc Natl Acad Sci U S A* 95:6469-6473.
- Stadelmann-Ingrand S, Pontcharraud R, Fauconneau B (2004) Evidence for the reactivity of fatty aldehydes released from oxidized plasmalogens with phosphatidylethanolamine to form Schiff base adducts in rat brain homogenates. *Chem Phys Lipids* 131:93-105.
- Stefanis L (2012) alpha-Synuclein in Parkinson's disease. *Cold Spring Harb Perspect Med* 2:a009399.
- Stein M, B., Heuser, I.J., Juncos, J.L., Uhde, T.W. (1990) Anxiety disorder in patient with Parkinson's disease. *Am J Psychiatry* 147:217-220.
- Strachan J, Roach L, Sokratous K, Tooth D, Long J, Garner TP, Searle MS, Oldham NJ, Layfield R (2012) Insights into the molecular composition of endogenous unanchored polyubiquitin chains. *Journal of proteome research* 11:1969-1980.
- Strey CW, Spellman D, Stieber A, Gonatas JO, Wang X, Lambris JD, Gonatas NK (2004) Dysregulation of stathmin, a microtubule-destabilizing protein, and up-regulation of Hsp25, Hsp27, and the antioxidant peroxiredoxin 6 in a mouse model of familial amyotrophic lateral sclerosis. *Am J Pathol* 165:1701-1718.
- Sujith O, Lane C (2009) Therapeutic options for continuous dopaminergic stimulation in Parkinson's disease. *Ther Adv Neurol Disord* 2:105-113.
- Sun L, Xu S, Zhou M, Wang C, Wu Y, Chan P (2010) Effects of cysteamine on MPTP-induced dopaminergic neurodegeneration in mice. *Brain Res* 1335:74-82.
- Tariq M, Khan HA, Al Moutaery K, Al Deeb S (2001) Protective effect of quinacrine on striatal dopamine levels in 6-OHDA and MPTP models of Parkinsonism in rodents. *Brain Res Bull* 54:77-82.
- Thomas BaG, L. (2006) Historical background, In *Dementia with lewy bodies*,. John O'Brien et al, Editors Taylor & Francis Press:1-8.
- Thorsell A, Bjerke M, Gobom J, Brunhage E, Vanmechelen E, Andreasen N, Hansson O, Minthon L, Zetterberg H, Blennow K (2010) Neurogranin in cerebrospinal fluid as a marker of synaptic degeneration in Alzheimer's disease. *Brain research* 1362:13-22.
- Tonoki A, Kuranaga E, Tomioka T, Hamazaki J, Murata S, Tanaka K, Miura M (2009) Genetic evidence linking age-dependent attenuation of the 26S proteasome with the aging process. *Mol Cell Biol* 29:1095-1106.
- Trojanowski, Goedert M, Iwatsubo T, VM. L (1998) Fatal attractions: abnormal protein aggregation and neuron death in Parkinson's disease and Lewy body dementia. *Cell Death Differ* 10:832-837.
- Trojanowski J (2003) Rotenone neurotoxicity: a new window on environmental causes of Parkinson's disease and related brain amyloidoses. *Exp Neurol* 179:6-8.
- Unlü M MM, Minden JS (1997) Differential gel electrophoresis: A single gel method for detecting changes in protein extracts. *Electrophoresis* 18:2071-2077.
- Unno M, Mizushima T, Morimoto Y, Tomisugi Y, Tanaka K, Yasuoka N, Tsukihara T (2002) The structure of the mammalian 20S proteasome at 2.75 Å⁰ resolution. *Structure* 10:609-618.

- Vanden Hoek TL, Li C, Shao Z, Schumacker PT, Becker LB (1997) Significant levels of oxidants are generated by isolated cardiomyocytes during ischemia prior to reperfusion. *J Mol Cell Cardiol* 29:2571-2583.
- Ventadour S, Jarzaguet M, Wing SS, Chambon C, Combaret L, Bechet D, Attaix D, Taillandier D (2007) A new method of purification of proteasome substrates reveals polyubiquitination of 20 S proteasome subunits. *J Biol Chem* 282:5302-5309.
- Walz W (2000) Role of astrocytes in the clearance of excess extracellular potassium. *Neurochem Int* 36:291-300.
- Wang E-S SY, Guo J-G, Gao X, Hu J-W, Zhou L, Hu J, Jiang C-C. (2010) Tetranectin and apolipoprotein A-I in cerebrospinal fluid as potential biomarkers for Parkinson's disease *Acta Neurol Scand* 122:350–359.
- Wang H-R, Kania M, Baumeister W, Nederlof PM (1997) Import of human and *Thermoplasma* 20S proteasomes into nuclei of HeLa cells requires functional NLS sequences. *European journal of cell biology* 73:105.
- Watson JB, Battenberg EF, Wong KK, Bloom FE, Sutcliffe JG (1990) Subtractive cDNA cloning of RC3, a rodent cortex-enriched mRNA encoding a novel 78 residue protein. *J Neurosci Res* 26:397-408.
- Weissman AM (2001) Themes and variations on ubiquitylation. *Nat Rev Mol Cell Biol* 2:169-178.
- Whitehouse PJ, Hedreen JC, White CL, 3rd, Price DL (1983) Basal forebrain neurons in the dementia of Parkinson disease. *Ann Neurol* 13:243-248.
- Wiborg O, Pedersen MS, Wind A, Berglund LE, Marcker KA, Vuust J (1985) The human ubiquitin multigene family: some genes contain multiple directly repeated ubiquitin coding sequences. *EMBO J* 4:755-759.
- Wong CM, Cheema AK, Zhang L, Suzuki YJ (2008) Protein carbonylation as a novel mechanism in redox signaling. *Circulation research* 102:310-318.
- Wood ZA, Schroder E, Robin Harris J, Poole LB (2003) Structure, mechanism and regulation of peroxiredoxins. *Trends Biochem Sci* 28:32-40.
- Wu Y, Feinstein SI, Manevich Y, Chowdhury I, Pak JH, Kazi A, Dodia C, Speicher DW, Fisher AB (2009) Mitogen-activated protein kinase-mediated phosphorylation of peroxiredoxin 6 regulates its phospholipase A(2) activity. *Biochem J* 419:669-679.
- Xia ZP, Sun L, Chen X, Pineda G, Jiang X, Adhikari A, Zeng W, Chen ZJ (2009) Direct activation of protein kinases by unanchored polyubiquitin chains. *Nature* 461:114-119.
- Xu P, Duong DM, Seyfried NT, Cheng D, Xie Y, Robert J, Rush J, Hochstrasser M, Finley D, Peng J (2009) Quantitative proteomics reveals the function of unconventional ubiquitin chains in proteasomal degradation. *Cell* 137:133-145.
- Yamada T, Kawamata T, Walker DG, McGeer PL (1992) Vimentin immunoreactivity in normal and pathological human brain tissue. *Acta Neuropathol* 84:157-162.
- Yamagata A, Kristensen DB, Takeda Y, Miyamoto Y, Okada K, Inamatsu M, Yoshizato K (2002) Mapping of phosphorylated proteins on two-dimensional polyacrylamide gels using protein phosphatase. *Proteomics* 2:1267-1276.
- Yan MH, Wang X, Zhu X (2012) Mitochondrial Defects and Oxidative Stress in Alzheimer's Disease and Parkinson's Disease. *Free Radic Biol Med*.
- Yang D, Song Y, Wang X, Sun J, Ben Y, An X, Tong L, Bi J, Bai C (2011) Deletion of peroxiredoxin 6 potentiates lipopolysaccharide-induced acute lung injury in mice. *Crit Care Med* 39:756-764.

- Yata K OS, Sasaki R, Shindo A, Yang R, Murata M, Kanamaru K, Tomimoto H (2011) Astrocytic neuroprotection through induction of cytoprotective molecules; a proteomic analysis of mutant P301S tau-transgenic mouse. *Brain Res* 1410:12-23.
- Yoon S, Cong WT, Bang Y, Lee SN, Yoon CS, Kwack SJ, Kang TS, Lee KY, Choi JK, Choi HJ (2009) Proteome response to ochratoxin A-induced apoptotic cell death in mouse hippocampal HT22 cells. *Neurotoxicology* 30:666-676.
- Yoshida M (2007) Multiple system atrophy: alpha-synuclein and neuronal degeneration. *Neuropathology* 27:484-493.
- Zaccai J, McCracken C, Brayne C (2005) A systematic review of prevalence and incidence studies of dementia with Lewy bodies. *Age Ageing* 34:561-566.
- Zarranz JJ, Alegre J, Gomez-Esteban JC, Lezcano E, Ros R, Ampuero I, Vidal L, Hoenicka J, Rodriguez O, Atares B, Llorens V, Gomez Tortosa E, del Ser T, Munoz DG, de Yebenes JG (2004) The new mutation, E46K, of alpha-synuclein causes Parkinson and Lewy body dementia. *Ann Neurol* 55:164-173.
- Zeng W, Sun L, Jiang X, Chen X, Hou F, Adhikari A, Xu M, Chen ZJ (2010) Reconstitution of the RIG-I pathway reveals a signaling role of unanchored polyubiquitin chains in innate immunity. *Cell* 141:315-330.
- Zhang, Xie W, Qu S, Pan T, Wang X, W. L (2005) Neuroprotection by iron chelator against proteasome inhibitor-induced nigral degeneration. *Biochem Biophys Res Commun* 333:544-549.
- Zhang DD (2006) Mechanistic studies of the Nrf2-Keap1 signaling pathway. *Drug Metab Rev* 38:769-789.
- Zhao F, Hu Y, Zhang Y, Zhu Q, Zhang X, Luo J, Xu Y, Wang X (2012) Abnormal expression of stathmin 1 in brain tissue of patients with intractable temporal lobe epilepsy and a rat model. *Synapse* 66:781-791.
- Zhou T, Liang B, Su GY, Gong WL, Li HY, Tian LF, He K, Zhao J, Man JH, Li T (2007) Identification of ubiquitin target proteins using cell-based arrays. *Journal of proteome research* 6:4397-4406.
- Zinn AB, Kerr DS, Hoppel CL (1986) Fumarase deficiency: a new cause of mitochondrial encephalomyopathy. *N Engl J Med* 315:469-475.

Appendix I

A. Sequence of primers used for mice genotyping

Primer	Forward Primer (5'-3')	Reverse Primer (5'-3')
Cre	GGTAGCACCCGAGGTGTAG	CTAATCGCCATCTTCCAGCAG
Psmc1-LB3	TACGAACCTCCTGTCCCAAC	-
Psmc1-D1360	CAGAAATACAGCCAGTGACC	-
Psmc1-X316	-	CTGGAACTCAGTGGATTGAG

B. DNA Sequencing p GEX-fwd for ZNF216 wild (Query) and C30/33A ZNF216 mutant (Sbjct)- (<http://blast.ncbi.nlm.nih.gov/Blast>.)

```

wild      1      ATGGCTCAGGAGACTAACCAGACCCAGGGCCCATGCTGTGTAGTACTGGATGTGGCTTT 60
|||||
mutant    1      ATGGCTCAGGAGACTAACCAGACCCAGGGCCCATGCTGTGTAGTACTGGATGTGGCTTT 60

wild      61      TATGGGAATCCTAGGACAAATGGAATG TCTTCTGTT TGTCTACAAAGAACATCTTCAGAGA 120
|||||
mutant    61      TATGGGAATCCTAGGACAAATGGAATG GCTTCTGTT TGTCTACAAAGAACATCTTCAGAGA 120

wild      121     CAGCAGAATAGTGGCAGAATGAGCCCAATGGGGACAGCTAGTGGTTCCAACAGTCCTACC 180
|||||
Mutant    121     CAGCAGAATAGTGGCAGAATGAGCCCAATGGGGACAGCTAGTGGTTCCAACAGTCCTACC 180

wild      181     TCAGACTCTGCGTCTGTACAAAGAGCAGATGCTACTTTAAACAACGTGAAGGTGCTGCT 240
|||||
Mutant    181     TCAGACTCTGCGTCTGTACAAAGAGCAGATGCTACTTTAAACAACGTGAAGGTGCTGCT 240

wild      241     GGCAGCACATCTGAAAAATCAAGAAATGTGCCTGTGGCTGCCTTGCTGTAACCAACAA 300
|||||
Mutant    241     GGCAGCACATCTGAAAAATCAAGAAATGTGCCTGTGGCTGCCTTGCTGTAACCAACAA 300

wild      301     ATGACAGAAATGAGCATTTCAAGAGAGGACAAAATAACCTCCCCGAAAACAGAGGTGTCA 360
|||||
mutant    301     ATGACAGAAATGAGCATTTCAAGAGAGGACAAAATAACCTCCCCGAAAACAGAGGTGTCA 360

wild      361     GAGCCAGTTGTCACCTCAGCCAGTCCATCAGTTTCTCAGCCAGTTCTTCTCAAAGTGAA 420
|||||
mutant    361     GAGCCAGTTGTCACCTCAGCCAGTCCATCAGTTTCTCAGCCAGTTCTTCTCAAAGTGAA 420

wild      421     GAAAAAGCTCCTGAGTTGCCCAAACCAAAGAAGAACAGATGTTTTATGTGTAGAAAGAAA 480
|||||
mutant    421     GAAAAAGCTCCTGAGTTGCCCAAACCAAAGAAGAACAGATGTTTTATGTGTAGAAAGAAA 480

wild      481     GTTGGCCTTACAGGGTTTGACTGCCGATGTGGAAATTTGTTTTGTGGACTTCACCGTTAC 540
|||||
mutant    481     GTTGGCCTTACAGGGTTTGACTGCCGATGTGGAAATTTGTTTTGTGGACTTCACCGTTAC 540

wild      541     TCTGACAAGCACAACCTGTCCTTATGATTACAAAGCAGAAGCTGCAGCAAAAATCAGAAAA 600
|||||
mutant    541     TCTGACAAGCACAACCTGTCCTTATGATTACAAAGCAGAAGCTGCAGCAAAAATCAGAAAA 600

wild      601     GAAAATCCAGTTGTTGTGGCTGAAAAATCCAGAGAATATAA 642
|||||
mutant    601     GAAAATCCAGTTGTTGTGGCTGAAAAATCCAGAGAATATAA 642

```

C. Comparing the amino sequences of ZNF216 wild and C30/33A ZNF216 mutant.

wild M A Q E T N Q T P G P M L C S T G C G F-20
mutant M A Q E T N Q T P G P M L C S T G C G F

wild Y G N P R T N G M C S V C Y K E H L Q R-40
mutant Y G N P R T N G M A S V A Y K E H L Q R

wild Q Q N S G R M S P M G T A S G S N S P T-60
mutant Q Q N S G R M S P M G T A S G S N S P T

wild S D S A S V Q R A D A T L N N C E G A A-80
mutant S D S A S V Q R A D A T L N N C E G A A

wild G S T S E K S R N V P V A A L P V T Q Q-100
mutant G S T S E K S R N V P V A A L P V T Q Q

wild M T E M S I S R E D K I T S P K T E V S-120
mutant M T E M S I S R E D K I T S P K T E V S

wild E P V V T Q P S P S V S Q P S S S Q S E-140
mutant E P V V T Q P S P S V S Q P S S S Q S E

wild E K A P E L P K P K K N R C F M C R K K-160
mutant E K A P E L P K P K K N R C F M C R K K

wild V G L T G F D C R C G N L F C G L H R Y-180
mutant V G L T G F D C R C G N L F C G L H R Y

wild S D K H N C P Y D Y K A E A A A K I R K-200
mutant S D K H N C P Y D Y K A E A A A K I R K

wild E N P V V V A E K I Q R I **Stop**
mutant E N P V V V A E K I Q R I **Stop**

Table I, Antibodies used throughout all protein analysis








Antibody for indicated proteins	Animal source	Concentration. Used mostly	Buffer used for western blot	Manufacturing company
Ubiquitin	rabbit	1:1000	TBST	House made
PRDX-6	rabbit	1:1000	TBST	GenTex 115262
ACTN	Rabbit / mouse	1:1000/1: 5000	TBST	Sigma-A2066
GFAP	mouse	1:1000	TBST	Sigma-G 3893
Nitrotyrosine HM 11	mouse	1:250	PBST	Santa Cruz-sc-32733
SEPT7	rabbit	1:500	PBST	Gene Tex GTX101533
COX5A	rabbit	1:1000	TBST	Gene Tex GTX101487
β - SNAP	rabbit	1:250	PBST	Gene Tex GTX116728
HSC 71/ HSP70	mouse	1:5000	TBST	-----
FUMH	rabbit	1:500	PBST	Gene Tex GTX109877
STMN-1	rabbit	1:250	PBST	Gene Tex GTX113341
VIME	rabbit	1:1000	TBST	Gene Tex GTX100619
GAPDH	rabbit	1:1000	TBST	Sigma, G9545

Appendix II





















CaMKII-alpha-cortex April 2011 Report created: 03/05/2011 13:26:37





Experiment Design:

Condition	control	<i>Psmc1^{fl/fl};CaMKIIa-Cre</i>
Replicates	4	4

Tags	
	Edited
	Anova p-value ≤ 0.05
	All condition p ≤ 0.05 Fold > 1.1
	control > <i>Psmc1^{fl/fl};CaMKIIa-Cre</i>
	pick "up" expressed in control mice
	pick up expressed in <i>Psmc1^{fl/fl};CaMKIIa-Cre</i> mice
	<i>Psmc1^{fl/fl};CaMKIIa-Cre</i> > control

Results of SameSpot analyses:

Spot No.	Anova (p)	Fold	Tags	Notes	pI	MW	Average Normalised Volumes	
							control	mutant
529	1.016e-004	3.2					0.293	0.947
668	1.757e-004	1.6					0.667	1.091
1039	4.173e-004	1.3					1.038	1.400
708	9.766e-004	1.2					1.027	1.245
1250	0.002	1.4					1.428	1.048
1089	0.003	1.2					1.130	1.376
1072	0.003	1.5					1.767	1.194
474	0.003	1.4					0.640	0.915
770	0.005	1.7					0.671	1.117
908	0.006	1.4					0.817	1.184
1130	0.008	1.2					0.908	1.087
705	0.008	1.4					1.011	0.716
1249	0.008	1.4					1.495	1.077
1174	0.012	1.2					1.370	1.096
832	0.014	1.2					1.190	1.012
988	0.019	1.2					0.923	0.776
527	0.022	1.3					1.003	0.759
1253	0.023	1.2					1.520	1.303
506	0.025	1.3					0.923	0.686
767	0.025	1.2					0.932	0.762

903	0.035	1.4					0.957		1.336
1140	0.038	1.3					0.923		1.180
531	0.043	1.4					1.042		0.765
1231	0.046	1.3					1.370		1.835

Identified proteins by MALDI -TOF mass spectrometer:

Spot No. 529. Mascot search peptides matches for **GFAP**

Protein sequence coverage: 82%

The identified peptide highlighted red

```

1 MERRRITSAR RSYASETVVR GLGPSRQLGT MPRFSLSRMT PPLPARVDFS
51 LAGALNAGFK ETRASERAEM MELNDRFASY IEKVRFLEQQ NKALAAELNQ
101 LRAKEPTKLA DVYQAEIREL RLRLDQLTAN SARLEVERDN FAQDLGTLRQ
151 KLQDETNLRL EAENNLAAAYR QEADEATLAR VDLERKVESL EEEIQFLRKI
201 YEEEVRELRE QLAQQQVHVE MDVAKPDLTA ALREIRTQYE AVATSNMQET
251 EEWYRSKFAD LTDAASRNAE LLRQAKHEAN DYRRQLQALT CDLESRLRGTN
301 ESLERQMREQ EERHARESAS YQEALARLEE EGQSLKEEMA RHLQEYQDLL
351 NVKLALDIEI ATYRKLLEGE ENRITIPVQT FSNLQIRETS LDTKSVSEGH
401 LKRNIIVKTV EMRDGEVIKD SKQEHKDVVM

```

Spot No. 770. Mascot search peptides matches for **GFAP**

Protein sequence coverage: 47%

The identified peptide highlighted red

```

1 MERRRITSAR RSYASETVVR GLGPSRQLGT MPRFSLSRMT PPLPARVDFS
51 LAGALNAGFK ETRASERAEM MELNDRFASY IEKVRFLEQQ NKALAAELNQ
101 LRAKEPTKLA DVYQAEIREL RLRLDQLTAN SARLEVERDN FAQDLGTLRQ
151 KLQDETNLRL EAENNLAAAYR QEADEATLAR VDLERKVESL EEEIQFLRKI
201 YEEEVRELRE QLAQQQVHVE MDVAKPDLTA ALREIRTQYE AVATSNMQET
251 EEWYRSKFAD LTDAASRNAE LLRQAKHEAN DYRRQLQALT CDLESRLRGTN
301 ESLERQMREQ EERHARESAS YQEALARLEE EGQSLKEEMA RHLQEYQDLL
351 NVKLALDIEI ATYRKLLEGE ENRITIPVQT FSNLQIRETS LDTKSVSEGH
401 LKRNIIVKTV EMRDGEVIKD SKQEHKDVVM

```

Spot No. 1250, Mascot search peptides matches for Neurogranin

Protein sequence coverage: 58%

The identified peptide highlighted red

1 MDCCTESACS KPDDDILDIP LDDPGANAAA AK**IQASFRGH** **MARKKIKSGE**
51 **CGRKGGPGGG** **PGGAGGARGG** **AGGGPSGD**

Spot No. 1249, Mascot search peptides matches for Neurogranin

Protein sequence coverage: 57%

The identified peptide highlighted red

1 MDCCTESACS KPDDDILDIP LDDPGANAAA AK**IQASFRGH** **MARKKIKSGE**
51 **CGRKGGPGGG** **PGGAGGARGG** **AGGGPSGD**

Spot No. 908, Mascot search peptides matches for Peroxiredoxin-6

Protein sequence coverage: 84%

The identified peptide highlighted red

1 **MPGGLLLGDE** **APNFEANTTI** **GRIRFHDFLG** **DSWGILFSHP** **RDFTPVCTTE**
51 **LGRAAKLAPE** **FAKRNVKLI** **LSIDSVEDHL** **AWSKDINAYN** **GETPTEKLPF**
101 **PIIDDKGRDL** **AILLGMLDPV** **EKDDNNMPVT** **ARVVFIFGPD** **KKLKLSILYP**
151 **ATTGRNFDEI** **LRVVDLQLT** **GTKPVATPVD** **WKKGESVMVV** **PTLSEEEAKQ**
201 **CFPKGVTKE** **LPSGKKYLRY** **TPQP**

Spot No. 474, Mascot search peptides matches for Vimentin

Protein sequence coverage: 69%

The identified peptide highlighted red

1 MSTR**SVSSSS** **YRRMFGGSGT** **SSRPSSNRSY** **VTTSTRTYSL** **GSALRPSTSR**
51 **SLYSSSPGGA** **YVTRSSAVRL** **RSSVPGVRL** **QDSVDFSLAD** **AINTEFKNTR**
101 **TNEKVELQEL** **NDRFANYIDK** **VERFLEQQNKI** **LLAELEQLKG** **QGKSR LGDLY**
151 **EEMRELRQ** **VDQLTNDKAR** **VEVERDNLAE** **DIMRLREKLQ** **EEMLQREEAE**
201 **STLQSFQDV** **DNASLARLDL** **ERKVESLQEE** **IAFLKKLHDE** **EIQELQAQIQ**
251 **EQHVQIDVDV** **SKPDLTAALR** **DVRQQYESVA** **AKNLQEAEEW** **YKSKFADLSE**
301 **AANRNNDALR** **QAKQESNEYR** **RQVQSLTCEV** **DALKGTNESL** **ERQMREMEEN**
351 **FALEAANYQD** **TIGRLQDEIQ** **NMKEEMARHL** **REYQDLLNVK** **MALDIEIATY**
401 **RKLEGEESR** **ISLPLPTFSS** **LNLRETNLES** **LPLVDTHSKR** **TLIKTVETR**
451 **DGQVINETSQ** **HHDDLE**

Spot No. 527, Mascot search peptides matches for **Fumarate hydratase, mitochondrial**

Protein sequence coverage: 26%

The identified peptide highlighted red

1	MYRALRLLAR	SRLLLRVPSA	GAAVSGEATT	LPRCAPNVAR	MASQNSFRVE
51	FDTFGELKVP	TDKYYGAQTV	RSTMNFKIGG	ATER MPIPVI	QAFGILKRAA
101	AEVNQEYGLD	PKIASAIMKA	ADEVAEGKLN	DHFPLVVWQT	GSGTQTNMNV
151	NEVISNR AIE	MLGGELGSKK	PVHPNDHVNK	SQSSNDTFPT	AMHIAAAVEV
201	HKVLLPGLQK	LHDALSAS SK	EFAQVIKIGR	THTQDAVPLT	LGQEFSGYVQ
251	QVQYAMVR IK	AAMPRIYELA	AGGTAVGTGL	NTRIGFAEKV	AAKVAALTGL
301	PFVTAPNKFE	ALAAHDALVE	LSGAMNTAAC	SLMK IANDIR	FLGSGPRSGL
351	GELILPENEP	GSSIMPGKVN	PTQCEAMTMV	AAQVMGNHVA	VTVGGSNHGF
401	ELNVFKPMMI	KNVLHSARLL	GDASVSFTDN	CVVGIQANTE	RINKLMNESL
451	MLVTALNPHI	GYDKAAKIAK	TAHKNGSTLK	ETAIELGYLT	AEQFDEWVKP
501	KDMLGPK				

Spot No. 1253, Mascot search peptides matches for **Stathmin-1**

Protein sequence coverage: 111%

The identified peptide highlighted red

1	MASSDIQVKE	LEKRASQAF	ELILSPRSKE	SVPDFPLSPP	KKKDLSEEEI
51	QKKLEAAEER	RKSHEAEVLK	QLAEKREHEK	EVLQKAIEEN	NNFSKMAEEK
101	LTHKMEANKE	NREAQMAAKL	ERLREKDKHV	EEVRKNKESK	DPADETEAD